Università degli Studi della Calabria

Facoltà di Farmacia e Scienze della Nutrizione e della Salute
Dipartimento Farmaco-Biologico (MED/04 PATOLOGIA GENERALE)

Dottorato di Ricerca in "Biochimica Cellulare ed Attività dei Farmaci in Oncologia" (XIX ciclo)

Relevance of Nuclear IRS-1 in Breast Cancer

Docente Tutor
Prof. Diego SISCI

Dottoranda
D.ssa Catia MORELLI

Coordinatore
Ch.mo Prof. Sebastiano ANDO'

Anno Accademico 2005-2006

INDEX

1) Sisci D, **Morelli C**, Garofalo C, Romeo F, Morabito L, Casaburi F, Middea E, Cascio S, Brunelli E, Ando' S, Surmacz E. Expression of nuclear insulin receptor substrate 1 (IRS-1) in breast cancer. J Clin Pathol. 2006 Aug 1; [Epub ahead of print]

2) Bonofiglio D, Aquila S, Catalano S, Gabriele S, Belmonte M, Middea E, Hongyan Q, **Morelli C**, Gentile M, Maggiolini M, Andò S. Peroxisome Proliferator-Activated Receptor (PPAR) gamma activates p53 gene promoter binding to the NF*k*B sequence in human MCF7 breast cancer cells. Molecular Endocrinology. September 28, 2006 [Epub ahead of print]

3) Panno ML, Giordano F., Mastroianni F., **Morelli C.**, Brunelli E., Palma MF, Pellegrino M., Aquila S., Miglietta A., Mauro L., Andò S. Evidence that low doses of Taxol enhance the functional transactivatory properties of p53 on p21 waf promoter in MCF-7 breast cancer cells. FEBS Letters 2006 Mar; 580:2371-2380.

4) Panno M.L., Mauro L., Marsico S., Bellizzi D., Rizza P., **Morelli C.**, Salerno M., Giordano F., Andò S. Evidence that the mouse insulin receptor substrate-1 belongs to the gene family on which the promoter is activated by estrogen receptor alpha through its interaction with Sp-1. J Mol Endocrinol. 2006 Feb;36(1):91-105.

5) Aquila S., Gentile M., Middea E., Catalano S., **Morelli C.**, Pezzi V., Andò S. Leptin secretion by human ejaculated spermatozoa. J. Clin..Endocrinol Metab. 2005 Aug 90(8):4753-61.

6) del Rincon S.V., Guo Q., **Morelli C.**, Shiu H.Y., Surmacz E., Miller W.H. Retinoic acid mediates degradation of IRS-1 by the ubiquitin-proteasome pathway, via a PKC-dependant mechanism. Oncogene. 2004 Dec 9;23(57):9269-79.

7) **Morelli C**., Garofalo C., Sisci D., del Rincon S., Cascio S., Tu X., Vecchione A., Sauter E.R., Miller W.H Jr, Surmacz E**.** Nuclear insulin receptor substrate 1 interacts with estrogen receptor alpha at ERE promoters. Oncogene. 2004 Sep 30;23(45):7517-26.

8) Sauter, E. R., Garofalo, C., Hewett, J., **Morelli, C.,** Surmacz, E. Leptin expression in breast nipple aspirate fluid (NAF) is influenced by body mass index (BMI) in premenopausal women. . Horm Metab Res. 2004 May; 36(5):336-40.

Atti di convegno

Pasqua, L., **Morelli, C.**, Testa, F., Sisci, D., Aiello, R. and Andò, S. Synthesis of mesoporous silica microsphere for drug targeting. **Atti del Convegno** "VIII Congresso Nazionale AIMAT, Palermo 27 Giugno-1 Luglio 2006".

Abstract

Insulin receptor substrate 1 (IRS-1), one of the major molecules transmitting signals from the insulin and insulin-like growth factor 1 receptors, has been implicated in breast cancer. Recently, data obtained in different cell models, suggested that in addition to its conventional role as a cytoplasmic signal transducer, IRS-1 can function in the nuclear compartment. However, the role of nuclear IRS-1 in breast cancer has never been addressed. Experiments undertaken in our laboratory showed that in estrogen receptor α (ERα)-positive MCF-7 cells 1) a fraction of IRS-1 is translocated to the nucleus upon 17-β-estradiol (E2) treatment; 2) E2-dependent nuclear translocation of IRS-1 is blocked with the antiestrogen ICI 182,780; 3) nuclear IRS-1 colocalizes and coprecipitates with ERα; 4) the nuclear IRS-1:ERα complex is recruited to the E2-sensitive pS2 gene promoter. Furthermore, transfection reporter assays with E2-sensitive promoters suggested that the presence of IRS-1 modulates ERα activity at estrogen response element (ERE)-containing DNA.

Furthermore, since the expression of nuclear IRS-1 in breast cancer biopsies has never been examined, we wanted to assess whether nuclear IRS-1 is present in breast cancer and non-cancer mammary epithelium and if it correlates with other markers, especially ERα. Parallel studies were done for cytoplasmic IRS-1. IRS-1 and ERα expression was assessed by immunohistochemistry. Data were evaluated using Pearson correlation, linear regression, and ROC analysis. Nuclear IRS-1 was expressed at low levels in normal mammary epithelial cells and at higher levels in benign tumors, ductal carcinoma, and lobular carcinoma. Similarly, ERα expression was low in normal cells and benign tumors, but high in ductal and lobular cancer. Nuclear IRS-1 and ERα positively correlated in ductal breast cancer and benign tumors, but were not associated in lobular cancer and normal mammary epithelium. In ductal carcinoma, both nuclear IRS-1 and ERα negatively correlated with tumor grade, size, mitotic index, and lymph node involvement. Cytoplasmic IRS-1 was expressed in all specimens and positively correlated with ERα in ductal cancer. A positive association between nuclear IRS-1 and ERα is a characteristic for ductal breast cancer and marks a more differentiated, non-metastatic phenotype. In summary, our data suggest the existence of interactions between IRS-1 and ERα occurring in the nucleus. These interactions might represent a novel aspect of ER/IGF-I crosstalk in breast cancer.

Introduction

Recent experimental and clinical evidence suggests the involvement of the insulin-like growth factor I (IGF-I) receptor (IGF-IR) in breast cancer development and progression (Bartucci et al., 2001; Pollak, 1998; Sachdev and Yee, 2001; Surmacz, 2000; Surmacz, 2003; Surmacz and Bartucci, 2004). The tumorigenic action of IGF-IR is executed through multiple antiapoptotic, growth promoting, and/or pro-metastatic pathways (Baserga, 2000; Baserga et al., 2003; Mauro et al., 2003; Surmacz, 2003; Surmacz and Bartucci, 2004). Many of these pathways stem from IRS-1, a major IGF-I signaling molecule that becomes phosphorylated on multiple tyrosine residues upon IGF-IR activation. Tyrosine phosphorylated IRS-1 acts as a scaffolding protein sequestering downstream signaling molecules and propagating IGF-I signal through the PI-3K/Akt, Ras/Raf/ERK1/2, Jak2/Stat3 and other pathways (Myers et al., 1994; Myers and White, 1996; White, 1997; White, 1998).

Overexpression or downregulation of IRS-1 in breast cancer cell models suggested that the molecule controls several aspects of the neoplastic phenotype, especially anchorage-dependent and -independent cell growth and survival (Nolan et al., 1997; Surmacz and Burgaud, 1995). In breast cancer cell lines, IRS-1 appears to be expressed at higher levels in ERα-positive than in ERα-negative cells and there is evidence supporting the existence of crosstalk between IRS-1 and ERα systems (Bartucci et al., 2001; Lee et al., 2000; Lee et al., 1999; Rocha et al., 1997; Surmacz, 2000; Surmacz and Bartucci, 2004).

Overexpression of IRS-1 in MCF-7 ERα-positive cells has been shown to induce estrogen-independence and mediate antiestrogen-resistance (Guvakova and Surmacz, 1997; Salerno et al., 1999; Surmacz, 2000; Surmacz and Burgaud, 1995). These effects have been attributed to increased tyrosine phosphorylation of IRS-1 and potentiation of its downstream signaling to Akt (Sachdev and Yee, 2001; Surmacz, 2000).

High expression of IRS-1 can be in part attributed to ERα activity, as 17-beta-estradiol (E2) can upregulate IRS-1 expression and function (Lee et al., 1999; Mauro et al.,

2001; Molloy et al., 2000), while antiestrogens reduce IRS-1 mRNA and protein levels and inhibit IRS-1 signaling (Chan et al., 2001; Guvakova and Surmacz, 1997; Salerno et al., 1999). It has recently been well established that ERα can activate IRS-1 transcription acting on IRS-1 promoter (Lee et al., 1999; Mauro et al., 2001; Molloy et al., 2000; Panno et al., 2006). Furthermore , our recent data suggested that unliganded ERα can directly interact with IRS-1, increasing its stability and potentiating its downstream signaling to Akt (Morelli et al., 2003). Notably, increased activity of IRS-1 is likely to modulate ERα, via ERK1/2- and Akt-mediated phosphorylation of ERα on Ser-118 and Ser-167, respectively (Campbell et al., 2001; Kato et al., 1995; Stoica et al., 2000).

Recent reports suggested that in addition to its cytoplasmic signaling function, IRS-1 is able to regulate nuclear processes in different cell models (Chen et al., 2005; Drakas et al., 2004; Lassak et al., 2002; Prisco et al., 2002; Trojanek et al., 2005). Several rigorously controlled studies demonstrated that nuclear IRS-1 can be found in cells transformed by oncogenic proteins, e.g., T antigens of the JCV (Lassak et al., 2002; Trojanek et al., 2003) and SV40 (Prisco et al., 2002) viruses, and v-src (Tu et al., 2002).

The biological relevance of nuclear IRS-1 in various cell backgrounds has yet to be determined. Recent studies demonstrated that in mouse embryo fibroblasts stimulated with IGF-I, IRS-1 accumulated in the nucleoli and interacted with the upstream binding factor 1 (UBF1), a regulator of RNA polymerase I (Tu et al., 2002); the presence of nucleolar IRS-1 coincided with increased rRNA synthesis and cell growth in size (i.e., rDNA) (Drakas et al., 2004; Tu et al., 2002). In the same cell model, IGF-I induced nuclear IRS-1 modulates the expression of genes controlling cell proliferation (i.e., Cyclin D1) by physically interacting with transcriptional complexes of beta-catenin (Drakas et al., 2004). Nuclear translocation of IRS-1 has also been described in 32D murine cells (Sciacca et al., 2003), osteoblasts (Seol and Kim, 2003) and hepatocytes (Boylan and Gruppuso, 2002).

The mechanism by which IRS-1 is targeted to the nucleus is unknown. The observations from different cell models suggested that although IRS-1 contains putative nuclear localization signals (NLS), it is most likely chaperoned to the nucleus by other proteins, such as viral antigens (Prisco et al., 2002; Tu et al., 2002). The nuclear localization of IRS-1 requires specific IRS-1 domains, but these requirements appear to be different depending on the experimental system. For instance, in JCV T antigen expressing cells, nuclear localization of IRS-1 depends on its pleckstrin homology domain (Lassak et al., 2002), while in IGF-I stimulated cells, the phosphotyrosine binding domain is required (Prisco et al., 2002).

The possible role of nuclear IRS-1 in breast cancer has never been addressed. Here we studied whether E2 can induce nuclear translocation of IRS-1 and if nuclear IRS-1 can associate with and modulate the action of ERα.

Moreover, despite the evidence that IRS-1 signaling may play a critical role in tumorigenesis, only limited studies examined the clinical significance of IRS-1 expression in human breast cancer specimens (Finlayson et al., 2003; Koda et al., 2005; Rocha et al., 1997; Schnarr et al., 2000). In one study, cytoplasmatic IRS-1 has been reported as a bad prognostic marker, as its abundance correlated with a less differentiated tumor phenotype (G3) and lymph node involvement (Koda et al., 2005). Another study correlated IRS-1 with shorter disease-free survival in patients with smaller tumors (Rocha et al., 1997). In contrast, Schnarr et al. found that IRS-1 marks a more differentiated phenotype and better prognosis (Schnarr et al., 2000). Furthermore, one study examining cancer and normal specimens reported similar IRS-1 tyrosine phosphorylation in all tissues (Finlayson et al., 2003), while other analysis found decreased IRS-1 levels in poorly differentiated cancers relative to normal tissue and benign tumors (Schnarr et al., 2000).

Regarding nuclear IRS-1, its presence in breast cancer specimens has been noted by Schnarr et al. (Schnarr et al., 2000) and Koda et al. (Koda et al., 2005), but the clinical

significance of this marker has never been formally addressed. Consequently, we examined the expression of nuclear IRS-1 in normal mammary tissue, benign breast tumors and breast cancer in relation to ERα and other markers and clinicopathological features. Parallel studies were done for cytoplasmatic IRS-1.

Materials and Methods

Cell lines. MCF-7, MDA-MB-231, BT-20, COS-7, and HeLa cells were obtained from ATCC. MDA-MB-231 cells stably expressing ERα have been developed in our laboratory (Morelli et al., 2003).

Cell culture. MCF-7 and MDA-MB-231cells were grown in DMEM:F12 containing 5% calf serum (CS). MDA-MB-231/ER cells were grown in DMEM:F12 plus 5% CS plus 0.05 mg/ml G418. BT-20 cells were grown in DMEM:F12 with 10% fetal bovine serum (FBS). COS-7 and HeLa cells were grown in DMEM supplemented with 10% FBS. In the experiments requiring E2- and serum-free conditions, the cells were cultured in phenol red-free serum-free medium (SFM) (Guvakova and Surmacz, 1997).

Cell treatments. E2 (Sigma) and the antiestrogen ICI 182,780 (Tocris Cookson) were used at the concentration of 10 nM.

Detection of IRS-1 and ERα by confocal microscopy. Confluent cultures (50%) grown on coverslips were fixed in 3% paraformaldehyde, permeabilized with 0.2% Triton X-100, washed three times with PBS, and incubated for 1 h with a mixture of primary antibodies (Abs) recognizing IRS-1 and ERα. The anti-IRS-1 CT (UBI) or anti-IRS-1 pre-CT (UBI) at 2 μg/ml was used for IRS-1 staining; F-10 monoclonal Ab (mAb) (Santa Cruz) at 2 μg /ml was used to detect ERα. Following the incubation with primary Abs, the slides were washed three times with PBS, and incubated with a mixture of secondary antibodies. A fluorescein-conjugated donkey anti-mouse IgG (Calbiochem) was used as a secondary Ab for ERα and a rhodamine-conjugated donkey anti-rabbit IgG (Calbiochem) was used for IRS-1. The cellular localization of IRS-1 and ERα was studied with Bio-Rad MRC 1024 confocal microscope connected to a Zeiss Axiovert 135M inverted microscope with 600 x magnification. The optical sections were taken at the central plane. The fluorophores were imaged separately to

ensure no excitation/emission wavelength overlap. In control samples, the staining was performed with the omission of the primary Abs.

Immunoprecipitation (IP) and Western Blotting (WB). The cytoplasmic and nuclear proteins were obtained from 70% cultures. The cytoplasmic lysis buffer contained: 50 mM HEPES pH 7.5, 150 mM NaCl, 1% Triton X-100, 1.5 mM $MgCl_2$, EGTA 10 mM pH 7.5, glycerol 10%, inhibitors (0.1 mM Na_3VO_4, 1% PMSF, 20 μg/ml aprotinin). Following the collection of cytoplasmic proteins, the nuclei were lysed with the buffer containing 20 mM HEPES pH 8, 0.1 mM EDTA, 5 mM $MgCl_2$, 0.5 M NaCl, 20% glycerol, 1% NP-40, inhibitors (as above). 25-50 μg of protein lysates were used for WB, while 500 μg for IP. The following Abs were employed: anti-IRS-1 CT pAb (UBI) for WB and IP; anti-ERα F-10 mAb (Santa Cruz) for WB and IP; anti-GAP-DH mAb (Research Diagnostics Inc.) for WB, anti-c-Jun mAb (Santa Cruz) for WB, anti-GRB2 mAb (Transduction Laboratories) for WB.

In all IPs, protein lysates were first incubated with primary Abs at 4°C for 4 h in HNTG buffer (20 mM HEPES pH 7.5, 150 mM NaCl, 0.1% Triton X-100, 10% glycerol, 0.1 mM Na_3VO_4), and then immune complexes were precipitated for 1 h with appropriate beads, specifically, with Protein A agarose (Calbiochem) for IPs with polyclonal Abs and anti-mouse IgG agarose (Sigma) for IPs with mouse monoclonal Abs. In control samples, the primary Abs were substituted with nonimmune IgGs (rabbit or mouse, depending on the source of the primary Abs). The immunoprecipitated proteins were washed three times with HNTG buffer, separated on a 4-15% polyacrylamide denaturing gel, analyzed by WB, and visualized by ECL chemiluminescence (Amersham). The intensity of bands representing relevant proteins was measured by Scion Image laser densitometry scanning program.

Luciferase reporter assays. The experiments were performed using COS-7, BT-20 and MCF-7 cell lines. The cells were grown in 24-well plates. At 70% confluence, the cultures were transfected for 6 h with 0.5 μg DNA/well using Fugene 6 (Roche) (DNA:Fugene 3:1). All transfection mixtures contained 0.3 μg of the reporter plasmid, ERE-Luc, encoding the

firefly luciferase (Luc) cDNA under the control of the TK promoter and three estrogen responsive element (ERE) sequences. ERE-Luc was cotransfected with the ERα expression vector pSG5-HEGO alone or in combination with the IRS-1 expression vector pCMV-IRS-1. To maintain the same DNA input in all transfection mixtures, the samples were adjusted with an empty vector (pcDNA3 or pSG5). In addition, to assess transfection efficiency, each of the DNA mixtures contained 50 ng of pRL-TK-Luc, a plasmid encoding renilla luciferase (RI Luc) (Promega). Upon transfection, the cells were shifted to SFM for 12 h and then treated with 10 nM E2 for 24 h, or left untreated in SFM. Luciferase activity (Luc and RI Luc) in cell lysates was measured using Dual Luciferase Assay System (Promega) following manufacturer's instructions. The values obtained for Luc were normalized to that of RI Luc to generate relative Luc units representing ERE-dependent transcription.

Chromatin immunoprecipitation. We followed ChIP methodology described by Shang et al. (2000) with minor modifications. MCF-7, MDA-MB-231, and MDA-MB-231/ER cells were grown in 100 mm plates. Confluent cultures (90%) were shifted to SFM for 24 h and then treated with 10 nM E2 for 1–24 h, or left untreated in SFM. Following treatment, the cells were washed twice with PBS and crosslinked with 1% formaldehyde at 37°C for 10 min. Next, the cells were washed twice with PBS at 41C, collected and resuspended in 200 ml of lysis buffer (1% SDS, 10 mM EDTA, 50 mM Tris-HCl pH 8.1) and left on ice for 10 min. Then, the cells were sonicated four times for 10 s at 30% of maximal power (Fisher Sonic Dismembrator) and collected by centrifugation at 4°C for 10 min at 14 000 rpm. The supernatants were collected and diluted in 1.3 ml of IP buffer (0.01% SDS, 1.1% Triton X-100, 1.2 mM EDTA, 16.7 mM Tris-HCl pH 8.1, 16.7 mM NaCl) followed by immunoclearing with 80 ml of sonicated salmon sperm DNA/ protein A agarose (UBI) for 1 h at 41C. The precleared chromatin was immunoprecipitated for 12 h with specific Abs, specifically anti-ERaC-terminus mAb F-10 (Santa Cruz) for ERa, and anti-IRS-1 C-terminus pAb (UBI) for IRS-1, anti-pol II CTD4H8 mAb for pol II (UBI), and anti-SRC1 1135 mAb

for SRC1 (UBI). After this, 60 ml of salmon sperm DNA/ protein A agarose was added and precipitation was continued for 2 h at 41C. After pelleting, precipitates were washed sequentially for 5 min with the following buffers: Wash A (0.1% SDS, 1% Triton X-100, 2 mM EDTA, 20 mM Tris-HCl pH 8.1, 150 mM NaCl), Wash B (0.1% SDS, 1% Triton X-100, 2mM EDTA, 20 mM Tris-HCl pH 8.1, 500 mM NaCl), and Wash C (0.25 M LiCl, 1% NP-40, 1% sodium deoxycholate, 1mM EDTA, 10 mM Tris-HCl pH 8.1), and then twice with TE buffer (10 mM Tris, 1 mM EDTA). The immune complexes were eluted with elution buffer (1% SDS, 0.1 M NaHCO3). The eluates were reverse crosslinked by heating at 651C for 12 h and digested with proteinase K (0.5 mg/ml) at 451C for 1 h. DNA was obtained by phenol and phenol/chloroform extractions. A 2 ml portion of 10 mg/ml of yeast tRNA was added to each sample and DNA was precipitated with EtOH for 12 h at 41C and then resuspended in 20 ml of TEbuffer. A 5 ml volume of each sample was used for PCR with pS2 promoter primers flanking ERE-containing pS2 promoter fragment: upstream 5'-GATTACAGCGTGAGCCACTG-3', and downstream 5'-TGGTCAAGCTACATGGAAGG-3'. The primers for GAPDH promoter were 5'-GCTACTAGCGGTTTTACGGG-3' (forward) and 5'-AAGATGCGGCTGACTGTCGAA-3' (reverse). The PCR conditions were 45 s at 94°C, 40 s at 58°C, and 90 s at 72°C. The amplification products obtained in 25 and 35 cycles were analysed in a 2% agarose gel and visualized by ethidium bromide staining. The intensity of bands representing relevant proteins was measured by Scion Image laser densitometry scanning program. In control samples, non-immune IgG (rabbit for IRS-1 Abs and mouse for all other Abs, Santa Cruz) was used instead of the primary Abs.

Reverse ChIP (Re-ChIP). We followed methodology described by Reid *et al* (2003). The pellets obtained by immunoprecipitation of soluble chromatin with IRS-1 and ERα Abs were eluted with 500 μl of Re-ChIP buffer (0.5mM DTT, 1% Triton X-100, 2mM EDTA, 150mM NaCl, 20mM TRIS-HCl pH 8.1). Next, the elute from ERα IP was precipitated with IRS-1 Ab (UBI) and the eluate from IRS-1 IP was precipitated with ERα Ab (Santa Cruz). The presence

of the pS2 promoter sequences in the resulting Re-ChIP pellets was examined as described above for one-step ChIP.

RT–PCR. COS-7 cells were transfected with different plasmids for 24 h, as described in the transactivation assays methodology. Total RNA was isolated using TRIzol reagent (Invitrogen) according to the manufacturer's instructions. A 5 mg portion of total RNA was reverse transcribed (RT) at 371C for 30 min in 20 ml of buffer containing 200 U of M-MLV reverse transcriptase (Promega), 0.4 mg oligo-dT, 0.5 mM deoxynucleotide triphosphate (dNTP), and 24 U RNAsin. The reaction was terminated by heat denaturation for 5 min at 95°C. A 2 ml portion of RT products was used to simultaneously amplify pS2 and 36B4 (control) DNA sequences. The pS2 cDNA fragment (210 bp) was amplified using the following primers: 50-TTCTATCCTAATACCATCGACG-30 (forward) and 50-TTTGAGTAGTCAAAGTCAGAGC-30 (reverse). The 408 bp fragment of the 36B4 ribosomal phosphoprotein DNA was amplified with the following primers: 50-CTCAA-CATCTCCCCCTTCTC-30 (forward) and 50-CAAATCCCA-TATCCTCGTCC-30 (reverse) (Maggiolini et al., 2001). The PCR amplification was performed using 1.25 U GoTaq DNA polymerase (Promega), 1 PCR buffer (10 mM Tris-HCl, 50 mM KCl), 2.5 mM MgCl2, 0.2 mM of each dNTP, and 1.5 pM of primers for pS2 or 0.5 pM primers for 36B4. PCR conditions were 30 s at 94°C, 40 s at 59°C, and 60 s at 72°C for 30 cycles. PCR products (10 ml) were separated on a 1.2% agarose gel.

Patients and tissue specimens. Tab. 1 summarizes information of patient and specimen characteristics. The histopathological examination of sections was based on the WHO and pTN classification of breast tumors. Tumor size (pT) was scored as follows: 0, primary tumor not detectable; 1, tumor largest diameter <2cm; 2, diameter <5cm; 3, diameter >5cm; 4, inflammatory carcinoma of any size. Lymph node status (pN) was scored from 0, no node involvement; 1, proximal node involved; 2, distal node involved. The protocol of the present study was reviewed and approved by the local ethical committee.

Table 1. Patient characteristics and clinical parameters of breast tissues and cancers

Sample characteristics

	Cancers	Controls
Total specimens	60	34
Ductal carcinoma	38	
Lobular carcinoma	22	
Benign breast tumors		19
Macromasty		14

Patient Age

	Normal	Benign	Ductal	Lobular
Mean±SE	53.6±3.3	45.4±3.1	62.9±2.4	64.5±2.7
Median (Range)	56.5 (33-68)	43 (20-68)	61.5 (43-94)	66 (48-78)
Menopause (%)	64	39	87	82

Clinical parameters of breast cancer tissues

	Ductal (38)		Lobular (22)	
	G2 (19)	G3 (19)	G2 (10)	G3 (12)
pT	1-4	0-4	2-4	0-4
pN	0-2	0-2	0-1	0-2
Ki67	7.7 ± 0.9 (4-14)	14.2±1.3 (6-21)	7.2±1.5 (4-12)	9.0±1.9 (3-15)

The age of patients in each group is given as mean value ± SE with median age (range) for each population. The percentage of postmenopausal patients is indicated in each group. The range is reported for tumor size (pT), and lymph node involvement (pN); median frequency of expression ±SE (range) is shown for Ki67.

Immunohistochemistry. Immediately after excision, tissue samples were fixed in 10% buffered formaldehyde solution and embedded in paraffin blocks at 56°C. ERα and IRS-1 were analyzed by immunohistochemical (IHC) staining using 3µm-thick consecutive paraffin

sections. The sections were dewaxed in xylene and rehydrated in graded alcohols. After antigen retrieval by boiling in 0.01M citrate buffer pH 6 and endogenous peroxidase removal with 3% H_2O_2, nonspecific binding was blocked by incubating the slides for 30 min with 1.5% BSA in PBS. Next, the sections were incubated with the primary antibodies (Abs) for 1h at room temperature. ERα was detected using ERα mouse monoclonal Ab (mAb) (Dako Cytomation, Denmark) at dilution 1:35. IRS-1 was detected using the C-terminus IRS-1 rabbit polyclonal Ab (pAb) (Upstate, USA) at a concentration 4μg/ml. Ab-antigen reactions were revealed using Streptavidin-biotin-peroxidase complex (LSAB kit, Dako Cytomation, Denmark). All slides were counterstained with hematoxylin. Breast specimens previously classified as positive for the expression of the studied markers were used for control and protocol standardization. In negative controls, primary Abs were omitted. The expression of ERα and IRS-1 was independently scored by two investigators (CM and CG) by light microscopy in 10 different section fields. For all nuclear markers, mean and median percentage, and the range of epithelial cells displaying positive staining was scored. In some analyses, specimens were grouped into ERα-negative (less than 5% of epithelial cells exhibiting ERα expression) and ERα-positive (5% or more of cells with ERα). The expression of cytoplasmic IRS-1 was classified using a four-point scale: 0, <10% positive cells with any staining intensity; 1+, 10-50% positive cells with weak or moderate staining; 2+, >50% positive cells with weak or moderate staining; 3+, >50% positive cells with strong staining. No samples with less than 50% of positive cells with strong staining were recorded.

Statistical analysis. Student's t-test was used to analyze WB and transactivation data. Statistical significance was assumed at $P<0.05$. Descriptive statistic for nuclear IRS-1 and ERα in normal, benign and tumor samples was reported as mean, standard error (±SE), median value and range. The relationship between nuclear IRS-1 and ERα was analyzed by linear regression and the statistical significance was evaluated by the Pearson correlation test.

The distribution of ERα and nuclear IRS-1 in respect to tumor size, grade, and lymph node involvement are reported in scatterplots. The correlations between nuclear IRS-1, ERα, cytoplasmatic IRS-1 and selected clinicopathologic features were examined with the Pearson correlation test.

The value of nuclear ERα or IRS-1 expression as diagnostic marker of tumor grade, pT, pN and Ki67 was evaluated calculating the areas under the receiver operating characteristic (ROC) curves (Greiner et al., 2000; Vanagas, 2004; Wynne-Jones et al., 2000; Zweig, 1993), which assess the performance of a diagnostic test . In the graphical representation of the ROC curve, the X-axis is the false-positive rate (1-specificity) and the Y-axis is the true positive rate (sensitivity). The diagonal line (from 0,0 to 1,1) reflects the characteristics of a test with no discriminating power. ROC curve was analyzed using MedCalc (MedCalc Software, Mariakerke, B).

Results

E2 stimulates nuclear translocation of IRS-1 in MCF-7 cells, and nuclear IRS-1 interacts with ERα

The subcellular localization of IRS-1 and ERα was studied in MCF-7 cells stimulated with E2 for different times, from 15 min to 72 h. The images obtained by immunostaining and confocal microscopy are shown in Figure 1. Under serum-free medium (SFM) conditions, IRS-1 was present mainly in the cytoplasm, especially in the perinuclear area, while ERα localized in the nucleus and was weakly detectable in the cytoplasm (Figure 1). In 95% of untreated cells (SFM), colocalization of IRS-1 and ERα was not observed. At 15 min of E2 treatment, the staining of both proteins resembled that at time 0. At 1 and 4 h, 80% of cells displayed weak nuclear IRS-1 staining and strong nuclear expression of ERα. At these time points, nuclear colocalization of ERα and IRS-1 was detectable in ~25% of cells (data not shown). At 8, 24, and 48 h of E2 treatment, ERα was expressed almost exclusively in the nucleus, while IRS-1 was abundant in both cellular compartments (Figure 1). Furthermore, at these time points, evident nuclear colocalization of ERα and IRS-1 was observed in 60–70% of the cells (Figure 1). At 72 h, nuclear presence of IRS-1 became greatly reduced compared with that of earlier time points, while ERα remained nuclear. At this time, colocalization of ERα and IRS-1 was nearly undetectable (data not shown).

The above experiments were repeated several times with reproducible results. The specificity of IRS-1 staining was confirmed with other anti-IRS-1 polyclonal antibodies (pAbs), specifically anti-IRS-1 CT and anti-IRS-1 pre-CT (both from UBI), and pAb C20 (Santa Cruz). The staining was negative when the primary Abs were omitted or blocking peptide was used, as shown by us before in other cell models (Tu et al., 2002). In addition, we evaluated the specificity of staining procedures using BT-20 breast cancer cells, which are ERα and IRS-1 negative but express IRS-2 (Figure 1, inset). BT-20 cells were treated for 24 and 48 h

with E2 and subjected to the same staining protocol as described for MCF-7 cells. Both IRS-1 and ERα were undetectable in BT-20 cells (Figure 1).

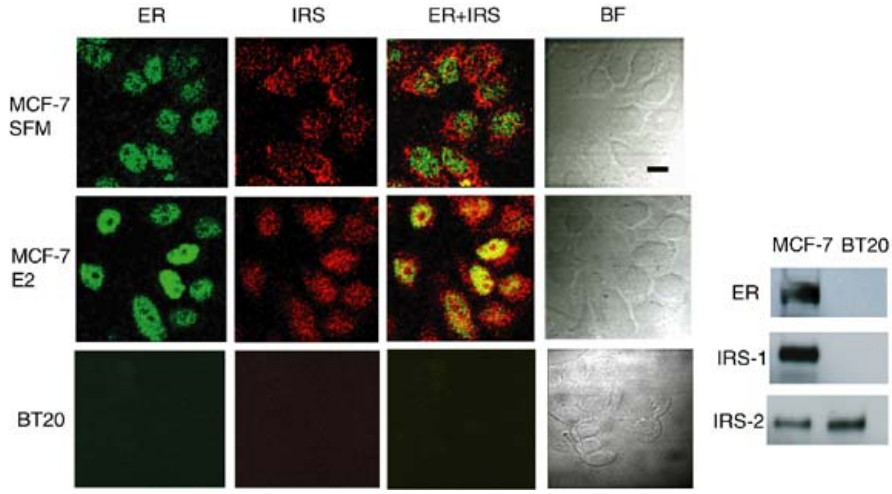

Figure 1. Subcellular localization of IRS-1 and ERα by confocal microscopy. MCF-7 cells synchronized in SFM for 24 h were treated with 10 nM E2 for 24 h (E2) or were left untreated (SFM). BT-20 cells were stimulated with E2 for 24 h. The localization of IRS-1 and ERα was studied by immunostaining and confocal microscopy as detailed in Materials and methods. The captured images of IRS-1 (IRS, red fluorescence), ERα (ER, green fluorescence), merged IRS-1 and ERα (IRS ER, yellow fluorescence), and bright field (BF) are shown. Scale bar equals 20 mm. Inset: The expression of ERα (ER), IRS-1, and IRS-2 was detected by WB in 50 mg of total protein lysates obtained from growing MCF-7 and BT-20 cells.

The localization of ERα and IRS-1 was further pursued in subcellular protein fractions. Cytoplasmic and nuclear proteins were obtained from MCF-7 cells treated with E2 for 24 h or left untreated. Under SFM conditions, ERα was present in the cytoplasmic and nuclear compartments. As expected, upon E2 treatment the nuclear abundance of ERα significantly increased, while the abundance of the cytoplasmic ERα significantly decreased (Figure 2a). In parallel, E2 stimulation significantly (~3.0-fold) upregulated nuclear amounts of IRS-1 (Figure 2). Despite nuclear translocation of IRS-1, its abundance in the cytoplasm remained similar in treated and untreated cells (Figure 2a), which is consistent with the fact that E2 can induce IRS-1 expression (Lee et al., 1999; Molloy et al., 2000). The expression of two

cytoplasmic proteins GRB-2 and GAP-DH, and a nuclear protein c-Jun, was assessed as control of lysate purity (Figure 2a).

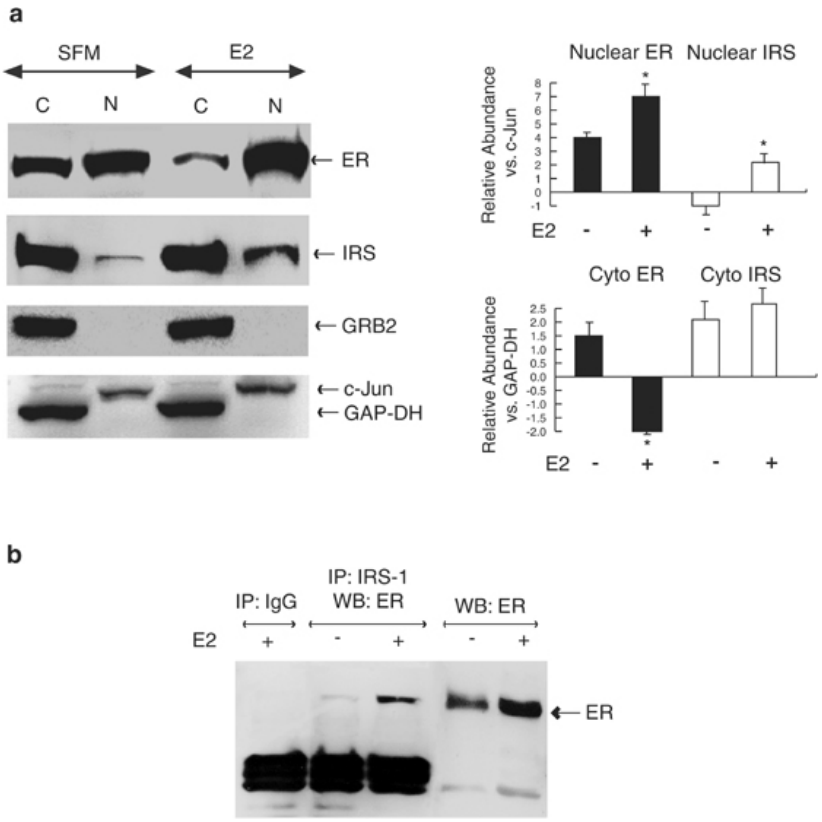

Figure 2. Subcellular localization of ERα and IRS-1 in E2-treated MCF-7 cells. (a) MCF-7 cells synchronized in SFM were treated with 10 nM E2 for 24 h (E2) or were left untreated (SFM). The expression of ERα (ER, ~67 kDa), IRS-1 (IRS, ~180 kDa), GRB-2 (~25 kDa), c-Jun (~39 kDa), and GAP-DH (~36 kDa) was assessed by WB in 100 μg of cytoplasmic (C) and nuclear (N) proteins using specific Abs, as described in Materials and methods. The graphs represent relative abundance of nuclear and cytoplasmic (Cyto) ERα and IRS-1 in unstimulated and E2-stimulated cells. Nuclear and cytoplasmic levels of ERα and IRS-1 were normalized to c-Jun and GAP-DH, respectively (relative values 1). The asterisks indicate statistically significant ($P<0.05$) differences between the amounts in stimulated vs unstimulated cells. The results were obtained after repetitive stripping and reprobing of the same filter. (b) Nuclear lysates from MCF-7 cells (300 μg) were immunoprecipitated with anti-IRS-1 Ab (CT-IRS-1, UBI) or nonimmune rabbit IgG, and the amounts of ERα in the IPs were probed by WB. A 50 μg portion of nuclear proteins was run in parallel.

Confocal microscopy results suggested nuclear colocalization of IRS-1 and ERα To confirm this observation, we studied IRS-1 and ERα interactions by immunoprecipitation (IP) and Western blotting (WB) using nuclear protein fractions obtained form MCF-7 cells grown in SFM or treated with E2 for 24 h (Figure 2b). ERα was found in IRS-1 immunoprecipitates in

treated and untreated cells, with greater abundance of ERα/IRS-1 complexes in E2-stimulated cells (Figure 2b). Similarly, IRS-1 co-precipitated with nuclear ERα under E2 treatment (data not shown). Comparison of ERα content in total nuclear proteins vs IRS-1-associated proteins suggested that only a fraction (~10%) of ERα co-precipitates with IRS-1.

IRS-1 is recruited to the ERE-containing pS2 promoter in MCF-7 cells

Nuclear colocalization and co-precipitation of ERα and IRS-1 suggested that both molecules could be recruited to the same regulatory sequences in DNA. The binding of ERα and IRS-1 to the estrogen-responsive element (ERE)-containing domain of the pS2 gene promoter was assessed with chromatin immunoprecipitation (ChIP) and reverse ChIP (Re-ChIP) assays (Figure 3).

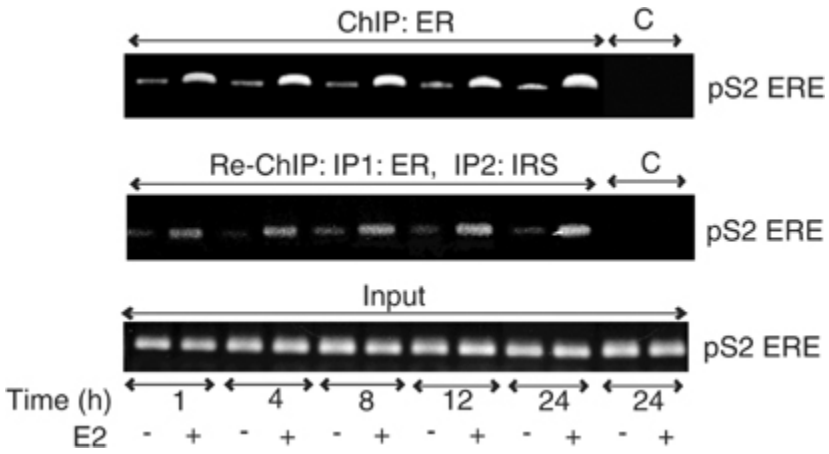

Figure 3. Time course of ERα and IRS-1 association with the pS2 promoter. Soluble chromatin was isolated from MCF-7 cells stimulated with E2 for 1, 4, 8, 12, and 24 h, and from untreated cells at the same time points. ERα ChIP (ChIP: ER) experiments were performed as described in Materials and methods. IRS-1 Re-ChIPs were obtained from ERα ChIP samples after reprecipitation with IRS-1 Abs (Re-ChIP: IP1: ER, IP2: IRS). DNA recovered from the immune complexes was tested for the presence of the ERE-containing pS2 promoter sequences (pS2 ERE) by PCR with specific primers listed in Materials and methods. PCR products obtained after 35 cycles are shown. ChIP pellets obtained using nonimmune IgG were analysed as controls of Ab specificity (C). The abundance of the pS2 promoter sequences in all samples before IP is shown as control of input DNA (Input)

First, we tested the dynamics of ERα association with the pS2 promoter sequences. Soluble chromatin obtained from MCF-7 cells untreated or treated with E2 for 1, 4, 8, 12, and 24 h was immunoprecipitated with anti- ERα Abs and the presence of pS2 promoter DNA in ERα precipitates was detected by PCR. As illustrated in Figure 3, E2 treatment increased ERα

occupancy on the pS2 promoter at all time points. The association of ERα with pS2 DNA was maximal at 24 h after E2 addition (~3.5-fold increase vs untreated) (Figure 3).

To test whether IRS-1 belongs to the ERα multicomplex recruited to the pS2 promoter, we performed Re-ChIP experiments, following the protocol described for ERα interacting proteins (Reid et al., 2003). In our Re-ChIP experiments, the original ERα ChIP pellets were eluted and precipitated with IRS-1 Abs and the pS2 promoter sequences were detected in IRS-1 Re-ChIPs by PCR. We found pS2 DNA in IRS-1 Re-ChIPs at all time points, which indicated that IRS-1 and ERα belong to the same protein complex, and that the complex is associated with the ERE-pS2 promoter in E2-stimulated MCF-7 cells. Notably, the greatest amounts of pS2 DNA in IRS-1 Re-ChIPs were present in cells stimulated with E2 for 24 h (Figure 3).

To extend the above observations, we examined the presence of other regulatory proteins in ERα transcriptional complexes in MCF-7 cells stimulated with E2 for 24 h. Figure 4 illustrates pS2 promoter occupancy by two proteins known to regulate ERα-dependent transcription, ERα coactivator SRC-1 and polymerase II (pol II). In parallel, the association of ERα and IRS-1 under the same conditions was assessed by ChIP and two-way Re-ChIP assays. The results confirmed that E2 stimulates the recruitment of the ERα:IRS-1 complex to the pS2 promoter in MCF-7 cells (Figure 4a and b). In the same experiment, neither ERα nor IRS-1 was recruited to the GAP-DH promoter that is not regulated by ERα (Metivier et al., 2002) (Figure 4c). Notably, the association of ERα and IRS-1 with pS2 DNA coincided with the recruitment of SRC-1 and pol II to the same promoter (Figure 4d).

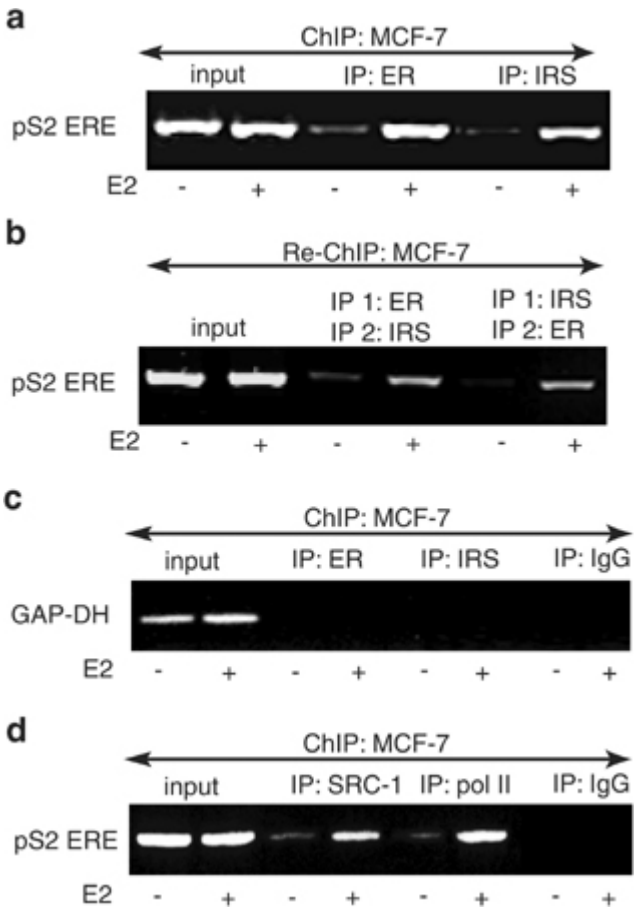

Figure 4. Association of the ERα:IRS-1 complex, SRC-1, and pol II with the pS2 promoter. MCF-7 cells were stimulated with E2 for 24 h, and the presence of the pS2 promoter sequences (pS2 ERE) in (a) ERα and IRS-1 ChIPs, (b)ERα:IRS-1 direct and reverse Re-ChIPs, and (d) SRC-1 and pol II ChIPs was detected by PCR as described in Materials and methods. The occupancy of ERα and IRS-1 on the GAP-DH promoter (not regulated by E2) was tested with specific GAP-DH primers in ERα and IRS-1 ChIP preparations (c). ChIP with nonimmune IgG was used as a control (IP: IgG).

Absence of ERα blocks nuclear IRS-1 translocation

The role of ERα in the nuclear translocation of IRS-1 was probed in MCF-7 cells pretreated with the antiestrogen ICI 182,780 (ICI) for 6 h (Figure 5). This treatment has been chosen based on preliminary tests establishing the dynamics of ICI-dependent downregulation of ERα and IRS-1. IRS-1 is a stable protein with a half-life of ~10 h (Morelli et al., 2003) and only a long-term ICI treatment (48–74 h) can substantially decrease its levels (Salerno et al., 1999), while short-term ICI exposure is sufficient to degrade ERα (Reid et al., 2003). Indeed, a 6 h ICI treatment dramatically reduced cytoplasmatic and nuclear ERα expression without affecting IRS-1 levels (Figure 5a and b).

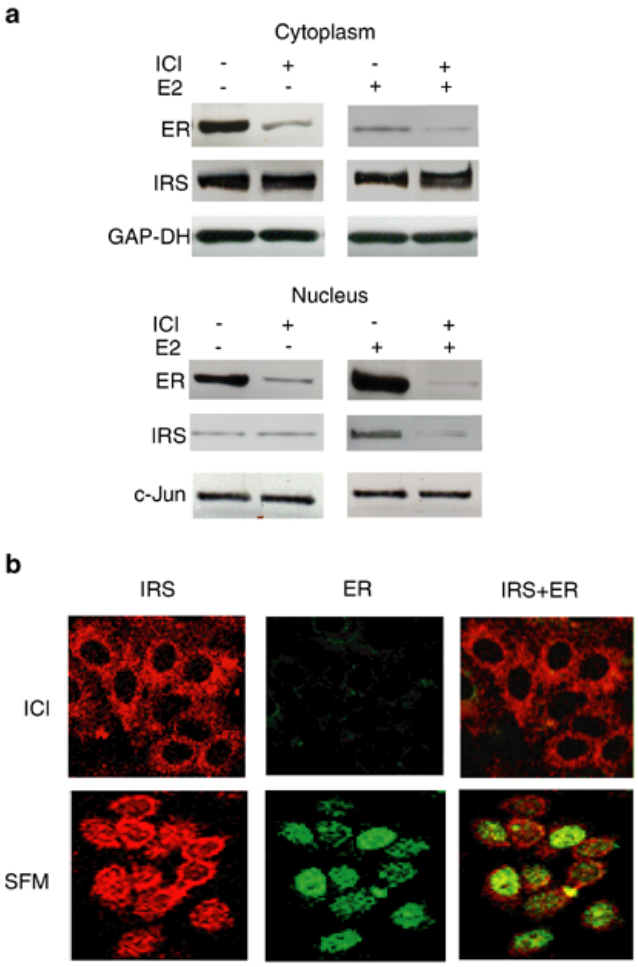

Figure 5. Effects of ERα downregulation on nuclear translocation of IRS-1. MCF-7 cells synchronized in SFM were pretreated with 10 nM ICI 182,780 for 6 h, and then stimulated with 10 nM E2 for 24 h or left untreated in SFM (a). The levels of IRS-1 (IRS) and ERα (ER) were detected in 50 μg of cytoplasmatic and nuclear proteins with specific Abs, as described in Materials and methods. The results were obtained after repetitive stripping and reprobing of the same filter. (b) MCF-7 cells were pretreated with ICI and then stimulated with E2 or left in SFM as described in (a). The localization of IRS-1 (IRS) and ERα (ER) was studied by confocal microscopy, as described in Figure 1. Scale bar equals 50 μm

In ICI pretreated cells, E2 did not stimulate nuclear translocation of IRS-1, as demonstrated by WB (Figure 5a) and confocal microscopy (Figure 5b). However, E2 induced nuclear translocation of IRS-1 in untreated cells expressing normal ERα levels (Figures 1, 2 and 5a). Low amounts of nuclear IRS-1 were found under SFM conditions, possibly reflecting IRS-1 translocation induced by basal ERα activity (Figures 1, 2, 5a and b).

IRS-1 does not associate with the pS2 promoter in ERα-negative MDA-MB-231 cells

The requirement of ERα for E2-dependent nuclear translocation of IRS-1 was further investigated with MDA-MB-231 and MDA-MB-231/ER breast cancer cells (Figure 6). MDA-MB-231 cells are ERα–negative but express IRS-1 on a level similar to that found in MCF-7 cells (Bartucci et al., 2001; Morelli et al., 2003). MDA-MB-231/ER cells have been developed in our laboratory by stable transfection of MDA-MB-231 cells with an ERα expression vector (Morelli et al., 2003). The association of ERα and IRS-1 with the pS2

promoter was studied in both cell lines by ChIP assays. In MDAMB-231 cells, neither ERα nor IRS-1 was found on the pS2 promoter. However, reintroduction of ERα allowed the association of both molecules with pS2 ERE sequences in response to E2 treatment (Figure 6).

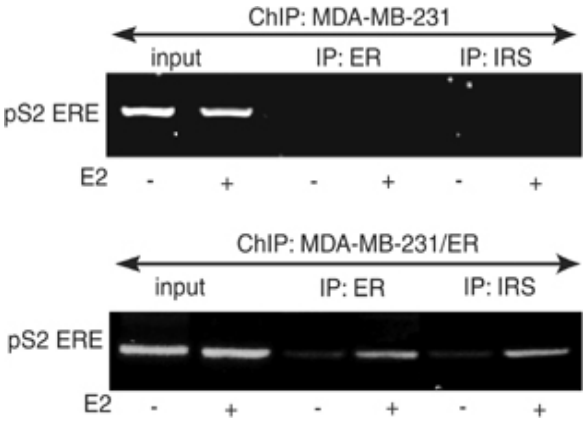

Figure 6. Recruitment of ERα and IRS-1 to the pS2 gene promoter in MDA-MB-231 and MDA-MB-231/ER cells. MDA-MB-231 and MDA-MB-231/ER cells were stimulated with E2 for 24 h or were left untreated in SFM. The presence of ERα and IRS-1 on the pS2 promoter (pS2 ERE) was detected by ChIP assays, as described in Materials and methods

IRS-1 modulates ERα transcriptional activity

Because IRS-1 and ERα are recruited to E2-sensitive promoters, we tested whether the presence of IRS-1 may affect ERα transcriptional activity at ERE sites. This possibility was examined with transactivation assays employing an ERE reporter plasmid. The plasmid, ERE-Luc, was transiently transfected into cells either together with ERα expression vector only or with a mixture of ERα and IRS-1 expression plasmids. The transfected cells were left untreated or were treated with E2 for 24 h (Figure 7). To assess E2-dependent transcription in a controlled environment, we used ERα- and IRS-1-negative COS-7 and BT-20 cells (Figures 1 and 7b), which allowed measurements of transcriptional activity in the presence or absence of studied molecules. In addition, transactivation experiments were performed in MCF-7 cells expressing endogenous IRS-1 and ERα. The transactivation assays indicated that the presence of IRS-1 significantly decreased ERα activation of ERE promoters in all cell lines stimulated with E2 (Figure 7a).

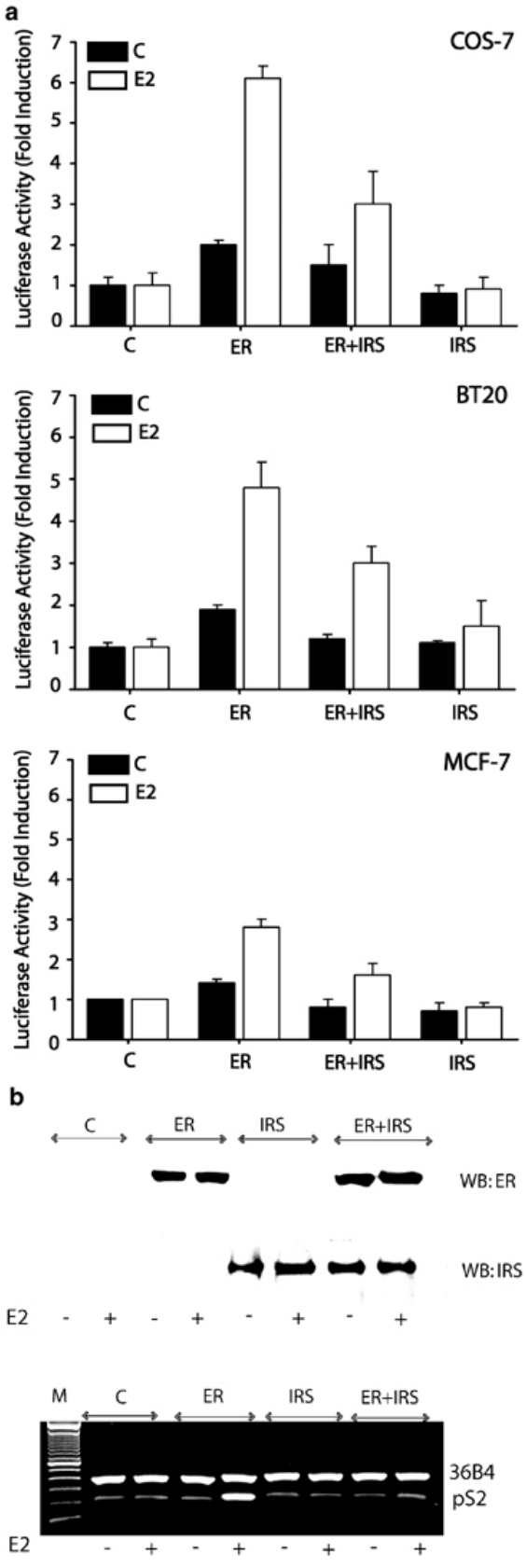

Figure 7. Effects of IRS-1 on ERα transcriptional activity at ERE promoters. (a) Transactivation assays. The transcriptional activity of ERα on ERE promoters in the presence or absence of IRS-1 was evaluated using luciferase reporter system, as described in Materials and methods. COS-7, BT-20, and MCF-7 cells were transfected with DNA mixtures containing ERE reporter plasmid alone (C), ERE + plasmid pHEGO encoding ERα (ER), ERE + ER + plasmid encoding IRS-1 (ER + IRS), or ERE + IRS1 (IRS). The activity of the ERE promoter in each experimental setting is represented by relative Luc units. The results are means ± s.e. from several experiments. In all experimental systems, the difference between E2-stimulated Luc activities in ER vs ER + IRS transfectants was statistically significant ($P<0.05$). (b) Effect of IRS-1 expression on pS2 mRNA levels. Upper panel: COS-7 cells were transfected with different plasmids and stimulated with E2 or left untreated, as described above. ERα and IRS-1 expression in transfected cells was detected by WB in 50 μg of total protein lysates. Lower panel: The abundance of pS2 and 36B4 mRNAs in COS-7 cells transfected with different plasmids was detected by RT–PCR, as described in Materials and methods

Specifically, in COS-7, BT-20, and MCF-7 cells, cotransfection of IRS-1 reduced ERα activation of ERE by ~50, ~39, and ~44%, respectively. The transfection of IRS-1 alone did not stimulate ERE transcription (Figure 7a). In addition to ERE reporter assays with reporter plasmids, we assessed transcriptional activation of the pS2 gene in COS-7 cells transfected with either ERα, IRS-1, or a combination of ERα plus IRS-1. COS-7 cells were selected for this assay as they proved to be the most E2-responsive and the best transfectable cell model (Figure 7a). The levels of pS2 mRNA in COS-7 cells transfected with different plasmids were studied using RT–PCR (Figure 7b). The amounts of a constitutively expressed 36B4 mRNA were assessed in the same samples. The results suggested that E2 stimulated pS2 mRNA expression (~3-fold) in ERα-transfected cells, compared with vector-only-transfected cells. This effect of E2 was significantly reduced in cells cotransfected with ERα and IRS-1, confirming the trend observed in ERE luciferase reporter assays. Notably, ERα expression was similar in the 'ER' and 'ER+IRS' populations, ruling out the possibility that differences in pS2 transcription were related to unequal ERα expression (Figure 7b).

Nuclear IRS-1and ERα expression in normal mammary epithelium and benign breast tumors

To assess nuclear IRS-1 relevance *in vivo*, we tested its expression in breast biopsies and evaluated if it was correlated with major clinicopathological features.

In general, the expression of nuclear IRS-1 in normal tissues was very low (~2% of positive cells) (Tab. 2 and data not shown). ERα was expressed in 11 of 14 samples at the median frequency 30% (Fig. 8A, B and Tab. 2). In 9 of 11 ERα-positive specimens, 1.8% of epithelial cells contained nuclear IRS-1 (Tab. 2). Low frequency (3.5%) of nuclear IRS-1 was also recorded in 2 specimens that did not express ERα. (Tab. 2 and data not shown).

Compared with normal epithelium, benign tumors expressed higher levels of nuclear IRS-1 (21%), while the levels of ERα were similar (23%). Nuclear IRS-1 was found in 16 of

19 ERα-positive specimens, but was not present in any of ERα-negative cases. (Fig. 8C, D and Tab. 2).

Cytoplasmic IRS-1 was expressed in all epithelial cells of normal epithelium and benign tumors at the levels 1+ to 3+ (Fig. 8B, D and Tab. 5), while no evidence of cytoplasmic ERα staining was revealed in any of the specimens (Fig. 8A).

Table 2. Descriptive statistics of nuclear IRS-1 and ERα in ERα-positive specimens.

	Normal Epithelium		**Benign Tumors**	
	ERα	**IRS-1**	**ERα**	**IRS-1**
Mean±SE	30.2±6.8	2.1±0.6	26±4.2	22.9±5.4
Median (Range)	30 (7-60)	1.8 (0-6)	23 (5-70)	21 (0-60)

Ductal Carcinoma	**G2+G3**		**G2**		**G3**	
	ERα	**IRS-1**	**ERα**	**IRS-1**	**ERα**	**IRS-1**
Mean±SE	58±8.1	25.1±6.7	72.5±6.4	31.3±8.7	21.7±8.4	9.5±3.2
Median (Range)	65 (5-92)	12.5 (0-72)	81 (30-92)	21 (5-72)	21 (5-40)	12 (0-14)

Lobular Carcinoma	**G2+G3**		**G2**		**G3**	
	ERα	**IRS-1**	**ERα**	**IRS-1**	**ERα**	**IRS-1**
Mean±SE	66.8±8.2	37.7±9.1	79.5±6.8	40±16.8	50±11.5	34.6±1.4
Median (Range)	70 (30-90)	35 (0-80)	84 (60-90)	40 (0-80)	50 (30-70)	35 (32-37)

The mean (±SE) expression with median (range) values for nuclear IRS-1 and ERα in ERα-positive samples is given. Cancer samples of ductal and lobular origin were grouped into G2+G3 or analyzed as separate G2 and G3 populations.

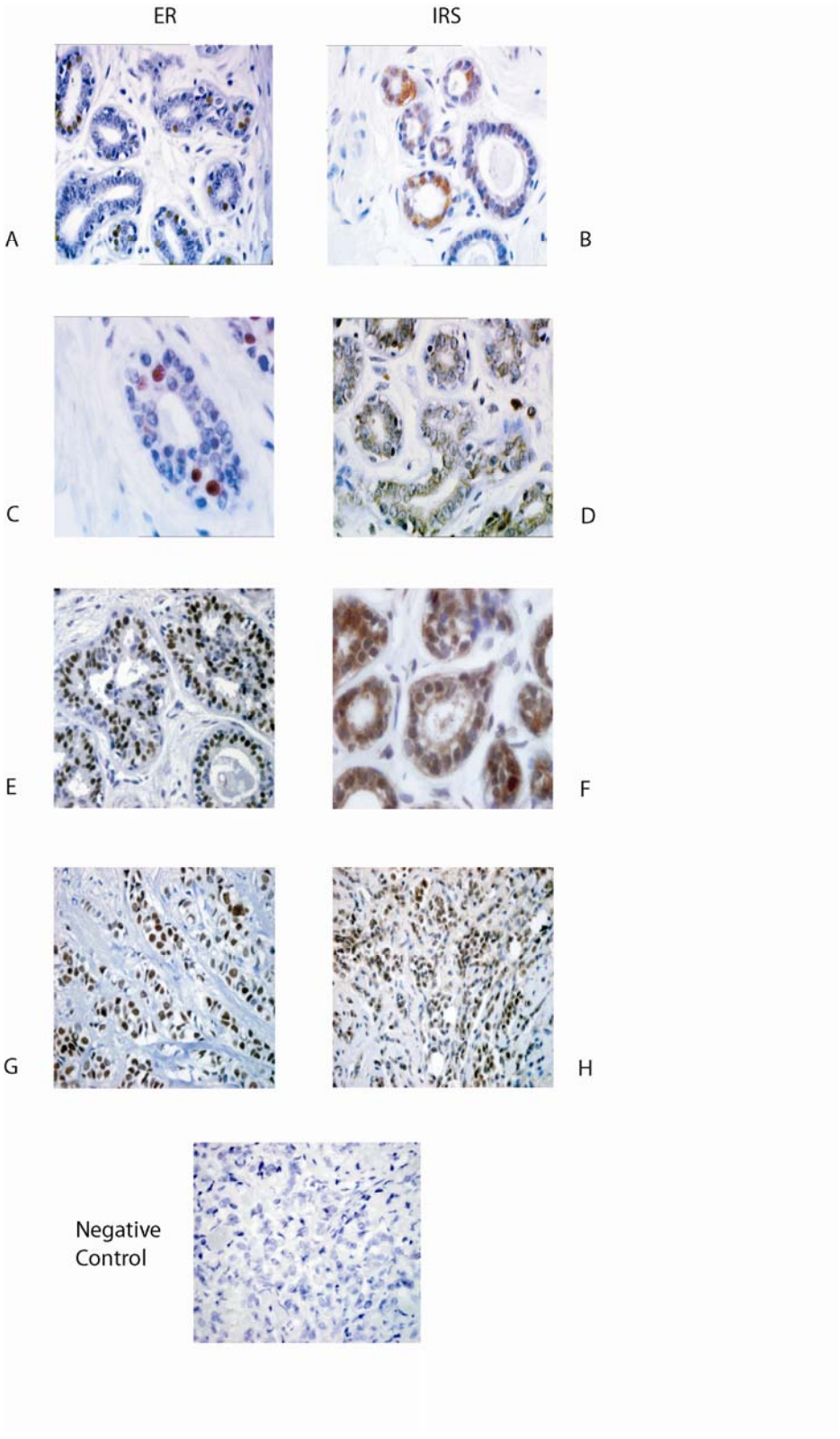

Figure 8. ERα and IRS-1 expression in normal mammary epithelium, benign breast tumors and breast cancers. The expression of ERα (ER) and IRS-1 (IRS) were examined by IHC, as described in Materials and Methods. Normal breast tissue (A, B); benign breast tumor (C, D); invasive ductal ERα-positive carcinoma (E, F); ERα-positive lobular breast cancer (G, H). Negative control; IHC of lobular carcinomas with primary Abs substituted with PBS.

IRS-1 expression in ERα-positive and ERα-negative breast carcinoma

In invasive ductal carcinoma, nuclear IRS-1 was found in 22 of 38 of specimens at the median level 12.5%, while ERα was detected in 20 of 38 of the samples with a median value of 65% (Fig. 8E, F and Tab. 2). Twenty two specimens (15 of 19 in G2, and 7 of 19 in G3) expressed nuclear IRS-1 (Fig. 8F, Tab. 2). Among nuclear IRS-1-positive samples, 18 also expressed ERα, while 4 were ERα-negative. Thirteen of G2 ductal carcinomas and 5 of G3 were positive for both IRS-1 and ERα. In 2 of 38 specimens, ERα was expressed in the absence of nuclear IRS-1.

In lobular cancer, nuclear IRS-1 staining was observed in 16 of 22 samples with the median frequency 35% (Fig. 8H, Tab. 2). Eleven of these 16 samples were also ERα-positive. In G2 lobular carcinomas, 6 of 10 (median 40%) displayed nuclear IRS-1 staining; all these samples were ERα-positive (Tab. 2). In the G3 subgroup, 10 of 12 tumors expressed nuclear IRS-1 (median 37%, data not shown) and 5 of 10 expressed ERα (median 35%). In 5 of 16 specimens, nuclear IRS-1 was found in the absence of ERα. ERα was expressed in 14 of 22 samples with the median frequency 70% (84 and 50%, in G2 and G3 subgroups, respectively) (Tab. 2).

Cytoplasmatic IRS-1 was identified in all ductal and lobular cancer samples displaying a weak to strong staining intensity (Tab. 5). In all specimens, the neoplasm surrounding tissue appeared normal and the pattern of ERα and IRS-staining comparable to that of the normal samples.

Correlation between nuclear IRS-1and ERα in breast cancer, benign tumors, and normal mammary epithelium

A very strong positive correlation ($p<0.001$) between nuclear IRS-1 and ERα was found in invasive ductal breast cancer. The markers were also positively associated ($p<0.01$)

in benign tumors cancer samples (Fig. 9). However, no correlations were found between nuclear IRS-1 and ERα in normal tissues (p=0.28) and lobular breast cancer (p=0.24) (Fig. 9).

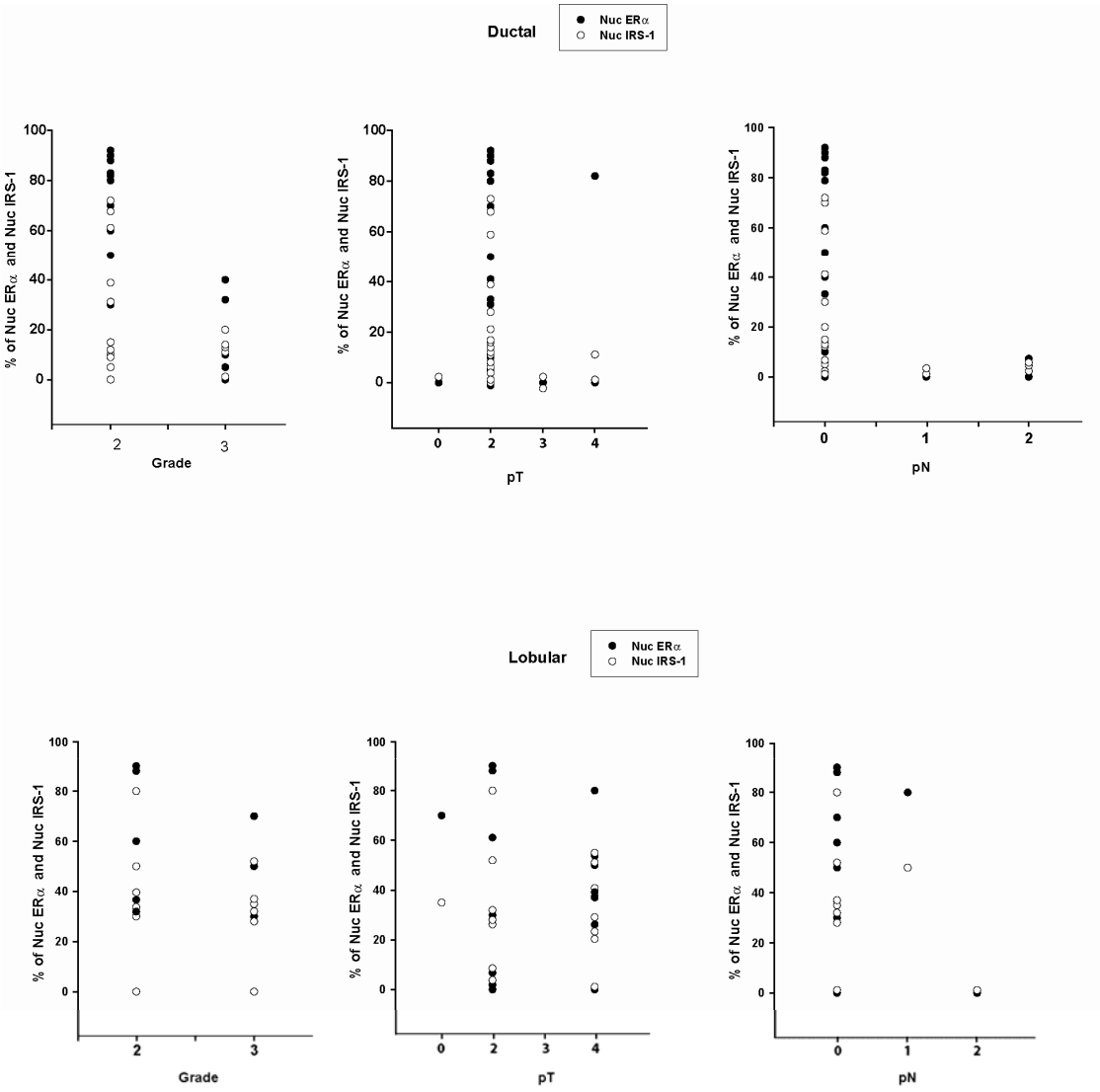

Figure 9. Correlations between nuclear IRS-1 and ERα in normal breast tissues, benign breast tumors and breast cancers. Associations between nuclear IRS-1 and ERα in different tissues were analyzed with Pearson correlation test. For each linear regression graph, the linear equation, the correlation coefficient (R), and the statistical significance (p) is reported.

Nuclear IRS-1 and ERα are correlated with some clinicopathological features in invasive ductal carcinomas

The distribution of nuclear ERα and nuclear IRS-1 was analyzed with respect to tumor grade, tumor size, lymph node involvement, and proliferation index (Fig. 10).

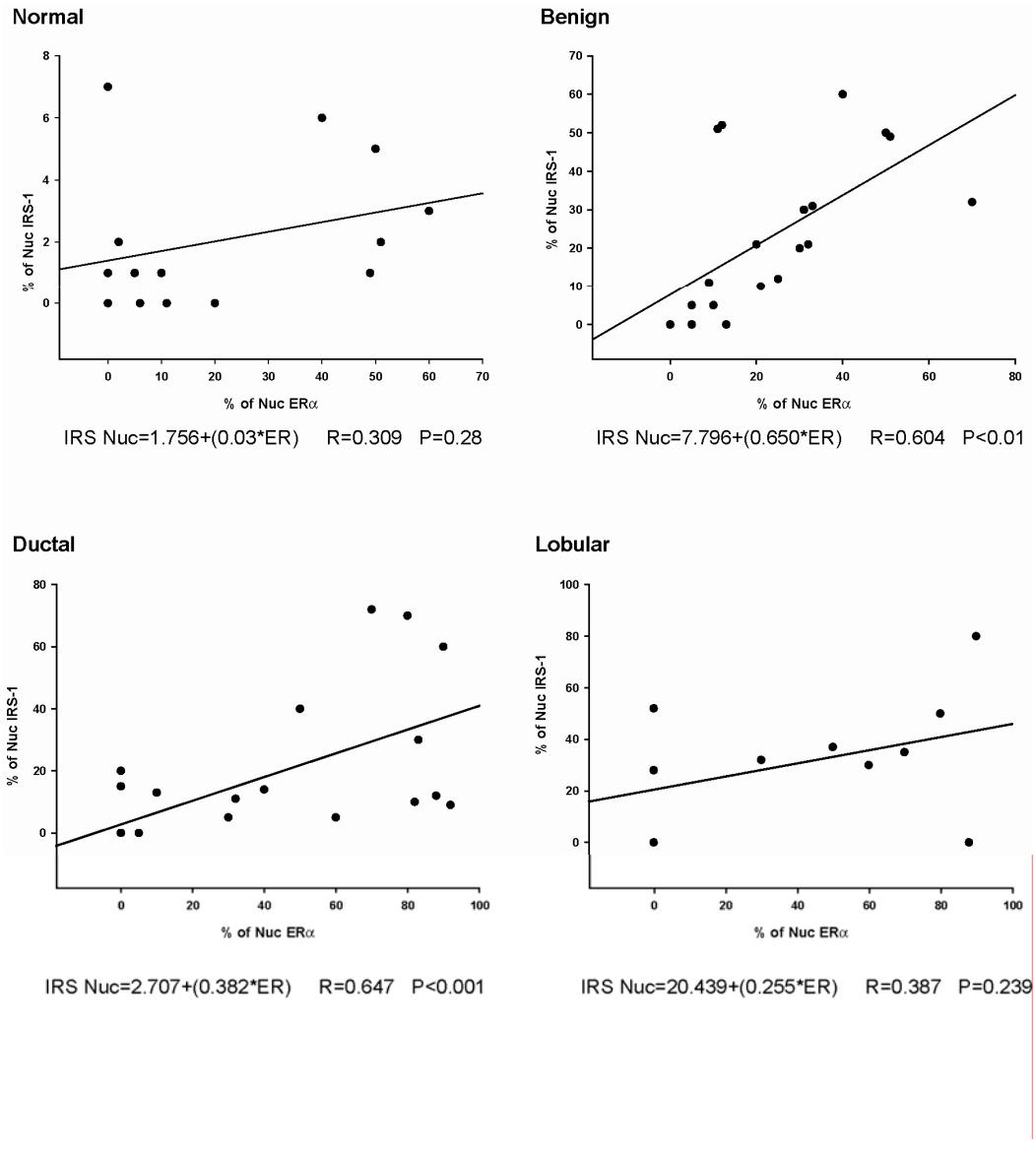

Figure 10. Distribution of nuclear IRS-1 and ERα in ductal and lobular breast cancers. Distributions of nuclear IRS-1 (%) and ERα (%) relative to tumor grade (Grade), size (pT), and the lymph node involvement (pN) in ductal and lobular breast cancers are shown in scatterplots.

The frequency of both ERα and nuclear IRS-1 expression was the highest in node-negative G2 invasive ductal carcinomas of smaller size (Fig. 10). In the same group, a significant negative correlation between nuclear IRS-1 or ERα and differentiation grade, the tumor size, lymph node involvement and proliferation rate was found (Tab. 3).

In contrast, in lobular breast carcinomas, the distribution of nuclear IRS-1 or ERα appeared to be independent of and not correlated with tumor grade, size, or Ki67 expression (Fig. 9 and Tab. 3). Interestingly, both nuclear IRS-1 and ERα were more abundant in lymph node-negative samples (Fig. 10), but no significant associations were determined between these markers and lymph node status (Tab. 3).

Table 3. Correlation between nuclear IRS-1, ERα and selected clinicopathological tumor features.

		Ductal Carcinoma		Lobular Carcinoma	
		ERα	IRS-1	ERα	IRS-1
G	r	**-0.573**	**-0.511**	-0.563	0.029
	p	**0.0015**	**0.0057**	0.065	0.94
pT	r	**-0.393**	**-0.382**	-0.326	0.153
	p	**0.039**	**0.044**	0.310	0.633
pN	r	**-0.381**	**-0.454**	-0.082	-0.122
	p	**0.044**	**0.015**	0.797	0.714
Ki67	r	**-0.591**	**-0.538**	-0.329	-0.016
	p	**0.0001**	**0.003**	0.31	0.94

The association between nuclear IRS-1 or ERa and tumor grade (G), size (pT), lymph node involvement (pN), and the expression of the proliferation marker Ki67 was statistically analyzed with Pearson correlation test; r, correlation coefficient; p, statistical significance. The statistically significant correlations are bolded.

The specificity and sensitivity of nuclear IRS-1 or ERα as a marker of tumor differentiation grade, tumor size and lymph node involvement was evaluated by the ROC curve analysis. The comparison of the areas under the ROC curves obtained for nuclear IRS-1 and ERα indicated that both nuclear IRS-1 and ERα are good markers for tumor grading in invasive ductal carcinomas, while in lobular carcinomas only ERα could be considered a marker for grading (Tab. 4 and Fig. 11).

Neither ERα nor nuclear IRS-1 was a useful marker of tumor size, node involvement, or tumor proliferation (data not shown). The distribution of nuclear IRS-1 or ERα was not related to patient's age and menopausal status in cancer, benign and normal samples (data not shown).

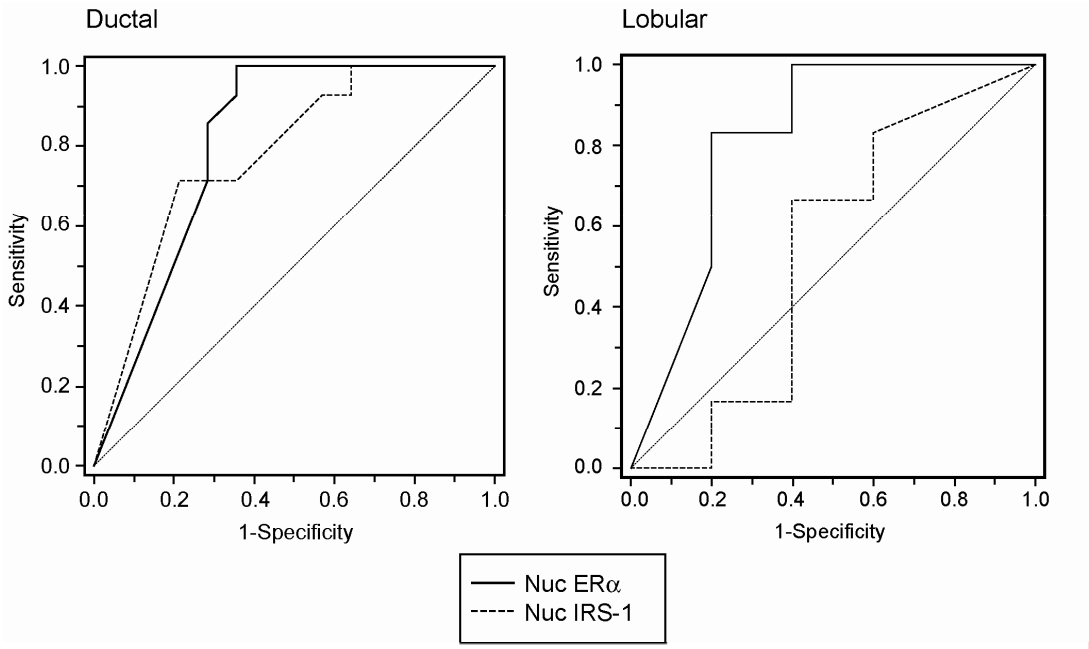

Figure 11. Value of nuclear IRS-1 and ERα as diagnostic markers of tumor grading. Graphic evaluation of ERα and nuclear IRS-1 in respect to tumor differentiation grade in invasive ductal and lobular carcinomas, showing the true-positive rate (sensitivity) and the false-positive rate (specificity) of the analysis as a function of all possible cut-points for the two markers. ERα, solid line; nuclear IRS-1, dotted line.

Table 4. Association between nuclear IRS-1, ERα and tumor grade.

Diagnostic Marker	ROC analysis for tumor grade		
	AUC estimate (95% CI)	**Area under the ROC curve**	**Mann-Whitney test (p value)**
Ductal Carcinoma			
ERα	71.4 (41.9-91.4)	0.809	**0.001**
IRS-1	78.6 (49.2-95.1)	0.778	**0.001**
Lobular Carcinoma			
ERα	80.0 (28.8-96.7)	0.817	**0.02**
IRS-1	60.0 (15.4-93.5)	0.533	0.85

The analysis was performed with ROC curves, as described in Materials and Methods. The area under the ROC (receiver operating characteristic) curve (AUC) describes the value of nuclear IRS-1 or ERα to discriminate between G2 and G3 tumors. AUC estimate reports the confidence intervals considering an error of 5%. The statistical significance was evaluated by Mann-Whitney test for an area =0.5. Statistical significances are bolded.

Table 5. Descriptive statistics of cytoplasmatic IRS-1 in all samples

Cytoplasmic IRS-1 Expression (% of Cases in Class)	Normal	Benign	Ductal	Lobular
0	0	0	0	0
1+	29	21	16	0
2+	29	21	52	63
3+	42	58	32	37

Samples are grouped in 4 classes as described in Materials and Methods. The percentage of specimens with cytoplasmic IRS-1 in each staining category is given.

Relationship between cytoplasmatic IRS-1 and clinicopathological features

In ductal carcinomas, cytoplasmic IRS-1 (each staining intensity group) positively correlated with ERα. Moreover, in ductal cancer low and moderate IRS-1 expression was positively associated with tumor size, while high IRS-1 levels negatively correlated with tumor grade (Tab. 6).

In lobular carcinomas, high expression of cytoplasmic IRS-1 directly correlated with Ki67 (Tab. 6). In benign tumors, low expression of cytoplasmatic IRS-1 was negatively

associated with ERα, while higher IRS-1 levels were not linked to ERα. No correlations between the two markers were found in normal samples (data not shown). Similarly, cytoplasmic IRS-1 expression was not related to age or menopausal status in all analyzed material (data not shown).

Table 6. Correlations between cytoplasmatic IRS-1 and selected clinicopathological features in ERα-positive tumors.

		Ductal				Lobular			
		0	**1+**	**2+**	**3+**	**0+**	**1+**	**2+**	**3+**
ERα	**r**	-	**0.978**	**0.637**	**0.987**	-	-	0.198	-0.029
	p		**0.025**	**0.019**	**0.013**			0.671	0.970
G	**r**	-	0.375	-0.082	**-0.962**	-	-	0.204	-0.376
	p		0.625	0.790	**0.037**			0.661	0.624
pT	**r**	-	**0.973**	**0.553**	-0.577	-	-	0.009	-0.225
	p		**0.026**	**0.050**	0.423			0.984	0.775
pN	**r**	-	0.00	0.301	-	-	-	-0.069	-
	p		1.00	0.318				0.883	
Ki67	**r**	-	0.724	-0.241	-0.905	-	-	-0.223	**0.978**
	p		0.276	0.428	0.095			0.631	**0.022**

The associations between cytoplasmatic IRS-1 and ERα positivity (ERα), tumor grade (G), tumor size (pT), lymph node involvement (pN), and the expression of the proliferation marker Ki67 were statistically analyzed with the Pearson correlation test; r, correlation coefficient; p, statistical significance. The statistically significant correlations are bolded. The absence of value is due to either the absence of samples in the group or to the homogeneity of samples (variance =0).

Discussion

The interactions between IGF-IR and ER signaling systems have been implicated in the development of the neoplastic phenotype in mammary epithelial cells (Sachdev and Yee, 2001; Surmacz, 2000; Yee and Lee, 2000). In this context, IRS-1, a molecule that activates multiple growth and survival pathways, has been found to be one of the central elements of IGF-IR/ER crosstalk. Several reports documented that E2 can increase IRS-1 transcription, while ICI inhibits IRS-1 mRNA levels (Sachdev and Yee, 2001; Surmacz, 2000; Yee and Lee, 2000). Furthermore, the expression of ERα seems to stabilize IRS-1 protein and potentiate IRS-1 signaling through the PI-3K/Akt pathway (Morelli et al., 2003). In turn, the activation of IRS-1/PI-3K/ Akt by growth factors can stimulate ERα by increasing its phosphorylation (Lannigan, 2003). In MCF-7 cells, overexpression of IRS-1 has been shown to induce estrogen independence (Surmacz and Burgaud, 1995), while downregulation of IRS-1 resulted in increased sensitivity to E2 (Ando et al., 1998).

Here we report on a novel aspect of ERα/IGF-I crosstalk involving nuclear ERα/IRS-1 interactions. Specifically, we demonstrated that (1) in MCF-7 cells, IRS-1 can be translocated from the cytoplasm to the nucleus following E2 treatment; (2) nuclear transloca tion of IRS-1 is blocked with ICI and does not occur in ERα-negative cells; (3) nuclear IRS-1 interacts with ERα; (4) nuclear IRS-1 is corecruited with ERα to the ERE-containing pS2 promoter; and (5) the presence of IRS-1 decreases ERα transcription at ERE promoters.

Nuclear localization of IRS-1 has recently been described in different cellular systems (Lassak et al., 2002; Prisco et al., 2002; Sciacca et al., 2003; Sun et al., 2003; Tu et al., 2002). The mechanism by which IRS-1 enters cell nucleus is still not clear. Although IRS-1 contains putative NLS, it is thought that IRS-1 is chaperoned to the nucleus by other proteins, for instance, by T antigens of the SV40 and JC viruses (Lassak et al., 2002). The transporting molecules involved in IGF-IR-dependent IRS-1 nuclear translocation are yet unknown.

In our experimental system, E2-dependent nuclear translocation of IRS-1 and its interaction with the pS2 promoter were totally blocked when ERα was down-regulated by ICI (Figure 5) and did not occur in MDA-MB-231 cells that are ERα–negative but express ERβ (Vladusic et al., 2000) (Figure 6). However, re-expression of ERα allowed association of IRS-1 with the pS2 sequences. These observations suggest that nuclear function of IRS-1 in response to E2 requires ERα. Notably, a small amount of nuclear IRS-1 was found in unstimulated MCF-7 cells, which could result from basal ERα activity.

The prerequisite for nuclear translocation of IRS-1 in response to E2 is most likely the formation of the ERα:IRS-1 complex in the cytoplasm. ERα association with cytoplasmic signaling molecules is not unusual. Recently, ERα has been shown to bind the PI-3K/Akt complex (Simoncini et al., 2000; Sun et al., 2001), and to interact with growth factor receptor docking protein Shc (Song et al., 2002) as well as with IGF-IR (Kahlert et al., 2000). Similarly, we reported that unliganded ERα can associate with cytoplasmic IRS-1 in MDA-MB-231/ER cells (Morelli et al., 2003). Our preliminary data suggest that ERα /IRS-1 binding involves at least two different IRS-1 domains, and does not depend on IRS-1 tyrosine phosphorylation (Surmacz et al., unpublished data).

Our previous findings (Morelli et al., 2003) and this report suggest that only a fraction of ERα binds to IRS-1(~10% of nuclear ERα) (Figure 2b), according to rough estimations based on coprecipitation procedures. However, if the linkage between ERα and IRS-1 is labile, coprecipitation assays might underestimate the actual extent of their association. In fact, the results obtained with confocal microscopy in intact cells suggested that in some cells, ~30% of ERα colocalized with IRS-1. Because only a fraction of ERα associates with IRS-1, it is understandable that nuclear accumulation of IRS-1 upon E2 stimulation might occur slower than that of ERα. The nuclear presence of IRS-1 in E2 treated MCF-7 cells was limited to ~72 h, while ERα remained nuclear for longer times. It needs to be discovered

whether IRS-1 disappearance from the nucleus is caused by proteolysis or by translocation to the cytoplasmic compartment.

In this work, we report for the first time that nuclear IRS-1 can interact with ERα on ERE-containing chromatin regions. In our experimental system, IRS-1 was recruited together with ERα and other proteins involved in ERα transcription (SRC-1 and Pol II) to the pS2 promoter (Figures 3, 4, and 6). The possibility that IRS-1 modulates ERα-dependent transcription was addressed with transient transfection reporter assays. With this methodology, we noted inhibition of ERα activity by IRS-1 in several cell lines (Figure 7a). We also found that overexpression of IRS-1 inhibits E2/ ERα-dependent transcription of the endogenous pS2 gene in COS-7 cells (Figure 7b). A hypothetical model explaining the inhibitory effect of IRS-1 could be proposed on the basis of the recent discovery that ERα-dependent transcription from ERE sites requires cyclic proteasomal degradation of ERα (Reid et al., 2003). Because IRS-1 and ERα compete for the same degradation machinery (Morelli et al., 2003), it is possible that the presence of nuclear IRS-1 interferes with ERα proteolysis, and thus with ERα transcription. IRS-1 modification of ERα activity is probably restricted to certain transcriptional complexes, as we did not observe significant effects of IRS-1 on ERα -dependent transcription at AP-1 sites. In addition, our new data suggest that the association of IRS-1 with ERE promoters can be transiently inhibited by its recruitment to activated IGF-I receptors (Surmacz et al., unpublished data).

The presence of nuclear IRS-1 in cellular systems was further evaluated in human clinical material. Until now, analysis of breast cancer samples did not establish a clear association between IGF-IR and breast cancer progression. Several studies demonstrated higher expression of IGF-IR compared with non-cancer mammary epithelium, however this feature has been associated with either favorable or unfavorable breast cancer prognosis (Happerfield et al., 1997; Koda et al., 2003; Lee et al., 1998; Papa et al., 1993; Peyrat et al.,

1989; Pezzino et al., 1996; Railo et al., 1994; Surmacz, 2000; Turner et al., 1997; Yee, 1994). The value of cytoplasmatic IRS-1 as a breast cancer marker is even less clear. Some studies provided evidence that IRS-1 expression is higher in cancer than in non-cancer breast epithelium, while others (including this study) reported that IRS-1 levels do not increase (but can decrease) during cancer development and progression (Finlayson et al., 2003; Rocha et al., 1997; Schnarr et al., 2000). Moreover, cytoplasmatic IRS-1 has been found either to correlate with ERα and associate with a more differentiated phenotype or be independent from ERα and associated with a more aggressive phenotype (Ando et al., 1998; Koda et al., 2003; Lee et al., 1999; Schnarr et al., 2000). The significance of nuclear IRS-1 as a marker of breast cancer has never been addressed.

In view of the importance of cytoplasmatic and nuclear IRS-1 in breast cancer growth evidenced in vitro and conflicting or lacking data in vivo, we set out to investigate IRS-1 expression in normal mammary epithelium, benign tumors and breast cancer. Using IHC, we assessed cytoplasmic and nuclear IRS-1 abundance and examined its association with other markers and features, especially ERα.

Our data on cytoplasmic IRS-1 are consistent with those reported by Schnarr *et al.* who noted moderate to strong IRS-1 expression in normal and benign tissues, and in well differentiated carcinomas of both ductal and lobular origin (Schnarr et al., 2000). Similarly, Finlayson *et al.* found no difference of IRS-1 phosphorylation in homogenates of normal and breast cancer tissues (Finlayson et al., 2003). On the other hand, other groups reported low IRS-1 expression in normal tissue and overexpression in poorly differentiated tumors (Koda et al., 2005; Lee et al., 1998; Rocha et al., 1997). In agreement with Schnarr et al. we found a positive association between cytoplasmatic IRS-1 and ERα and a negative correlation between high expression of IRS-1 an tumor grade in ductal carcinomas. This observation is also consistent with coexpression of IRS-1 and ERα noted in less invasive breast cancer cell lines (Surmacz and Bartucci, 2004). In other studies ERα and IRS-1 were not positively

correlated in primary tumors (Koda et al., 2005; Rocha et al., 1997). The causes for these different results are unclear, but could be related to different IHC protocols, including different Abs used.

We did not find any correlation between cytoplasmic IRS1 and lymph node involvement in ductal and lobular cancers. This partially confirms data of Koda *et al.*, who did not observe such a correlation in the whole group of primary tumours, but only in the subgroup of better differentiated (G2) cancers (Koda et al., 2005). Our results also suggested a positive correlation between cytoplasmatic IRS-1 (weak to moderate) and tumor size in ERα-positive ductal cancers. This association has not been noted by others. Regarding cell proliferation, we found a positive correlation of IRS-1 and Ki-67 only in ERα-positive lobular cancers expressing high levels of IRS-1 and no associations in all other samples. Similarly, no link between cell proliferation and cytoplasmatic IRS-1 levels was reported by Rocha et al. In contrast, a negative correlation was reported by Schnarr et al., while Koda et al., noted a positive IRS-1/Ki-67 correlation in ERα-positive primary tumors (Koda et al., 2005; Schnarr et al., 2000). Taken together, these data are still too few and inconsistent to suggest cytoplasmic IRS-1 as a marker for breast cancer prognosis and diagnosis.

Instead, our results suggest that nuclear IRS-1 is tightly linked to ERα expression and might serve as an additional clinical breast cancer marker. As expected, ERα levels were similar in normal and benign tumors and strongly increased in moderately differentiated (G2) cancers. ERα expression was downregulated in poorly differentiated (G3) ductal cancers but not in G3 lobular cancers, confirming the value of ERα as a marker of differentiation in ductal carcinoma (Desombre, 1984; Mansour et al., 1994; McGuire, 1973). Similarly, the levels of nuclear IRS-1, unlike cytoplasmatic IRS-1, were very low in normal tissue and increased in benign tumors and breast cancer. Furthermore, a very strong correlation was found between nuclear IRS-1 and ERα in ductal, while this association was not present in

lobular carcinomas. Importantly, in ductal cancers, but not in lobular, each nuclear IRS-1 and ERα negatively correlated with tumor grade, tumor size, lymph node involvement and proliferation rate, suggesting their association with a less aggressive phenotype. The ROC analysis confirmed that nuclear IRS-1 and ERα are both highly reliable as diagnostic markers of differentiation grade.

In summary, our data suggest that IRS-1 can interact with ERα in the nucleus of breast cancer cells and modulate ERα transcriptional activity and that nuclear IRS-1 can serve as a novel predictive marker of good prognosis in ductal cancer. The lack of association between nuclear IRS-1 and ERα in lobular cancer might suggest that in this setting IGF-I and ERα systems are not tightly linked, similar to the situation seen in benign tumors. We postulate that nuclear ERα/IRS-1 interactions represent a new paradigm in IGF-IR/ER crosstalk.

References

Ando, S., Panno, M.L., Salerno, M., Sisci, D., Mauro, L., Lanzino, M. and Surmacz, E. (1998) Role of IRS-1 signaling in insulin-induced modulation of estrogen receptors in breast cancer cells. *Biochem Biophys Res Commun*, **253**, 315-319.

Bartucci, M., Morelli, C., Mauro, L., Ando, S. and Surmacz, E. (2001) Differential insulin-like growth factor I receptor signaling and function in estrogen receptor (ER)-positive MCF-7 and ER-negative MDA-MB-231 breast cancer cells. *Cancer Res*, **61**, 6747-6754.

Baserga, R. (2000) The contradictions of the insulin-like growth factor 1 receptor. *Oncogene*, **19**, 5574-5581.

Baserga, R., Peruzzi, F. and Reiss, K. (2003) The IGF-1 receptor in cancer biology. *Int J Cancer*, **107**, 873-877.

Boylan, J.M. and Gruppuso, P.A. (2002) Insulin receptor substrate-1 is present in hepatocyte nuclei from intact rats. *Endocrinology*, **143**, 4178-4183.

Campbell, R.A., Bhat-Nakshatri, P., Patel, N.M., Constantinidou, D., Ali, S. and Nakshatri, H. (2001) Phosphatidylinositol 3-kinase/AKT-mediated activation of estrogen receptor alpha: a new model for anti-estrogen resistance. *J Biol Chem*, **276**, 9817-9824.

Chan, T.W., Pollak, M. and Huynh, H. (2001) Inhibition of insulin-like growth factor signaling pathways in mammary gland by pure antiestrogen ICI 182,780. *Clin Cancer Res*, **7**, 2545-2554.

Chen, J., Wu, A., Sun, H., Drakas, R., Garofalo, C., Cascio, S., Surmacz, E. and Baserga, R. (2005) Functional significance of IGF-1-mediated nuclear translocation of the insulin receptor substrate-1 and beta -catenin. *J Biol Chem*.

Desombre, E.R. (1984) Steroid receptors in breast cancer. *Monogr Pathol*, 149-174.

Drakas, R., Tu, X. and Baserga, R. (2004) Control of cell size through phosphorylation of upstream binding factor 1 by nuclear phosphatidylinositol 3-kinase. *Proc Natl Acad Sci U S A*, **101**, 9272-9276.

Finlayson, C.A., Chappell, J., Leitner, J.W., Goalstone, M.L., Garrity, M., Nawaz, S., Ciaraldi, T.P. and Draznin, B. (2003) Enhanced insulin signaling via Shc in human breast cancer. *Metabolism*, **52**, 1606-1611.

Greiner, M., Pfeiffer, D. and Smith, R.D. (2000) Principles and practical application of the receiver-operating characteristic analysis for diagnostic tests. *Prev Vet Med*, **45**, 23-41.

Guvakova, M.A. and Surmacz, E. (1997) Tamoxifen interferes with the insulin-like growth factor I receptor (IGF-IR) signaling pathway in breast cancer cells. *Cancer Res*, **57**, 2606-2610.

Happerfield, L.C., Miles, D.W., Barnes, D.M., Thomsen, L.L., Smith, P. and Hanby, A. (1997) The localization of the insulin-like growth factor receptor 1 (IGFR-1) in benign and malignant breast tissue. *J Pathol*, **183**, 412-417.

Kahlert, S., Nuedling, S., van Eickels, M., Vetter, H., Meyer, R. and Grohe, C. (2000) Estrogen receptor alpha rapidly activates the IGF-1 receptor pathway. *J Biol Chem*, **275**, 18447-18453.

Kato, S., Endoh, H., Masuhiro, Y., Kitamoto, T., Uchiyama, S., Sasaki, H., Masushige, S., Gotoh, Y., Nishida, E., Kawashima, H., Metzger, D. and Chambon, P. (1995) Activation of the estrogen receptor through phosphorylation by mitogen-activated protein kinase. *Science*, **270**, 1491-1494.

Koda, M., Sulkowska, M., Kanczuga-Koda, L. and Sulkowski, S. (2005) Expression of insulin receptor substrate 1 in primary breast cancer and lymph node metastases. *J Clin Pathol*, **58**, 645-649.

Koda, M., Sulkowski, S., Garofalo, C., Kanczuga-Koda, L., Sulkowska, M. and Surmacz, E. (2003) Expression of the insulin-like growth factor-I receptor in primary breast cancer and lymph node metastases: correlations with estrogen receptors alpha and beta. *Horm Metab Res*, **35**, 794-801.

Lannigan, D.A. (2003) Estrogen receptor phosphorylation. *Steroids*, **68**, 1-9.

Lassak, A., Del Valle, L., Peruzzi, F., Wang, J.Y., Enam, S., Croul, S., Khalili, K. and Reiss, K. (2002) Insulin receptor substrate 1 translocation to the nucleus by the human JC virus T-antigen. *J Biol Chem*, **277**, 17231-17238.

Lee, A.V., Guler, B.L., Sun, X., Oesterreich, S., Zhang, Q.P., Curran, E.M. and Welshons, W.V. (2000) Oestrogen receptor is a critical component required for insulin-like growth factor (IGF)-mediated signalling and growth in MCF-7 cells. *Eur J Cancer*, **36 Suppl 4**, 109-110.

Lee, A.V., Hilsenbeck, S.G. and Yee, D. (1998) IGF system components as prognostic markers in breast cancer. *Breast Cancer Res Treat*, **47**, 295-302.

Lee, A.V., Jackson, J.G., Gooch, J.L., Hilsenbeck, S.G., Coronado-Heinsohn, E., Osborne, C.K. and Yee, D. (1999) Enhancement of insulin-like growth factor signaling in human breast cancer: estrogen regulation of insulin receptor substrate-1 expression in vitro and in vivo. *Mol Endocrinol*, **13**, 787-796.

Mansour, E.G., Ravdin, P.M. and Dressler, L. (1994) Prognostic factors in early breast carcinoma. *Cancer*, **74**, 381-400.

Mauro, L., Salerno, M., Morelli, C., Boterberg, T., Bracke, M.E. and Surmacz, E. (2003) Role of the IGF-I receptor in the regulation of cell-cell adhesion: implications in cancer development and progression. *J Cell Physiol*, **194**, 108-116.

Mauro, L., Salerno, M., Panno, M.L., Bellizzi, D., Sisci, D., Miglietta, A., Surmacz, E. and Ando, S. (2001) Estradiol increases IRS-1 gene expression and insulin signaling in breast cancer cells. *Biochem Biophys Res Commun*, **288**, 685-689.

McGuire, W.L. (1973) Estrogen receptors in human breast cancer. *J Clin Invest*, **52**, 73-77.

Metivier, R., Stark, A., Flouriot, G., Hubner, M.R., Brand, H., Penot, G., Manu, D., Denger, S., Reid, G., Kos, M., Russell, R.B., Kah, O., Pakdel, F. and Gannon, F. (2002) A dynamic structural model for estrogen receptor-alpha activation by ligands, emphasizing the role of interactions between distant A and E domains. *Mol Cell*, **10**, 1019-1032.

Molloy, C.A., May, F.E. and Westley, B.R. (2000) Insulin receptor substrate-1 expression is regulated by estrogen in the MCF-7 human breast cancer cell line. *J Biol Chem*, **275**, 12565-12571.

Morelli, C., Garofalo, C., Bartucci, M. and Surmacz, E. (2003) Estrogen receptor-alpha regulates the degradation of insulin receptor substrates 1 and 2 in breast cancer cells. *Oncogene*, **22**, 4007-4016.

Myers, M.G., Jr., Sun, X.J. and White, M.F. (1994) The IRS-1 signaling system. *Trends Biochem Sci*, **19**, 289-293.

Myers, M.G., Jr. and White, M.F. (1996) Insulin signal transduction and the IRS proteins. *Annu Rev Pharmacol Toxicol*, **36**, 615-658.

Nolan, M.K., Jankowska, L., Prisco, M., Xu, S., Guvakova, M.A. and Surmacz, E. (1997) Differential roles of IRS-1 and SHC signaling pathways in breast cancer cells. *Int J Cancer*, **72**, 828-834.

Panno, M.L., Mauro, L., Marsico, S., Bellizzi, D., Rizza, P., Morelli, C., Salerno, M., Giordano, F. and Ando, S. (2006) Evidence that the mouse insulin receptor substrate-1 belongs to the gene family on which the promoter is activated by estrogen receptor alpha through its interaction with Sp1. *J Mol Endocrinol*, **36**, 91-105.

Papa, V., Gliozzo, B., Clark, G.M., McGuire, W.L., Moore, D., Fujita-Yamaguchi, Y., Vigneri, R., Goldfine, I.D. and Pezzino, V. (1993) Insulin-like growth factor-I

receptors are overexpressed and predict a low risk in human breast cancer. *Cancer Res*, **53**, 3736-3740.

Peyrat, J.P., Bonneterre, J., Dusanter-Fourt, I., Leroy-Martin, B., Djiane, J. and Demaille, A. (1989) Characterization of insulin-like growth factor 1 receptors (IGF1-R) in human breast cancer cell lines. *Bull Cancer*, **76**, 311-319.

Pezzino, V., Papa, V., Milazzo, G., Gliozzo, B., Russo, P. and Scalia, P.L. (1996) Insulin-like growth factor-I (IGF-I) receptors in breast cancer. *Ann N Y Acad Sci*, **784**, 189-201.

Pollak, M. (1998) IGF-I physiology and breast cancer. *Recent Results Cancer Res*, **152**, 63-70.

Prisco, M., Santini, F., Baffa, R., Liu, M., Drakas, R., Wu, A. and Baserga, R. (2002) Nuclear translocation of insulin receptor substrate-1 by the simian virus 40 T antigen and the activated type 1 insulin-like growth factor receptor. *J Biol Chem*, **277**, 32078-32085.

Railo, M.J., von Smitten, K. and Pekonen, F. (1994) The prognostic value of insulin-like growth factor-I in breast cancer patients. Results of a follow-up study on 126 patients. *Eur J Cancer*, **30A**, 307-311.

Reid, G., Hubner, M.R., Metivier, R., Brand, H., Denger, S., Manu, D., Beaudouin, J., Ellenberg, J. and Gannon, F. (2003) Cyclic, proteasome-mediated turnover of unliganded and liganded ERalpha on responsive promoters is an integral feature of estrogen signaling. *Mol Cell*, **11**, 695-707.

Rocha, R.L., Hilsenbeck, S.G., Jackson, J.G., VanDenBerg, C.L., Weng, C., Lee, A.V. and Yee, D. (1997) Insulin-like growth factor binding protein-3 and insulin receptor substrate-1 in breast cancer: correlation with clinical parameters and disease-free survival. *Clin Cancer Res*, **3**, 103-109.

Sachdev, D. and Yee, D. (2001) The IGF system and breast cancer. *Endocr Relat Cancer*, **8**, 197-209.

Salerno, M., Sisci, D., Mauro, L., Guvakova, M.A., Ando, S. and Surmacz, E. (1999) Insulin receptor substrate 1 is a target for the pure antiestrogen ICI 182,780 in breast cancer cells. *Int J Cancer*, **81**, 299-304.

Schnarr, B., Strunz, K., Ohsam, J., Benner, A., Wacker, J. and Mayer, D. (2000) Down-regulation of insulin-like growth factor-I receptor and insulin receptor substrate-1 expression in advanced human breast cancer. *Int J Cancer*, **89**, 506-513.

Sciacca, L., Prisco, M., Wu, A., Belfiore, A., Vigneri, R. and Baserga, R. (2003) Signaling differences from the A and B isoforms of the insulin receptor (IR) in 32D cells in the presence or absence of IR substrate-1. *Endocrinology*, **144**, 2650-2658.

Seol, K.C. and Kim, S.J. (2003) Nuclear matrix association of insulin receptor and IRS-1 by insulin in osteoblast-like UMR-106 cells. *Biochem Biophys Res Commun*, **306**, 898-904.

Simoncini, T., Hafezi-Moghadam, A., Brazil, D.P., Ley, K., Chin, W.W. and Liao, J.K. (2000) Interaction of oestrogen receptor with the regulatory subunit of phosphatidylinositol-3-OH kinase. *Nature*, **407**, 538-541.

Song, R.X., McPherson, R.A., Adam, L., Bao, Y., Shupnik, M., Kumar, R. and Santen, R.J. (2002) Linkage of rapid estrogen action to MAPK activation by ERalpha-Shc association and Shc pathway activation. *Mol Endocrinol*, **16**, 116-127.

Stoica, A., Saceda, M., Fakhro, A., Joyner, M. and Martin, M.B. (2000) Role of insulin-like growth factor-I in regulating estrogen receptor-alpha gene expression. *J Cell Biochem*, **76**, 605-614.

Sun, H., Tu, X., Prisco, M., Wu, A., Casiburi, I. and Baserga, R. (2003) Insulin-like growth factor I receptor signaling and nuclear translocation of insulin receptor substrates 1 and 2. *Mol Endocrinol*, **17**, 472-486.

Sun, M., Paciga, J.E., Feldman, R.I., Yuan, Z., Coppola, D., Lu, Y.Y., Shelley, S.A., Nicosia, S.V. and Cheng, J.Q. (2001) Phosphatidylinositol-3-OH Kinase (PI3K)/AKT2,

activated in breast cancer, regulates and is induced by estrogen receptor alpha (ERalpha) via interaction between ERalpha and PI3K. *Cancer Res*, **61**, 5985-5991.

Surmacz, E. (2000) Function of the IGF-I receptor in breast cancer. *J Mammary Gland Biol Neoplasia*, **5**, 95-105.

Surmacz, E. (2003) Growth factor receptors as therapeutic targets: strategies to inhibit the insulin-like growth factor I receptor. *Oncogene*, **22**, 6589-6597.

Surmacz, E. and Bartucci, M. (2004) Role of estrogen receptor alpha in modulating IGF-I receptor signaling and function in breast cancer. *J Exp Clin Cancer Res*, **23**, 385-394.

Surmacz, E. and Burgaud, J.L. (1995) Overexpression of insulin receptor substrate 1 (IRS-1) in the human breast cancer cell line MCF-7 induces loss of estrogen requirements for growth and transformation. *Clin Cancer Res*, **1**, 1429-1436.

Trojanek, J., Croul, S., Ho, T., Wang, J.Y., Darbinyan, A., Nowicki, M., Valle, L.D., Skorski, T., Khalili, K. and Reiss, K. (2005) T-antigen of the human polyomavirus JC attenuates faithful DNA repair by forcing nuclear interaction between IRS-1 and Rad51. *J Cell Physiol*.

Trojanek, J., Ho, T., Del Valle, L., Nowicki, M., Wang, J.Y., Lassak, A., Peruzzi, F., Khalili, K., Skorski, T. and Reiss, K. (2003) Role of the insulin-like growth factor I/insulin receptor substrate 1 axis in Rad51 trafficking and DNA repair by homologous recombination. *Mol Cell Biol*, **23**, 7510-7524.

Tu, X., Batta, P., Innocent, N., Prisco, M., Casaburi, I., Belletti, B. and Baserga, R. (2002) Nuclear translocation of insulin receptor substrate-1 by oncogenes and Igf-I. Effect on ribosomal RNA synthesis. *J Biol Chem*, **277**, 44357-44365.

Turner, B.C., Haffty, B.G., Narayanan, L., Yuan, J., Havre, P.A., Gumbs, A.A., Kaplan, L., Burgaud, J.L., Carter, D., Baserga, R. and Glazer, P.M. (1997) Insulin-like growth factor-I receptor overexpression mediates cellular radioresistance and local breast cancer recurrence after lumpectomy and radiation. *Cancer Res*, **57**, 3079-3083.

Vanagas, G. (2004) Receiver operating characteristic curves and comparison of cardiac surgery risk stratification systems. *Interact CardioVasc Thorac Surg*, **3**, 319-322.

Vladusic, E.A., Hornby, A.E., Guerra-Vladusic, F.K., Lakins, J. and Lupu, R. (2000) Expression and regulation of estrogen receptor beta in human breast tumors and cell lines. *Oncol Rep*, **7**, 157-167.

White, M.F. (1997) The insulin signalling system and the IRS proteins. *Diabetologia*, **40 Suppl 2**, S2-17.

White, M.F. (1998) The IRS-signaling system: a network of docking proteins that mediate insulin and cytokine action. *Recent Prog Horm Res*, **53**, 119-138.

Wynne-Jones, K., Jackson, M., Grotte, G. and Bridgewater, B. (2000) Limitations of the Parsonnet score for measuring risk stratified mortality in the north west of England. The North West Regional Cardiac Surgery Audit Steering Group. *Heart*, **84**, 71-78.

Yee, D. (1994) The insulin-like growth factor system as a target in breast cancer. *Breast Cancer Res Treat*, **32**, 85-95.

Yee, D. and Lee, A.V. (2000) Crosstalk between the insulin-like growth factors and estrogens in breast cancer. *J Mammary Gland Biol Neoplasia*, **5**, 107-115.

Zweig, M.H. (1993) ROC plots display test accuracy, but are still limited by the study design. *Clin Chem*, **39**, 1345-1346.

SCIENTIFIC RESEARCH PERFORMED DURING THE PhD PROGRAM

Expression of Nuclear Insulin Receptor Substrate 1 (IRS-1) in Breast Cancer

Diego Sisci[1§] , Catia Morelli[1§], Cecilia Garofalo[1], Francesco Romeo[2], Lucio Morabito[2], Filomena Casaburi[2], Emilia Middea[1] , Sandra Cascio[3], Elvira Brunelli[4], Sebastiano Andò[5] and Eva Surmacz[3*]

[1] Department of Pharmaco-Biology, Faculty of Pharmacy, University of Calabria, Arcavacata di Rende, Italy; [2] Division of Anatomo-Pathology, Annunziata Hospital, Cosenza, Italy; [3]Sbarro Institute for Cancer Research and Molecular Medicine, Temple University, Philadelphia, PA, USA, [4]Department of Natural Science and [5]Department of Cellular Biology, Faculty of Pharmacy, University of Calabria, Arcavacata di Rende, Italy.

[§] D.S. and C.M. contributed equally to this work

***Corresponding author:** Eva Surmacz, Ph.D.
Sbarro Institute for cancer Research and Molecular Medicine
College of Science and Technology, Temple University
1900 N 12th St. Rm. 446, Philadelphia, PA 19122
Tel. 001/215-204-0306, Fax 001/215-204-0303
e-mail surmacz@temple.edu

Word count (Abstract included): 3475
Structured abstract: 251 words.

Abstract

Aims: Insulin receptor substrate 1 (IRS-1), a cytoplasmic protein transmitting signals from the insulin and insulin-like growth factor 1 receptors, has been implicated in breast cancer. Previously, we reported that IRS-1 can be translocated to the nucleus and modulate estrogen receptor α (ERα) activity in vitro. However, the expression of nuclear IRS-1 in breast cancer biopsies has never been examined. Consequently, we assessed whether nuclear IRS-1 is present in breast cancer and non-cancer mammary epithelium and if it correlates with other markers, especially ERα. Parallel studies were done for cytoplasmatic IRS-1.

Methods: IRS-1 and ERα expression was assessed by immunohistochemistry. Data were evaluated using Pearson correlation, linear regression, and ROC analysis.

Results: Median nuclear IRS-1 expression was low in normal mammary epithelial cells (1.6%) and higher in benign tumors (20.5%), ductal grade 2 carcinoma (11.0%), and lobular carcinoma (~30%). Median ERα expression in normal epithelium, benign tumors, ductal cancer grade 2 and 3 and lobular cancer grade 2 and 3 was 10.5, 20.5, 65.0, 0.0, 80, and 15%, respectively. Nuclear IRS-1 and ERα positively correlated in ductal cancer ($p<0.001$) and benign tumors ($p< 0.01$), but were not associated in lobular cancer and normal mammary epithelium. In ductal carcinoma, both nuclear IRS-1 and ERα negatively correlated with tumor grade, size, mitotic index, and lymph node involvement. Cytoplasmic IRS-1 was expressed in all specimens and positively correlated with ERα in ductal cancer.

Conclusions: A positive association between nuclear IRS-1 and ERα is a characteristic for ductal breast cancer and marks a more differentiated, non-metastatic phenotype.

Take-home messages

1. This is the first report examining the expression of nuclear IRS-1 in normal mammary tissue, benign breast tumors and breast cancer in relation to ERα and clinicopathological features.

2. Nuclear IRS-1 is more prevalent in cancer specimens than in normal mammary tissues.
3. Nuclear IRS-1 and ERα negatively correlated with tumor grade, size, mitotic index, and lymph node involvement.
4. A positive association between nuclear IRS-1 and ERα is a characteristic for ductal breast cancer and marks a more differentiated, non-metastatic phenotype.

Introduction

Recent experimental and clinical evidence suggests the involvement of the insulin-like growth factor I (IGF-I) receptor (IGF-IR) in breast cancer development and progression [1-6]. The tumorigenic action of IGF-IR is executed through multiple antiapoptotic, growth promoting, and/or pro-metastatic pathways [5-9]. Many of these pathways stem from IRS-1, a major IGF-I signaling molecule that becomes phosphorylated on multiple tyrosine residues upon IGF-IR activation. Tyrosine phosphorylated IRS-1 acts as a scaffolding protein sequestering downstream signaling molecules and propagating IGF-I signal through the PI-3K/Akt, Ras/Raf/ERK1/2, Jak2/Stat3 and other pathways [10-13].

Overexpression or downregulation of IRS-1 in breast cancer cell models suggested that the molecule controls several aspects of the neoplastic phenotype, especially anchorage-dependent and -independent cell growth and survival [14 15]. In breast cancer cell lines, IRS-1 appears to be expressed at higher levels in ERα-positive than in ERα-negative cells and there is evidence supporting the existence of a crosstalk between IRS-1 and ERα systems [1 4 6 16-18]. Overexpression of IRS-1 in MCF-7 ERα-positive cells has been shown to induce estrogen-independence and mediate antiestrogen-resistance [14 19 20]. High expression of IRS-1 can be in part attributed to ERα activity, as 17β-estradiol (E2) can upregulate IRS-1 expression and function [16 21 22], while antiestrogens reduce IRS-1 mRNA and protein levels and inhibit IRS-1 signaling [19 20 23]. In addition, ERα can directly interact with IRS-1, increasing its stability and potentiating its downstream signaling to Akt [24]. Notably, increased activity of IRS-1 is likely to modulate ERα, via ERK1/2- and Akt-mediated phosphorylation of ERα on Ser-118 and Ser-167, respectively [25-27].

Recent reports suggested that in addition to its cytoplasmic signaling function, IRS-1 is able to regulate nuclear processes in different cell models [28-33]. For instance, in mouse fibroblasts treated with IGF-I, a fraction of IRS-1 is translocated from the cytoplasm to the nuclear and nucleolar

compartments where it modulates the expression of genes controlling cell proliferation (i.e., Cyclin D1) and cell growth in size (i.e., rDNA) by physically interacting with transcriptional complexes of β-catenin and upstream binding factor 1 (UBF1), respectively [31 32]. Our recent work demonstrated that nuclear IRS-1 is also found in breast cancer cell lines. For instance, in MCF-7 cells treated with E2 nuclear IRS-1 physically interacted with ERα modulating its transcriptional activity at estrogen response element (ERE) DNA motifs [33]. The exact mechanism of nuclear IRS-1 transport is not clear, but most likely it involves other proteins containing nuclear localization signals (ERα, T antigen, importins).

Despite the evidence that IRS-1 signaling may play a critical role in tumorigenesis, only limited studies examined the clinical significance of IRS-1 expression in human breast cancer specimens [18 34-36]. In one study, cytoplasmatic IRS-1 has been reported to correlate with poorly differentiated breast tumor phenotype (G3) and lymph node involvement [35]. Another study correlated IRS-1 with shorter disease-free survival in patients with smaller tumors [18]. In contrast, Schnarr et al. found that IRS-1 marks a more differentiated phenotype and better prognosis [34]. Furthermore, one study examining cancer and normal specimens reported similar IRS-1 tyrosine phosphorylation in all tissues [36], while other analysis found decreased IRS-1 levels in poorly differentiated cancers relative to normal tissue and benign tumors [34].

Regarding nuclear IRS-1, its presence in breast cancer specimens has been noted by Schnarr et al. [34] and Koda et al. [35], but any association with the disease has never been formally addressed. Consequently, we examined the expression of nuclear IRS-1 in normal mammary tissue, benign breast tumors and breast cancer in relation to ERα and clinicopathological features. Parallel studies were done for cytoplasmatic IRS-1.

Materials and Methods

Patients and tissue specimens

Table 1 summarizes information on patient and specimen characteristics. The histopathological examination of sections was based on the WHO and pTN classification of breast tumors. Tumor size (pT) was scored as follows: 0, primary tumor not detectable; 1, tumor largest diameter <2cm; 2, diameter <5cm; 3, diameter >5cm; 4, inflammatory carcinoma of any size. Lymph node status (pN) was scored from 0, no node involvement; 1, proximal node involved; 2, distal node involved. The protocol of the present study was reviewed and approved by the local ethical committee.

Table 1. Patient characteristics and clinical parameters of breast tissues and cancers

Sample characteristics

	Cancers	**Controls**
Total specimens	60	34
Ductal carcinoma	38	
Lobular carcinoma	22	
Benign tumors		19
Macromasty		14

Patient Age

	Normal	**Benign**	**Ductal**	**Lobular**
Mean±SE	53.6±3.3	45.4±3.1	62.9±2.4	64.5±2.7
Median (Range)	56.5 (33-68)	43 (20-68)	61.5 (43-94)	66 (48-78)
Menopause (%)	64	39	87	82

Clinical parameters of breast cancer tissues

	Ductal (38)		**Lobular (22)**	
	G2 (19)	**G3 (19)**	**G2 (10)**	**G3 (12)**
pT	1-4	0-4	2-4	0-4
pN	0-2	0-2	0-1	0-2
Ki67	7.7 ± 0.9 (4-14)	14.2±1.3 (6-21)	7.2±1.5 (4-12)	9.0±1.9 (3-15)

The age of patients in each group is given as mean value ± SE with median age (range) for each population. The percentage of postmenopausal patients is indicated in each group. The range is

reported for tumor size (pT), and lymph node involvement (pN); median frequency of expression ±SE (range) is shown for Ki67.

Immunohistochemistry and confocal microscopy

Samples preparation

Immediately after excision, tissue samples were fixed in 10% buffered formaldehyde solution and embedded in paraffin blocks at 56°C. ERα and IRS-1 were analyzed by immunohistochemical (IHC) staining using 3µm-thick consecutive paraffin sections. The sections were dewaxed in xylene and rehydrated in graded alcohols. After antigen retrieval by boiling in 0.01M citrate buffer pH 6.

Immunohistochemistry

Endogenous peroxidase was removed with 3% H_2O_2; nonspecific binding was blocked by incubating the slides for 30 min with 1.5% BSA in PBS. Next, the sections were incubated with the primary antibodies (Abs) for 1h at room temperature. ERα was detected using ERα mouse monoclonal Ab (mAb) (DakoCytomation, Denmark) at dilution 1:35. IRS-1 was detected using the C-terminus IRS-1 rabbit polyclonal Ab (pAb) (Upstate, USA) at a concentration 4µg/ml. Ab-antigen reactions were revealed using Streptavidin-biotin-peroxidase complex (LSAB kit, DakoCytomation, Denmark). All slides were counterstained with hematoxylin. Breast specimens previously classified as positive for the expression of the studied markers were used for control and protocol standardization. In negative controls, primary Abs were omitted. The expression of ERα and IRS-1 was independently scored by two investigators (CM and CG) by light microscopy in 10 different section fields. For all nuclear markers, mean and median percentage, and the range of epithelial cells displaying positive staining was scored. In some analyses, specimens were grouped into ERα-negative (less than 5% of epithelial cells exhibiting ERα expression) and ERα-positive (5% or more of cells with ERα). The expression of cytoplasmic IRS-1 was classified using a four-point scale: 0, <10% positive cells with any staining

intensity; 1+, 10-50% positive cells with weak or moderate staining; 2+, >50% positive cells with weak or moderate staining; 3+, >50% positive cells with strong staining. No samples with less than 50% of positive cells with strong staining were recorded.

Confocal microscopy

Tissues sections were incubated for 30 min with 3% BSA in PBS to avoid nonspecific bindin, then for 1 h with a mixture of primary Abs (pAbs) recognizing IRS-1 and ERα.

The anti-IRS-1 pAb (UBI) at 4 μg/ml was used for IRS-1 staining; anti-ERa F-10 monoclonal Ab (mAb) (Santa Cruz) at 2 μg/ml was used to detect ERα. Following the incubation with primary Abs, the slides were washed three times with PBS, and incubated with a mixture of secondary Abs. A rhodamine-conjugated donkey anti-mouse IgG (Calbiochem) was used as a secondary Ab for ERα and a fluorescein-conjugated donkey anti-rabbit IgG (Calbiochem) was used for IRS-1. The cellular localization of IRS-1 and ERα was studied using the Bio-Rad MRC 1024 confocal microscope connected to a Zeiss Axiovert 135M inverted microscope with x1000 magnification. The optical sections were taken at the central plane. The fluorophores were imaged separately to ensure no excitation/emission wavelength overlap. In control samples, the staining was performed with the omission of the primary Abs.

Statistical analysis

Descriptive statistic for nuclear IRS-1 and ERα in normal, benign and tumor samples was reported as mean, standard error (±SE), median value and range. The relationship between nuclear IRS-1 and ERα was analyzed by linear regression and the statistical significance was evaluated by the Pearson correlation test. The distribution of ERα and nuclear IRS-1 in respect to tumor size, grade, and lymph node involvement are reported in scatterplots. The correlations between nuclear IRS-1, ERα,

cytoplasmatic IRS-1 and selected clinicopathologic features were examined with the Pearson correlation test.

The value of nuclear ERα or IRS-1 expression as diagnostic marker of tumor grade, pT, pN and Ki67 was evaluated calculating the areas under the receiver operating characteristic (ROC) curves [37], which assess the performance of a diagnostic test [38-40]. In the graphical representation of the ROC curve, the X-axis is the false-positive rate (1-specificity) and the Y-axis is the true positive rate (sensitivity). The diagonal line (from 0,0 to 1,1) reflects the characteristics of a test with no discriminating power. ROC curve was analyzed using MedCalc (MedCalc Software, Mariakerke, B).

Results

Nuclear IRS-1and ERα expression in normal mammary epithelium and benign breast tumors.

In general, the expression of nuclear IRS-1 in normal tissues was very low (~2% of positive cells) (Tab. 2). ERα was expressed in 11 of 14 samples; the median frequency of ERα in all samples was 10.5% (Fig. 1A, B and Tab. 2). Nuclear IRS-1 was found in 9 of 11 ERα-positive specimens at the median frequency 1.8%. Low expression (3.5%) of nuclear IRS-1 was also recorded in 2 specimens that did not express ERα (data not shown).

Compared with normal epithelium, benign tumors expressed higher median levels of nuclear IRS-1 (20.5%) and ERα (20.5.0%) (Tab. 2). Nuclear IRS-1 was found in 16 of 19 ERα-positive specimens, but was not present in any of ERα-negative cases. (Fig. 1C, D and data not shown).

Cytoplasmic IRS-1 was expressed in all epithelial cells of normal epithelium and benign tumors at the levels 1+ to 3+ (Fig. 1B, D and Tab. 3), while no evidence of cytoplasmic ERα staining was revealed in any of the specimens (Fig. 1A). The co-localization of nuclear IRS-1 and ERα was determined by confocal microscopy (Fig. 2).

Table 2. Descriptive statistics of nuclear IRS-1 and ERα in all samples.

	Normal Epithelium		Benign Tumors	
	ERα	**IRS-1**	**ERα**	**IRS-1**
Mean±SE	21.7±6.1	2.3±0.6	23.4±4.2	23±4.5
Median (Range)	10.5 (0-60)	1.6 (0-7)	20.5 (0-70)	20.5 (0-60)

Ductal Carcinoma	G2		G3	
	ERα	**IRS-1**	**ERα**	**IRS-1**
Mean±SE	51.8±10.1	23.4±7.1	6.2±3.4	4.1±1.8
Median (Range)	65 (0-92)	11 (0-72)	0 (0-40)	0 (0-20)

Lobular Carcinoma	G2		G3	
	ERα	**IRS-1**	**ERα**	**IRS-1**
Mean±SE	64.8±11.3	32±9.7	26.7±8.9	30.7±4.7
Median (Range)	80 (0-90)	35 (0-80)	15 (0-80)	33.5 (0-52)

The mean (±SE) expression with median (range) values for nuclear IRS-1 and ERα in all specimens (ERα-positive and ERα-negative) is given. Cancer samples of ductal and lobular origin were grouped into separate G2 and G3 populations.

Table 3. Descriptive statistics of cytoplasmatic IRS-1 in all samples

Cytoplasmic IRS-1 Expression (% of Cases in Class)				
Class	**Normal**	**Benign**	**Ductal**	**Lobular**
0	0	0	0	0
1+	29	21	16	0
2+	29	21	52	63
3+	42	58	32	37

Samples are grouped in 4 classes as described in Materials and Methods. The percentage of specimens with cytoplasmic IRS-1 in each staining category is given.

IRS-1 expression in ERα-positive and ERα-negative breast carcinoma.

In invasive ductal carcinoma, nuclear IRS-1 was found in 22 of 38 of specimens. The median level of expression in these samples was 13.7%. ERα was detected in 20 of 38 of specimens with a median expression of 29.2% (Fig. 1E, F). Twenty two specimens (15 of 19 in G2, and 7 of 19 in G3) expressed nuclear IRS-1 (Fig. 1F, Tab. 2). Among nuclear IRS-1-positive samples, 18 also expressed ERα, while 4 were ERα-negative. Thirteen of G2 ductal carcinomas and 5 of G3 cancers were positive for both IRS-1 and ERα. In 2 of 38 specimens, ERα was expressed in the absence of nuclear IRS-1.

In lobular cancer, nuclear IRS-1 staining was observed in 16 of 22 samples with the median frequency 31.2% (Fig. 1H). Eleven of these 16 samples were also ERα-positive. Within G2 lobular carcinomas, 6 of 10 specimens displayed nuclear IRS-1 at the median level 35.0%; all these samples expressed ERα at the median frequency 80.0% (Tab. 2). In the G3 subgroup, 10 of 12 tumors expressed nuclear IRS-1 (median 33.5%) and 5 of 10 expressed ERα (median 15.0%). In 5 of 16 lobular cancers, nuclear IRS-1 was found in the absence of ERα (Tab. 2).

Cytoplasmatic IRS-1 was identified in all ductal and lobular cancer samples displaying a weak to strong staining intensity (Tab. 3). In all specimens, the neoplasm surrounding tissue appeared normal and the pattern of ERα and IRS-staining comparable to that of the normal samples.

Correlation between nuclear IRS-1and ERα in breast cancer, benign tumors, and normal mammary epithelium.

A very strong positive correlation ($p<0.001$) between nuclear IRS-1 and ERα was found in invasive ductal breast cancer. The markers were also positively associated ($p<0.01$) in benign tumors cancer samples (Fig. 4). However, no correlations were found between nuclear IRS-1 and ERα in normal tissues ($p=0.28$) and lobular breast cancer ($p=0.24$) (Fig. 4).

Nuclear IRS-1 and ERα are correlated with some clinicopathological features in invasive ductal carcinomas.

The distribution of nuclear ERα and nuclear IRS-1 was analyzed with respect to tumor grade, tumor size, lymph node involvement, and proliferation index (Fig. 3). The frequency of both ERα and nuclear IRS-1 expression was the highest in node-negative G2 invasive ductal carcinomas of smaller size (Fig. 3). In the same group, a significant negative correlation between nuclear IRS-1 or ERα and differentiation grade, the tumor size, lymph node involvement and proliferation rate was found (Tab. 4).

In contrast, in lobular breast carcinomas, the distribution of nuclear IRS-1 or ERα appeared to be independent of and not correlated with tumor grade, size, or Ki67 expression (Fig. 3 and Tab. 4). Interestingly, both nuclear IRS-1 and ERα were more abundant in lymph node-negative samples (Fig. 3), but no significant associations were determined between these markers and lymph node status (Tab. 4).

The specificity and sensitivity of nuclear IRS-1 or ERα as a marker of tumor differentiation grade, tumor size and lymph node involvement was evaluated by the ROC curve analysis. The comparison of the areas under the ROC curves obtained for nuclear IRS-1 and ERα indicated that both nuclear IRS-1 and ERα are good markers for tumor grading in invasive ductal carcinomas, while in lobular carcinomas only ERα could be considered a marker for grading (Tab. 5 and Fig. 5).

Neither ERα nor nuclear IRS-1 was a useful marker of tumor size, node involvement, or tumor proliferation (data not shown). The distribution of nuclear IRS-1 or ERα was not related to patient's age and menopausal status in cancer, benign and normal samples (data not shown).

Table 4. Correlation between nuclear IRS-1, ERα and selected clinicopathological tumor features.

		Ductal Carcinoma		Lobular Carcinoma	
		ERα	IRS-1	ERα	IRS-1
G	r	**-0.573**	**-0.511**	-0.563	0.029
	p	**0.0015**	**0.0057**	0.065	0.94
pT	r	**-0.393**	**-0.382**	-0.326	0.153
	p	**0.039**	**0.044**	0.310	0.633
pN	r	**-0.381**	**-0.454**	-0.082	-0.122
	p	**0.044**	**0.015**	0.797	0.714
Ki67	r	**-0.591**	**-0.538**	-0.329	-0.016
	p	**0.0001**	**0.003**	0.31	0.94

The association between nuclear IRS-1 or ERa and tumor grade (G), size (pT), lymph node involvement (pN), and the expression of the proliferation marker Ki67 was statistically analyzed with Pearson correlation test; r, correlation coefficient; p, statistical significance. The statistically significant correlations are bolded.

Table 5. Association between nuclear IRS-1, ERα and tumor grade.

Diagnostic Marker	**ROC analysis for tumor grade**		
	AUC estimate (95% CI)	**Area under the ROC curve**	**Mann-Whitney test (p value)**
Ductal Carcinoma			
ERα	71.4 (41.9-91.4)	0.809	**0.001**
IRS-1	78.6 (49.2-95.1)	0.778	**0.001**
Lobular Carcinoma			
ERα	80.0 (28.8-96.7)	0.817	**0.02**
IRS-1	60.0 (15.4-93.5)	0.533	0.85

The analysis was performed with ROC curves, as described in Materials and Methods. The area under the ROC (receiver operating characteristic) curve (AUC) describes the value of nuclear IRS-1 or ERα to discriminate between G2 and G3 tumors. AUC estimate reports the confidence intervals considering an error of 5%. The statistical significance was evaluated by Mann-Whitney test for an area =0.5. Statistical significances are bolded.

Relationship between cytoplasmatic IRS-1 and clinicopathological features.

In ductal carcinomas, cytoplasmic IRS-1 (each staining intensity group) positively correlated with ERα. Moreover, in ductal cancer low and moderate IRS-1 expression was positively associated with tumor size, while high IRS-1 levels negatively correlated with tumor grade (Tab. 6).

In lobular carcinomas, high expression of cytoplasmic IRS-1 directly correlated with Ki67 (Tab. 6). In benign tumors, low expression of cytoplasmatic IRS-1 was negatively associated with ERα, while higher IRS-1 levels were not linked to ERα. No correlations between the two markers were found in normal samples (data not shown). Similarly, cytoplasmic IRS-1 expression was not related to age or menopausal status in all analyzed material (data not shown).

Table 6. Correlations between cytoplasmatic IRS-1 and selected clinicopathological features in ERα-positive tumors.

		Ductal				Lobular			
		0	**1+**	**2+**	**3+**	**0+**	**1+**	**2+**	**3+**
ERα	**r**	-	**0.978**	**0.637**	**0.987**	-	-	0.198	-0.029
	p		**0.025**	**0.019**	**0.013**			0.671	0.970
G	**r**	-	0.375	-0.082	**-0.962**	-	-	0.204	-0.376
	p		0.625	0.790	**0.037**			0.661	0.624
pT	**r**	-	**0.973**	**0.553**	-0.577	-	-	0.009	-0.225
	p		**0.026**	**0.050**	0.423			0.984	0.775
pN	**r**	-	0.00	0.301	-	-	-	-0.069	-
	p		1.00	0.318				0.883	
Ki67	**r**	-	0.724	-0.241	-0.905	-	-	-0.223	**0.978**
	p		0.276	0.428	0.095			0.631	**0.022**

The associations between cytoplasmatic IRS-1 and ERα positivity (ERα), tumor grade (G), tumor size (pT), lymph node involvement (pN), and the expression of the proliferation marker Ki67 were statistically analyzed with the Pearson correlation test; r, correlation coefficient; p, statistical significance. The statistically significant correlations are bolded. The absence of value is due to either the absence of samples in the group or to the homogeneity of samples (variance =0).

Discussion

Studies in cellular and animal models established that breast cancer cell growth is controlled by complex crosstalk between ERα and IGF-I systems [4-6 14 19 41-44]. However, while ERα is an established marker for breast cancer diagnosis and prognosis and a target for breast cancer therapy and prevention, the value of critical IGF-I system components like IGF-IR and IRS-1 as breast cancer markers needs

further examination. Until now, analysis of breast cancer samples did not establish a clear association between IGF-IR and breast cancer progression. Several studies demonstrated higher expression of IGF-IR compared with non-cancer mammary epithelium, however this feature has been associated with either favorable or unfavorable breast cancer prognosis [4 45-53]. The value of cytoplasmatic IRS-1 as a breast cancer marker is even less clear. Some studies provided evidence that IRS-1 expression is higher in cancer than in non-cancer breast epithelium, while others (including this study) reported that IRS-1 levels do not increase (but can decrease) during cancer development and progression [18 34 36]. Moreover, cytoplasmatic IRS-1 has been found either to correlate with ERα and associate with a more differentiated phenotype or be independent from ERα and associated with a more aggressive phenotype [16 34 41 52]. The significance of nuclear IRS-1 in breast cancer has never been addressed.

In view of the importance of cytoplasmatic and nuclear IRS-1 in breast cancer growth evidenced in vitro and conflicting or lacking data in vivo, we set out to investigate IRS-1 expression in normal mammary epithelium, benign tumors and breast cancer. Using IHC, we assessed cytoplasmic and nuclear IRS-1 abundance and examined its relations with some prognostic markers, especially ERα, and clinicopathological features.

Our data on cytoplasmic IRS-1 are consistent with those reported by Schnarr *et al.* who noted moderate to strong IRS-1 expression in normal and benign tissues, and in well differentiated carcinomas of both ductal and lobular origin [34]. Similarly, Finlayson *et al.* found no difference of IRS-1 phosphorylation in homogenates of normal and breast cancer tissues [36]. On the other hand, other groups reported low IRS-1 expression in normal tissue and overexpression in poorly differentiated tumors [18 35 48]. In agreement with Schnarr et al. we found a positive association between cytoplasmatic IRS-1 and ERα and a negative correlation between high expression of IRS-1 and tumor grade in ductal carcinomas. This observation is also consistent with coexpression of IRS-1 and ERα noted in less

invasive breast cancer cell lines [6]. In other studies ERα and IRS-1 were not positively correlated in primary tumors [18 35]. The causes for these different results are unclear, but could be related to different IHC protocols, including different Abs used.

We did not find any correlation between cytoplasmic IRS1 and lymph node involvement in ductal and lobular cancers. This partially confirms data of Koda *et al.*, who did not observe such a correlation in the whole group of primary tumours, but only in the subgroup of better differentiated (G2) cancers [35]. Our results also suggested a positive correlation between cytoplasmatic IRS-1 (weak to moderate) and tumor size in ERα-positive ductal cancers. This association has not been noted by others. Regarding cell proliferation, we found a positive correlation of IRS-1 and Ki-67 only in ERα-positive lobular cancers expressing high levels of IRS-1 and no associations in all other samples. Similarly, no link between cell proliferation and cytoplasmatic IRS-1 levels was reported by Rocha *et al*. In contrast, a negative correlation was reported by Schnarr *et al*., while Koda *et al*., noted a positive IRS-1/Ki-67 correlation in ERα-positive primary tumors [34 35]. Taken together, these data are still too few and inconsistent to suggest cytoplasmic IRS-1 as a marker for breast cancer prognosis and diagnosis.

Instead, our results suggest that nuclear IRS-1 is tightly linked to ERα expression and might serve as an additional clinical breast cancer marker. As expected, ERα levels were low in normal mammary epithelium, higher in benign tumors, and strongly increased in moderately differentiated (G2) cancers. ERα expression was downregulated in poorly differentiated (G3) ductal cancers but not in G3 lobular cancers, confirming the value of ERα as a marker of differentiation in ductal carcinoma [54-56]. Notably, the levels of nuclear IRS-1 were very low in normal tissue, increased in benign tumors and G2 ductal cancer, and decreased in G3 ductal cancer, displaying an expression trend similar to that of ERα.

In lobular cancer, the levels of nuclear IRS-1 were relatively high in both G2 and G3 tumors (~30%) and were not related to the abundance of ERα. Indeed, statistical analysis of data confirmed a very strong correlation between nuclear IRS-1 and ERα in ductal, but not lobular, cancers. Importantly, in ductal, but again not in lobular cancers, both nuclear IRS-1 and ERα negatively correlated with tumor grade, tumor size, lymph node involvement and proliferation rate, suggesting their association with a less aggressive phenotype. The ROC analysis confirmed that nuclear IRS-1 as for ERα, is highly reliable as diagnostic marker of differentiation grade. The observation that nuclear IRS-1 expression increases in benign as well as in highly and moderately differentiated tumors, compared to normal tissues, strongly supports this assumption.

Taken together, our data indicate that nuclear IRS-1 could serve as a novel predictive marker of good prognosis in ductal cancer. The lack of association between nuclear IRS-1 and ERα in lobular cancer and benign tumors, might suggest that, in this settings, IGF-I and ERα systems are not tightly linked.

List of Abbreviations

ERα (Estrogen Receptor alpha), IRS-1 (Insulin Receptor Substrate 1).

Authors'contributions

DS and CM participated in the design of the study, performed the statistical analysis and drafted the manuscript, CG carried out the immunostaining and participated to the statistical analysis, FR participated in the design of the study, LM participated to the statistical analysis, FC prepared the histological samples, EM carried out the immunostaining, SC participated to the statistical analysis, SA

participated in the design of the study and drafted the manuscript, ES designed the study and drafted the manuscript.

Acknowledgments: This work was supported by AIRC – 2004, MURST Ex 60% - 2005 and Sbarro Health Research Organization

References

1. Bartucci M, Morelli C, Mauro L, Ando S, Surmacz E. Differential insulin-like growth factor I receptor signaling and function in estrogen receptor (ER)-positive MCF-7 and ER-negative MDA-MB-231 breast cancer cells. *Cancer Res.* Sep 15 2001;61(18):6747-6754.
2. Pollak M. IGF-I physiology and breast cancer. *Recent Results Cancer Res.* 1998;152:63-70.
3. Sachdev D, Yee D. The IGF system and breast cancer. *Endocr Relat Cancer.* Sep 2001;8(3):197-209.
4. Surmacz E. Function of the IGF-I receptor in breast cancer. *J Mammary Gland Biol Neoplasia.* Jan 2000;5(1):95-105.
5. Surmacz E. Growth factor receptors as therapeutic targets: strategies to inhibit the insulin-like growth factor I receptor. *Oncogene.* Sep 29 2003;22(42):6589-6597.
6. Surmacz E, Bartucci M. Role of estrogen receptor alpha in modulating IGF-I receptor signaling and function in breast cancer. *J Exp Clin Cancer Res.* Sep 2004;23(3):385-394.
7. Baserga R. The contradictions of the insulin-like growth factor 1 receptor. *Oncogene.* Nov 20 2000;19(49):5574-5581.
8. Baserga R, Peruzzi F, Reiss K. The IGF-1 receptor in cancer biology. *Int J Cancer.* Dec 20 2003;107(6):873-877.
9. Mauro L, Salerno M, Morelli C, Boterberg T, Bracke ME, Surmacz E. Role of the IGF-I receptor in the regulation of cell-cell adhesion: implications in cancer development and progression. *J Cell Physiol.* Feb 2003;194(2):108-116.
10. Myers MG, Jr., Sun XJ, White MF. The IRS-1 signaling system. *Trends Biochem Sci.* Jul 1994;19(7):289-293.

11. Myers MG, Jr., White MF. Insulin signal transduction and the IRS proteins. *Annu Rev Pharmacol Toxicol.* 1996;36:615-658.
12. White MF. The insulin signalling system and the IRS proteins. *Diabetologia.* Jul 1997;40 Suppl 2:S2-17.
13. White MF. The IRS-signaling system: a network of docking proteins that mediate insulin and cytokine action. *Recent Prog Horm Res.* 1998;53:119-138.
14. Surmacz E, Burgaud JL. Overexpression of insulin receptor substrate 1 (IRS-1) in the human breast cancer cell line MCF-7 induces loss of estrogen requirements for growth and transformation. *Clin Cancer Res.* Nov 1995;1(11):1429-1436.
15. Nolan MK, Jankowska L, Prisco M, Xu S, Guvakova MA, Surmacz E. Differential roles of IRS-1 and SHC signaling pathways in breast cancer cells. *Int J Cancer.* Sep 4 1997;72(5):828-834.
16. Lee AV, Jackson JG, Gooch JL, et al. Enhancement of insulin-like growth factor signaling in human breast cancer: estrogen regulation of insulin receptor substrate-1 expression in vitro and in vivo. *Mol Endocrinol.* May 1999;13(5):787-796.
17. Lee AV, Guler BL, Sun X, et al. Oestrogen receptor is a critical component required for insulin-like growth factor (IGF)-mediated signalling and growth in MCF-7 cells. *Eur J Cancer.* Sep 2000;36 Suppl 4:109-110.
18. Rocha RL, Hilsenbeck SG, Jackson JG, et al. Insulin-like growth factor binding protein-3 and insulin receptor substrate-1 in breast cancer: correlation with clinical parameters and disease-free survival. *Clin Cancer Res.* Jan 1997;3(1):103-109.
19. Guvakova MA, Surmacz E. Tamoxifen interferes with the insulin-like growth factor I receptor (IGF-IR) signaling pathway in breast cancer cells. *Cancer Res.* Jul 1 1997;57(13):2606-2610.
20. Salerno M, Sisci D, Mauro L, Guvakova MA, Ando S, Surmacz E. Insulin receptor substrate 1 is a target for the pure antiestrogen ICI 182,780 in breast cancer cells. *Int J Cancer.* Apr 12 1999;81(2):299-304.
21. Mauro L, Salerno M, Panno ML, et al. Estradiol increases IRS-1 gene expression and insulin signaling in breast cancer cells. *Biochem Biophys Res Commun.* Nov 2 2001;288(3):685-689.
22. Molloy CA, May FE, Westley BR. Insulin receptor substrate-1 expression is regulated by estrogen in the MCF-7 human breast cancer cell line. *J Biol Chem.* Apr 28 2000;275(17):12565-12571.
23. Chan TW, Pollak M, Huynh H. Inhibition of insulin-like growth factor signaling pathways in mammary gland by pure antiestrogen ICI 182,780. *Clin Cancer Res.* Aug 2001;7(8):2545-2554.
24. Morelli C, Garofalo C, Bartucci M, Surmacz E. Estrogen receptor-alpha regulates the degradation of insulin receptor substrates 1 and 2 in breast cancer cells. *Oncogene.* Jun 26 2003;22(26):4007-4016.
25. Kato S, Endoh H, Masuhiro Y, et al. Activation of the estrogen receptor through phosphorylation by mitogen-activated protein kinase. *Science.* Dec 1 1995;270(5241):1491-1494.
26. Campbell RA, Bhat-Nakshatri P, Patel NM, Constantinidou D, Ali S, Nakshatri H. Phosphatidylinositol 3-kinase/AKT-mediated activation of estrogen receptor alpha: a new model for anti-estrogen resistance. *J Biol Chem.* Mar 30 2001;276(13):9817-9824.
27. Stoica A, Saceda M, Fakhro A, Joyner M, Martin MB. Role of insulin-like growth factor-I in regulating estrogen receptor-alpha gene expression. *J Cell Biochem.* Jan 2000;76(4):605-614.
28. Lassak A, Del Valle L, Peruzzi F, et al. Insulin receptor substrate 1 translocation to the nucleus by the human JC virus T-antigen. *J Biol Chem.* May 10 2002;277(19):17231-17238.

29. Prisco M, Santini F, Baffa R, et al. Nuclear translocation of insulin receptor substrate-1 by the simian virus 40 T antigen and the activated type 1 insulin-like growth factor receptor. *J Biol Chem.* Aug 30 2002;277(35):32078-32085.
30. Trojanek J, Croul S, Ho T, et al. T-antigen of the human polyomavirus JC attenuates faithful DNA repair by forcing nuclear interaction between IRS-1 and Rad51. *J Cell Physiol.* Jan 2006;206(1):35-46.
31. Chen J, Wu A, Sun H, et al. Functional significance of type 1 insulin-like growth factor-mediated nuclear translocation of the insulin receptor substrate-1 and beta-catenin. *J Biol Chem.* Aug 19 2005;280(33):29912-29920.
32. Drakas R, Tu X, Baserga R. Control of cell size through phosphorylation of upstream binding factor 1 by nuclear phosphatidylinositol 3-kinase. *Proc Natl Acad Sci U S A.* Jun 22 2004;101(25):9272-9276.
33. Morelli C, Garofalo C, Sisci D, et al. Nuclear insulin receptor substrate 1 interacts with estrogen receptor alpha at ERE promoters. *Oncogene.* Sep 30 2004;23(45):7517-7526.
34. Schnarr B, Strunz K, Ohsam J, Benner A, Wacker J, Mayer D. Down-regulation of insulin-like growth factor-I receptor and insulin receptor substrate-1 expression in advanced human breast cancer. *Int J Cancer.* Nov 20 2000;89(6):506-513.
35. Koda M, Sulkowska M, Kanczuga-Koda L, Sulkowski S. Expression of insulin receptor substrate 1 in primary breast cancer and lymph node metastases. *J Clin Pathol.* Jun 2005;58(6):645-649.
36. Finlayson CA, Chappell J, Leitner JW, et al. Enhanced insulin signaling via Shc in human breast cancer. *Metabolism.* Dec 2003;52(12):1606-1611.
37. Vanagas G. Receiver operating characteristic curves and comparison of cardiac surgery risk stratification systems. *Interact CardioVasc Thorac Surg.* 2004;3:319-322.
38. Greiner M, Pfeiffer D, Smith RD. Principles and practical application of the receiver-operating characteristic analysis for diagnostic tests. *Prev Vet Med.* May 30 2000;45(1-2):23-41.
39. Wynne-Jones K, Jackson M, Grotte G, Bridgewater B. Limitations of the Parsonnet score for measuring risk stratified mortality in the north west of England. The North West Regional Cardiac Surgery Audit Steering Group. *Heart.* Jul 2000;84(1):71-78.
40. Zweig MH. ROC plots display test accuracy, but are still limited by the study design. *Clin Chem.* Jun 1993;39(6):1345-1346.
41. Ando S, Panno ML, Salerno M, et al. Role of IRS-1 signaling in insulin-induced modulation of estrogen receptors in breast cancer cells. *Biochem Biophys Res Commun.* Dec 18 1998;253(2):315-319.
42. Huynh H, Nickerson T, Pollak M, Yang X. Regulation of insulin-like growth factor I receptor expression by the pure antiestrogen ICI 182780. *Clin Cancer Res.* Dec 1996;2(12):2037-2042.
43. Ignar-Trowbridge DM, Pimentel M, Parker MG, McLachlan JA, Korach KS. Peptide growth factor cross-talk with the estrogen receptor requires the A/B domain and occurs independently of protein kinase C or estradiol. *Endocrinology.* May 1996;137(5):1735-1744.
44. Migliaccio M, Di Domenico M, Castoria G, et al. Tyrosine kinase/p21ras/MAP-kinase pathway activation by estradiol-receptor complex in MCF-7 cells. *EMBO J.* 1996;15:1292-1300.
45. Pezzino V, Papa V, Milazzo G, Gliozzo B, Russo P, Scalia PL. Insulin-like growth factor-I (IGF-I) receptors in breast cancer. *Ann N Y Acad Sci.* Apr 30 1996;784:189-201.
46. Railo MJ, von Smitten K, Pekonen F. The prognostic value of insulin-like growth factor-I in breast cancer patients. Results of a follow-up study on 126 patients. *Eur J Cancer.* 1994;30A(3):307-311.

47. Papa V, Gliozzo B, Clark GM, et al. Insulin-like growth factor-I receptors are overexpressed and predict a low risk in human breast cancer. *Cancer Res.* Aug 15 1993;53(16):3736-3740.
48. Lee AV, Hilsenbeck SG, Yee D. IGF system components as prognostic markers in breast cancer. *Breast Cancer Res Treat.* Feb 1998;47(3):295-302.
49. Yee D. The insulin-like growth factor system as a target in breast cancer. *Breast Cancer Res Treat.* 1994;32(1):85-95.
50. Turner BC, Haffty BG, Narayanan L, et al. Insulin-like growth factor-I receptor overexpression mediates cellular radioresistance and local breast cancer recurrence after lumpectomy and radiation. *Cancer Res.* Aug 1 1997;57(15):3079-3083.
51. Happerfield LC, Miles DW, Barnes DM, Thomsen LL, Smith P, Hanby A. The localization of the insulin-like growth factor receptor 1 (IGFR-1) in benign and malignant breast tissue. *J Pathol.* Dec 1997;183(4):412-417.
52. Koda M, Sulkowski S, Garofalo C, Kanczuga-Koda L, Sulkowska M, Surmacz E. Expression of the insulin-like growth factor-I receptor in primary breast cancer and lymph node metastases: correlations with estrogen receptors alpha and beta. *Horm Metab Res.* Nov-Dec 2003;35(11-12):794-801.
53. Peyrat JP, Bonneterre J, Dusanter-Fourt I, Leroy-Martin B, Djiane J, Demaille A. Characterization of insulin-like growth factor 1 receptors (IGF1-R) in human breast cancer cell lines. *Bull Cancer.* 1989;76(3):311-319.
54. Mansour EG, Ravdin PM, Dressler L. Prognostic factors in early breast carcinoma. *Cancer.* Jul 1 1994;74(1 Suppl):381-400.
55. McGuire WL. Estrogen receptors in human breast cancer. *J Clin Invest.* Jan 1973;52(1):73-77.
56. Desombre ER. Steroid receptors in breast cancer. *Monogr Pathol.* 1984(25):149-174.

Figure Legends

Fig. 1. ERα and IRS-1 expression in normal mammary epithelium, benign breast tumors and breast cancers.

The expression of ERα (ER) and IRS-1 (IRS) were examined by IHC, as described in Materials and Methods. Normal breast tissue (A, B); benign breast tumor (C, D); invasive ductal ERα-positive carcinoma (E, F); ERα-positive lobular breast cancer (G, H). Negative control; IHC of lobular carcinomas with primary Abs substituted with PBS. Higher magnification of specific areas is reported as inset in the original images.

Fig. 2. Subcellular localization of IRS-1 and ERα in breast tumors.

The localization of IRS-1 and ERα in ductal cancers was analyzed by immunostaining and confocal microscopy as detailed in Materials and methods. The captured images of IRS-1 (green fluorescence), ERα (red fluorescence) and merged IRS-1 and ERα (yellow fluorescence) are shown in a representative ductal cancer tissue section.

Fig. 3. Correlations between nuclear IRS-1 and ERα in normal breast tissues, benign breast tumors and breast cancers.

Associations between nuclear IRS-1 and ERα in different tissues were analyzed with Pearson correlation test. For each linear regression graph, the linear equation, the correlation coefficient (R), and the statistical significance (p) is reported.

Fig. 4. Distribution of nuclear IRS-1 and ERα in ductal and lobular breast cancers.

Distributions of nuclear IRS-1 (%) and ERα (%) relative to tumor grade (Grade), size (pT), and the lymph node involvement (pN) in ductal and lobular breast cancers are shown in scatterplots.

Fig. 5. Value of nuclear IRS-1 and ERα as diagnostic markers of tumor grading.

Graphic evaluation of ERα and nuclear IRS-1 in respect to tumor differentiation grade in invasive ductal and lobular carcinomas, showing the true-positive rate (sensitivity) and the false-positive rate (specificity) of the analysis as a function of all possible cut-points for the two markers. ERα, solid line; nuclear IRS-1, dotted line.

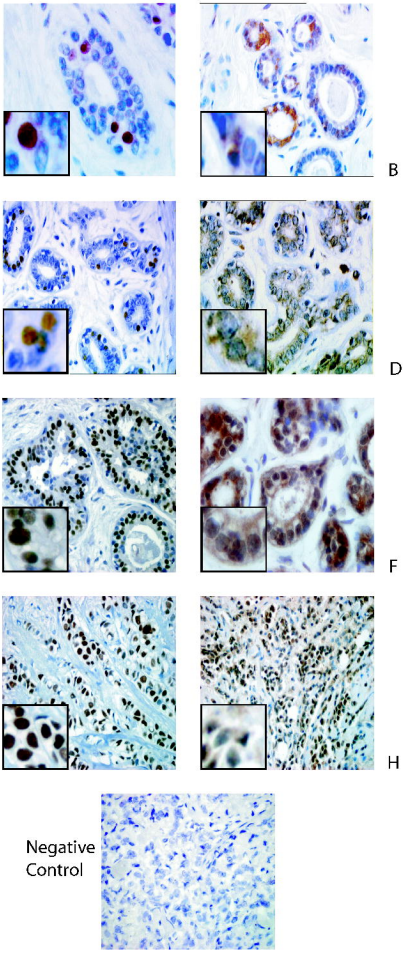

Figure 1

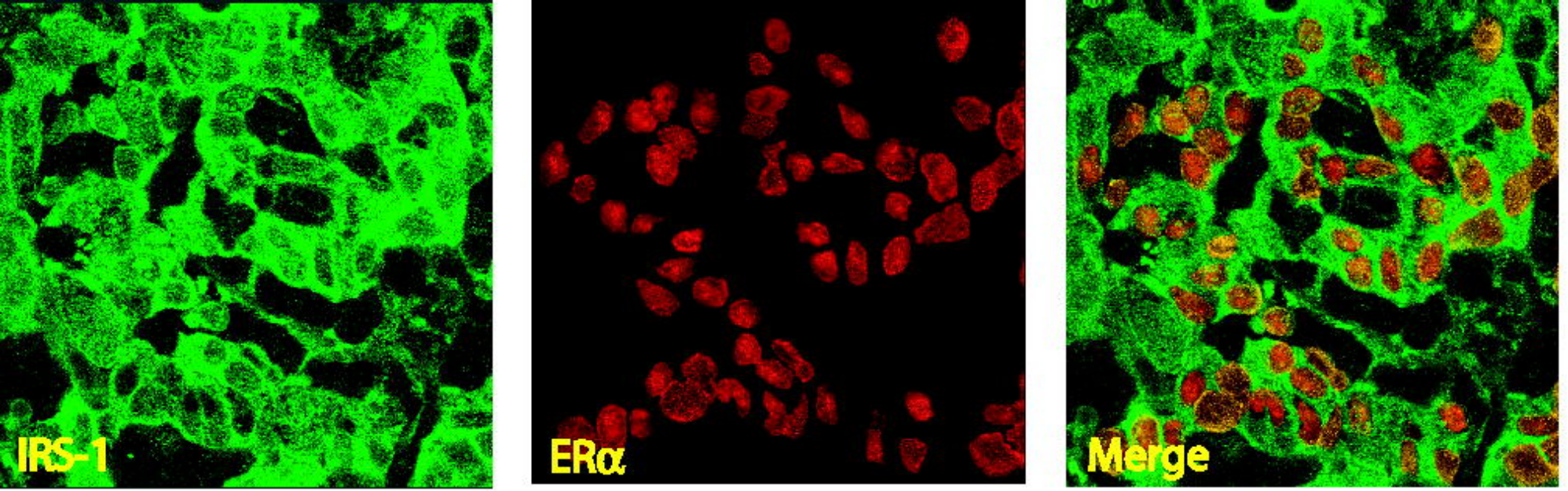

Figure 2

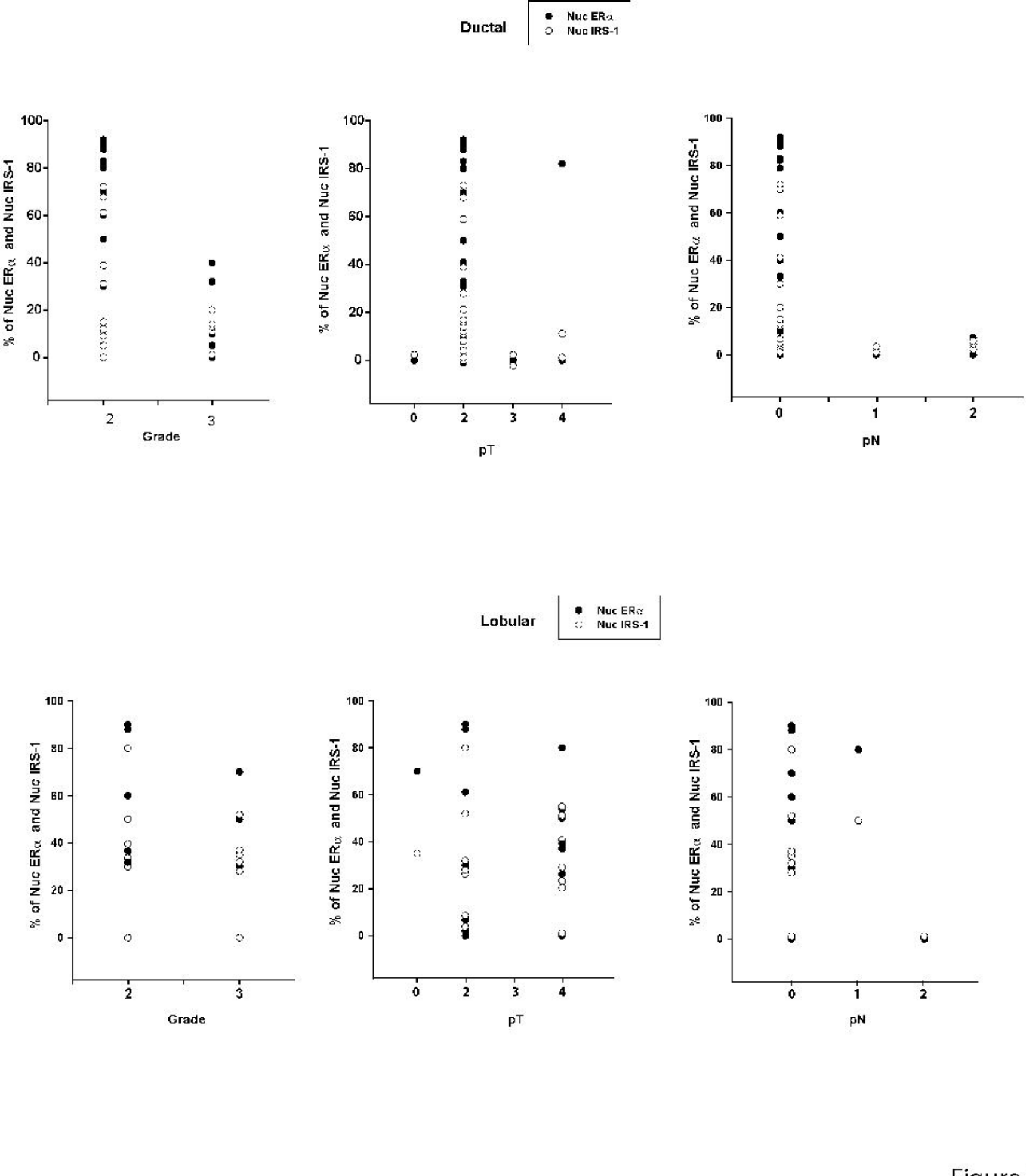
Ductal
Nuc ERα
Nuc IRS-1
% of Nuc ERα and Nuc IRS-1
Grade
pT
pN
Lobular
Nuc ERα
Nuc IRS-1
% of Nuc ERα and Nuc IRS-1
Grade
pT
pN

Figure 3

Normal

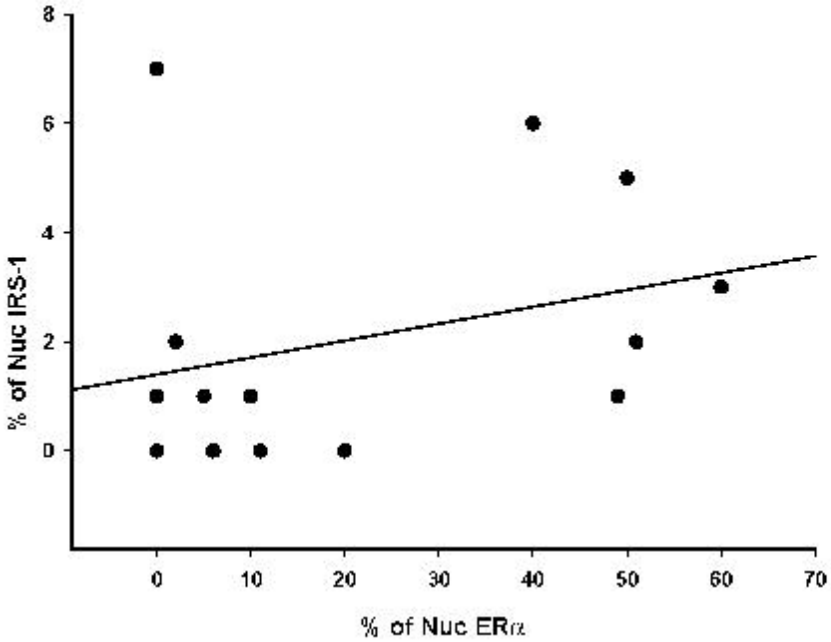

IRS Nuc=1.756+(0.03*ER) R=0.309 P=0.28

Benign

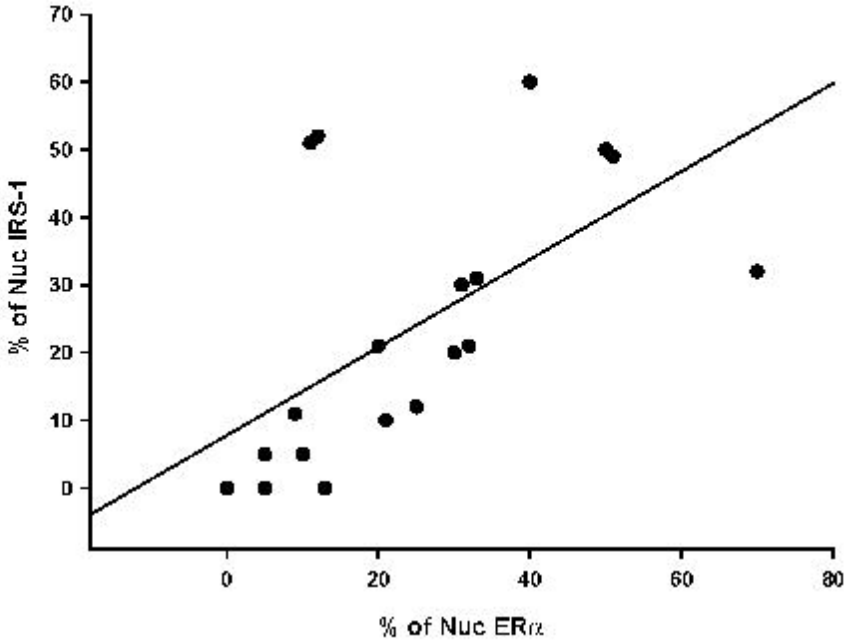

IRS Nuc=7.796+(0.650*ER) R=0.604 P<0.01

Ductal

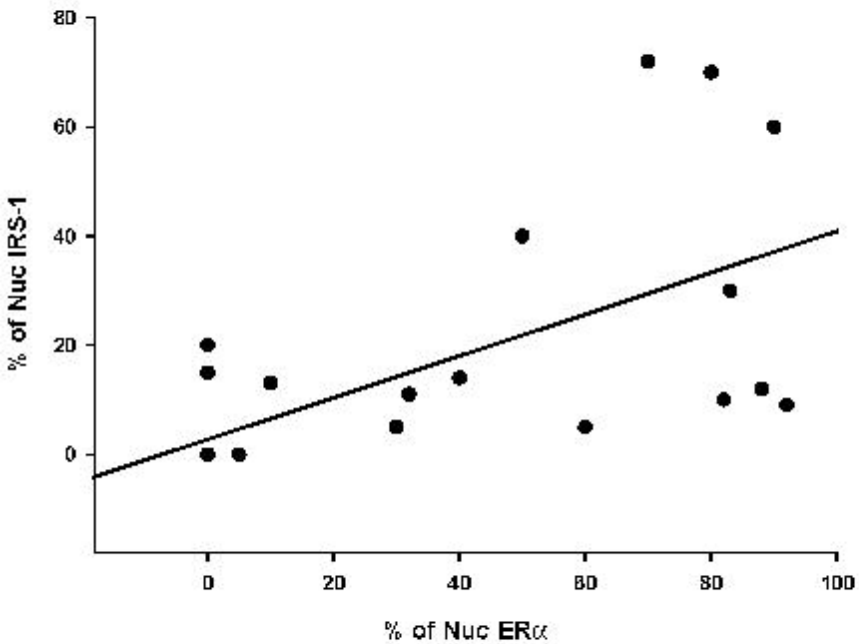

IRS Nuc=2.707+(0.382*ER) R=0.647 P<0.001

Lobular

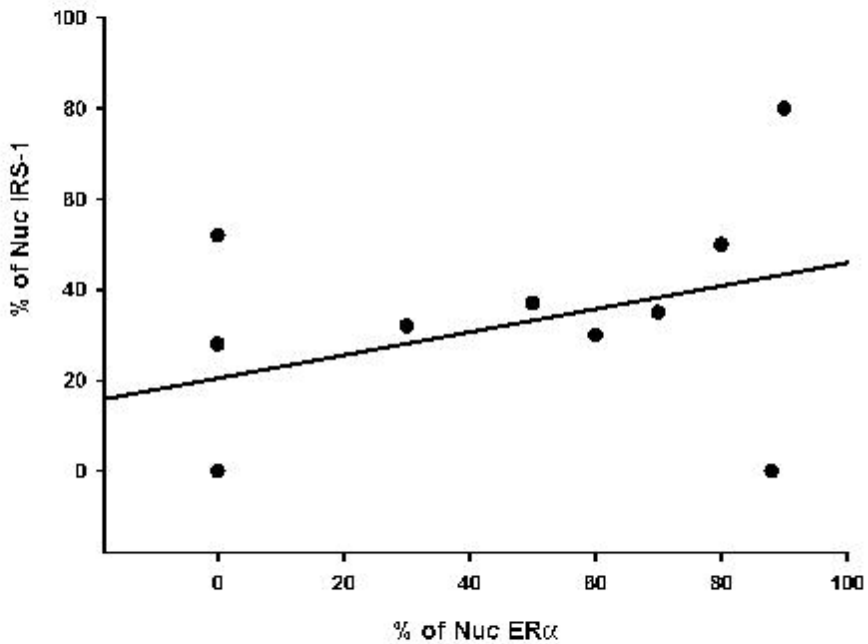

IRS Nuc=20.439+(0.255*ER) R=0.387 P=0.239

Figure 4

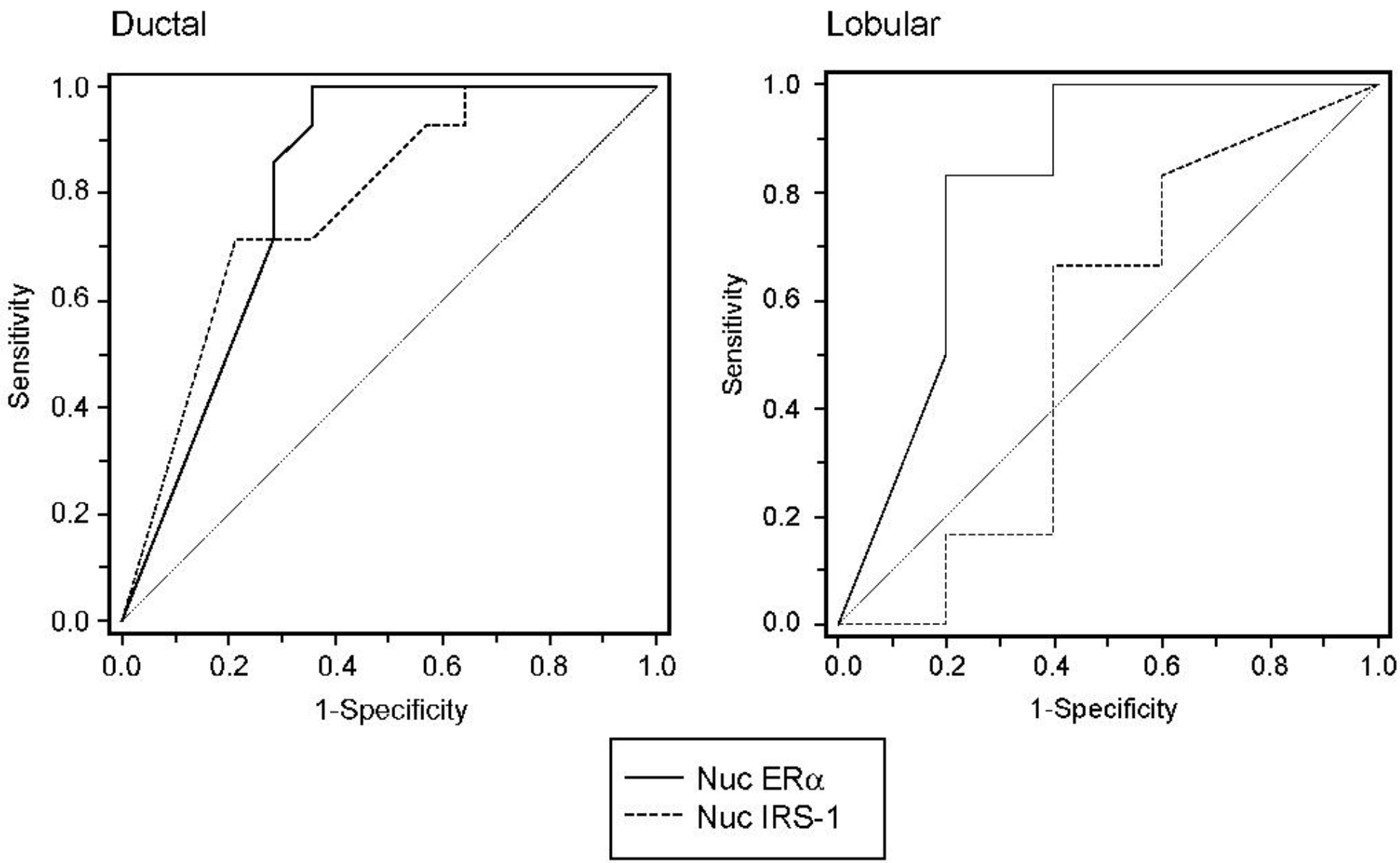
Ductal
Lobular
Sensitivity
1-Specificity
0.0
0.2
0.4
0.6
0.8
1.0
Nuc ERα
Nuc IRS-1

Figure 5

Molecular Endocrinology. First published ahead of print September 28, 2006 as doi:10.1210/me.2006-0192

Title page

Peroxisome Proliferator-Activated Receptor (PPAR) gamma activates p53 gene promoter binding to the NF*k*B sequence in human MCF7 breast cancer cells

Bonofiglio Daniela[1*], Aquila Saveria[1*], Catalano Stefania[1], Gabriele Sabrina[1], Belmonte Maria[1], Middea Emilia[1], Qi Hongyan[1], Morelli Catia[1], Gentile Mariaelena[2], Maggiolini Marcello[1] and Andò Sebastiano[2, 3]

[1]*Dept. Pharmaco-Biology,* [2] *Dept. Cellular Biology,* [3]*Faculty of Pharmacy University of Calabria 87030 Arcavacata di Rende (CS) Italy*

Key words: PPAR γ, p53, p21$^{WAF1/Cip1}$, breast cancer cells, rosiglitazone

Running title: PPAR γ activates p53 in MCF7 cells

Corresponding Author: Prof. Sebastiano Andò

Faculty of Pharmacy-University of Calabria

Arcavacata - Rende (Cosenza) 87036

ITALY

TEL: +39 0984 496201

E-mail: sebastiano.ando@unical.it

E-mail: daniela.bonofiglio@tin.it

Footnotes: * The two authors equally contributed to this work.

This work was supported by Associazione Italiana Ricerca sul Cancro (AIRC), Ministero dell'Istruzione Università e Ricerca and Ministero della Salute

ABSTRACT

The aim of the present study was to provide new mechanistic insight into the growth arrest and apoptosis elicited by Peroxisome proliferator-activated receptor (PPAR) γ in breast cancer cells. We ascertained that PPARγ mediates the inhibition of cycle progression in MCF7 cells exerted by the specific PPARγ agonist rosiglitazone (BRL), since this response was no longer notable in presence of the receptor antagonist GW9662 (GW). We also evidenced that BRL is able to up-regulate in a time- and dose-dependent manner mRNA and protein levels of the tumor suppressor gene p53 and its effector $p21^{WAF1/Cip1}$. Moreover, in transfection experiments with deletion mutants of the p53 gene promoter, we documented that the Nuclear Factor *k*B (NF*k*B) sequence is required for the transcriptional response to BRL. Interestingly, electrophoretic mobility shift assay showed that PPARγ binds directly to the NF*k*B site located in the promoter region of p53 and chromatin immunoprecipitation experiments demonstrated that BRL increases the recruitment of PPARγ on the p53 promoter sequence. Next, both PPARγ and p53 were involved in the cleavage of caspases-9 and DNA fragmentation induced by BRL, given that GW and an expression vector for p53 antisense blunted these effects. Our findings evidenced that the PPARγ agonist BRL promotes the growth arrest and apoptosis in MCF7 cells, at least in part, through a crosstalk between p53 and PPARγ which may be considered an additional target for novel therapeutic interventions in breast cancer patients.

INTRODUCTION

Peroxisome proliferator-activated receptor γ (PPARγ) is a prototypical member of the nuclear receptor superfamily and integrates the control of energy, lipid, and glucose homeostasis (1-4). PPARγ regulates differentiation and induces cell growth arrest and apoptosis in a large variety of cells (5 and references therein), including both primary and metastatic breast malignancy (6-7). However, the molecular mechanisms involved in the inhibitory effects mediated by PPARγ remain to be elucidated.

It is well known that the p53 tumor suppressor gene regulates the transcription of effectors that are also responsible for growth arrest and apoptosis (reviewed in reference 8). Among the p53 target genes, the $p21^{WAF1/Cip1}$ has been recognized to exert an essential role in mediating cell cycle arrest at both G1 and G2/M checkpoints (9-11). $p21^{WAF1/Cip1}$ inhibits cyclin D1 or E/CDK in G1 and cyclin B/cdc2 in G2/M arrest, eliciting regulatory effects on DNA replication and repair (12). Moreover, it has been reported that p53 is able to promote apoptosis in certain cell types in a transcription independent manner (13).

The function of p53 as a tumor suppressor is finely tuned through an interaction with other transduction pathways regulating the cell network (14-18). For instance, a striking evidence has recently emerged for a crosstalk between p53 and relevant transcription factors, such as the glucocorticoid, androgen and estrogen receptors (19). It was therefore proved that these nuclear receptors are able to induce a cytosolic accumulation of p53, altering its stability and, consequently, its function (19).

In the present study, we provide new insight into the molecular mechanisms by which the specific PPARγ ligand rosiglitazone (BRL) induces the growth arrest and apoptosis in MCF7 human breast cancer cells. Performing a panel of different assays, we have demonstrated that the biological effects of BRL are triggered, at least in part, by PPARγ binding to the Nuclear Factor *k*B

1 sequence located within the p53 promoter region. Our findings have evidenced a crosstalk between
2 p53 and PPARγ which assumes a biological relevance in order to suggest new pharmacological
3 strategies in breast cancer.

RESULTS

BRL induces G_0/G_1 cycle arrest in MCF7 cells

On the basis of our (20) and other (21-22) studies demonstrating the inhibitory effects of the PPARγ-agonists on proliferation of breast cancer cells, we first investigated the activity of BRL on MCF7 cell cycle progression. A 48-h exposure to BRL caused in a dose-dependent manner the inhibition of G0-G1→S phase progression with concomitant decrease in the proportion of cells entering in S phase (TAB. 1). Of note, this effect was mediated by PPARγ, since it was no longer notable in presence of the specific antagonist GW9662 (GW).

BRL up-regulates p53 and $p21^{WAF1/Cip1}$ expression in MCF7 cells

Considering that the tumor suppressor gene p53 is mainly involved in the growth arrest promoted by different factors, we aimed to examine the potential ability of PPARγ to modulate the expression of p53 along with its natural target gene $p21^{WAF1/CIP1}$. The mRNA (Fig. 1) and protein (Fig. 2) levels of both p53 and $p21^{WAF1/CIP1}$ were up-regulated in a time- and dose-dependent manner in MCF7 cells treated with BRL. These stimulations were abrogated by GW (figures 1 and 2) suggesting a direct involvement of PPARγ.

BRL transactivates p53 gene promoter

The aforementioned observations prompted us to investigate whether PPARγ is able to transactivate an expression vector encoding p53 promoter gene. Thus, MCF7 cells were transiently transfected with a luciferase reporter construct (named p53-1) containing the upstream region of the p53 gene spanning from –1800 to +12 (Fig. 3A) and treated with increasing concentrations of BRL for 24-h. Interestingly, the dose-dependent activation of p53-1 by BRL was reversed in presence of GW indicating that a PPARγ-mediated mechanism was involved in the transcriptional response to BRL (Fig. 3B).

To identify the region within the p53 promoter responsible for transactivation, we used deletion constructs expressing different binding sites such as CTF-1/YY1, nuclear factor-Y (NF-Y) and NF*k*B (Fig. 3A). In transfection experiments performed using the mutants p53-6 and p-53-13 encoding the regions from -106 to +12 and from -106 to -40, respectively, the responsiveness to BRL was still observed, while using the mutant p53-14 encoding the sequence from -106 to -49 we did not detect increase in luciferase activity (Fig. 3C). Consequently, the region from -49 to -40, which corresponds to the NF*k*B site (Fig. 3A), was required for the transactivation of p53 by BRL.

PPARγ binds to NFkB sequence in EMSA

In order to further evaluate whether the NF*k*B site is responsible for the action triggered by BRL, we performed EMSA experiments. Using synthetic oligodeoxyribonucleotides corresponding to the NF*k*B sequence, we observed in nuclear extracts from MCF7 cells the formation of a single band (Fig. 4A, lane 1) which was abrogated by 100-fold molar excess of unlabeled probe (Fig. 4A, lane 2), demonstrating the specificity of the DNA binding complex. Of note, BRL treatment induced a strong increase in the specific band (Fig. 4A, lane 3), which was immunodepleted and supershifted using anti-PPARγ (Fig. 4A, lane 4) and anti-NF*k*B (Fig. 4A, lane 5) antibodies. Interestingly, the PPARγ transcribed and translated protein was able to bind to [^{32}P]-NF*k*B oligonucleotide (Fig. 4A, lane 6). The specificity of the band was proved by a 100-fold excess of cold probe (Fig. 4A, lane 7) and confirmed by a consensus PPRE used as a cold competitor (Fig. 4A, lane 8). Besides, the immunodepleted band obtained using the anti-PPARγ antibody (Fig. 4A, lane 9), but not evidenced with the anti-NF*k*B antibody (Fig. 4A, lane 10), confirmed that PPARγ binds in a specific manner to the NF*k*B site present in the promoter of p53. As next controls, we used NF*k*B protein alone (Fig. 4B, lane 1) and in combination with either cold competitor (Fig. 4B, lane 2) or the anti-NF*k*B antibody (Fig. 4B, lane 3).

Functional interaction of PPARγ with p53 in ChIP assay

The interaction of PPARγ with p53 was further elucidated by ChIP experiments. MCF7 cells were treated with formaldehyde to form DNA-protein cross-links and then sonicated. Thereafter, using anti-PPARγ, anti-NF*k*B and anti-RNA Pol II antibodies we immunoprecipitated the complexes and the binding of PPARγ, NF*k*B and, respectively RNA Pol II, respectively, to the NF*k*B site within the p53 promoter was revealed by PCR. As shown in panel A of figure 5, BRL increased the recruitment of PPARγ to the promoter of p53. The BRL-induced effect was slightly reduced by TGFβ, but not altered in presence of the specific inhibitor of NF*k*B parthenolide (P) (23) (Fig. 5A). As it concerns the recruitment of NF*k*B to p53, evaluated using the anti-NF*k*B antibody, TGFβ enhanced such interaction which was abolished by P (Fig.5A). Moreover, P was able to prevent the binding of RNA Pol II to p53 induced by TGFβ, but not that determined by BRL (Fig. 5A). These findings confirmed the ability of PPARγ to stimulate the transcription of p53 in a NF*k*B independent manner (Fig. 5A). Next, the anti-PPARγ antibody did not immunoprecipitate a region upstream the NF*k*B site located within the p53 promoter gene (Fig. 5B).

BRL induces caspase-9 cleavage and DNA fragmentation in MCF7 cells

Having demonstrated that PPARγ mediates p53 expression induced by BRL, we investigated the cleavage of caspase 9, which is an important component of the intrinsic apoptotic process (24). Notably, the treatment of MCF7 cells with BRL for 48-h promoted the caspase-9 activation which was prevented by GW and in presence of an expression vector encoding p53 antisense (AS/p53) (Fig. 6A), which abolished p53 expression (Fig. 6B). On the contrary, the effect of BRL on the cleavage of caspase 9 was still notable using the NF*k*B inhibitor P (Fig. 6A), which abrogating the NF*k*B protein levels (Fig. 6C) excluded the contribution of such factor in the action elicited by BRL.

As evidenced in DNA fragmentation assay, PPARγ was also involved in the apoptotic process triggered by BRL since this effect was completely and partially reversed by GW and the AS/p53, respectively (Fig. 6D). Again, P did not modify the activity of BRL (Fig. 6D). Taken together, these results indicate that, at least in part, a crosstalk between PPARγ and p53 may be responsible for the growth arrest and apoptosis induced by BRL in MCF7 cells.

DISCUSSION

In recent years, a great deal of attention focused on the antiproliferative effects of PPARγ in a variety of cancer cell types. Treatments with PPARγ ligands have been demonstrated to induce cell cycle arrest and apoptosis in different cancer models (6-7, 25). Besides, an interaction between PPARγ and p53 was hypothesized but not clarified at molecular level in cholangiocarcinoma (26), in human gastric cancer cells (27) and even in rat vascular smooth muscle cells (28). In addition, from our and other studies emerged the ability of PPARγ to up-regulate the expression of the tumor suppressor gene PTEN which is required for both a negative modulation of PI3K/Akt-dependent cell proliferation (20, 29-30) and a p53-mediated regulation of cell survival and apoptosis (31). Consequently, PPARγ and p53 may converge in a tumor suppressor activity which remains to be further elucidated.

In order to provide new insight into the inhibitory action exerted by the cognate PPARγ-ligand BRL, we first demonstrated that PPARγ mediates the growth arrest in G0-G1 phase induced by BRL in MCF7 cells. Besides, considering the key role elicited by p53 in the growth inhibition and apoptosis (14, 17), we have evaluated whether PPARγ signalling converges on p53 transduction pathway in MCF7 cells. Of interest, we found that BRL exposure up-regulates both p53 mRNA and protein levels with a concomitant increase of $p21^{WAF1/Cip1}$ expression. These effects were abrogated in presence of the specific antagonist GW, addressing a PPARγ-mediated mechanism. Therefore, investigating the potential ability of BRL to modulate p53 promoter gene, we performed transient transfections in MCF7 cells using diverse deletion mutants of p53 promoter gene (32). The dose-dependent transactivation of p53 by BRL involved directly PPARγ since the transcriptional activity was prevented by GW treatment. Moreover, we documented that the region spanning from -49 to -40, which corresponds to the NF*k*B site, is required for the responsiveness to BRL.

It deserves to be mentioned that the transcription factor NF*k*B can regulate both pro- and antiapoptotic signalling pathways depending on cell type, the extent of NF*k*B activation and the nature of the apoptotic stimuli (33). NF*k*B was reported to physically interact with PPARγ (34), which in some circumstances binds to DNA cooperatively with NF*k*B (35-36), further enhancing the NF*k*B-DNA binding (37). Besides, PPARγ agonists were able to enhance the binding of NF*k*B to the upstream *k*B regulatory element site of c-*myc* (38). Our EMSA experiments extended the aforementioned observations since nuclear extracts of MCF7 cells treated with BRL showed an increased binding to the NF*k*B sequence located in the p53 promoter region. Given that the anti-PPARγ and anti-NF*k*B antibodies were both able to induce shifted bands, we performed an EMSA study using a cell free system to ascertain the potential direct interaction of PPARγ with NF*k*B site. Interestingly, we observed the formation of a single DNA-binding complex which was again shifted by the anti-PPARγ antibody. These findings were supported by ChIP assay in MCF7 cells demonstrating the ability of BRL to enhance the recruitment of PPARγ and RNA Pol II to the promoter of p53 even in presence of the NF*k*B inhibitor P. Overall, these data indicate that the PPARγ-mediated growth arrest upon addition of BRL in MCF7 cells involves, at least in part, the direct stimulation of p53 transcription.

p53 acts as a tumor suppressor depending on its physical and functional interaction with diverse cellular proteins (39), like some nuclear receptors that in turn exert an inhibitory activity on p53 biological outcomes (19). In *Supplemental Data* we show an evident co-immunoprecipitation and co-localization of PPARγ and p53 after BRL treatment. However, additional experiments are required to better characterize such interaction and its functional consequences.

A large body of evidence has suggested the straightforward role of p53 signalling in the apoptotic cascades which include the activation of caspases, a family of cytoplasmic cysteine proteases (40). The intrinsic apoptotic pathway involves a mitochondria-dependent process, which

results in cytochrome *c* release and, thereafter, activation of caspase-9 (24). Besides, apoptosis is characterized by distinct morphological changes including the internucleosomal cleavage of DNA, which is recognized as a 'DNA ladder' (24 and references therein). Notably, we evidenced that in a consecutive series of events BRL i) up-regulates the expression of p53 and ii) its effector $p21^{WAF1/Cip1}$, iii) triggers the cleavage of caspases-9, and iv) induces DNA fragmentation in a PPARγ-mediated manner. Given the ability of AS/p53 to reduce the last two biological effects of BRL, it may be argued an involvement of p53 in such PPARγ-dependent activity. On the contrary, the cleavage of caspase-9 and DNA fragmentation observed upon BRL treatment did not show changes suppressing the NF*k*B at protein level with P, suggesting that this factor is not required for the apoptotic events elicited by BRL.

In the present study we have provided new insight into the molecular mechanism through which PPARγ mediates the growth arrest and apoptosis induced by BRL in MCF7 cells. Our findings suggest that a crosstalk between p53 and PPARγ may assume biological relevance in setting novel therapeutic interventions in breast cancer.

MATERIALS AND METHODS

Reagents

Rosiglitazone, BRL49653, was a gift from GlaxoSmithKline (West Sussex, UK), the irreversible PPARγ-antagonist GW9662 was purchased by Sigma (Milan, Italy), human recombinant TGFβ was obtained from ICN Biomedicals (DBA, Milan, Italy), and the Parthenolide was purchased by Alexis (San Diego, CA USA).

Plasmids

The p53 promoter-luciferase reporters, constructed using pGL2 for cloning of p53–1 and -6, and TpGL2 for p53–13 and -14 were kindly provided by Dr. Stephen H. Safe (Texas A&M University, Texas, USA). The constructs used were generated by Safe (32) from the human p53 gene promoter: p53-1 (containing the -1800 to +12 region), p53-6 (containing the – 106 to +12 region), p53-13 (containing the – 106 to -40 region) and p53-14 (containing the – 106 to -49 region).

As an internal transfection control, we co-transfected the plasmid pRL-CMV (Promega Corp., Milan, Italy) that expresses Renilla luciferase enzymatically distinguishable from firefly luciferase by the strong cytomegalovirus enhancer/promoter. The p53 antisense plasmid (AS/p53) and PPARγ expression plasmid were gifts from Dr. Moshe Oren (Weizmann Institute of Science, Rehovot, Israel) and Dr. R. Evans (The Salk Institute, San Diego, CA, USA), respectively.

Cell cultures

Wild-type human breast cancer MCF7 cells (a gift from Dr. Ewa Surmacz, Sbarro Institute for Cancer Research and Molecular Medicine, Philadelphia, USA) were grown in DMEM plus glutamax containing 10 % fetal calf serum (FCS) (Invitrogen, Milan, Italy) and 1 mg/ml penicillin-streptomycin.

DNA Flow cytometry

MCF7 cells at 50-60 % confluence were shifted to serum free medium (SFM) for 24 hours and then treatments were added in SFM for 48 hours. Thereafter, cells were trypsinized, centrifuged at 1500 rpm for 3 minutes, washed with PBS, and then treated with 20 μg/ml RNase A (Calbiochem, La Jolla, CA). DNA was stained with 100 μg/ml propidium iodide for 30 minutes at 4°C protected from light, and cells were analyzed with the FACScan (Becton, Dickinson, NJ).

RT-PCR assay

MCF7 cells were grown in 10-cm dishes to 70-80 % confluence and exposed to treatments for 24 and 48 hours in SFM. Total cellular RNA was extracted using TRIZOL reagent (Invitrogen) as suggested by the manufacturer. The purity and integrity were checked spectroscopically and by gel electrophoresis before carrying out the analytical procedures. The evaluation of gene expression was performed by semiquantitative RT-PCR method as previously described (41). For p53, $p21^{WAF1/Cip1}$, and the internal control gene 36B4, the primers were: 5'-GTGGAAGGAAATTTGCGTGT-3' (p53 forward) and 5'-CCAGTGTGATGATGGTGAGG-3' (p53 reverse), 5'-GCTTCATGCCAGCTACTTCC-3' (p21 forward) and 5'-CTGTGCTCACTTCAGGGTCA-3' (p21 reverse), 5'-CTCAACATCTCCCCCTTCTC-3' (36B4 forward) and 5'-CAAATCCCATATCCTCGTCC-3' (36B4 reverse) to yield respectively products of 190 bp with 18 cycles, 270 bp with 18 cycles and 408 bp with 12 cycles. The results obtained as optical density arbitrary values were transformed to percentage of the control (percent control) taking the samples from untreated cells as 100 %.

Transfection assay

MCF7 cells were transferred into 24-well plates with 500 μl of regular growth medium/well the day before transfection. The medium was replaced with SFM on the day of transfection, which was performed using Fugene 6 reagent as recommended by the manufacturer (Roche Diagnostics,

Mannheim, Germany) with a mixture containing 0.5 μg of promoter-luc reporter plasmid, 5 ng of pRL-CMV. After 24 hours transfection, treatments were added in SFM as indicated and cells were incubated for further 24 hours. Firefly and Renilla luciferase activities were measured using the Dual Luciferase Kit (Promega, Madison, WI). The firefly luciferase values of each sample were normalized by Renilla luciferase activity and data were reported as Relative Light Units (RLU) values.

MCF7 cells plated into 10-cm dishes were transfected with 5 μg of AS/p53 using Fugene 6 reagent as recommended by the manufacturer (Roche Diagnostics, Mannheim, Germany). The activity of AS/p53 was verified utilizing western blot to detect changes in p53 protein levels. Time course analysis revealed that p53 levels were effectively suppressed at 18 hours after transfection (data not shown). Empty vector was used to ensure that DNA concentrations were constant in each transfection.

Electrophoretic Mobility Shift Assay (EMSA)

Nuclear extracts from MCF7 cells were prepared as previously described for EMSA (42). Briefly, MCF7 cells plated into 10-cm dishes were grown to 70-80 % confluence shifted to SFM for 24 hours and then treated with 10 μM BRL for 6 hours. Thereafter, cells were scraped into 1.5 ml of cold phosphate-buffered saline (PBS). Cells were pelleted for 10 seconds and resuspended in 400 μl cold buffer A (10 mM HEPES-KOH pH 7.9 at 4 °C, 1.5mM $MgCl_2$, 10 mM KCl, 0.5 mM dithiothreitol, 0.2 mM PMSF, 1 mM leupeptin) by flicking the tube. The cells were allowed to swell on ice for 10 minutes and then vortexed for 10 seconds. Samples were then centrifuged for 10 seconds and the supernatant fraction discarded. The pellet was resuspended in 50 μl of cold Buffer B (20 mM HEPES-KOH pH 7.9, 25 % glycerol, 1.5 mM $MgCl_2$, 420 mM NaCl, 0.2 mM EDTA, 0.5 mM dithiothreitol, 0.2 mM PMSF, 1 mM leupeptin) and incubated in ice for 20 minutes for high-salt extraction. Cellular debris were removed by centrifugation for 2 minutes at 4 °C and the

supernatant fraction (containing DNA binding proteins) was stored at –70 °C. *In vitro* transcribed and translated PPARγ was synthesized using the T7 polymerase in the rabbit reticulocyte lysate system from PPARγ plasmid as directed by the manufacturer (Promega). The probe was generated by annealing single stranded oligonucleotides and labeled with [γ^{32}P] ATP (Amersham Pharmacia, Buckinghamshire, UK) and T4 polynucleotide kinase (Promega) and then purified using Sephadex G50 spin columns (Amersham Pharmacia). The DNA sequence of the nuclear factor *k*B (NF*k*B) used as probe or as cold competitor is the following: NF*k*B, 5'-AGT TGA GGG GAC TTT CCC AGG C-3' (Sigma Genosys, Cambridge, UK). As cold competitor we also used PPRE oligonucleotide: 5'-GGGACCAGGACAAAGGTCACGTT-3' (Sigma Genosys). The protein binding reactions were carried out in 20 μl of buffer [20 mM Hepes pH 8, 1 mM EDTA, 50 mM KCl, 10 mM DTT, 10% glicerol, 1mg/ml BSA, 50 μg/ml poly dI/dC] with 50000 cpm of labeled probe, 5 μg of MCF7 nuclear protein, or 2 μl of transcribed and translated *in vitro* PPARγ protein, or 1 μl of NF*k*B protein (Promega), and 5 μg of poly (dI-dC). The mixtures were incubated at room temperature for 20 minutes in the presence or absence of unlabeled competitor oligonucleotides. For the experiments involving anti-PPARγ and anti-NF*k*B antibodies (Santa Cruz Biotechnology, Santa Cruz, CA), the reaction mixture was incubated with these antibodies at 4 °C for 30 minutes before addition of labeled probe. The entire reaction mixture was electrophoresed through a 6 % polyacrylamide gel in 0.25 X Tris borate-EDTA for 3 hours at 150 V. Gel was dried and subjected to autoradiography at –70 °C.

Chromatin immunoprecipitation (ChIP)

MCF7 cells were grown in 10-cm dishes to 50-60 % confluence, shifted to SFM for 24 hours and then treated with 10 μM BRL for 1 hour. Thereafter, cells were washed twice with PBS and crosslinked with 1 % formaldehyde at 37 °C for 10 minutes. Next, cells were washed twice with PBS at 4 °C, collected and resuspended in 200 μl of lysis buffer (1% SDS, 10 mM EDTA, 50

mM Tris-HCl pH 8.1) and left on ice for 10 minutes. Then, cells were sonicated four times for 10 seconds at 30 % of maximal power (Sonics, Vibra Cell 500 W) and collected by centrifugation at 4 °C for 10 minutes at 14,000 rpm. The supernatants were diluted in 1.3 ml of IP buffer (0.01 % SDS, 1.1 % Triton X-100, 1.2 mM EDTA, 16.7 mM Tris-HCl pH 8.1, 16.7 mM NaCl) followed by immunoclearing with 80 µl of sonicated salmon sperm DNA/protein A agarose (UBI, DBA Srl, Milan - Italy) for 1 hour at 4 °C. The precleared chromatin was immunoprecipitated with anti-PPARγ, anti-NF*k*B and anti-RNA Pol II antibodies (Santa Cruz Biotechnology). At this point, 60 µl salmon sperm DNA/protein A agarose were added and precipitation was further continued for 2 hours at 4 °C. After pelleting, precipitates were washed sequentially for 5 minutes with the following buffers: Wash A (0.1 % SDS, 1 % Triton X-100, 2 mM EDTA, 20 mM Tris-HCl pH 8.1, 150 mM NaCl), Wash B (0.1 % SDS, 1 % Triton X-100, 2 mM EDTA, 20 mM Tris-HCl pH 8.1, 500 mM NaCl), and Wash C (0.25 M LiCl, 1 % NP-40, 1 % sodium deoxycholate, 1 mM EDTA, 10 mM Tris-HCl pH 8.1), and then twice with TE buffer (10 mM Tris, 1 mM EDTA). The immunocomplexes were eluted with elution buffer (1 % SDS, 0.1 M $NaHCO_3$). The eluates were reverse crosslinked by heating at 65 °C and digested with proteinase K (0.5 mg/ml) at 45 °C for 1 hour. DNA was obtained by phenol/chloroform/isoamyl alcohol extraction. 2 µl of 10 mg/ml yeast tRNA (Sigma) were added to each sample and DNA was precipitated with 70 % ethanol for 24 hours at –20 °C, and then washed with 95 % ethanol and resuspended in 20 µl of TE buffer. A 5 µl volume of each sample was used for PCR with primers flanking a sequence present in the p53 promoter: 5'-CTGAGAGCAAACGCAAAAG-3' (forward) and 5'-CAGCCCGAACGCAAAGTGTC-3' (reverse) containing the *k*B site from -254 to -42 region and 5'-GAAAACGTTAGGGTGTGG-3' (forward) and 5'-GGTGCAGAGTCAGGATTC-3' (reverse) upstream of the *k*B site from -528 to -452 region (Gene Bank AC: J0423). The PCR conditions for the two p53 promoter fragments were respectively 45 seconds at 94 °C, 40 seconds at 57 °C, 90

seconds at 72 °C and 45 seconds at 94 °C, 40 seconds at 55 °C, 90 seconds at 72 °C. The amplification products obtained in 30 cycles were analysed in a 2 % agarose gel and visualized by ethidium bromide staining. The negative control was provided by PCR amplification without DNA sample. The specificity of reactions was ensured using normal mouse and rabbit IgG (Santa Cruz Biotechnology).

Immunoblotting

MCF7 cells were grown in 10-cm dishes to 70-80% confluence and exposed to treatments for 24 and 48 hours in SFM as indicated. Cells were then harvested in cold PBS and resuspended in lysis buffer containing 20 mM HEPES pH 8, 0.1mM EDTA, 5mM $MgCl_2$, 0.5M NaCl, 20 % glycerol, 1 % NP-40, inhibitors (0.1mM Na_3VO_4, 1 % PMSF, 20 mg/ml aprotinin). Protein concentration was determined by Bio-Rad Protein Assay (Bio-Rad Laboratories, Hercules, CA).

A 50 μg portion of protein lysates was used for Western Blotting (WB), resolved on a 10 % SDS-polyacrylamide gel, transferred to a nitrocellulose membrane and probed with an antibody directed against the p53, $p21^{WAF1/Cip1}$, caspases-9 and NF*k*B (Santa Cruz Biotechnology). As internal control, all membranes were subsequently stripped (glycine 0.2 M, pH 2.6 for 30 minutes at room temperature) of the first antibody and reprobed with anti-β-actin antibody.

The antigen-antibody complex was detected by incubation of the membranes for 1 hour at room temperature with peroxidase-coupled goat anti-mouse or anti-rabbit IgG and revealed using the enhanced chemiluminescence system (ECL system, Amersham Pharmacia). Blots were then exposed to film (Kodak film, Sigma).The intensity of bands representing relevant proteins was measured by Scion Image laser densitometry scanning program.

DNA Fragmentation

DNA fragmentation was determined by gel electrophoresis. MCF7 cells were grown in 10-cm dishes to 70 % confluence and treated with 10 μM BRL and/or 10 μM GW and /or 15 μM P. After 72 hours cells were collected and washed with PBS and pelletted at 1800 rpm for 5 minutes. The samples were resuspended in 0.5 ml of extraction buffer (50 mM Trios-HCl pH 8, 10mM EDTA, O.5% SDS) for 20 minutes in rotation at 4 °C. DNA was extracted with phenol/chloroform for 3 times and once with chloroform. The aqueous phase was used to precipitate acids nucleic with 0.1 volumes or of 3 M sodium acetate and 2.5 volumes cold EtOH overnight at -20 °C. The DNA pellet was resuspended in 15 μl of H_2O treated with RNAse A for 30 minutes at 37 °C. The absorbance of the DNA solution at 260 and 280 nm was determined by spectrophotometry. The extracted DNA (40 μg/lane) was subjected to electrophoresis on 1.5 % agarose gels. The gels were stained with ethidium bromide and then photographed.

STATISTICAL ANALYSIS

Statistical analysis was performed using ANOVA followed by Newman-Keuls testing to determine differences in means. $p<0.05$ was considered as statistically significant.

REFERENCES

1. Shearer BG, Hoekstra WJ 2003Recent advances in peroxisome proliferator-activated receptor science. Curr Med Chem 10:267–280
2. Francis GA, Fayard E, Picard F, Auwerx J 2003Nuclear receptors and the control of metabolism. Ann Rev Physiol 65:261–311
3. Chawla A, Repa JJ, Evans RM, Mangelsdorf DJ 2001Nuclear receptors and lipid physiology: opening the X-files. Science 294:1866–1870
4. Yamauchi T, Kamon J, Waki H, Murakami K, Motojima K, Komeda K, Ide T, Kubota N, Terauchi Y, Tobe K, Miki H, Tsuchida A, Akanuma Y, Nagai R, Kimura S, Kadowaki T 2001 The mechanisms by which both heterozygous peroxisome proliferator-activated receptor gamma (PPARgamma) deficiency and PPAR gamma agonist improve insulin resistance. J Biol Chem 276:41245-41254
5. Fajas L, Egler V, Reiter R, Miard S, Lefebvre AM, Auwerx J 2003 PPAR gamma controls cell proliferation and apoptosis in an RB-dependent manner. Oncogene 22: 4186–4193
6. Mueller E, Sarraf P, Tontonoz P, Evans RM, Martin KJ, Zhang M, Fletcher C, Singer S, Spiegelman BM 1998 Terminal differentiation of human breast cancer through PPAR gamma. Mol Cell 1:465-470
7. Elstner E, Muller C, Koshizuka K, Williamson EA, Park D, Asou H, Shintaku P, Said JW, Heber D, Koeffler HP 1998 Ligands for peroxisome proliferator-activated receptor gamma and retinoic acid receptor inhibit growth and induce apoptosis of human breast cancer cells in vitro and in BNX mice. Proc Natl Acad Sci USA 95:8806-8811
8. Vousden KH, Lu X 2002 Live or let die: the cell's response to p53. Nat Rev Cancer 2:594-604
9. Liu G, Lozano G 2005 p21 stability: linking chaperones to a cell cycle checkpoint. Cancer Cell 7:113-114

10. el-Deiry WS, Tokino T, Velculescu VE, Levy DB, Parsons R, Trent JM, Lin D, Mercer WE, Kinzler KW, Vogelstein B 1993 WAF1, a potential mediator of p53 tumor suppression. Cell 75:817-825
11. Harper JW, Adami GR, Wei N, Keyomarsi K, Elledge SJ 1993 The p21 Cdk-interacting protein Cip1 is a potent inhibitor of G1 cyclin-dependent kinases. Cell 75:805-816
12. Tom S, Ranalli TA, Podust VN, Bambara RA 2001 Regulatory roles of p21 and apurinic/apyrimidinic endonuclease 1 in base excision repair. J Biol Chem 276:48781-48789
13. Caelles C, Helmberg A, Karin M 1994 p53-dependent apoptosis in the absence of transcriptional activation of p53-target genes. Nature 370:220-223
14. Yu J, Zhang L 2005 The transcriptional targets of p53 in apoptosis control. Biochem Biophys Res Commun 331:851-858
15. O'Brate A, Giannakakou P 2003 The importance of p53 location: nuclear or cytoplasmic zip code? Drug Resistance Updates 6:313-322
16. Appella E 2001 Modulation of p53 function in cellular regulation. Eur J Biochem 268:2763
17. Haupt S, Berger M, Goldberg Z, Haupt Y 2003 Apoptosis - the p53 network. J Cell Sci 116:4077-4085
18. Woods DB, Vousden KH 2001 Regulation of p53 function. Exp Cell Res 264:56-66
19. Sengupta S, Wasylyk B 2004 Physiological and pathological consequences of the interactions of the p53 tumor suppressor with the glucocorticoid, androgen, and estrogen receptors. Ann N Y Acad Sci 1024:54–71
20. Bonofiglio D, Gabriele S, Aquila S, Catalano S, Gentile M, Middea E, Giordano F, Andò S 2005 Estrogen Receptor alpha binds to Peroxisome Proliferator-Activated Receptor (PPAR) Response Element and negatively interferes with PPAR gamma signalling in breast cancer cells. Clin Cancer Res 11:6139-6147

21. Patel L, Pass I, Coxon P, Downes CP, Smith SA, Macphee CH 2001 Tumor suppressor and anti-inflammatory actions of PPARγ agonist are mediated via upregulation of PTEN. Curr Biol 11:764-768
22. Clay CE, Namen AM, Atsumi G, Willingham MC, High KP, Kute TE, Trimboli AJ, Fonteh AN, Dawson PA, Chilton FH 1999 Influence of J series prostaglandins on apoptosis and tumorigenesis of breast cancer cells. Carcinogenesis 20:1905-1911
23. Hehner SP, Heinrich M, Bork PM, Vogt M, Ratter F, Lehmann V, Schulze-Osthoff K, Droge W, Schmitz ML 1998 Sesquiterpene lactones specifically inhibit activation of NF-kappa B by preventing the degradation of I kappa B-alpha and I kappa B-beta. J Biol Chem 273:1288-1297
24. Cohen GM 1997 Caspases: the executioners of apoptosis. Biochem J 326:1-16
25. Brockman JA, Gupta RA, Dubois RN 1998 Activation of PPAR gamma leads to inhibition of anchorage-independent growth of human colorectal cancer cells. Gastroenterology 115:1049-1055
26. Han C, Demetris AJ, Michalopoulos GK, Zhan Q, Shelhamer JH, Wu T 2003 PPARgamma ligands inhibit cholangiocarcinoma cell growth through p53-dependent GADD45 and p21 pathway. Hepatology 38:167-177
27. Nagamine M, Okumura T, Tanno S, Sawamukai M, Motomura W, Takahashi N, Kohgo Y 2003 PPAR gamma ligand-induced apoptosis through a p53-dependent mechanism in human gastric cancer cells. Cancer Sci 94:338-343
28. Okura T, Nakamura M, Takata Y, Watanabe S, Kitami Y, Hiwada K 2000 Troglitazone induces apoptosis via the p53 and Gadd45 pathway in vascular smooth muscle cells. Eur J Pharmacol 407:227-235
29. Di Cristofano A, Pandolfi PP 2000 The multiple roles of PTEN in tumor suppression. Cell 100:387-390

30. Yamada KM, Araki M 2001 Tumor suppressor PTEN: modulator of cell signaling, growth, migration and apoptosis. J Cell Sci 114:2375-2382
31. Stambolic V, MacPherson D, Sas D, Lin Y, Snow B, Jang Y, Benchimol S, Mak TW 2001 Regulation of PTEN transcription by p53. Mol Cell 8:317-325
32. Qin C, Nguyen T, Stewart J, Samudio I, Burghardt R, Safe S 2002 Estrogen up-regulation of p53 gene expression in MCF-7 breast cancer cells is mediated by calmodulin kinase IV-dependent activation of a nuclear factor kappaB/CCAAT-binding transcription factor-1 complex. Mol Endocrinol 16:1793-1809
33. Fujioka S, Schmidt C, Sclabas GM, Li Z, Pelicano H, Peng B, Yao A, Niu J, Zhang W, Evans DB, Abbruzzese JL, Huang P, Chiao PJ 2004 Stabilization of p53 is a novel mechanism for proapoptotic function of NF-kappaB. J Biol Chem 279:27549-27559
34. Chung SW, Kang BY, Kim SH, Pak YK, Cho D, Trinchieri G, Kim TS 2000 Oxidized low density lipoprotein inhibits interleukin-12 production in lipopolysaccharide-activated mouse macrophages via direct interactions between peroxisome proliferator-activated receptor-gamma and nuclear factor-kappa B. J Biol Chem 275:32681-32687
35. Coutureir C, Brouillet A, Couriaud C, Koumanov K, Bereziat G, Andreani M 1999 Interleukin 1β induces type II-secreted phospholipase A_2 gene in vascular smooth muscle cells by a nuclear factor kB and peroxisome proliferator-activated receptor-mediated process. J Biol Chem 274:23085-23093
36. Sun YX, Wright HT, Janciasukiene S 2002 α1-Antichymotrypsin/Alzheimer's peptide Aβ (1–42) complex perturbs lipid metabolism and activates transcription factors PPARγ and NF*k*B in human neuroblastoma (Kelly) cells. J Neurosci Res 67:511-522

37. Ikawa H, Kameda H, Kamitani H, Baek SJ, Nixon JB, Hsi LC, Eling TE 2001 Effect of PPAR activators on cytokine-stimulated cyclooxygenase-2 expression in human colorectal carcinoma cells. Exp Cell Res 267:73-80
38. Schlezinger JJ, Jensen BA, Mann KK, Ryu HY, Sherr DH 2002 Peroxisome proliferator-activated receptor gamma-mediated NF-kappa B activation and apoptosis in pre-B cells. J Immunol 169:6831-6841
39. Oren M, Damalas A, Gottlieb T, Michael D, Taplick J, Leal JF, Maya R, Moas M, Seger R, Taya Y, Ben-Ze'Ev A 2002 Regulation of p53: intricate loops and delicate balances. Ann N Y Acad Sci 973:374-383
40. Schuler M, Green DR 2001 Mechanisms of p53-dependent apoptosis Biochem Soc Trans 29:684–688
41. Maggiolini M, Donzé O, Picard D 1999 A non-radioactive method for inexpensive quantitative RT-PCR. Biol Chem 380:695-697
42. Andrews NC, Faller DV 1991 A rapid micropreparation technique for extraction of DNA-binding proteins from limiting numbers of mammalian cells. Nucleic Acids Res 19:2499

ACKNOWLEDGMENTS

Our thanks to Dr. Stephen H. Safe to provide us the human p53 gene promoter and the deletion mutants, to Moshe Oren and R.M. Evans for the gifts of the p53 antisense and PPARγ expression plasmid, respectively. We also thank D. Sturino (Faculty of Pharmacy, University of Calabria – Italy) for the English review. This work was supported by Associazione Italiana Ricerca sul Cancro (AIRC), Ministero dell'Istruzione Università e Ricerca and Ministero della Salute.

FIGURE LEGENDS

Table 1 BRL induces G_0/G_1 arrest of cell cycle progression in MCF7 cells. MCF7 cells were treated as indicated. DNA was stained with 100 μg/ml propidium iodide for 30 minutes at 4 °C protected from light and then the cells were analyzed with the FACScan (Becton, Dickinson, NJ). Each data point represents the percentage of three independent experiments performed in triplicate. The data are presented as mean ± S.D. *p<0.05 and **p<0.01 BRL-treated *vs* untreated cells.

Figure 1 BRL up-regulates p53 and $p21^{WAF1/Cip1}$ mRNA expression in MCF7 cells. Semiquantitative RT-PCR evaluation of p53 and $p21^{WAF1/Cip1}$ mRNAs expression. MCF7 cells were treated for 24 **(A)** and 48 **(B)** hours with increasing concentrations of BRL as indicated, 10 μM GW alone or in combination with 1 μM BRL. 36B4 mRNA levels were determined as control. The *side panels* show the quantitative representation of data (mean ± S.D.) of three independent experiments after densitometry and correction for 36B4 expression. *p<0.05 and **p<0.01 BRL-treated *vs* untreated cells

Figure 2 BRL up-regulates p53 and $p21^{WAF1/Cip1}$ protein expression in MCF7 cells. Immunoblots of p53 and $p21^{WAF1/Cip1}$ from MCF7 cells extracts treated for 24 h (**A**) and 48 (**B**) with increasing BRL concentrations, 10 μM GW alone or in combination with 1 μM BRL. β-actin was used as loading control. The *side panels* show the quantitative representations of data (mean ± S.D.) of three independent experiments performed for each condition. * p<0.05 and **p<0.01 BRL-treated *vs* untreated cells

Figure 3 Effects of BRL on p53-gene promoter-luciferase reporter constructs in MCF7 cells. **A**: Schematic map of the p53 promoter fragments used in this study. **B:** MCF7 cells were transiently transfected with p53 gene promoter-luciferase reporter construct (p53-1) and treated for 24 hours with increasing BRL concentrations, 10 μM GW alone or in combination with 1 μM BRL. **C**: MCF7 cells were transiently transfected with p53 gene promoter-luc reporter constructs (p53-1,

p53-6, p53-13, p53-14) and treated for 24 hours with 1 μM BRL and/or 10 μM GW. The luciferase activities were normalized to the Renilla luciferase as internal transfection control and data were reported as RLU values. Columns are mean ± S.D. of three independent experiments performed in triplicate. *p<0.05 BRL-treated *vs* untreated cells. pGL_2: basal activity measured in cells transfected with pGL_2 basal vector; RLU, Relative Light Units. CTF-1, CCAAT-binding transcription factor-1; NF-Y, nuclear factor-Y; NF*k*B, nuclear factor *k*B.

Figure 4 PPARγ binds to NF*k*B site in the p53 promoter region in EMSA.

A: Nuclear extracts from MCF7 cells (lane 1) or 2 μl of PPARγ translated protein (lane 6) were incubated with a double-stranded NF*k*B sequence probe labeled with [γ^{32}P] and subjected to electrophoresis in a 6% polyacrylamide gel. Competition experiments were performed adding as competitor a 100-fold molar excess of unlabeled NF*k*B probe (lanes 2 and 7) or as cold competitor PPRE (lane 8). In lane 3, nuclear extracts from MCF7 were treated with 10 μM BRL. Anti-PPARγ and anti-NF*k*B Abs were incubated with nuclear extracts from MCF7 cells treated with 10 μM BRL (lanes 4 and 5, respectively) or added to PPARγ protein (lanes 9 and 10, respectively). Lane 11 contains probe alone, lane 12 contains 2 μl of unprogrammed rabbit reticulocyte lysate incubated with NF*k*B (URRL). **B:** 1 μl of NF*k*B protein (lane 1) was incubated with a double-stranded NF*k*B sequence probe labeled with [γ^{32}P] and subjected to electrophoresis in a 6% polyacrylamide gel. A 100-fold molar excess of unlabeled NF*k*B probe (lanes 2) or anti-NF*k*B antibody (lane 3) was added to NF*k*B protein.

Figure 5 Functional interaction of PPARγ and p53 in ChIP assay. MCF7 cells were treated for 1 hour with 10 μM BRL, 10 ng/ml TGFβ, 15 μM Parthenolide (P), as indicated. The soluble chromatin was immunoprecipitated with anti-PPARγ, anti-NFkB and anti-RNA Pol II antibodies. The p53 promoter sequence including the NF*k*B site (panel A) and that located upstream the NF*k*B

site (panel B) were detected by PCR with specific primers, as described in *Materials and Methods*. To control input DNA, p53 promoter was amplified from 30 μl of initial preparations of soluble chromatin (before immunoprecipitations). Normal rabbit antiserum was used as negative control (N).

Figure 6 BRL induces cleavage of caspase-9 and DNA laddering. **A:** MCF7 cells were treated with BRL alone or in combination with GW or parthenolide (P) for 48-h as indicated, or transfected with an expression plasmid encoding for p53 antisense (AS/p53). Positions of procaspase-9 and its cleavage products are indicated by *arrowheads* to the *right*. One of three similar experiments is presented. β-actin was used as loading control on the same stripped blot. **B:** p53 protein expression (evaluated by WB) in MCF7 cells transfected with an empty vector (v) or a AS/p53 and treated as indicated. β-actin was used as loading control. **C**: NF*k*B expression in MCF7 cells untreated or treated with P as indicated. β-actin was used as loading control. **D**: DNA laddering was performed in MCF7 cells treated for 72-h as indicated, or transfected with AS/p53.

Table 1

Treatment	μM	Cell cycle phase (%)		
		G_0 - G_1	S	G_2 - M
C		53 ± 7.2	30 ± 4.4	17 ± 2.1
BRL	1	67* ± 7.4	20* ± 3.3	13 ± 2.2
BRL	10	76* ± 8.1	14* ± 3.1	10* ± 2.6
BRL	50	82** ± 8.3	10** ± 2.4	8** ± 1.2
GW	10	54 ± 6.5	29 ± 3.5	17 ± 2.1
BRL + GW	1+10	53 ±6.1	29 ± 3.2	18 ± 2.3

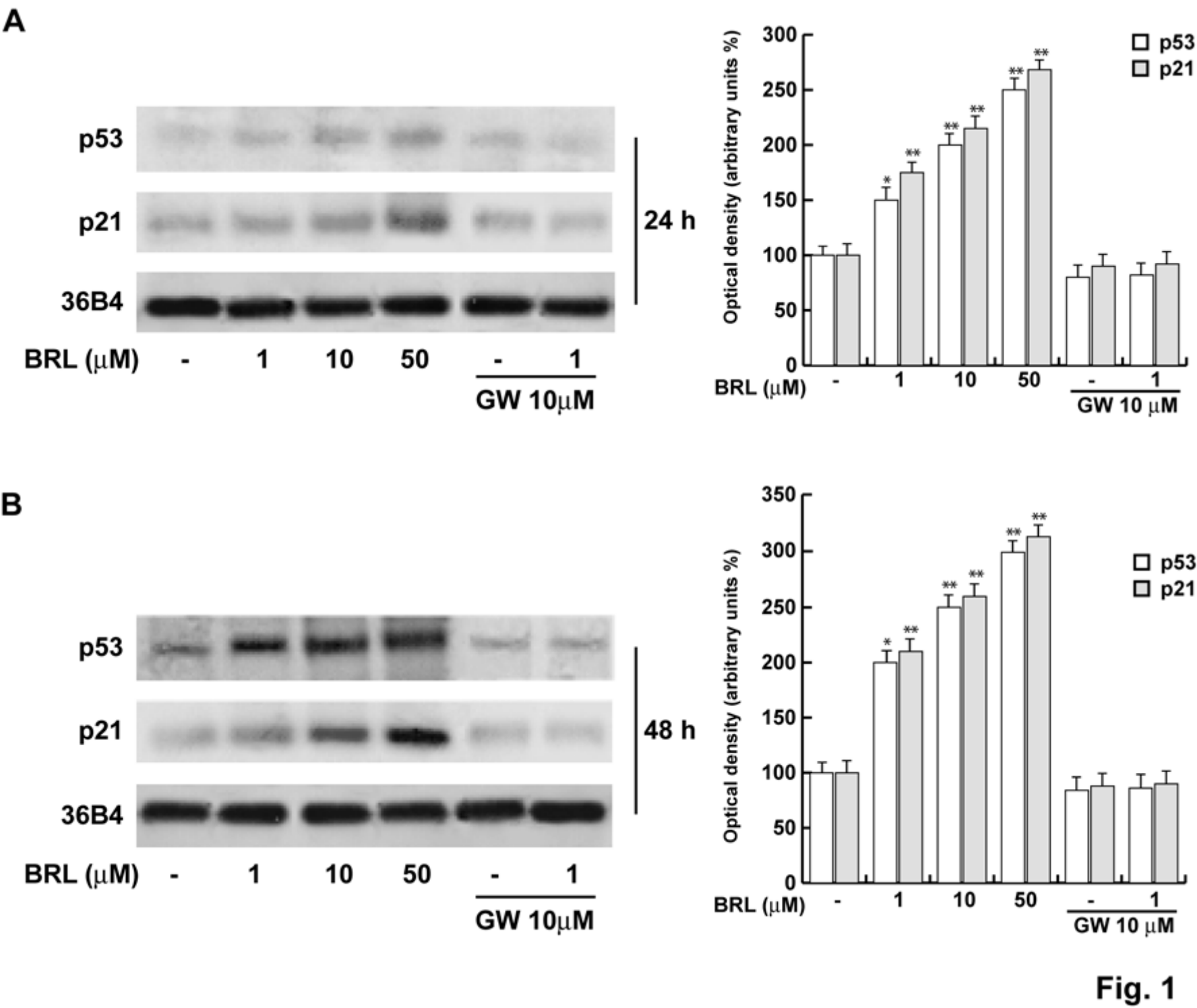
A
p53
p21
36B4
24 h
BRL (μM) - 1 10 50 - 1
GW 10μM
Optical density (arbitrary units %)
300
250
200
150
100
50
0
p53
p21
*
**
BRL (μM) - 1 10 50 - 1
GW 10 μM
B
p53
p21
36B4
48 h
BRL (μM) - 1 10 50 - 1
GW 10μM
Optical density (arbitrary units %)
350
300
250
200
150
100
50
0
p53
p21
*
**
BRL (μM) - 1 10 50 - 1
GW 10 μM

Fig. 1

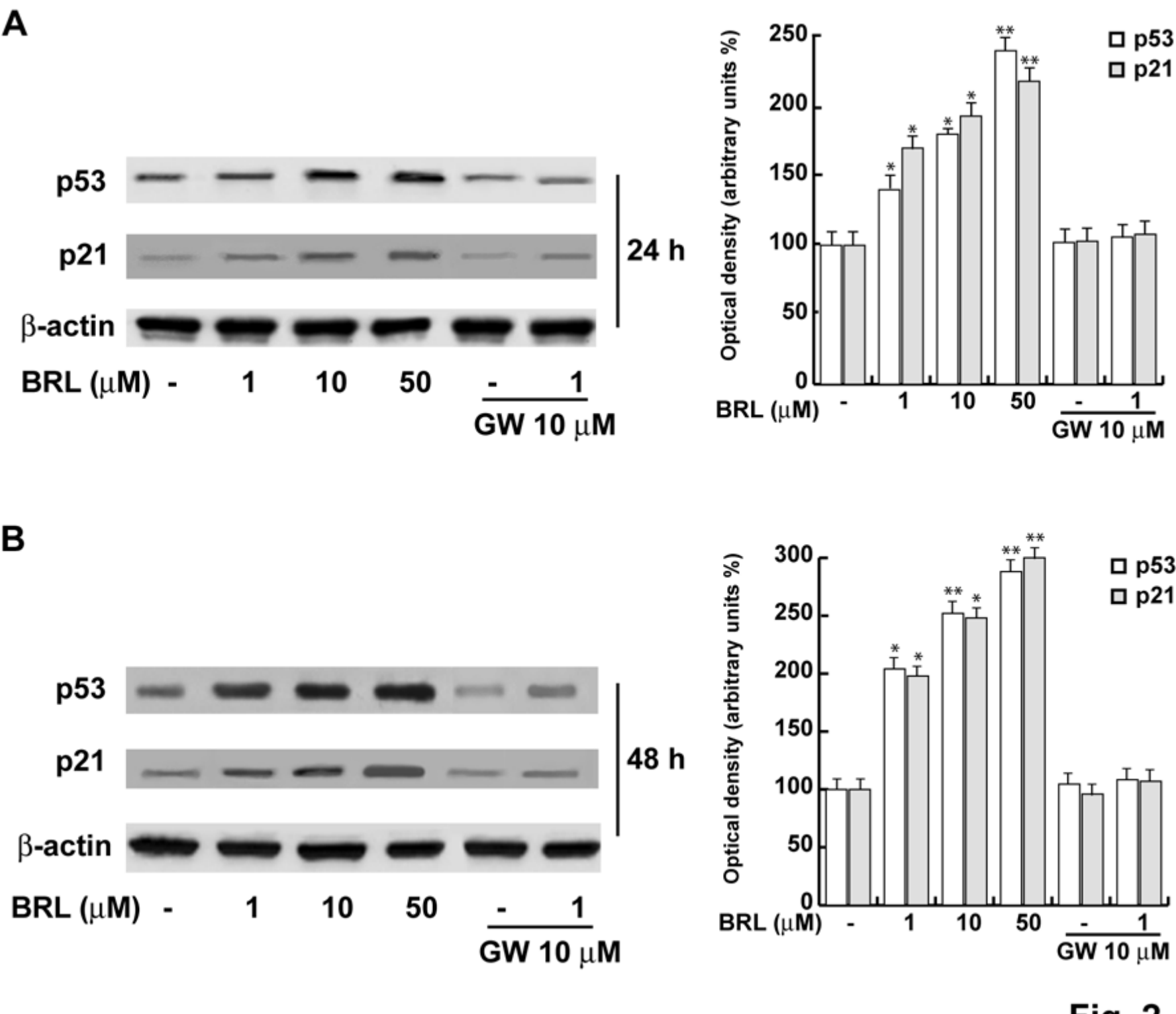
A
p53
p21
β-actin
24 h
BRL (μM) - 1 10 50 - 1
GW 10 μM
Optical density (arbitrary units %)
250
200
150
100
50
0
p53
p21
BRL (μM) - 1 10 50 - 1
GW 10 μM
B
p53
p21
β-actin
48 h
BRL (μM) - 1 10 50 - 1
GW 10 μM
Optical density (arbitrary units %)
300
250
200
150
100
50
0
p53
p21
BRL (μM) - 1 10 50 - 1
GW 10 μM

Fig. 2

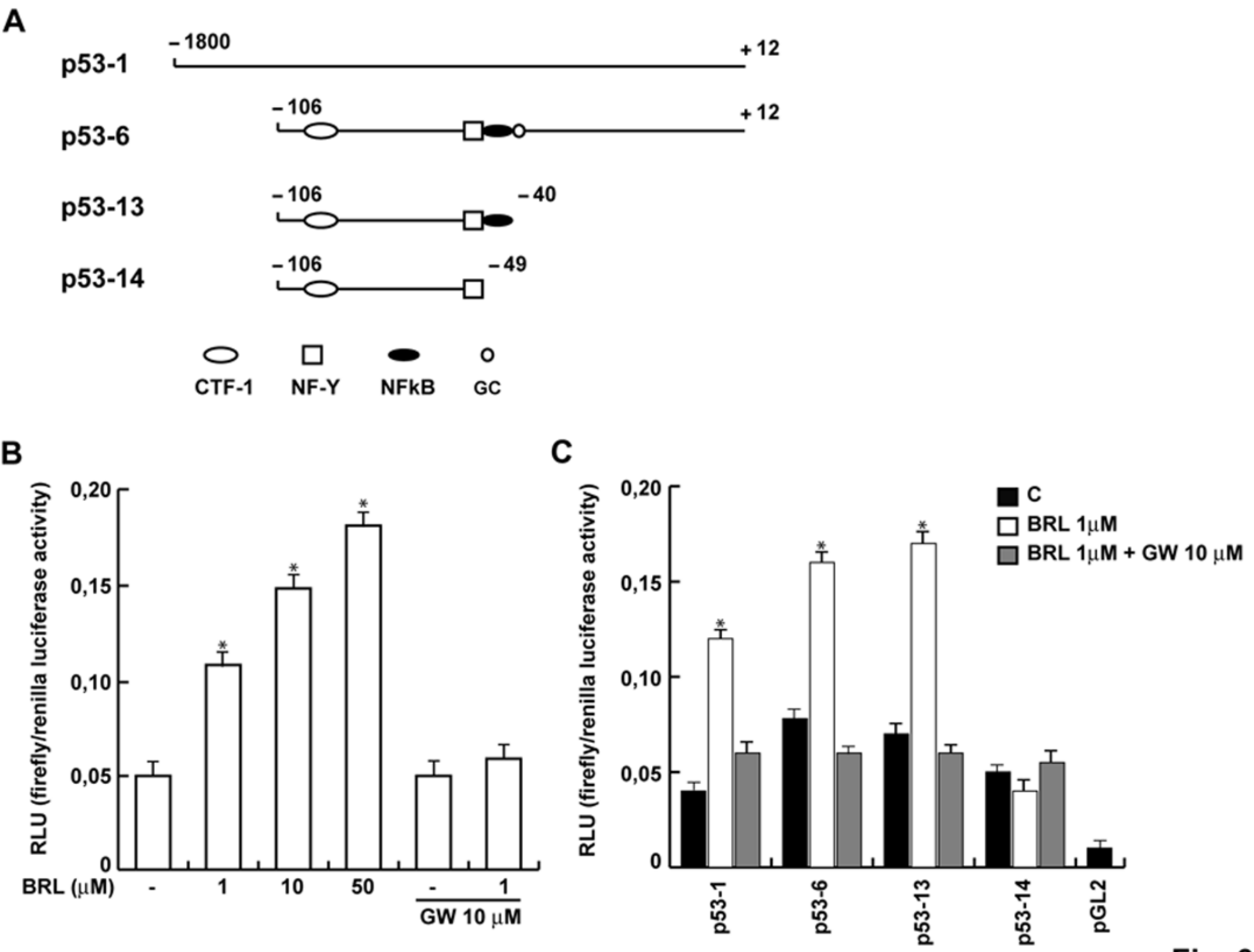
A
p53-1
−1800
+12
p53-6
−106
+12
p53-13
−106
−40
p53-14
−106
−49
CTF-1
NF-Y
NFkB
GC
B
RLU (firefly/renilla luciferase activity)
0,20
0,15
0,10
0,05
0
BRL (μM)
-
1
10
50
-
1
GW 10 μM
C
RLU (firefly/renilla luciferase activity)
0,20
0,15
0,10
0,05
0
C
BRL 1μM
BRL 1μM + GW 10 μM
p53-1
p53-6
p53-13
p53-14
pGL2

Fig. 3

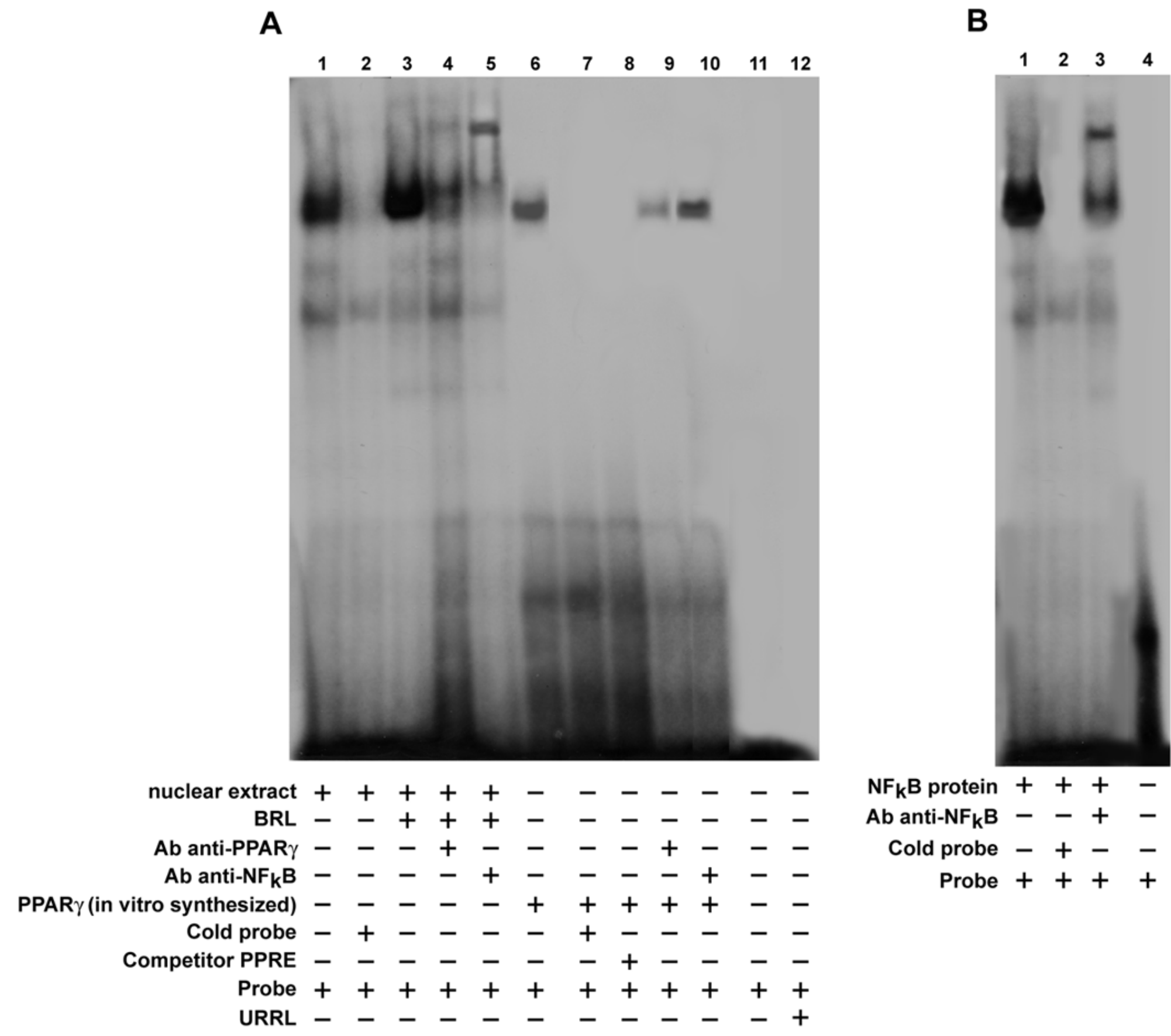
A
1 2 3 4 5 6 7 8 9 10 11 12
nuclear extract + + + + + − − − − − − −
BRL − − + + + − − − − − − −
Ab anti-PPARγ − − − + − − − − + − − −
Ab anti-NFkB − − − − + − − − − + − −
PPARγ (in vitro synthesized) − − − − − + + + + + − −
Cold probe − + − − − − + − − − − −
Competitor PPRE − − − − − − − + − − − −
Probe + + + + + + + + + + + +
URRL − − − − − − − − − − − +
B
1 2 3 4
NFkB protein + + + −
Ab anti-NFkB − − + −
Cold probe − + − −
Probe + + + +

Fig. 4

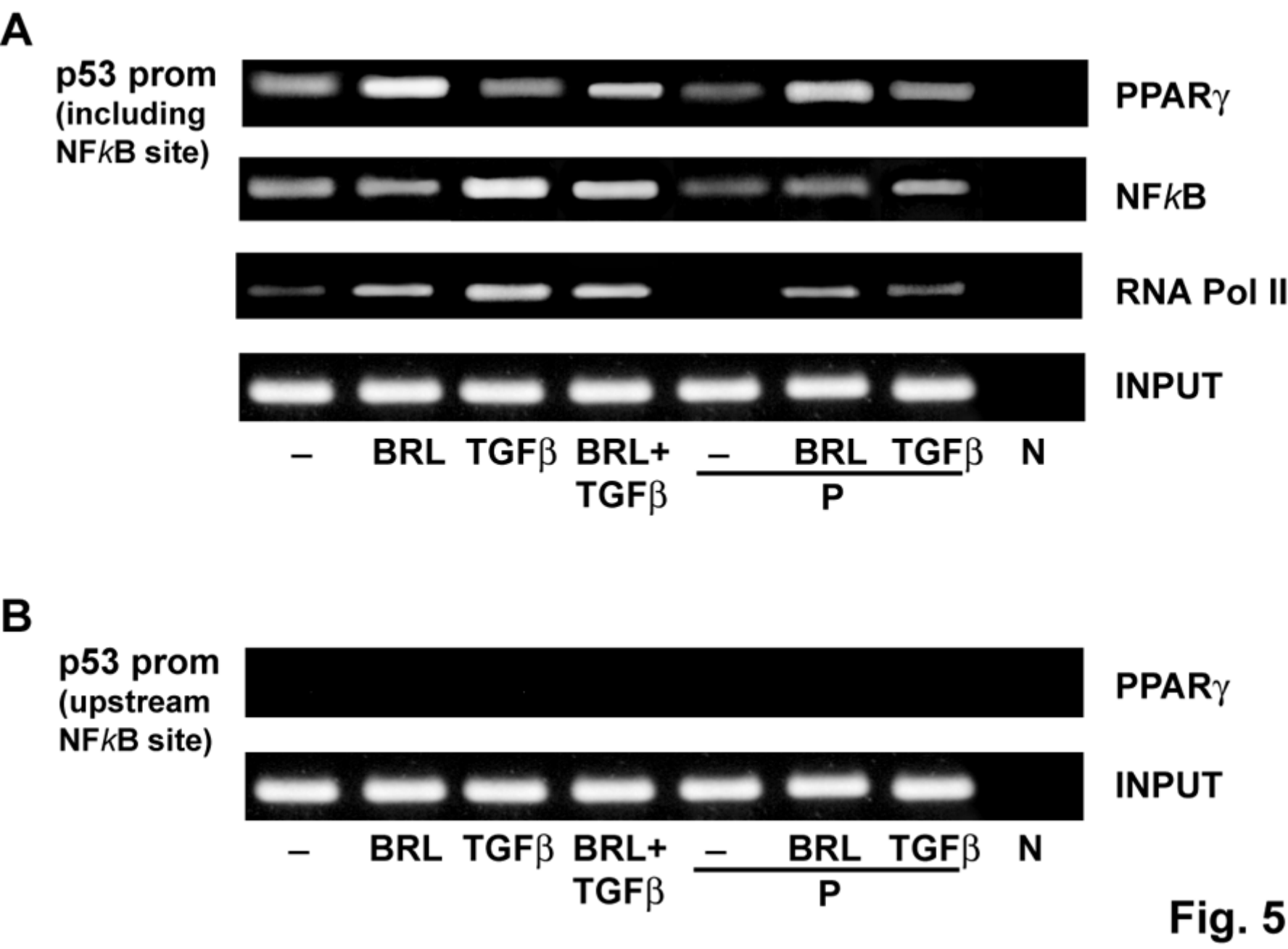
A
p53 prom
(including
NFkB site)
PPARγ
NFkB
RNA Pol II
INPUT
–
BRL
TGFβ
BRL+
TGFβ
–
BRL
TGFβ
N
P
B
p53 prom
(upstream
NFkB site)
PPARγ
INPUT
–
BRL
TGFβ
BRL+
TGFβ
–
BRL
TGFβ
N
P

Fig. 5

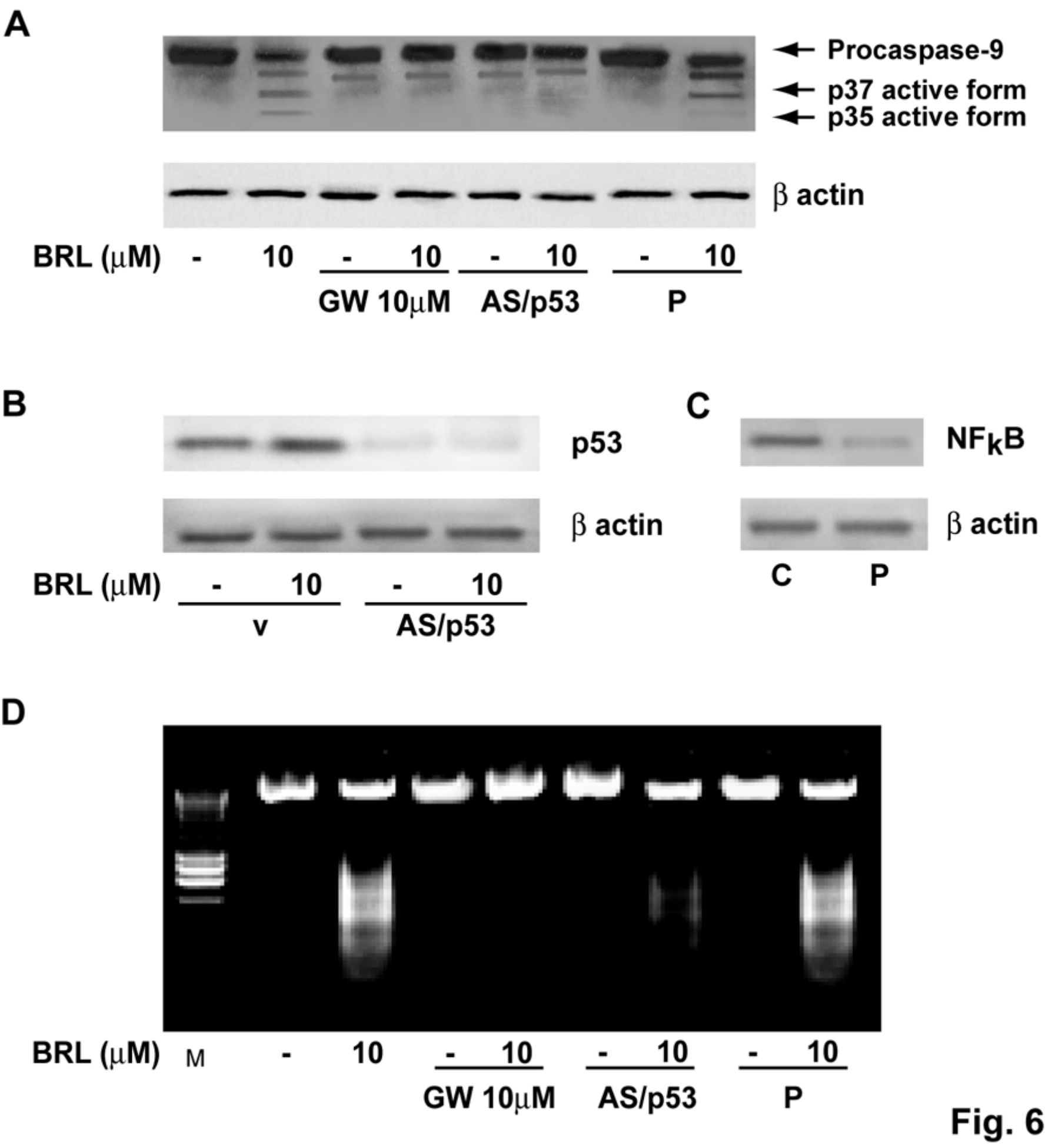
A
Procaspase-9
p37 active form
p35 active form
β actin
BRL (μM) - 10 - 10 - 10 - 10
GW 10μM
AS/p53
P
B
p53
β actin
BRL (μM) - 10 - 10
v
AS/p53
C
NFkB
β actin
C
P
D
BRL (μM) M - 10 - 10 - 10 - 10
GW 10μM
AS/p53
P

Fig. 6

FEBS Letters 580 (2006) 2371–2380

Evidence that low doses of Taxol enhance the functional transactivatory properties of p53 on p21 waf promoter in MCF-7 breast cancer cells

M. Luisa Panno[a,*], Francesca Giordano[a], Fabrizia Mastroianni[b], Catia Morelli[b], Elvira Brunelli[c], M. Grazia Palma[b], Michele Pellegrino[b], Saveria Aquila[b], Antonella Miglietta[d], Loredana Mauro[a], Daniela Bonofiglio[b], Sebastiano Andò[a,b,*]

[a] *Department of Cellular Biology, University of Calabria, Ponte Pietro Bucci, Cubo 4C, 87030, Arcavacata di Rende, Cosenza, Italy*
[b] *Faculty of Pharmacy, University of Calabria, 87030, Arcavacata di Rende, Cosenza, Italy*
[c] *Department of Ecology, University of Calabria, Arcavacata di Rende, Cosenza, Italy*
[d] *Department of Experimental Medicine and Oncology, University of Torino, Turin, Italy*

Received 10 January 2006; revised 10 March 2006; accepted 14 March 2006

Available online 29 March 2006

Edited by Varda Rotter

Abstract In the present study, we evidence how in breast cancer cells low doses of Taxol for 18 h determined the upregulation of p53 and p21 waf expression concomitantly with a decrease of the anti-apoptotic Bcl-2. P53 and its gene product, the mdm2 protein, in treated cells exhibits a prevalent nuclear compartmentalization, thus potentiating p53 transactivatory properties. Indeed, the most important finding of this study consists with the evidence that Taxol at lower concentrations is able to produce the activation of p21 promoter via p53. Prolonged exposure of MCF-7 cells to Taxol (48 h) resulted in an increased co-association between p21 and PCNA compared to control and this well fits with the simultaneous block of cell cycle into the G2/M phase.

Keywords: Taxol; p21 waf; p53; Breast cancer cells

1. Introduction

Taxol is a chemotherapic drug specifically effective against prostate, ovarian, breast and lung cancer. Its primary mechanism of action is related to the ability to stabilize the microtubules and to disrupt their dynamic equilibrium [1–6].

Treatment of cells with Taxol interferes with the normal reorganization of the microtubule network, and inhibits the formation of normal spindle at metaphase required for mitosis and cell proliferation. These effects lead to an arrest of the cells in the G2/M phase of the cell cycle and eventually to apoptotic cell death [7–9].

The biological responses to Taxol may vary depending on cell type and drug concentration.

An aspect extremely intriguing rises from the evidence that low doses of Taxol in human lung cancer, though still unable to alter all microtubule network, upregulate p53 and its nuclear compartmentalization [10]. Indeed, the polymerization of microtubules with the extension of their minus end, induced by Taxol, may facilitate the translocation of p53, using dynein as carrier, from the cytosol into the nucleus [10,11].

In this compartment, p53 stimulates the expression of proteins involved in a wide network of signals that act through two major apoptotic pathways: the extrinsic death receptor signalling which triggers caspases activation and Bid cleavage, and the intrinsic mitochondrial pathway, which shifts the balance in the Bcl-2 family towards the pro-apoptotic members, enhancing mitochondrial permeabilization with consequent release of cytochrome *c* and direct caspases activation [12]. These events have been previously reported in human neuroblastoma, ovarian and breast carcinoma cells that underwent Taxol treatment [13–15].

Taxol-initiated apoptosis has been also associated with increase of p21 waf/Cip protein, a key regulator of cell cycle and DNA synthesis, which expression is regulated by p53-dependent and/or independent mechanisms [16–19].

P21 binds to various cyclin–CDK complexes and inhibits their activity, thus resulting in a block in cell cycle [20]. An alternative mechanism through which p21 inhibits cell cycle progression lays on its capability to recruit PCNA, then enabling this factor to interact with the DNA polymerase δ and ε activities [21,22].

In the present study, we have explored if low doses of Taxol "per se" are able to enhance the transactivatory properties of p53 producing the upregulation of p53-classically dependent gene, such as p21 waf, involved in the regulation of cell apoptosis and in the progression of cell cycle.

2. Materials and methods

2.1. Materials

DMEM/Ham's F-12, L-glutamine, penicillin/streptomycin, calf serum (CS), bovine serum albumin, aprotinin, leupeptin, phenylmethylsulfonyl fluoride (PMSF), sodium orthovanadate and Taxol were purchased from Sigma (Milan, Italy). FuGENE 6 was from Roche

*Corresponding authors. Fax: +39 0984 492911 (M.L. Panno), +39 0984 496203 (S. Andò).
E-mail addresses: mamissina@yahoo.it (M.L. Panno), sebastiano.ando@unical.it (S. Andò).

0014-5793/$32.00
doi:10.1016/j.febslet.2006.03.055

Applied Science (Milan, Italy). Dual luciferase kit and TK Renilla luciferase plasmid were provided by Promega (Madison, WI). [γ^{32}P]-ATP and ECL system come from Amersham Biosciences.

The plasmid WWP-Luc containing human p21 waf promoter (2.4 kb) was kindly given by Dr. Wafik El-Deiry (Howard Hughes Medical Institute, Philadelphia); pCMV-wt p53 plasmid, pCMV-p53 plasmid mutant and pCMV empty vector were generously provided by Dr. G. Daniel (Department of Health and Human Service, Natl. Inst. Env. Health Sci., Res. Triangle Park, NC). Thin layer chromatography (TLC) aluminium sheets were from MERK (Milan, Italy).

2.2. Cell lines and culture conditions

Human breast cancer MCF-7 cell line was cultured in DMEM/Ham's F12 (1:1) medium supplemented with 5% CS, 1% L-glutamine and 1% penicillin/streptomycin. The cells were cultured in phenol-red-free DMEM (PRF-SFM-DMEM) containing 0.5% bovine serum albumin, 1% L-glutamine and 1% penicillin/streptomycin, 24 h before each experiment. Next, the 70% confluent cells, synchronized in PRF-SFM-DMEM (day 0) [23] were treated with different doses of Taxol (2, 6, 12, 50, 100 nM) for 18 and 48 h.

2.3. Cell viability

The viability of the cells was assessed by morphological analysis using trypan blue exclusion assay. Cells in the exponential growth phase were plated and grown overnight; then, the medium was changed and shifted for 24 h with PRF-SFM-DMEM. At the end of this incubation the cells were exposed for 18 and 48 h to different concentrations of Taxol, as reported in Fig. 1. Cells were trypsinized and incubated in a 0.5% trypan blue solution for 10 min at room temperature and viable numbers were determined microscopically by counting trypan blue negative cells in a counting chamber (Burker, Brand, Germany).

2.4. Transfections and luciferase assay

MCF-7 cells were seeded (1×10^5 cells/well) in DMEM/F12 supplemented with 5% CS in 24-well plates. Cells were co-transfected with the plasmid WWP-Luc containing human p21 waf promoter and pCMV-empty vector or pCMV-p53 mutant plasmid or pCMV-wt p53 plasmid, in SFM using FuGENE6 according to the manufacture's instructions with a mixture containing 0.1 μg/well of each specific plasmid and 25 ng/well of TK Renilla luciferase plasmid. 24 h after the transfection the medium was changed and the cells were treated in PRF-SFM-DMEM in the presence of 2, 6 and 12 nM of Taxol for 18 h. The firefly and Renilla luciferase activities were measured by using a dual luciferase kit. The firefly luciferase data for each sample were normalized on the basis of the transfection efficiency measured by Renilla luciferase activity.

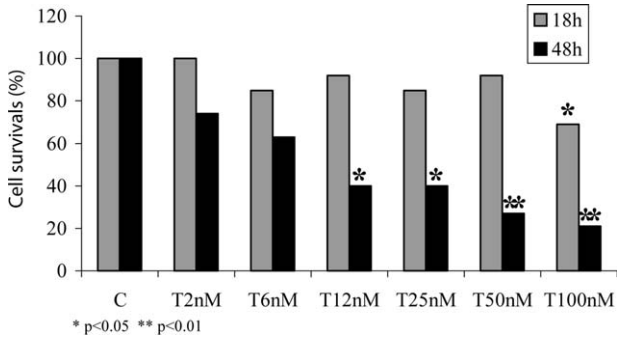

Fig. 1. Cell viability of MCF-7 cells after Taxol treatment. MCF-7 cells were plated in six-well plates at a density of 2×10^5 cells/well and grown 24 h to be completely attached to the surface of the plates. The day after, the medium was switched to serum-free medium for 24 h. Next, the cells were added of different doses of Taxol ranging from 2 nM until 100 nM and incubated for 18 and 48 h. Values are the average of four triplicate independent experiments, and are expressed as percentage of the controls, determined by standardizing untreated cells to 100%. $^{*}P < 0.05$ $^{**}P < 0.01$ as compared to untreated cells. The S.D. was lower than 0.25%.

2.5. Immunoprecipitation and Western blotting

MCF-7 cells were grown in 100 mm dishes to 70–80% confluence, shifted to SFM for 24 h and lysed. Cytoplasmic protein lysates were obtained with a buffer containing 50 mM HEPES, pH 7.5, 150 mM NaCl, 1.5 mM $MgCl_2$, 10 mM EGTA, pH 7.5, 10% glycerol, 1% Triton X-100 and protease inhibitors (2 μM Na_3VO_4, 1% PMSF, 20 μg/ml aprotinin). Following the collection of cytoplasmic proteins, the nuclei were lysed with the buffer containing 20 mM KOH–HEPES, pH 8, 0.1 mM EDTA, 5 mM $MgCl_2$, 0.5 M NaCl, 20% glycerol, 1% Np-40 and inhibitors (as above) [24].

The association of PCNA (Proliferating Cell Nuclear antigen) and p21 waf/Cip and/or phospho p21 (Thr 145) proteins was assessed by immunoprecipitation (IP) and Western blotting (WB) in 500 μg protein lysates using appropriate antibodies (as specified in the figure legends), while the association of dynein and p53 proteins was determined by immunoprecipitating the nuclear fractions with anti-dynein antibody and then blotting for anti-p53 antibody and anti-β-tubulin. In IPs, protein lysates were incubated in HNTG buffer (20 mM HEPES, pH 7.5, 150 mM NaCl, 0.1% Triton X-100, 10% glycerol and 0.2 mM Na_3VO_4) at 4 °C for 4 h with the primary antibodies, and then agarose beads conjugated with Protein A/G Agarose (Sigma) were added for another 1 h. The immunoprecipitated proteins were washed three times with the HNTG buffer and separated by SDS–PAGE (polyacrylamide gel electrophoresis).

The expression of different proteins was tested by WB in 50 μg of protein lysates or in 500 μg of immunoprecipitated cell proteins using an anti-p21 WAF, anti-phospho-p21 waf (Thr 145), anti-PCNA, anti-p53, anti-mdm2, anti β-actin, anti-p85, anti-Lamin B, anti-GAP-DH, anti-β-tubulin and anti-dynein pAbs from Santa Cruz Biotechnology (Heidelberg, Germany), anti-phospho-Akt (Ser 473), anti phospho p-Bcl-2 (Ser 70), anti-pBcl-2 and anti-caspase-9 pAbs from Cell Signaling Technology (Beverly, MA, USA).

Proteins were transferred to a nitrocellulose membrane, probed with primary antibody and then stripped and reprobed with the appropriate antibodies. The antigen–antibody complex was detected by incubation of the membranes for 1 h at room temperature with a peroxidase-coupled anti-IgG antibody and revealed using the ECL system. Blots were then exposed to film and bands of interest were quantified by densitometer (Mod 620 BioRad). The results obtained were expressed in term of arbitrary densitometric units.

2.6. Immunofluorescent microscopy

50% confluent cultures, grown on coverslips, were shifted to SFM for 24 h and then treated either for 18 or 48 h with 2, 6 or 50 nM of Taxol. Cells were then fixed in 4% paraformaldehyde, permeabilized with 0.2% Triton X-100, washed three times with PBS, and incubated for 1 h with a mixture of primary Abs recognizing p53 and p21. The anti-p53 monoclonal Ab (mAb) (Santa Cruz) at 2 mg/ml was used for p53 staining; anti p21 polyclonal Ab (pAb) (Santa Cruz) at 2 mg/ml was used to detect p21. Following the incubation with primary Abs, the slides were washed three times with PBS, and incubated with a mixture of two secondary Abs, each 1 mg/ml concentrated. A rhodamine-conjugated donkey anti-mouse IgG (Calbiochem) was used as a secondary Ab for p53 and a fluorescein-conjugated donkey anti-rabbit IgG (Calbiochem) was used for p21. The cellular localization of p53 and p21 was studied with confocal microscope with 1000× magnification. The optical sections were taken at the central plane.

2.7. FACS analysis

Serum-starved cells for 24 h were given Taxol for 18 and 48 h at the doses reported in the figures. After this incubation cells were trypsinized, washed with PBS and fixed for 1 h in ice-cold 70% ethanol. The samples were then washed once with PBS and resuspended in 1 ml of staining solution (10 mg/ml RNasi A, 10 mg/ml propidium iodide in PBS). The samples were then incubated at room temperature in the dark for at least 30 min. FACS analysis was performed using CellFeet software (Becton Dickinson, NJ). At least 2×10^4 cells/sample were measured.

2.8. PI-3 kinase activity

PI-3K activity associated with p85, was assessed by standard protocol provided by the manufacturer of the p85 antibody (Upstate Biotechnology). Briefly, p85 was IP from 500 μg of protein lysate with an anti-p85 p-Ab, the negative control was performed using a cell lysate where p110 catalyzing subunit of PI3K, was previously removed by pre-

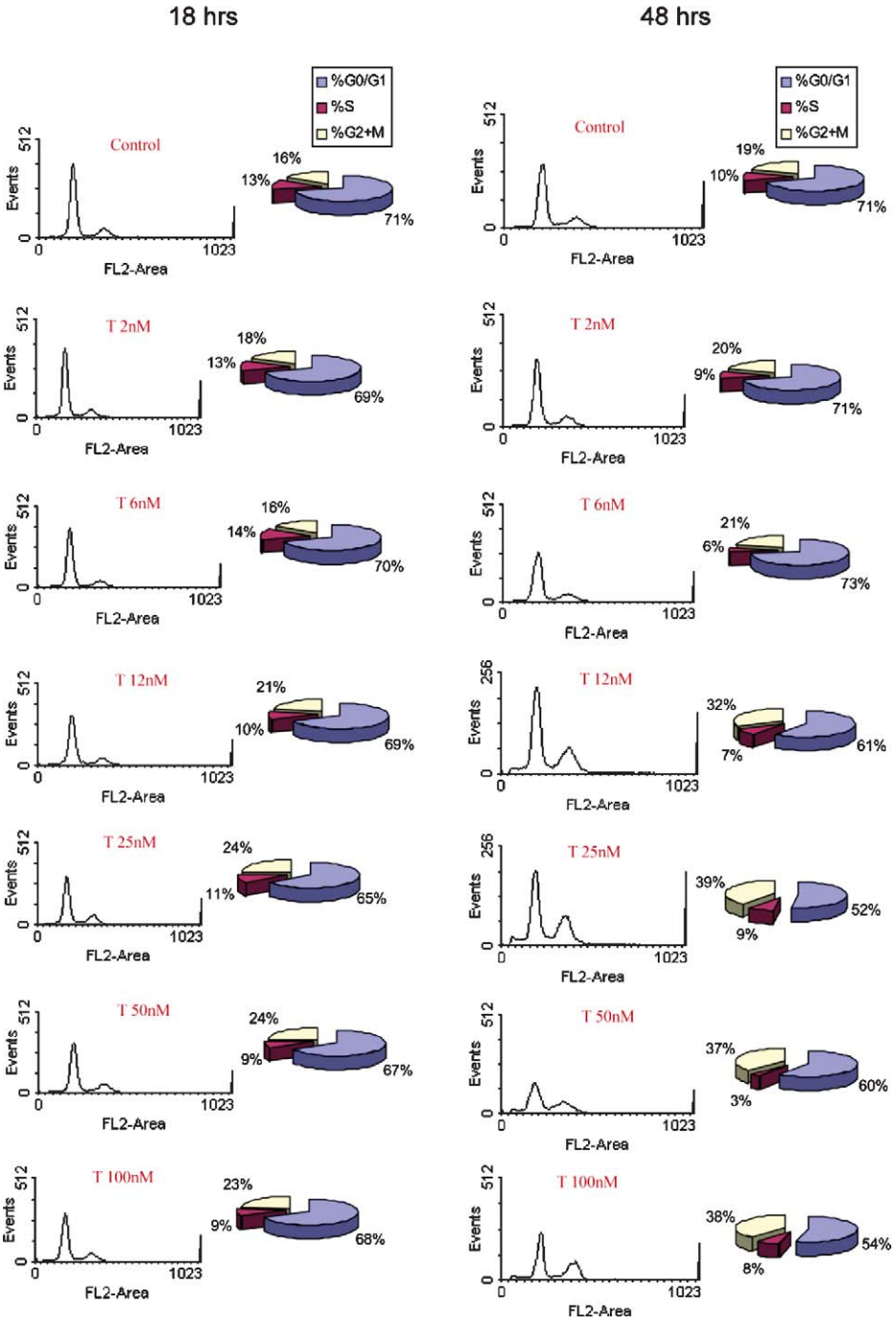

Fig. 2. Effect of different doses of Taxol on cell cycle progression of MCF-7 breast cancer cells. Serum-starved MCF-7 cells for 24 h were incubated for 18 and 48 h with the different concentrations of Taxol as shown in figure. Then the cells were collected and stained with propidium iodide (see Section 2) to be analyzed by FACS. DNA histograms were measured using Cell Fit software and the percentage of G0/G1, S and G2/M cells were calculated. Data are representative of four independent experiments.

incubation with the respective antibody (1 h at room temperature) and subsequently immunoprecipitated with Protein A/G-agarose. As a positive control, MCF-7 were treated with 100 nM insulin for 24 h before lysis and immunoprecipitated with anti-p85 from 500 μg of cell lysates. The immunoprecipitates were washed once with cold PBS, twice with 0.5 M LiCl, 0.1 M Tris (pH 7.4) and finally with 10 mM Tris, 100 mM NaCl, 1 mM EDTA. The presence of PI3K activity in immunoprecipitates was determined by incubating the beads with reaction buffer containing 10 mM HEPES (pH 7.4), 10 mM $MgCl_2$, 50 μM ATP, 20 μCi [γ^{32}-P] ATP, and 10 μg of L-α-phosphatidylinositol-4,5-bis phosphate (PI-4,5-P_2) for 20 min at 37 °C. The reactions were stopped by adding 100 μl of 1 M HCl. Phospholipids were extracted with 200 μl of $CHCl_3$/methanol. For extraction of lipids, 200 μl of chloroform:methanol (1:1, v/v) were added to the samples and vortexed for 20 s. Phase separation was facilitated by centrifugation at 5000 rpm for 2 min in a tabletop centrifuge. The upper phase was removed, and the lower chloroform phase was washed once more with clear upper phase. The washed chloroform phase was dried under a stream of nitrogen gas and redissolved in 30 μl of chloroform. The labelled products of the kinase reaction, the PI phosphates, then were spotted onto *trans*-1,2-diaminocyclohexane–*N*,*N*,*N*′,*N*′-tetraacetic acid-treated silica gel 60 TLC plates. Radioactive spots were visualized by autoradiography.

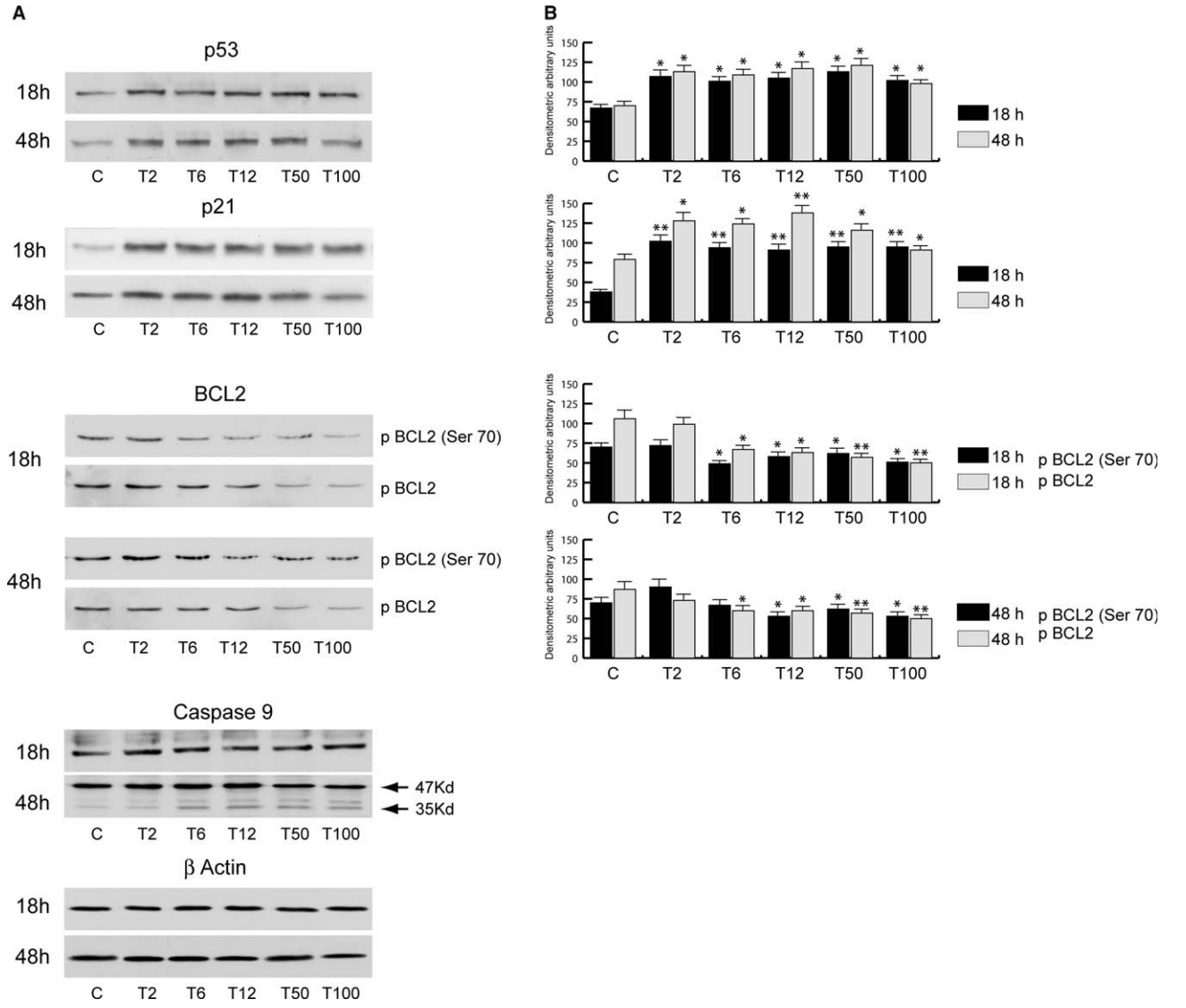

Fig. 3. Low doses of Taxol affect p53 expression and its target proteins p21 WAF and Bcl-2. (A) MCF-7 cells underwent Taxol treatment (from 2 to 100 nM) for 18 and 48 h were harvested and lysed to detect p53 protein expression in 50 μg of total cell lysates. The same filter was stripped and reprobed with anti-p21 waf, anti-Bcl-2, anti caspase-9 and anti-β-actin antibodies. C: control; T: Taxol at different nM concentrations. β-Actin serves as a loading control. Representative results are shown. (B) The histograms represent the mean ± S.D. of three separate experiments in which bands intensity for p53, p21 and Bcl-2 were evaluated in term of arbitrary densitometric units. $^{*}P < 0.05$; $^{**}P < 0.01$ vs C.

2.9. DNA ladder formation

The ladder assay is based on the oligonucleosomal DNA fragmentation of nuclear DNA that can be visualized by ethidium bromide staining following electrophoresis. MCF-7 cells were plated in 100-mm dishes (1×10^6 cells/dish); serum-starved cells were treated with Taxol (2, 6, 50 and 100 nM) for 48 h.

At the end of the incubation period cells were trypsinized and combined with floating cells in the same culture. DNA was isolated by lysing the cells in 400 μl of 0.2% Triton-X, 20 mM EDTA, and 10 mM Tris, pH 8.0, for 20 min on ice. The DNA fragments were harvested by centrifugation for 20 min at 12000 rpm. After the addition of 400 μl of phenol–chloroform the supernatant was centrifuged at 12000 rpm for 5 min and then was precipitated with sodium acetate (400 μl) and ethanol (800 μl) for 24 h at −20 °C.

Afterwards the supernatant was centrifuged at 12000 rpm for 20 min, dried and incubated for 1 h at room temperature with a buffer containing 500 μg/ml RNase A. The DNA fragments were resolved by electrophoresis at 75 V on 1% agarose gel impregnated with ethidium bromide, detected by UV transillumination, and photographed.

2.10. Statistical analysis

Each data point represents the mean ± S.D. of at least three experiments. The data were analyzed by analysis of variance using the STATPAC computer program.

3. Results

3.1. Taxol decreases basal growth rate of MCF-7 cells in a dose/time-related manner

High doses of Taxol (100 nM) since 18 h of treatment inhibited MCF-7 cells proliferation. The same inhibitor effects were produced by lower doses of Taxol starting from 12 nM after 48 h of incubation (Fig. 1). These results well correlates with FACS analysis demonstrating a block of MCF-7 cell cycle into the G2/M phase after 48 h of drug treatment at the doses ranging from 12 to 100 nM (Fig. 2).

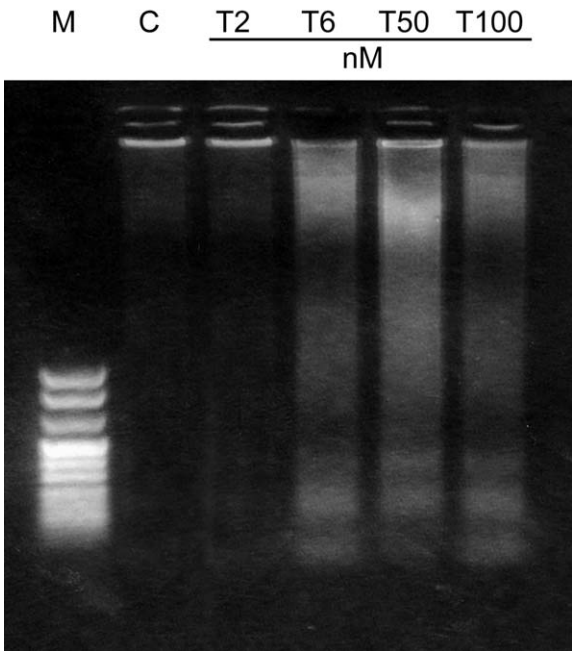

Fig. 4. Treatment of MCF-7 cells with Taxol induces DNA fragmentation. DNA gel electrophoresis of Taxol-treated (T) (lanes 2–5) and control (C) (lane 1) MCF-7 cells. DNA from MCF7 cell treated for 48 h with 2, 6, 50 and 100 nM of Taxol was extracted as detailed in Section 2, then separated in 1.5% agarose gel electrophoresis. DNA from a 48 h control (untreated) culture was prepared in the same way. M, Marker.

3.2. Cell survival pathway is affected by taxol

To investigate if Taxol "per se" might produce early changes in cell apoptotic and/or survival signals, first of all we focused our attention on the effects of the drug on p53 and p21 waf expression.

It is worth to mention that low doses of Taxol incubated for 18 and 48 h are able to enhance both p53 and p21 waf protein expressions, while the anti-apoptotic Bcl-2, in its total content and consequently in its phosphorylative status (phospho-Bcl Ser70) resulted downregulated (Fig. 3 A and B). However, it is note worthy to observe how the relative phospho-Bcl-2 levels tend to be enhanced by Taxol treatment since the decrease of Bcl-2 protein content occurs much faster than its phosphorylation. Indeed, the ratio of densitometric values of the bands between phospho-Bcl-2 /Bcl-2 protein varied from 0.6 in control sample, to 1.2 in treated sample. Drug treatment triggers cell apoptotic events only after 48 h, eliciting the cleavage of caspase-9, which is detectable from Taxol 6 nM and persists at the higher doses (Fig. 3A). This was also confirmed by agarose DNA electrophoresis that demonstrates the formation of the characteristic ladder of DNA at 6, 50 and 100 nM of Taxol (48 h), while it is absent at lower concentration of the drug as well as in the control sample (Fig. 4).

On the basis of the reported findings, even in the presence of low doses of Taxol, p53 may potentiate its transactivatory properties on the regulatory region of target gene through its faster translocation into the nucleus. To prove this we studied p53 nuclear/cytosolic compartmentalization in MCF-7 cells in the presence of low and high doses of the drug incubated for both 18 and 48 h.

3.3. Taxol induced P53 and P21 intracellular relocation

WB analysis performed, respectively, in the nuclear and cytosolic cell lysates showed that p53 and its gene product, the mdm2 protein, after 18 h of drug treatment, exhibit a prevalent nuclear compartmentalization, while p21 waf protein

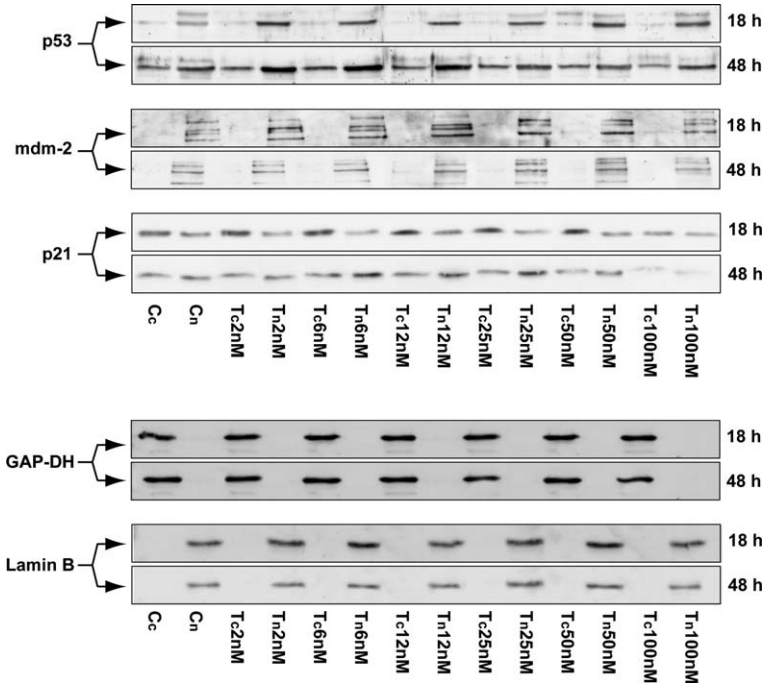

Fig. 5. Different subcellular compartmentalization of p53, mdm2 and p21 waf in cells treated with Taxol. MCF-7 cells treated with Taxol, at the concentrations reported in the figure, were harvested and cytosolic (c) and nuclear (n) protein lysates were subject to WB with an anti-p53, anti-mdm2, anti-p21 antibodies. C, control; T, Taxol-treated cells. The expressions of a nuclear protein, Lamin B, and a cytoplasmatic enzyme, GAP-DH, were assessed by stripping and reprobing the filters to verify the purity of fractions.

appears mostly localized in the cytosol (Fig. 5). Drug treatment of MCF-7 cells for 48 h increases p53 levels in both nuclear and cytosolic compartments until 25 nM of cell exposure to Taxol. At the same time, p21 waf protein tends to diffuse from the cytosol into the nucleus (Fig. 5). P53 uses dynein to translocate into the nucleus since it co-immunoprecipitates with the microtubule-motor protein and with β-tubulin (Fig. 6). In the end, we observed that the amount of protein bound to dynein in the nuclear compartment is increased upon Taxol treatment at 48 h.

The subcellular localization of both p53 and p21 proteins was also investigated by confocal microscopy using immunofluorescent staining of p53 (rhodamine-conjugated antibody, red staining) and p21 (fluorescein-conjugated antibody, green staining) proteins.

At 18 h of drug treatment, p53 tended to accumulate much more into the nucleus (a very strong nuclear staining was ob-

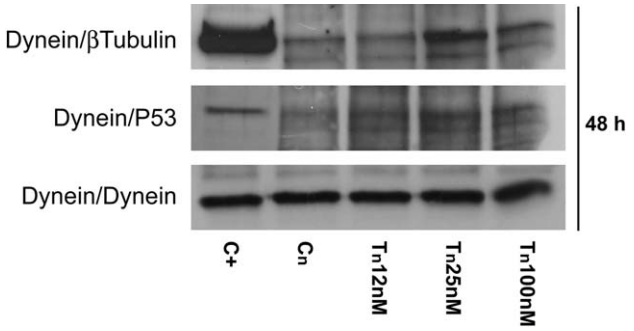

Fig. 6. P53 co-immunoprecipitates with dynein. MCF-7 cells treated with Taxol (12, 25, 100 nM) for 48 h were harvested and nuclear (n) protein lysates were subject to IP experiment by using an anti-dynein antibody/protein A/G complex followed by WB with anti-β-tubulin antibody; anti-p53 antibody; anti-dynein antibody. C+, 50 μg of soluble cell protein; Cn, nuclear control.

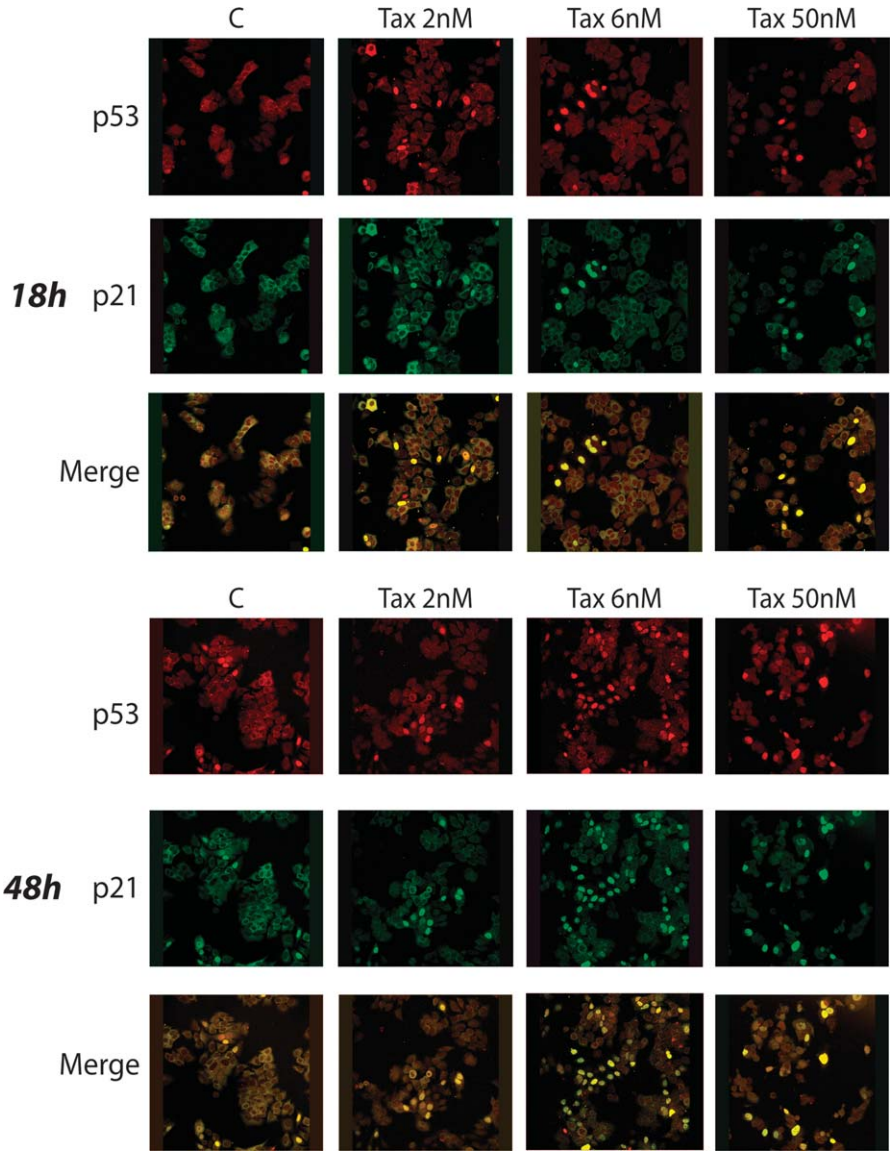

Fig. 7. Immunolocalization of p53 and p21 WAF in MCF-7 cells treated with Taxol. MCF-7 cells were treated with Taxol, at the indicated doses, for 18 and 48 h and subsequently fixed and stained with a rhodamine-conjugated donkey anti-mouse IgG as secondary Ab for p53 (red), or with a fluorescein-conjugated donkey anti-rabbit IgG for p21 (green). Staining was analysed by confocal laser-scanning microscopy. Co-localization of p53 and p21 waf is visible as yellow staining generated where the color images merge. Images are optical sections at intervals of 0.3 μm along the *z*-axis from the bottom of the cell to the top of the nucleus.

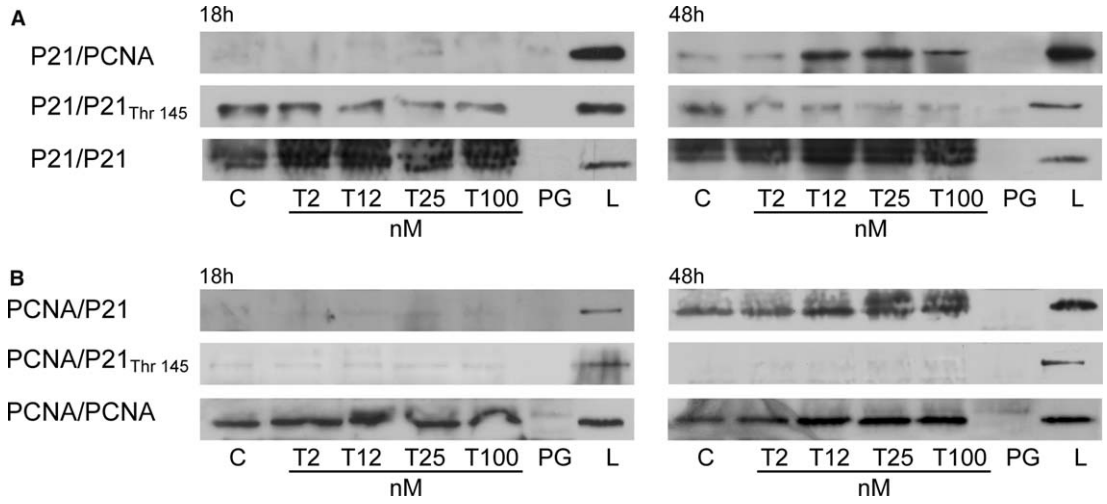

Fig. 8. Expression of p21-PCNA complex in MCF-7 cells treated with different doses of Taxol. MCF-7 cells treated with Taxol at the indicated concentrations (nM) for both 18 and 48 h were lysed and immunoprecipitated in (A) with: an anti-p21 waf antibody/protein A/G complex followed by WB with specific anti-PCNA antibody (upper panel), with anti-p21 (Thr 145) antibody (middle panel) and with anti-p21 antibody (lower panel); in B with: an anti PCNA antibody/protein A/G complex followed by WB with specific anti-p21 antibody (upper panel), with anti-p21 (Thr 145) antibody (middle panel) and with anti-PCNA antibody (lower panel). C, control; L, 50 μg of soluble cell protein not subjected to IP; PG, 0.5 mg of soluble cell protein immunoprecipitated only with protein A/G-agarose beads; T, Taxol treated cells. Results are representative of three independent experiments.

served in about 10% of cells treated with 2 and 6 nM Taxol, and in 30% of cells treated with 50 nM Taxol) respect to control sample, where, instead, a quite uniform localization in both nuclear and cytoplasmatic compartments is showed (Fig. 7). At the same time, in untreated cells, p21 resulted to be prevalently retained in the cytosol and following Taxol treatment it tends to translocate in the nucleus.

For instance, at 48 h of incubation, while 5% of control cells showed a strong nuclear co-localization of p53 and p21, in cells treated with 2 and 6 nM of Taxol the percentage increased to 15% and 50%, respectively. Nevertheless, it is worth to mention that the detectable cell compartmentalization of p53 and p21 waf proteins, in the presence of high concentrations of Taxol (50 nM), are in all likelihood not reliable since morphological changes turning cell polygonal shape into rounding ones occur and produces loss of adhesion (Fig. 7).

The cytosolic retention of p21 waf at 18 h, probably makes it unable to interact with nuclear proteins like PCNA and to inhibit cell cycle.

To determine if the level of co-association between p21 and PCNA in MCF-7 treated cells may correlate with the inhibition of cell cycle progression we performed, at both 18 and 48 h, two sets of IP experiments by using whole-cell lysates incubated:

(i) with anti-p21 waf antibody followed by immunoblotting with an anti-PCNA antibody (Fig. 8A); and
(ii) with anti-PCNA antibody followed by immunoblotting with an anti-p21 antibody (Fig. 8B).

As shown in Fig. 8A, PCNA protein was present in immunoprecipitates from MCF-7 cells treated for 48 h with 12, 25 and 100 nM of Taxol. The highest levels of co-IP of p21/PCNA were concomitant with the alteration of cell cycle.

The same filters obtained at 18 and 48 h of drug treatment were reprobed with an anti-phospho-p21 waf (Thr 145) antibody, that represents the phosphorylated form of the protein unable to inhibit cell cycle. In accordance, the results demonstrated that in untreated and treated MCF-7 cells the phospho-p21 waf (Thr 145) is present at 18 h and it slightly decreases under Taxol (Fig. 8A). On the other hand, Taxol treatment prolonged up to 48 h significantly reduced the level of phosphorylated p21 waf protein compared with that obtained at 18 h. To asses that p21 is immunoprecipitated in all experimental conditions we reprobed the same blots with an anti-p21 antibody.

In the reverse IP experiment (IP with anti-PCNA antibody and blot with anti-p21 antibody) (Fig. 8B) the results confirm that PCNA and p21 waf associated only following 48 h drug treatment, while phospho-p21 (Thr 145) is not present in the IPs both at 18 and 48 h. The same filters were then blotted for anti-PCNA antibody to verify PCNA protein in immunoprecipitates.

3.4. Evidence that low doses of taxol are able to potentiate transactivatory properties of P53

53 nuclear compartmentalization, induced by low doses of Taxol, leads us to assume that the treatment with the drug per se may potentiate the functional transactivating properties of this protein.

PTo support this assumption we treated MCF-7 transfected with a p21 promoter conjugated with a luciferase reporter gene. Our results show, for the first time, how low doses of Taxol are able to induce the activation of p21 promoter (Fig. 9). This activation was drastically potentiated by the ectopic overexpression of wild-type p53 and abrogated in the presence of p53 mutant construct.

3.5. Effect of low doses of taxol on PI3K/Akt signal

When we evaluated the effect of the drug on the PI3K/Akt pathway, which is crucial in maintaining cell survival signal, we observed that Taxol (25 and 100 nM) for 18 h induced an early activation of PI3K and consequently this leads to an increase of phospho-Akt levels (Fig. 10A and B). Such

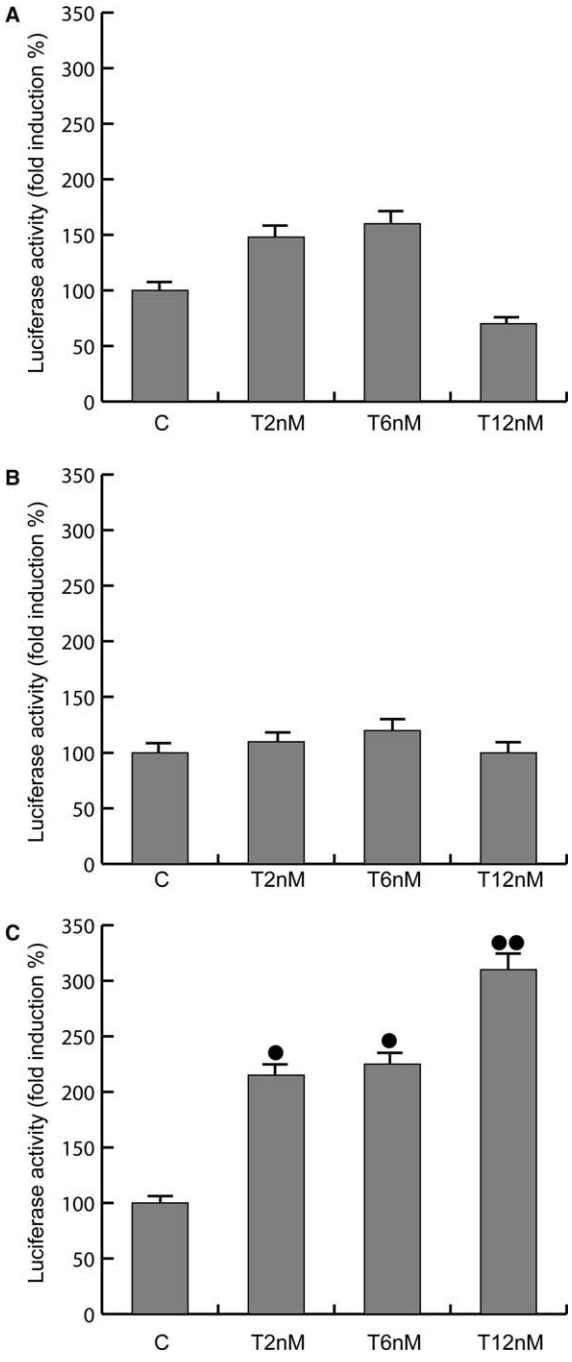

Fig. 9. Taxol induces p21 WAF promoter activity via p53. MCF-7 cells were co-transfected with the p21 waf promoter-luciferase construct and pCMV empty vector (A), pCMV-p53 mutant (B) and pCMV-p53 wild-type (C). After 8 h of transfection cells were treated with low doses of Taxol (T): 2, 6 and 12 nM for 18 h. MCF-7 cells were lysed and luciferase activities were measured using the dual luciferase reporter assay system as described under Section 2. Each column/bar represents the relative p21 waf promoter (luciferase) activity and is the mean ± S.D. of three independent experiments in triplicate. Levels of significance vs control (C): $^{\bullet}P < 0.05$; $^{\bullet\bullet}P < 0.01$.

effect is not longer noticeable at 48 h of drug exposure when G2/M cell population, analyzed in flow cytometry, appears to increase significantly together with a concomitant down regulation of the anti-apoptotic signal: Bcl-2 protein, as previously documented.

4. Discussion

Taxol has been shown to be effective as an anticancer agent in a variety of tumoral cell types [8,25–27].

As a result of cell exposure to Taxol, events characteristic to cell cycle arrest and apoptosis might take place. These effects seem to be linked to the different concentration of the drug as well as to the tissues and/or cell line used.

In the present study we demonstrate how low doses of Taxol have some apparent conflictory effects: an enhanced p53 expression involved in the regulation of programmed cell death on one hand, and the activation of PI3 kinase involved in cell survival on the other. The apparent contradictory effects have been previously reported by other authors in the same breast cancer cell type where the rapid enhancement of PI3K/Akt together with an increased of survivin expression, occurs only to counteract the increased p53 expression [28]. Indeed, it is well known how p53 might inhibit PI3K/Akt pathway by double mechanisms: first through the PTEN activation, a specific inhibitor of PI3K activity, as well as through an enhanced Akt degradation via proteosoma [29,30]. However, the functional effect of the enhanced PI3K/Akt signal, induced by low doses of Taxol, seems to be vanished by the decrease of the anti-apoptotic Bcl-2, which in such a way, fails to have any protective role in controlling mitochondrial permeability and then to inhibit the release of cytochrome *c*. Indeed, in the same circumstance, low doses of Taxol (6 nM) incubated for 48 h in MCF-7 cells are able to induce the cleavage of caspase-9 and the formation of DNA ladder. These apoptotic events precede the block of cell cycle, which occurs as from 12 nM of Taxol.

The reduced levels of Bcl-2, linked to the enhanced p53 expression under Taxol treatment, counteract the activation of PI3K/Akt pathway. P53 protein, in turn, through its binding to the negative response *cis*-elements of the Bcl-2 gene promoter may transcriptionally downregulate the expression of the anti-apoptotic protein [31].

Here, we observed that in the presence of low doses of Taxol, p53 co-immunoprecipitates with dynein, a microtubule-motor protein that requires ATP to move along microtubules with their cargoes.

Our data, together with previous results, suggest that in such circumstances p53 may use dynein to translocate into the nucleus, an event which is potentiated by Taxol treatment [10,11]. Besides, an other protein that comes down in a p53/dynein complex is the β-tubulin prevalently present in treated cells. Thus, the effect of the polymerizing agent on microtubule assemblement, consistent with their end elongation, might functionally contribute to p53 nuclear translocation where the p53-transactivatory properties would appear enhanced. The deep drop of Bcl-2 expression and the enhancement of p21 waf protein may stem from this.

Indeed, the most important finding of the present study is consistent with the evidence that Taxol, at lower concentrations, is able to transactivate p21 promoter resulting in the enhancing of p21 protein expression. This response is linked to p53 wild-type expression in MCF-7 cells, since the presence of a p53 mutant abrogates the transactivation of p21 promoter under Taxol treatment. In the same vein, the nuclear localization of p53 induced by low doses of Taxol after 18 h is followed by the enhancement of its gene product: the mdm2 protein, which shows the same sub-cellular distribution reported for p53.

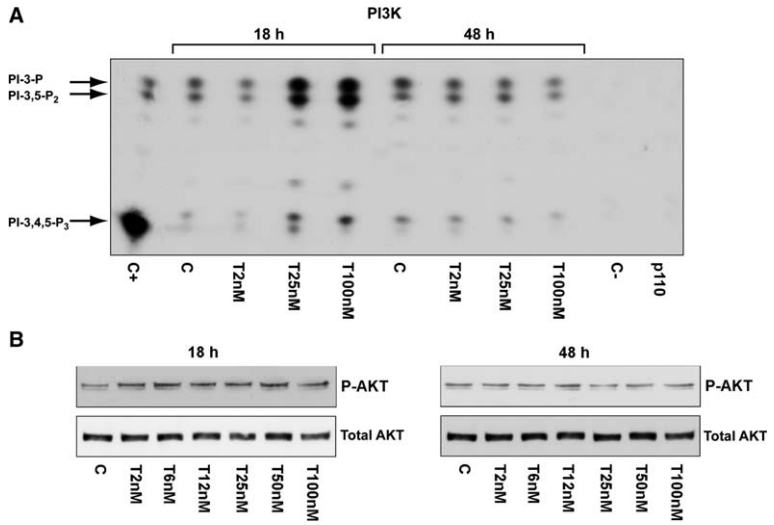

Fig. 10. Transitory Taxol activation of PI3 kinase pathway. (A) MCF-7 cells treated with Taxol (at the indicated doses) for 18 and 48 h were lysed and immunoprecipitated with an anti-p-85 antibody. The immunocomplexes were assayed for their ability to phosphorylate PI to PIP using [γ^{32}P]-ATP at 37 °C for 20 min. The PIP was resolved by TLC and autoradiographed. As a positive control (C+) MCF-7 cells were treated with 100 nM of insulin for 24 h. The negative control (p110) was performed using MCF-7 lysate, where p110, the catalyzing subunit of PI3K, was previously removed by preincubation with the respective antibody (1 h at room temperature) and subsequently immunoprecipitated with protein A/G-agarose. PI-3,4,5-P3: phosphatidylinositol 3,4,5-triphosphate; PI-3,5-P2: phosphatidylinositol 3,5-diphosphate; PI-3-P: phosphatidylinositol 3-phosphate. An additional negative control (C−) is represented by MCF-7 cells previously treated with worthmanin for 30 min. Untreated cells: (C), Taxol-treated cells: (T). The autoradiographs presented are representative of experiments that were performed at least three times with repetitive results. (B) WB of phospho-Akt (Ser 473) levels from MCF-7 cells treated with the indicated doses of Taxol (T) at 18 and 48 h of incubation. Total Akt levels are showed as a loading control. Results are representative of three independent experiments.

It is worth to observe that in this scenario MCF-7 cell cycle is not substantially modified, given that p21 waf result mostly stored in the cytosol and this could prevent its binding with nuclear factors such as PCNA [32–34]. Indeed, at the same time, the enhanced activation of phospho-Akt, as here reported, may serve to recruit p21 protein into the cytosol, where it is unable to act as an inhibitor of CDKs and thereby to inhibit cell cycle progression [16,33,34]. Results from this study showed that prolonged treatment of MCF-7 cells with Taxol up to 12 nM induced an evident co-association between p21 protein and PCNA which was concomitant with the decay of the phosphorylative status of p21 waf (Thr 145) together with the arrest of cell cycle. These findings supported the evidence that when phospho-Akt is not activated due to the prolonged treatment with Taxol, p21, mainly present in the ipo-phosphorylated form, is able to co-immunoprecipitate with PCNA. The latter event well correlates with the block of cell cycle into the G2/M phase that progressively increases with the elapsing of time of the drug exposure as well as with the dose of Taxol used.

In conclusion, in the present study we have demonstrated how low doses of Taxol, without affecting cell cycle, may induce the enhanced expression of p53 protein and its prevalent nuclear translocation with well featured apoptotic events occurring in breast cancer cells. This, furthermore, supports the potential benefit of the association of low doses of Taxol with the classic chemotherapic agents. The combined treatment may potentiate the effect of low doses of chemotherapics reducing thus the harmful systemic effects mostly occurring during the treatment of breast carcinomas.

Acknowledgements: We thank Dr. Wafik El-Deiry (Howard Hughes Medical Institute, Philadelphia) for kindly providing the plasmid WWP-Luc containing human p21 waf promoter and Dr. G. Daniel (Department of Health and Human Service, Natl. Inst. Env. Health Sci., Res. Triangle Park, NC) for his generous gift of the pCMV-wt p53 plasmid, pCMV-p53 plasmid mutant and pCMV empty vector.

We thank Prof. D. Sturino for English revision of the manuscript.

Financial support: This work was supported by A.I.R.C., 2003.

References

[1] Horwitz, S.B. (1992) Mechanism of action of taxol. Trends Pharmacol. Sci. 13, 131–136.
[2] Rao, S., Krauss, N.E., Heerding, J.M., Swindell, C.S., Ringell, L., Orr, G.A. and Horwitz, S.B. (1994) 3′-(*p*-Azidobenzamido)taxol photolabels the N-terminal 31 amino acids of beta-tubulin. J. Biol. Chem. 269, 3131–3134.
[3] Rao, S., Orr, G.A., Chaudhary, A.G., Kingston, D.G.Y. and Horwitz, S.B. (1995) Characterization of the taxol binding site on the microtubule. 2-(*m*-Azidobenzoyl) taxol photolabels a peptide (amino acids 217–231) of beta-tubulin. J. Biol. Chem. 270, 20235–20238.
[4] Jordan, M.A. and Wilson, L. (1998) Microtubules and actin filaments: dynamic targets for cancer chemotherapy. Curr. Opin. Cell. Biol. 10, 123–130.
[5] Caplow, M., Shanks, J. and Ruhlen, R. (1994) How taxol modulates microtubule disassembly. J. Biol. Chem. 38, 23399–23402.
[6] Horwitz, S.B. (1994) Taxol (paclitaxel): mechanisms of action. Ann. Oncol. 6, S3–S6.
[7] Woods, C.M., Zhu, J., McQueney, P.A., Bollag, D. and Lazarides, E. (1995) Taxol-induced mitotic block triggers rapid onset of a p53-independent apoptotic pathway. Mol. Med. 5, 506–526.
[8] Rowinsky, E.K. and Donehower, R.C. (1995) Paclitaxel (taxol). N. Engl. J. Med. 15, 004–1014.
[9] Eastman, A. and Rigas, J.R. (1999) Modulation of apoptosis signaling pathways and cell cycle regulation. Semin. Oncol. 26, 41–52.
[10] Giannakakou, P., Sackett, D.L., Ward, Y., Webster, K.R., Blagosklonny, M.W. and Fojo, T. (2000) p53 is associated with

cellular microtubules and is transported to the nucleus by dynein. Nat. Cell Biol. 2, 709–717.
[11] Giannakakou, P., Nakano, M., Nicolaou, K.C., O'Brate, A., Yu, J., Blagosklonny, M.W., Greber, U.F. and Fojo, T. (2002) Enhanced microtubule-dependent trafficking and p53 nuclear accumulation by suppression of microtubule dynamics. Proc. Natl. Acad. Sci. 16, 10855–10860.
[12] Haupt, S., Berger, M., Goldberg, Z. and Haupt, Y. (2003) Apoptosis-the p53 network. J. Cell Sci. 15, 4077–4085.
[13] Andre, N., Braguer, D., Brasseur, G., Goncalves, A., Lemesle-Meunier, D., Guise, S., Jordan, M.A. and Briand, C. (2000) Paclitaxel induces release of cytochrome *c* from mitochondria isolated from human neuroblastoma cells. Cancer Res. 19, 5349–5353.
[14] Ofir, R., Seidman, R., Rabinski, T., Krup, M., Yavelsky, V., Weinstein, Y. and Wolfson, M. (2002) Taxol-induced apoptosis in human SKOV3 ovarian and MCF7 breast carcinoma cells is caspase-3 and caspase-9 independent. Cell Death Differ. 9, 636–642.
[15] Park, S.J., Wu, C.H., Gordon, J.D., Zhong, X., Emami, A. and Safa, A.R. (2004) Taxol induces caspase-10 dependent apoptosis. J. Biol. Chem. 49, 51057–51067.
[16] Heliez, C., Baricault, L., Barboule, N. and Valette, A. (2003) Paclitaxel increases p21 synthesis and accumulation of its AKT-phosphorylated form in the cytoplasm of cancer cells. Oncogene 22, 3260–3268.
[17] Harper, J.W., Adami, G.R., Wei, N., Keyomarsi, K. and Elledge, S.J. (1993) The p21 Cdk-interacting protein Cip1 is a potent inhibitor of G1 cyclin-dependent kinases. Cell 75, 805–816.
[18] Michieli, P., Chedid, M., Lin, D., Pierce, J., Mercer, E. and Givol, D. (1994) Induction of WAF1/CIP1 by a p53 independent pathway. Cancer Res. 54, 3391–3395.
[19] Zeng, Y. and El-Deiry, W. (1996) Regulation of p21WAF1/CIP1 expression by p53-independent pathways. Oncogene 12, 1557–1564.
[20] Sherr, C. and Roberts, J. (1999) CDK inhibitors: positive and negative regulators of G1-phase progression. Genes Dev. 13, 1501–1512.
[21] Kelman, Z. and O'Donnell, M. (1995) Structural and functional similarities of prokaryotic and eukaryotic DNA polymerase sliding clamps. Nucleic Acids Res. 23, 3613–3620.
[22] Gulbis, J., Kelman, Z., Hurwitz, J., O'Donnell, M. and Kuriyan, J. (1996) Structure of the C-terminal region of p2(WAF1/CIP1) complexed with human PCNA. Cell 87, 297–306.
[23] Andò, S., Panno, M.L., Salerno, M., Sisci, D., Mauro, L., Lanzino, M. and Surmacz, E. (1998) Role of IRS-1 signaling in insulin-induced modulation of estrogen receptors in breast cancer cells. Biochem. Biophys. Res. Commun. 253, 315–319.
[24] Morelli, C., Garofalo, C., Bartucci, M. and Surmacz, E. (2003) Estrogen receptor alpha regulates the degradation of insulin receptor substrates 1 and 2 in breast cancer cells. Oncogene 22, 4007–4016.
[25] McGuire, W.P., Rowinsky, E.K., Rosenshein, E.K., Grumbine, F.C., Ettinger, D.S., Armstrong, D.K. and Donehower, R.C. (1989) Taxol: a unique antineoplastic agent with significant activity in advanced ovarian epithelial neoplasms. Ann. Intern. Med. 111, 273–279.
[26] Liebmann, J.E., Cook, J.A., Lipschultz, C., Teague, D., Fisher, J. and Mitchell, J.B. (1993) Cytotoxic studies of paclitaxel (Taxol) in human tumour cell lines. Br. J. Cancer 68, 1104–1109.
[27] Eisenhauer, E.A. and Vermorker, J.B. (1998) The taxoids. Comparative clinical pharmacology and therapeutic potential. Drugs 55, 5–30.
[28] Ling, X., Bernacki, R.J., Brattain, M.G. and Li, F. (2004) Induction of survivin expression by taxol (paclitaxel) is an early event, which is independent of taxol-mediated G2/M arrest. J. Biol. Chem. 279, 15196–15203.
[29] Mayo, L.D., Dixon, J.E., Durden, D.L., Tonks, N.K. and Donner, D.B. (2002) PTEN protects p53 from Mdm2 and sensitizes cancer cells to chemotherapy. J. Biol. Chem. 277, 5484–5489.
[30] Gottlieb, T.M., Leal, J.F., Seger, R., Taya, Y. and Oren, M. (2002) Cross-talk between Akt, p53 and Mdm2: possible implications for the regulation of apoptosis. Oncogene 218, 1299–1303.
[31] Miyashita, R., Krajewski, S., Krajewska, M., Wang, H.G., Lin, H.K., Liebermann, D.A., Hoffman, B. and Reed, J.C. (1994) Tumor suppressor p53 is a regulator of bcl-2 and bax gene expression in vitro and in vivo. Oncogene 9, 1799–1805.
[32] Nicholson, K.M. and Anderson, N.G. (2002) The protein kinase B/AKT signalling pathway in human malignancy. Cell. Signal. 14, 381–395.
[33] Li, Y., Dowbenco, D. and Lasky, L.A. (2001) AKT/PKB phosphorylation of p21 Cip/WAF1 enhances protein stability of p21 Cip/WAF1 and promotes cell survival. J. Biol. Chem. 277, 11352–11361.
[34] Rossig, L., Jadidi, A.S., Urbich, C., Badorff, C., Zeihr, A.M. and Dimmeler, S. (2001) AKT-dependent phosphorylation of $p21^{Cip1}$ regulates PCNA binding and proliferation of endothelial cells. Mol. Cell. Biol. 21, 5644–5657.

Evidence that the mouse insulin receptor substrate-1 belongs to the gene family on which the promoter is activated by estrogen receptor α through its interaction with Sp1

M L Panno[1*], L Mauro[1*], S Marsico[3], D Bellizzi[1], P Rizza[3], C Morelli[2], M Salerno[1], F Giordano[1] and S Ando'[1,2,3]

[1]Department of Cellular Biology, [2]Faculty of Pharmacy and [3]Centro Sanitario, University of Calabria, Via Pietro Bucci, cubo 4c, 87030 Arcavacata di Rende (CS), Italy

(Requests for offprints should be addressed to S Ando' at the Department of Cellular Biology, University of Calabria; Email: sebastiano.ando@unical.it)

*(M L Panno and L Mauro contributed equally to this work)

Abstract

In the present study, the molecular mechanism underlying the up-regulatory effect of estradiol (E_2) on mouse insulin receptor substrate-1 (IRS-1) promoter was investigated in CHO cells on which the same promoter had first been functionally characterized. The mouse IRS-1 promoter bears four consensus half Estrogen Responsive Elements (ERE) sequences and thirteen AP-1- and ten Sp1-binding elements. We performed molecular dissection of this promoter gene providing 3′ different deleted constructs, containing the same AP-1 rich region with a progressively increased number of ERE half sites located downstream. None of these constructs was responsive to E_2, while a downstream region (nt –1420 to –160) rich in GC elements was induced by E_2. However, the latter region lost its intrinsic E_2 responsiveness when the whole IRS-1 promoter was mutated for deletion in all four ERE half sites. Deletion analysis of the ERE half sites demonstrated that only ERE located at the position –1500 to –1495, close to the GC-rich region, was able to maintain the induced activatory effect of E_2 on the IRS-1 gene. Electrophoretic mobility shift and chromatin immunoprecipitation assays identified the region containing the half ERE/Sp1 (nt –1500 to –1477) as the one conferring E_2 responsiveness to the whole promoter. This effect occurs through the functional interaction between E_2/ERα and Sp1.

Journal of Molecular Endocrinology (2006) **36,** 91–105

Introduction

Estrogen and insulin-like growth factor (IGF) regulate breast cancer cell growth and survival through the activation of distinct transductional pathways (Dickson & Lippman 1987, 1995, Surmacz 2000). However, evidence of a cross-talk between estrogen and growth factors (such as IGFs) has been documented, addressing an additive effect of these two mitogenic systems on breast cancer cell growth and survival (Molloy *et al.* 2000, Yee & Lee 2000).

The previous findings of ourselves and others have disclosed novel arguments to sustain the cross-talk between the two signals, demonstrating how exposure of breast cancer cells to estradiol (E_2) enhances the expression of insulin receptor substrate-1 (IRS-1), a key molecule linked to phosphatidylinositol-3 kinase (PI-3K)/Akt and ERK1/ERK2 pathways, crucial for cell proliferative response and survival (Surmacz 2000, Molloy *et al.* 2000, Yee & Lee 2000, Mauro *et al.* 2001). This deduction fits well with previous evidence reporting on how the mitogenic effects of insulin or IGF-I were amplified by exposure to estrogen (Ando' *et al.* 1998, Lee *et al.* 1999). In addition, breast cancer cells overexpressing IRS-1 show a marked growth advantage and reduced or abrogated estrogen growth requirements (Guvakova & Surmacz 1997). Our recent data have demonstrated that E_2 is able to increase IRS-1 mRNA level through activation of the regulatory region of the IRS-1 gene (Mauro *et al.* 2001). Mouse IRS-1 promoter, characterized for the first time by Araki *et al.* (1995) in CHO cells, has furthermore been analyzed and our results show four consensus half Estrogen Responsive Elements (ERE) sequences and thirteen AP-1- and ten Sp1-binding elements. These might be important regulatory sites for the actions of estrogen. The up-regulatory effect induced by E_2 on this promoter activity in both MCF-7 and CHO cells, expressing estrogen receptor α (ERα), seems to underscore a general mechanism which is not strictly related to the cell type (Mauro *et al.* 2001).

In the present study, we have demonstrated, through a molecular dissection of the IRS-1 promoter, how the region bearing the ERE half site, separated by 12

0952–5041/06/036–091
DOI: 10.1677/jme.1.01848
Online version via http://www.endocrinology-journals.org

nucleotides from the Sp1 site (5′-AGGTCA$(N)_{12}$CCG CCC-3′) within nt –1500 to –1477, is responsible for the E_2-induced activation of the whole IRS-1 promoter. Both electrophoretic mobility shift assay (EMSA) and chromatin immunoprecipitation (ChIP) assay confirmed that the above-mentioned sequence is functionally involved in mediating the up-regulatory effect induced by E_2 on IRS-1 expression. The effect, as documented for other E_2-responsive genes, occurs through the interaction between ERα and Sp1 proteins, bound separately to the ERE half sequence and Sp1 responsive element respectively and present in the ERE/Sp1 region of the IRS-1 promoter (Dubik & Shiu 1992, Wu-Peng *et al.* 1992, Krishnan *et al.* 1994, Rishi *et al.* 1995, Porter *et al.* 1996, 1997, Scholz *et al.* 1998, Petz & Nardulli 2000, Saville *et al.* 2000, Khan *et al.* 2003).

Materials and methods

Materials

Dulbecco's modified essential medium (DMEM)/Ham's F-12, L-glutamine, penicillin/streptomycin, calf serum (CS), bovine serum albumin (BSA), aprotinin, leupeptin, phenylmethylsulfonyl fluoride (PMSF), sodium orthovanadate, 4-OH-tamoxifen and E_2 were purchased from Sigma (Milan, Italy). FuGENE 6 and poly (dI-dC) were from Roche Applied Science (Milan, Italy). Taq DNA polymerase, T4 polynucleotide kinase, 1 kb DNA ladder, dual luciferase kit, pGL_2 basic vector and timidine kinase promoter (TK) Renilla luciferase plasmid were provided by Promega (Madison, WI, USA). [γ^{32}P]ATP, Sephadex G50 spin columns and the enhanced chemoluminescence (ECL) system were from Amersham Biosciences. Sp1 (1C6), ERα F10 and β-actin antibodies were purchased from Santa Cruz Biotechnology (Santa Cruz, CA, USA). IRS-1 antibody was from UpState Biotechnology (New York, NY, USA). Human recombinant ERα and Sp1 proteins were obtained from Invitrogen (Carlsbad, CA, USA) and Alexis (Lausen, Switzerland) respectively.

The plasmid pBluescript SKII containing mouse IRS-1 promoter (3·3 kb) and a codifying region of the IRS-1 gene (3·4 kb) was kindly given by Dr Kaku Tsuruzoe (Research Division, Joslin Diabetes, Boston, MA, USA). pHEGO plasmid, containing the full length of ERα cDNA was generously provided by Dr Didier Picard (Department of Cellular Biology, University of Geneva, Geneva, Switzerland).

Plasmids

The sequence of the IRS-1 mouse promoter was analyzed by MatInspector V2·2 software to identify potential transcriptional regulatory sites, such as AP-1, Sp1 and ERE, other than that characterized by Araki *et al.* (1995). The MatInspector V2·2 software is available at the web url http://transfac.gbf.de/cgi-bin/matSearch/matsearch.pl; it allows the identification of consensus sequences of transcriptional factors through the TRANSFAC data base (http://transfact.gbf.de/TRANSFAC/) (Quandt *et al.*1995).

Plasmid pIRS-1-luciferase (luc) was generated by inserting the 3·3 kb fragment of the mouse IRS-1 gene promoter into the pGL_2 expression vector containing a luciferase gene. The sequence was confirmed by automated sequencing analysis with a BigDye terminator cycle sequencing ready reaction kit (Applied Biosystems, Foster City, CA, USA).

IRS-1 promoter fragments (pIRS-1A-luc, pIRS-1B-luc, pIRS-1C-luc) were synthesized by unidirectional deletion using the esonuclease III reaction (Ausubel *et al.* 1988). pIRS-1D-luc was obtained by PCR using 5′-CCC TCCCTCACTCCTGCGT-3′ and 5′-GGAAGATAG CCTGATCCGAG-3′ as the sense and antisense primers respectively.

All ligation products were transformed into competent *Escherichia coli* cells (Invitrogen). Plasmids were isolated, and clones were confirmed by DNA sequencing. pHEGO plasmid contains the full-length ERα cDNA. The Renilla luciferase reporter vector pRL-TK (Promega) was used as a transfection standard to normalize transfection efficiency.

PCR mutagenesis

The plasmids pEREmut-luc, pERE1,2,3,mut-luc and pERE4 mut-luc were generated by PCR mutagenesis (Clackson *et al.* 1991).

pEREmut-luc contained mutation of all ERE half sites, located at sites nt −2218 to −2213, −2128 to −2123, −2050 to −2045 and −1500 to –1495. To generate this plasmid, PCRs were performed using the primers 1s (3′-GGCACCTCAGAGCAGATGG-5′) and 2a (5′-TGGGGGCGCTGGGGCGGAGGGGACGAC CCAACAGGTAAAGGCGACCCCCG-3′) to obtain the amplified product A (nt −3350 to −2240); the non-mutagenic external primer 3s (3′-CGTCTAATGC TCGTGCAAAC-5′) and the mutagenic internal primer 6a (5′-TGGGGGCGCTGGGGCGGAGGGGACGAC CCAACAGGTAAAGGCGACCCCCG-3′) to obtain the amplified product B (nt −2026 to −1466); the mutagenic internal primer 5s (5′-CGGGGGTCGCCT TTACCTGTTGGGTCGTCCCCTCCGCCCCAGC GCCCCCA-3′) and the non-mutagenic external primer 4a (3′-AGGAAGATAGCCTGATCCGA-5′) to obtain the amplified product C (nt −1536 to −170). Products B and C were used as templates in a second PCR using the primers 3s and 4a (product D, nt −2026 to −170). Products A and D were restricted by BamHI (specific sites were present in primers 2a and 3s) and ligated to obtain product E, lacking all ERE half sites, which was further

digested by SacI and HindIII (specific sites were present in primers 1s and 4a) and inserted in the pGL_2 plasmid.

pERE1,2,3,mut-luc contained mutations of the three ERE half sites, located at the sites nt −2218 to −2213, −2128 to −2123 and −2050 to −2045, and was generated using product A, as described above, and product F (nt −2026 to −170) obtained by PCR using primers 3s and 4a. Products A and F were restricted by BamHI, ligated to obtain product G, lacking the three ERE half sites, which was further digested by SacI and HindIII and inserted in the pGL_2 plasmid.

pERE4 mut-luc was mutated in the ERE half sites corresponding to nt −1500 to −1495, and was constructed using product C, as described above, and product H (nt −3350 to −1466) obtained by PCR using the primers 1s and 6a. Products C and H were used as templates in a second PCR using the primers 1s and 4a to obtain product L. The latter product was digested by SacI and HindIII and inserted in the pGL_2 plasmid.

Point mutations were done by PCR-mediated site-specific mutagenesis using degenerate primers, replacing one G with T in the ERE sequences. Namely, the ERE half site was located at position nt −2218 to −2213: AGtTCA; the ERE half site was located at position nt −2128 to −2123: TtACCC; the ERE half site was located at position nt −2050 to −2045: TCAAtG; the ERE half site was located at position nt −1500 to −1495: AGtTCA (mutations are shown as lower case letters).

Cell lines and culture conditions

CHO cells were obtained from the American Type Culture Collection (Manassas, VA, USA). Wild-type human breast cancer (MCF-7) cells were a gift from Dr E Surmacz (Kimmel Cancer Institute, Philadelphia, PA, USA).The cell lines were cultured in DMEM/Ham's F12 (1:1) medium supplemented with 5% CS, 1% L-glutamine and 1% penicillin/streptomycin. The cells were cultured in phenol red-free, serum free medium, DMEM (PRF-SFM-DMEM) containing 0·5% BSA, 1% L-glutamine and 1% penicillin/streptomycin, 24 h before each experiment.

Transfections and luciferase assay

CHO and MCF-7 cells were seeded (1×10^5 cells/well) in DMEM/F-12 supplemented with 5% CS in 24-well plates. CHO cells were cotransfected with pIRS-1-luc promoter construct and pHEGO. Cells were transfected in SFM using FuGENE6 according to the manufacturer's instructions with a mixture containing 1 μg/well of each specific plasmid and 25 ng/well of TK Renilla luciferase plasmid. An empty pGL_2 vector was used as the control vector to measure basal activity. Twenty-four hours after the transfection the medium was changed and the cells were treated in PRF-SFM-DMEM in the presence of 10 pM and 1, 10 and 100 nM E_2. The firefly and Renilla luciferase activities were measured by using a dual luciferase kit. The firefly luciferase data for each sample were normalized on the basis of the transfection efficiency measured by Renilla luciferase activity.

Western blotting

CHO and MCF-7 cells were grown in 100 mm dishes to 70–80% confluence, shifted to SFM for 24 h and lysed. Protein lysates were obtained with a buffer containing 50 mM HEPES, pH 7·5, 150 mM NaCl, 1·5 mM $MgCl_2$, 10 mM EGTA, pH 7·5, 10% glycerol, 1% Triton X-100 and protease inhibitors (2 μM Na_3Vo_4, 1% PMSF and 20 μg/ml aprotinin).

The expression of IRS-1 was tested by Western blotting in 50 μg protein lysates using an anti-IRS-1 antibody. Proteins were separated by SDS-PAGE and then transferred to a nitrocellulose membrane, probed with primary antibody and then stripped and reprobed with β-actin antibody. The antigen–antibody complex was detected by incubation of the membranes for 1 h at room temperature with a peroxidase-coupled anti-IgG antibody and revealed using the ECL system. Blots were then exposed to film and bands were quantified by densitometer. The results obtained are expressed in terms of arbitrary densitometric units.

Gel mobility shift assay

Nuclear extracts were prepared from CHO cells as previously described (Andrews & Faller 1991). The probe was generated by annealing single stranded oligonucleotides and labeled with [γ^{32}P]ATP and T4 polynucleotide kinase, and then purified using Sephadex G50 spin columns. The DNA sequences used as probe or as cold competitors were as follows (the nucleotide motifs of interest are underlined, mutations are shown as lower case letters): Sp1 5′-GTTGGGACTTGGCAGCt CGCCTCCCCCTGCCCAAG-3′; ERE/Sp1 5′-GAG AGCTAGCAGtTCACCCGCGTCCCCTCtGCCCCA GCGCCCCCACCCTC-3′. The DNA sequence used as ERE cold competitor was as follows: 5′-TCCCCC TGCAAGGTCACGGTGGCCACCCCGTG-3′. Oligonucleotides were synthesized by MWGBiotech (Ebersberg, Germany). The protein binding reactions were carried out in 20 μl buffer (20 mM HEPES, pH 8, 1 mM EDTA, 50 mM KCl, 10 mM dithiothreitol (DTT), 10% glycerol, 1 mg/ml BSA, 50 μg/ml poly (dI-dC)) with 50 000 c.p.m. labeled probe, 20 μg CHO nuclear protein or an appropriate amount of ERα or Sp1 human recombinant proteins, and 5 μg poly (dI-dC). The mixtures were incubated at room temperature for 20 min in the presence or absence of unlabeled

competitor oligonucleotides. The specificity of the binding was tested by adding specific antibodies (anti-ERα and anti-Sp1) to the reaction mixture. The entire reaction mixture was electrophoresed through a 4% polyacrylamide gel in 0·25 × Tris borate-EDTA for 3 h at 150 V. The gel was dried and subjected to autoradiography at −70 °C.

ChIP and Reverse (Re)-ChIP assays

We followed the ChIP methodology described by Morelli *et al.* (2004). CHO cells were transiently transfected with pHEGO plasmid and treated with 100 nM E_2 for 1 h, or left untreated in SFM. The cells were then cross-linked with 1% formaldehyde and sonicated. Supernatants were immunocleared with sonicated salmon DNA/protein A agarose (Upstate Biotechnology Inc., New York, NY, USA) and immunoprecipitated with anti-ERα antibody (Ab) F-10 (Santa Cruz Biotechnology). Pellets were washed as reported in Morelli *et al.* (2004), eluted with elution buffer (1% SDS and 0·1 M $NaHCO_3$) and digested with proteinase K (Morelli *et al.* 2004). DNA was obtained by phenol/chloroform extractions and precipitated with EtOH. PCR was carried out with the ERE/Sp1 primers: upstream 5′-CTCACCCAGACAC CGACATC-3′ and downstream 5′-ACGCCCGTGC CACCCAGAGC-3′, or with the primers amplifying the IRS-1 promoter region containing the three upstream and non-functional ERE half sequences: upstream 5′-CAGGCAGTCTAGTGGATTGA-3′ and downstream 5′-TGTGTATATGTTAGCAGATGTTTG-3′.

In Re-ChIP experiments, complexes from ERα immunoprecipitations (IPs) were eluted in RE-ChIP buffer (0·5 mM DTT, 1% Triton X-100, 2 mM EDTA, 150 mM NaCl and 20 mM Tris–HCl, pH 8·1) and subjected again to the ChIP procedure by using anti-Sp1 antibody PEP2 (Santa Cruz Biotechnology). Inputs were used as loading control and were obtained by eluting DNA from 5 μl cell lysates prior to the IP step. Negative control was performed using normal IgGs in place of the primary antibody.

Statistical analysis

Each data point represents the means ± S.D. of at least three experiments. The data were analyzed by ANOVA using the STATPAC computer program (Statpac Inc., Bloomington, MN, USA).

Results

Analysis of the IRS-1 mouse promoter sequence

Sequencing of the IRS-1 mouse promoter by MatInspector V2·2 software (see Materials and methods) led us to the identification of new potential transcriptional regulatory sites, in addition to those characterized by Araki *et al.* (1995), namely thirteen AP-1, ten Sp1 and four ERE half sites (Fig. 1). All these sites could be potential targets of E_2 action resulting in the activation of the IRS-1 promoter.

Identification of an E_2-activated IRS-1 promoter region

In CHO cells transiently co-transfected with pHEGO and pIRS-1-luc, encoding the full length of IRS-1 gene promoter linked to the firefly luciferase reporter gene, E_2 (10 pM and 1, 10 and 100 nM) was able to induce luciferase activity (Fig. 2A). The same results were obtained in ER-positive human breast cancer MCF-7 cells transfected with pIRS-1-luc (Fig. 2B). E_2 up-regulated IRS-1 protein content in both CHO and MCF-7 cells in a dose-dependent manner (Fig. 3).

Previous findings have demonstrated that ER may indirectly modulate transcription by interaction with the AP-1 sites (Umayahara *et al.* 1994, Paech *et al.* 1997, Webb *et al.* 1999); thus, we checked the potential role of the AP-1-rich region in mediating the activatory effect induced by E_2 on the IRS-1 promoter. In the same vein, we checked how the four ERE half sites may work, together with AP-1, in mediating the up-regulatory effect of E_2 on the activity of the whole IRS-1 promoter. With this aim, we transiently co-transfected CHO cells with pHEGO and three different 3′-deleted constructs conjugated with a luciferase reporter gene containing the same AP-1-rich region with a progressively increased number of ERE half sites, namely: (i) pIRS-1A-luc, containing one ERE half site (nt −3370 to −2180), (ii) pIRS-1B-luc, containing three ERE half sites (nt −3370 to −1650) and (iii) pIRS-1C-luc, containing four ERE half sites (nt −3370 to −1308). None of these constructs was stimulated by E_2 (Fig. 4).

On the contrary, the plasmid pIRS-1D-luc, containing the residual downstream region (nt −1420 to −160), rich in GC elements, was responsive to E_2 action (Fig. 4). The potential positive influence of AP-1 sites in the construct rich in Sp1 sequences has been ruled out since in previous experiments the deletion of the AP-1 site in the construct pIRS-1D-luc did not elicit substantial effects in the E_2-responsiveness (data not shown). Earlier reports (Saville *et al.* 2000) have shown how Sp1 *cis*-elements located in the promoter region of some genes are responsive to E_2; we therefore ascertained if the IRS-1 CG-rich region, present in the full length of IRS-1 promoter, was able to yield estrogen responsiveness independently on the four ERE half sites. Consequently, we performed site-specific mutagenesis at the ERE half sites of the IRS-1 mouse promoter located upstream to the CG-rich region. The effects of the site-specific mutagenesis on basal activity and E_2

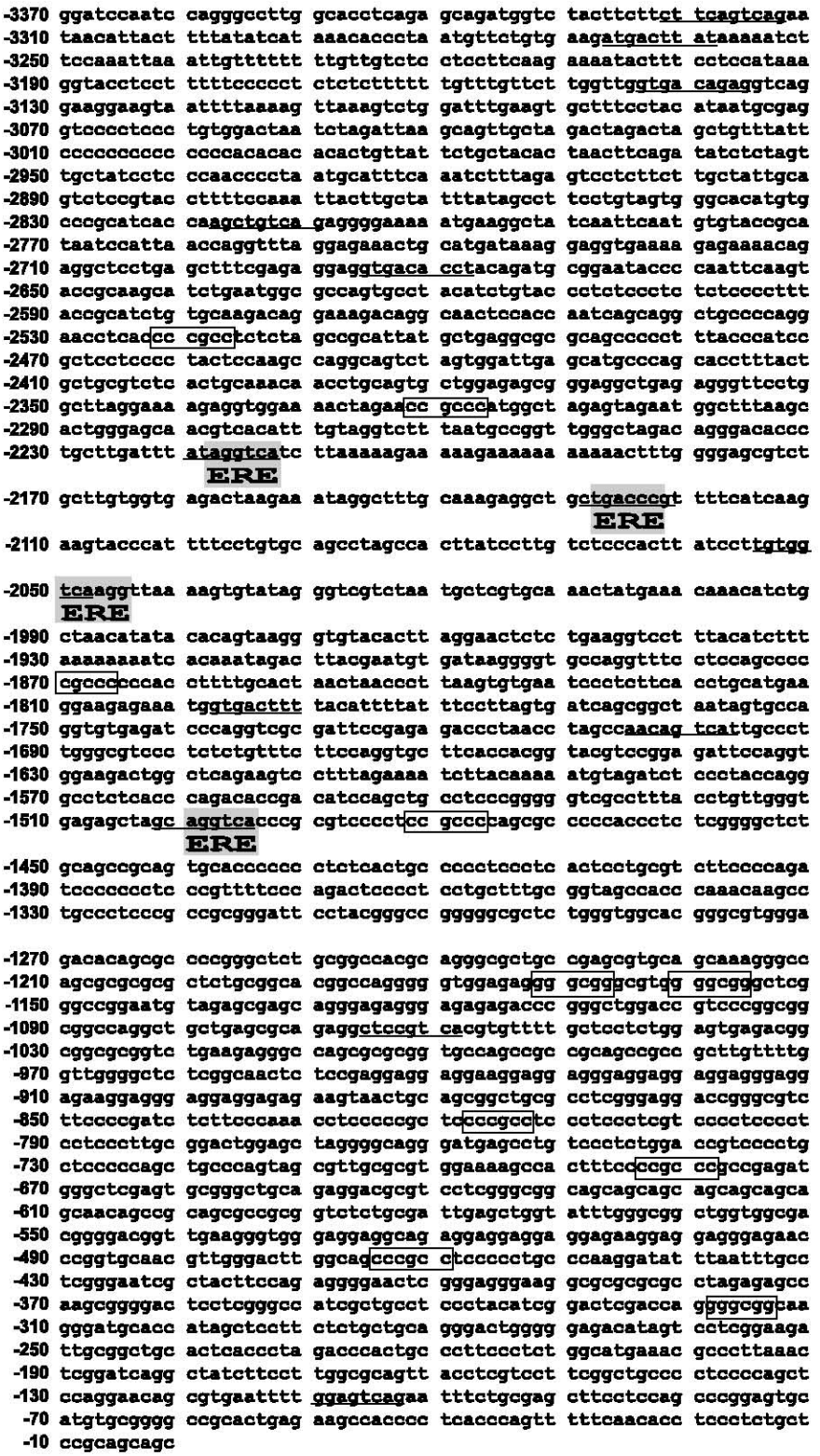

Figure 1 Regulatory sites of the IRS-1 mouse promoter. The analysis of the IRS-1 mouse promoter sequence by MatInspector V2·2 software allowed identification of 13 AP-1 (underlined nucleotides), ten Sp1 (nucleotides in the boxes) and four half ERE (nucleotides in grey boxes) potential regulatory sites.

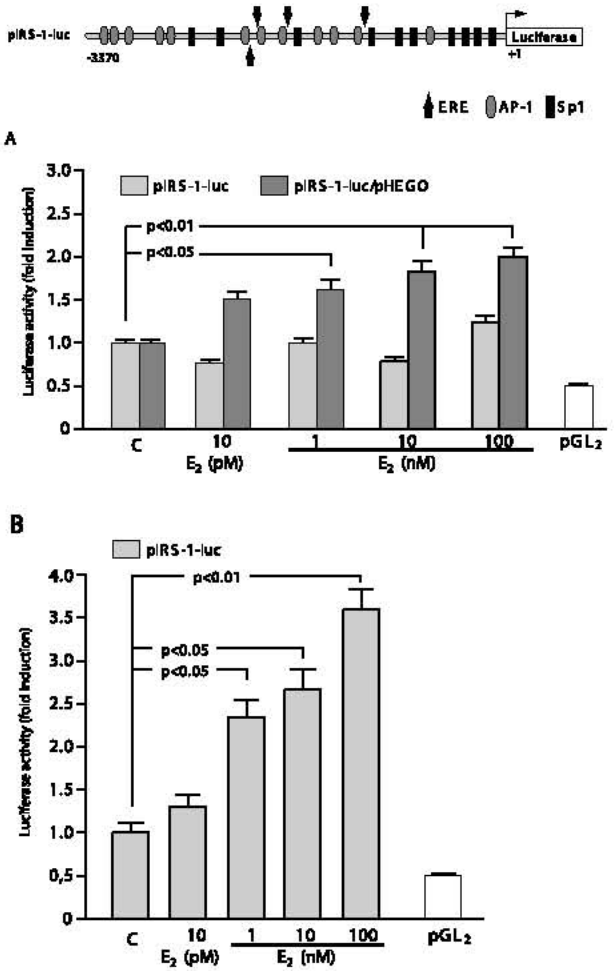

Figure 2 E_2 enhances IRS-1 promoter activity. (A) CHO cells were co-transfected with pIRS-1-luc and pHEGO together with pRL-TK. (B) MCF-7 cells were transiently transfected with DNA mixture containing pIRS-1-luc and pRL-TK. The transfectants were treated in the absence (C, control) or in the presence of 10 pM and 1, 10 and 100 nM E_2 for 24 h. These results represent the means±S.D. of five different experiments. In each experiment, the activities of the transfected plasmids were assayed in triplicate transfections. pGL_2 basal activity was measured in cells transfected with pGL_2 basal vector. The firefly luciferase data for each sample were normalized on the basis of the transfection efficiency measured by Renilla luciferase activity.

responsivness were determined in transient transfection studies using the plasmids pEREmut-luc, pERE4 mut-luc and pERE1,2,3 mut-luc (see Materials and methods) (Fig. 5A).

Using the IRS-1 promoter mutated for delection of all four ERE half sites, the CG-rich region, present in the full length of the IRS-1, was unable *per se* to yield E_2 responsiveness. On the contrary, only the ERE half site localized at the position nt − 1500 to −1495, close to the Sp1 elements, was crucial in maintaining the E_2

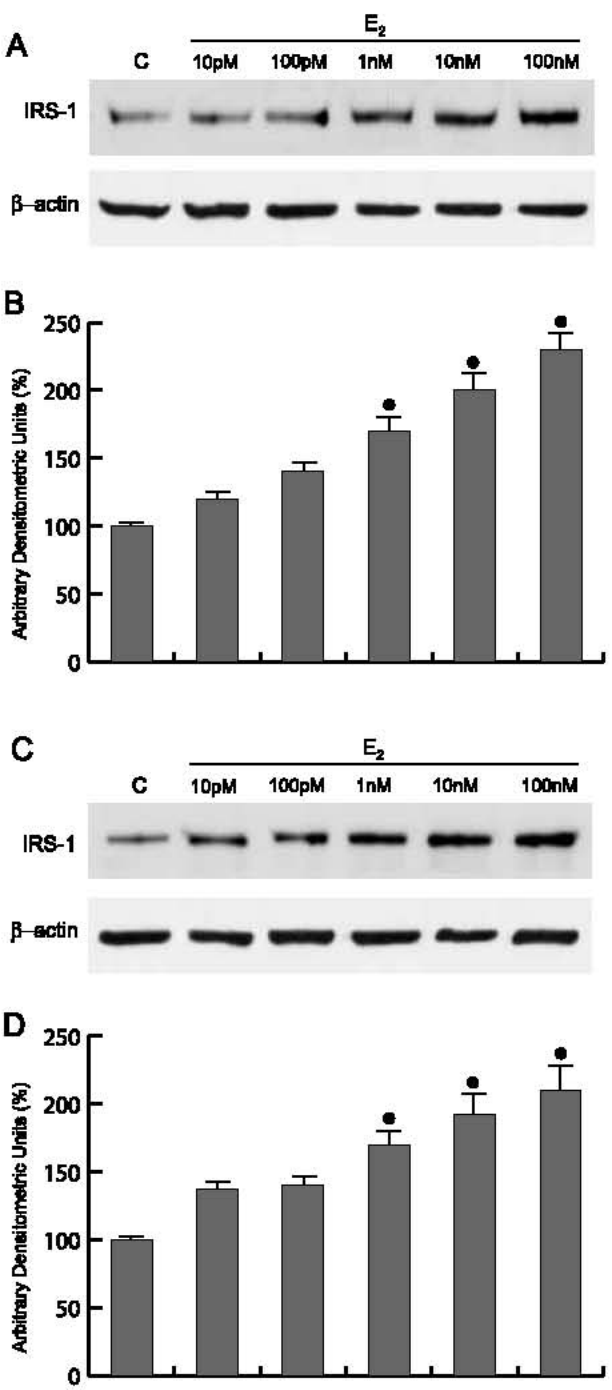

Figure 3 E_2 up-regulates IRS-1 protein expression. Protein expression of IRS-1 in (A) CHO and (C) MCF-7 cells treated in the presence or absence of 10 and 100 pM and 1, 10 and 100 nM E_2 for 24 h. β-actin served as loading control. Representative results are shown. The histograms represent the means±S.D. of three separate experiments performed in (B) CHO and (D) MCF-7 cells, in which the band intensities were evaluated in terms of arbitrary densitometric units and expressed as the percentage of the control assumed as 100%. ●$P<0{\cdot}01$ vs control.

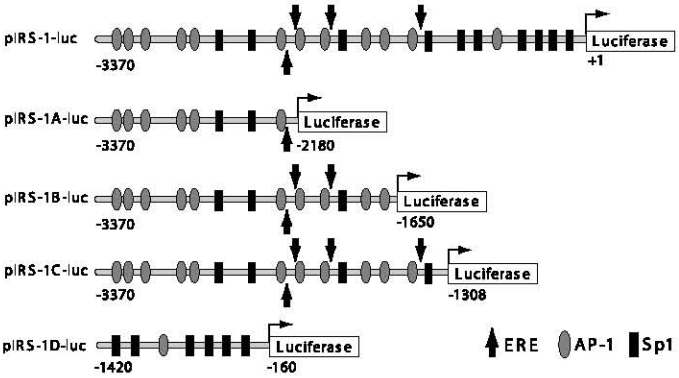

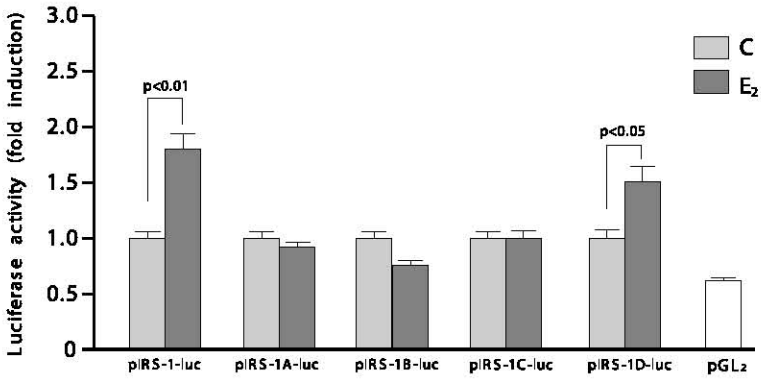

Figure 4 E_2 responsiveness of different IRS-1 promoter constructs. Transcriptional activity of CHO cells co-transfected with pHEGO and with different IRS-1 promoter luciferase reporter constructs are shown. CHO cells were transiently transfected with pIRS-1A-luc, pIRS-1B-luc, pIRS-1C-luc 3′-deleted constructs and pIRS-1D-luc (see Materials and methods) together with pRL-TK. Cells were treated in the absence (C, control) or in the presence of 10 nM E_2 for 24 h. These results represent the means±S.D. of five different experiments. In each experiment, the activities of the transfected plasmids were assayed in triplicate transfections. pGL_2 basal activity was measured in cells transfected with pGL_2 basal vector. The firefly luciferase data for each sample were normalized on the basis of the transfection efficiency measured by Renilla luciferase activity.

transactivation of the IRS-1 promoter. Similar results were obtained by performing point mutations in ERE half sequences (data not shown). The important role of the fourth ERE half site together with the Sp1 region in conferring E_2 responsiveness was confirmed by a functional study performed with the following construct bearing: (i) the whole IRS-1 promoter, (ii) the fragment containing the first three ERE half sites and (iii) the fragment containing the fourth ERE half site close to the Sp1 elements (Fig. 5B). The results showed that pERE4/Sp1-luc, transfected in CHO cells, reproduced the E_2 responsiveness pattern similar to the full length of IRS-1 promoter (Fig. 5B).

On the basis of these findings, our attention was focused on the sequence ERE/Sp1 assumed to be a putative regulatory region target of E_2 action.

EMSA study

Nuclear extracts of CHO cells were incubated in the presence of ERE/Sp1-labeled oligonucleotide to prove if this region was able to bind ERα and/or Sp1 proteins. Nuclear proteins from CHO cells revealed the presence of a single band (Fig. 6, lane 1), which was inhibited by a 100-fold molar excess of the homologous ERE/Sp1 cold competitor (Fig. 6, lane 2), but remained substantially unchanged in the presence of the cold mutated competitor (Fig. 6, lane 3). The results showed an enhanced binding of the nuclear extracts, obtained from CHO cells over-expressing ERα, to the ERE/Sp1-labeled oligonucleotide (Fig. 6, lane 5) and particularly evident upon E_2 treatment (Fig. 6, lane 8). Both bands were abrogated by a 100-fold molar excess of the cold

competitor (Fig. 6, lanes 6 and 9). The specificity of the binding was demonstrated by immunodepletion induced by ERα and Sp1 antibodies (Fig. 6, lanes 10 and 11).

Using a labeled Sp1 oligonucleotide containing a GC box motif present in the Sp1-rich region of the IRS-1 mouse promoter (from nt −490 to nt −455), in a cell-free system, ERα protein *per se* was unable to bind the Sp1 sequence (Fig. 7, lanes 1 and 2). However, the combined presence of ERα at a lower concentration and Sp1 proteins resulted in a clearly enhanced Sp1–DNA binding (Fig. 7, lanes 8 and 9) with respect to the one observed with Sp1 protein alone (Fig. 7, lanes 6 and 7). Sp1 protein was able to up-regulate its binding to the ERE/Sp1 sequence in a dose-related manner (Fig. 7, lanes 6 and 7). Such an up-regulatory effect produced by ERα was drastically attenuated in the presence of cold ERE oligonucleotide (Fig. 7, lanes 10 and 11). On performing a new set of experiments using the same ERE/Sp1-labeled oligonucleotide, as mentioned, it emerged that both Sp1 and ERα were able to bind this sequence (Fig. 8A, lanes 1 and 4). Both bindings were abrogated by a 100-fold molar excess of cold competitor (Fig. 8A, lanes 2 and 5) and restored in the presence of a mutated cold competitor (Fig. 8A, lanes 3 and 6). The specificity of the separate binding of the two proteins to the ERE/Sp1 sequence was demonstrated by the immunodepletion obtained in the presence of the two specific antibodies (Fig. 8A, lanes 8 and 9).

An increased amount of ERα enhanced Sp1 binding to the ERE/Sp1 sequence (Fig. 8B, lanes 6 and 7). In contrast, a progressive increase of Sp1 did not elicit any apparent influence on ERα binding (Fig. 8B, lanes 4 and 5). This up-regulatory effect was reversed by an excess of cold ERE oligonucleotide (Fig. 8B, lanes 8 and 9).

No cross-reaction was observed between the two specific antibodies (data not shown).

ERα and Sp1 are recruited to the ERE/Sp1 sequences of the IRS-1 promoter in CHO cells

The binding of ERα and Sp1 to the ERE/Sp1-containing sequence of the IRS-1 gene promoter was confirmed by ChIP assays. CHO cells were transiently transfected with pHEGO and treated or not treated with E_2 for 1 h. The chromatin was immunoprecipitated with anti-ERα anti-

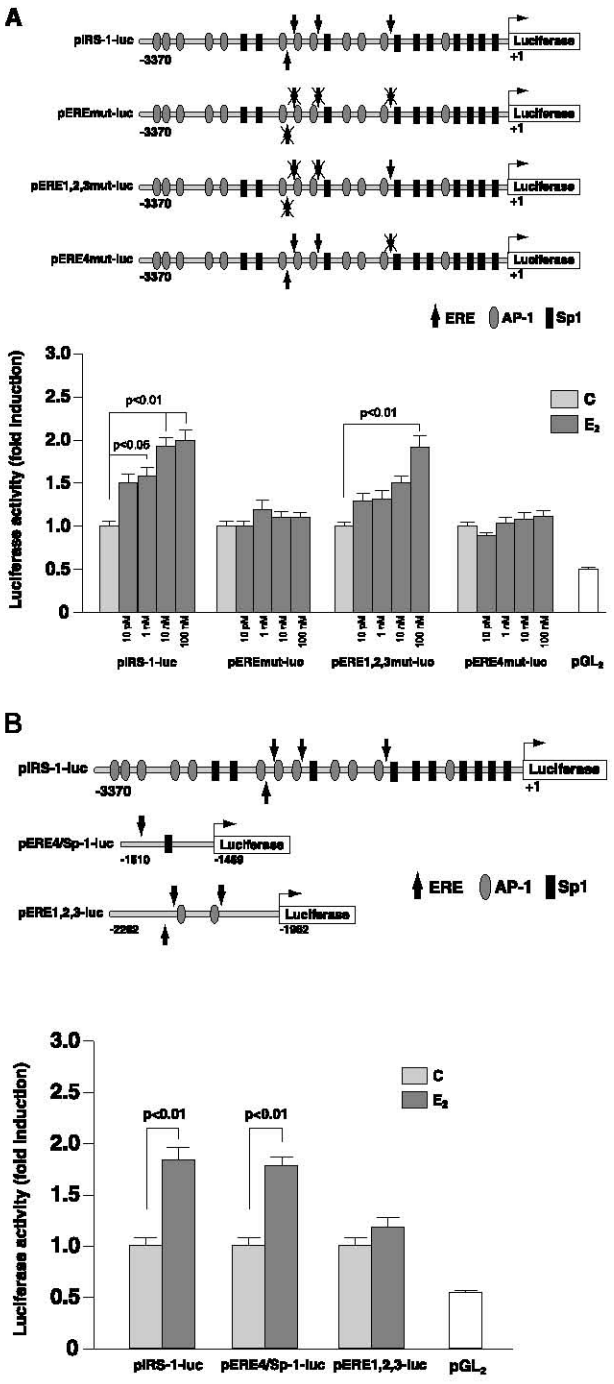

Figure 5 Identification of IRS-1 promoter region responsive to E_2. (A) CHO cells were transiently co-transfected with pHEGO and with pIRS-1-luc or with pEREmut-luc, pERE4 mut-luc and pERE1,2,3 mut-luc, obtained by site-specific mutagenesis of IRS-1 promoter plasmid (see Materials and methods) together with pRL-TK. Cells were treated in the absence (C, control) or in the presence of different doses of E_2 for 24 h. (B) Transcriptional activity of CHO cells co-transfected with pHEGO and with pIRS-1-luc or pERE4/Sp1-luc or pERE1,2,3-luc luciferase reporter constructs (see Materials and methods) together with pRL-TK are shown. Transfectants were treated in the absence (C, control) or in the presence of 100 nM E_2 for 24 h. The results represent the means±S.D. of five different experiments assayed in triplicate transfections. pGL_2 basal activity was measured in cells transfected with pGL_2 basal vector. The firefly luciferase data for each sample were normalized on the basis of the transfection efficiency measured by Renilla luciferase activity.

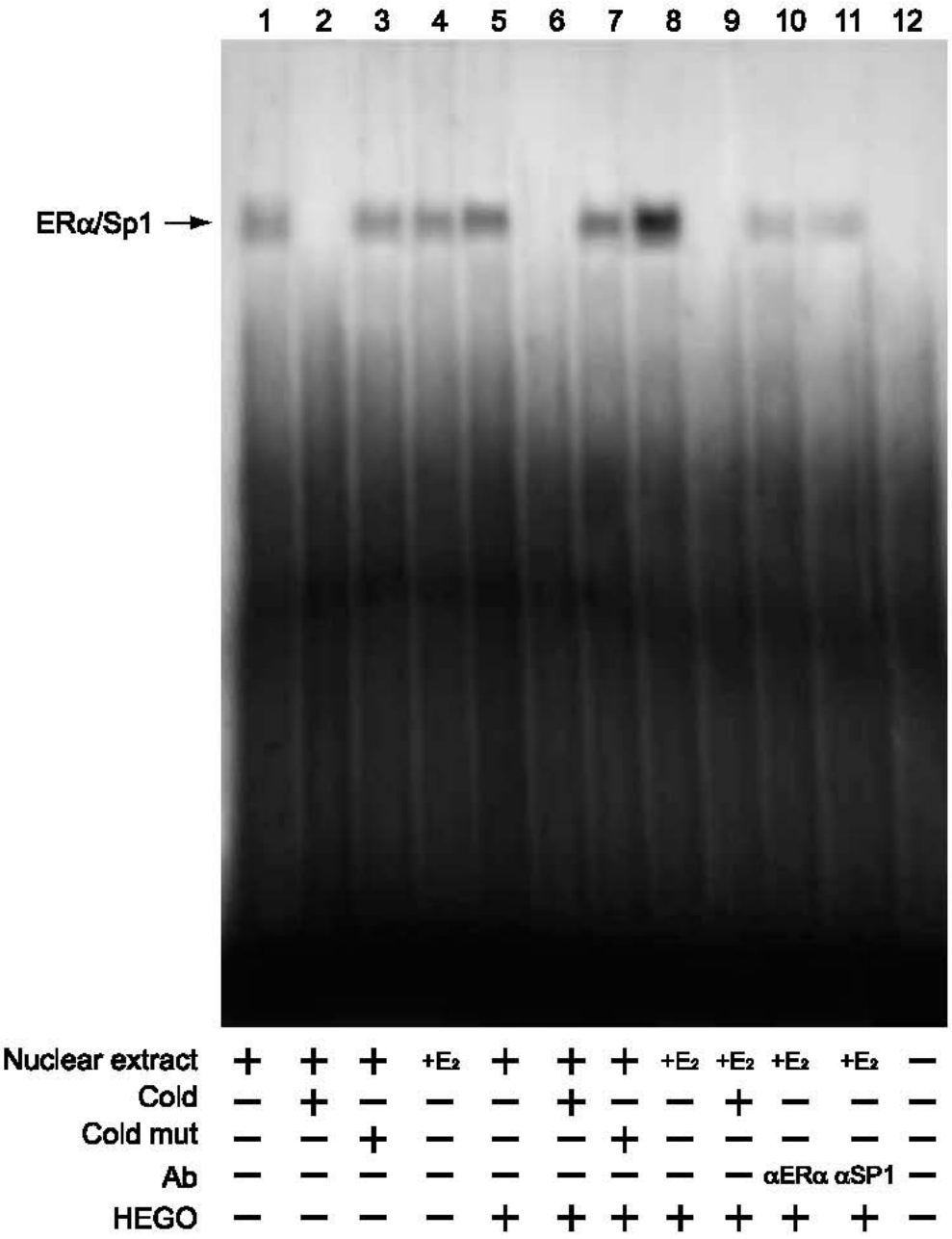

Figure 6 Binding of nuclear extracts from CHO cells and CHO cells transfected with pHEGO (CHO/HEGO) to ERE/Sp1 oligonucleotide. Nuclear extracts from CHO (lanes 1–4) and CHO/HEGO cells (lanes 5–11) were incubated with a double stranded ERE/Sp1 sequence probe labeled with [γ^{32}P]ATP and subject to electrophoresis in a 4% polyacrylamide gel. CHO and CHO/HEGO nuclear extracts treated with 100 nM E_2 for 24 h incubated with probe are shown in lanes 4 and 8 respectively. Competition experiments were performed by adding as competitor a 100-fold molar excess of unlabeled ERE/Sp1 probe (lanes 2, 6 and 9) or a cold mutated (mut) competitor (lanes 3 and 7). The specificity of the binding was tested by adding to the reaction mixture an ERα antibody (α) (lane 10) or an Sp1 antibody (α) (lane 11). Lane 12 contains probe alone. The location of the ERα/Sp1/DNA (ERα/Sp1) complex is indicated by the arrow.

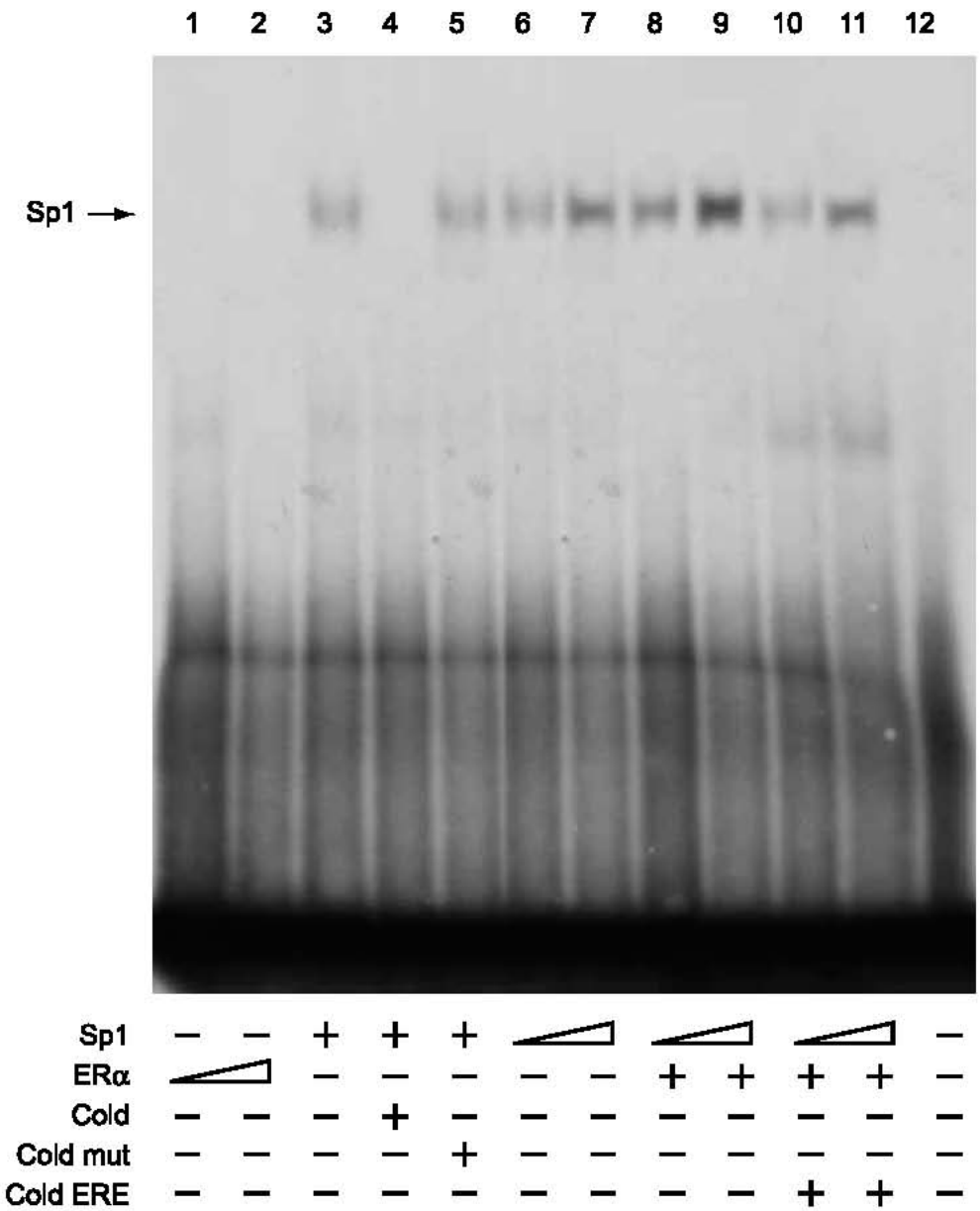

Figure 7 Binding of Sp1 to the Sp1 oligonucleotide in the presence of ERα. ^{32}P-labeled oligonucleotide containing the Sp1-binding site was incubated with: (i) 360 fmol (lane 1) or 540 fmol (lane 2) of ERα and (ii) 10 ng (lanes 3 and 6) or 15 ng (lane 7) of Sp1 and subjected to electrophoresis in a 4% polyacrylamide gel. ERα (360 fmol) was incubated in the presence of 10 ng (lane 8) or 15 ng (lane 9) Sp1 protein. A competition experiment was performed by adding as competitor a 100-fold molar excess of unlabeled probe (lane 4) or a cold mutated competitor (lane 5) or a cold ERE (lanes 10 and 11). Lane 12 contains probe alone. The location of the Sp1/DNA (Sp1) complex is indicated by the arrow.

body. Eluates from ERα IPs were re-immunoprecipitated with anti-Sp1 antibody (Re-ChIP) to confirm the co-existence of ERα/Sp1 complex on the promoter (Fig. 9). The recovered DNA, opportunely amplified by using specific primers mapping the ERE/Sp1-containing sequence, showed an increased occupancy of this region by the two proteins under E_2 treatment (Fig. 9). No effect was observed when the amplified DNA region contained the other three non-functional ERE half sequences (data not shown).

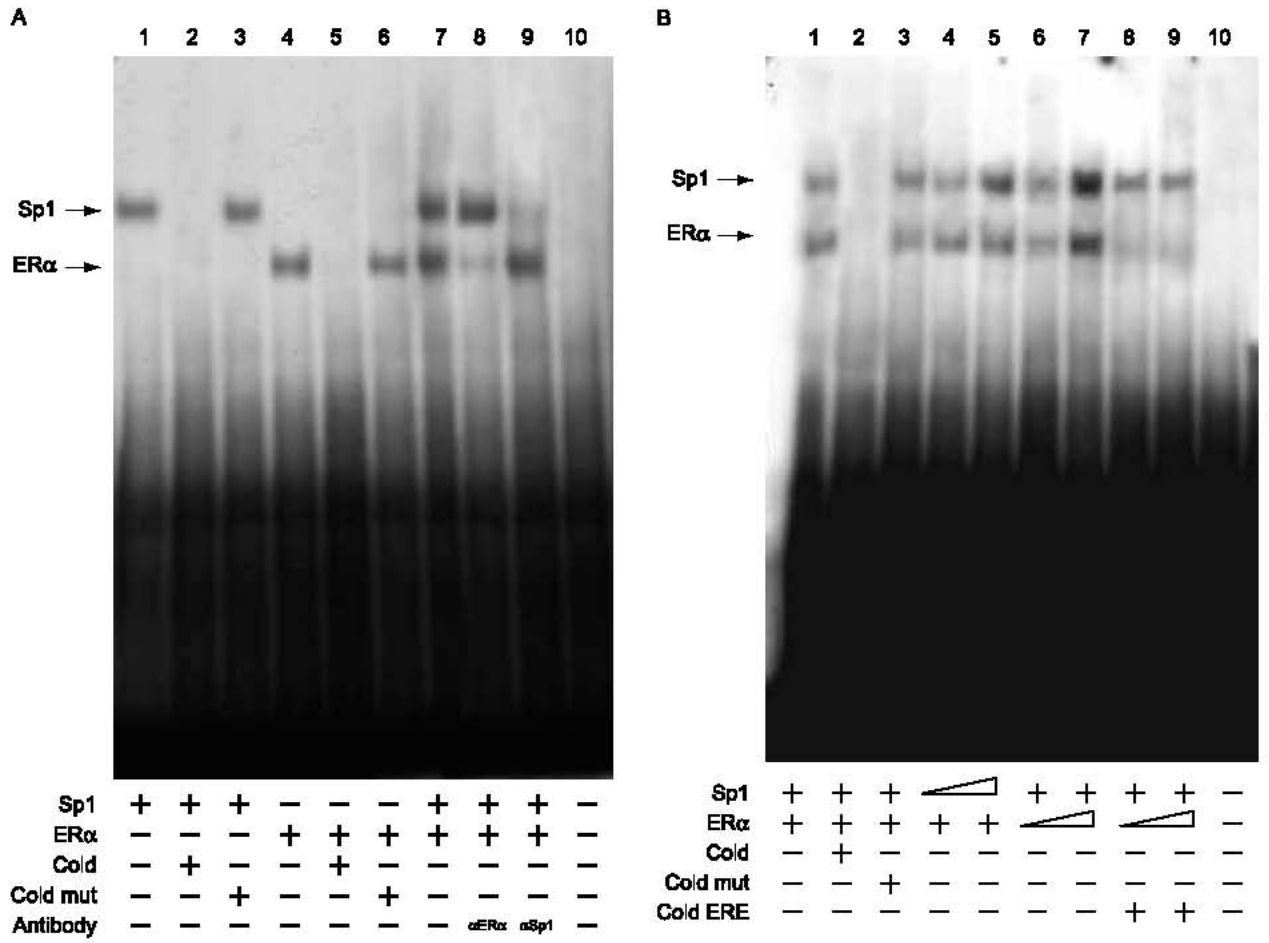

Figure 8 ER-enhanced binding of Sp1 to the half ERE/Sp1-binding site. (A) 10 ng Sp1 or 360 fmol ERα proteins were incubated with a double stranded ERE/Sp1 sequence probe labeled with [γ^{32}P]ATP and subject to electrophoresis in a 4% polyacrylamide gel (lanes 1 and 4 respectively). The specificity of the binding was proved by incubating the reaction mixture containing Sp1 and ERα proteins with an anti-Sp1 or anti-ERα antibodies (lanes 8 and 9 respectively). Competition experiments were performed by adding as competitor a 100-fold molar excess of unlabeled probe (lanes 2 and 5) or a cold mutated (mut) competitor (lanes 3 and 6). Lane 10 contains probe alone. The location of the Sp1/DNA (Sp1) and ERα/DNA (ERα) complexes are indicated by the arrows. (B) ^{32}P-labeled oligo containing the half ERE/Sp1-binding site was incubated with 10 ng Sp1 and 360 fmol ERα (lane 1) and subjected to electrophoresis in a 4% polyacrylamide gel. Competition experiments were performed by adding as competitor a 100-fold molar excess of unlabeled probe (lanes 2) or a cold mutated (mut) competitor (lanes 3). Binding reaction contained 10 ng (lane 4) or 15 ng (lane 5) Sp1 protein in combination with 360 fmol ERα protein. Sp1 (10 ng) was incubated with 360 fmol (lane 6) or 540 fmol (lane 7) ERα, in the absence (lanes 6 and 7) or presence (lanes 8 and 9) of cold ERE. Lane 10 contains probe alone. The location of the Sp1/DNA (Sp1) and ERα/DNA (ERα) complexes are indicated by the arrows.

Discussion

Our previous findings have shown how treatment of CHO cells and estrogen-responsive positive breast cancer cell lines with E_2, for up to 24 h, revealed an up-regulatory effect of E_2 on the regulator region of the mouse IRS-1 gene (Mauro *et al.* 2001). We have here demonstrated that E_2 at concentrations ranging from 10 pM to 100 nM produces the same up-regulatory effect on IRS-1 protein content in both CHO and human breast cancer MCF-7 cells. This suggests that there is a common regulatory mechanism controlling IRS-1 expression in the human and the mouse.

In order to investigate the molecular mechanism underlying the up-regulatory effect of E_2 on the mouse IRS-1 promoter we used the same cell type where it had been first functionally characterized. With this aim, we transiently co-transfected CHO cells with the mouse IRS-1 promoter and pHEGO and tested the response to different doses of E_2 ranging from 10 pM to 100 nM. The mouse IRS-1 gene, like other housekeeping genes, lacks the typical TATA and CAAT boxes (Araki *et al.*

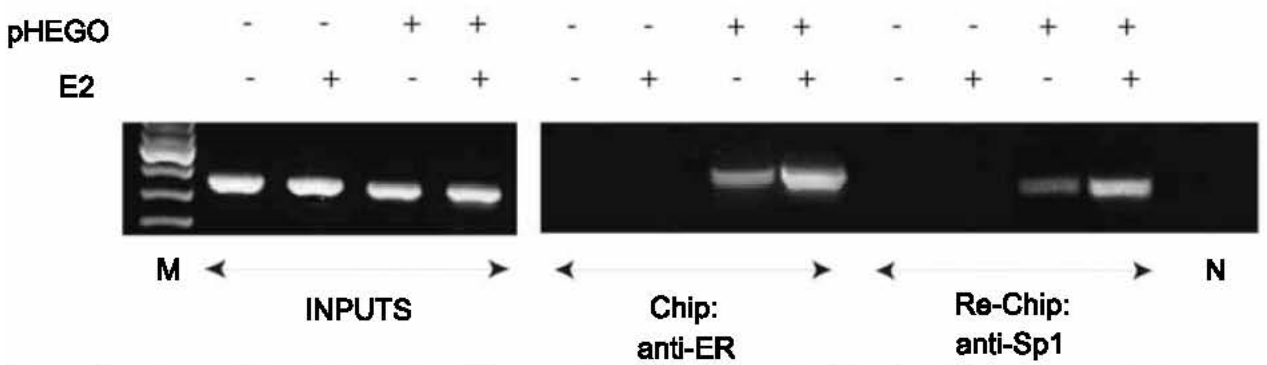

Figure 9 Recruitment of ERα and Sp1 to the ERE/Sp1-containing IRS-1 promoter in CHO cells. CHO cells were transiently transfected with pHEGO and treated with 100 nM E_2 for 1 h (+) or left untreated (−). The cells were then cross-linked with formaldehyde, lysed and soluble, precleared chromatin was obtained as described in Materials and Methods. Chromatin (200 µl) was immunoprecipitated with anti-ERα Ab (Santa Cruz Biotechnology) (ChIP:anti-ER) and eluates from this IP were re-immunoprecipitated with anti-Sp1 Ab (Santa Cruz Biotechnology) (Re-ChIP: anti-Sp1). The immune complexes were reverse cross-linked, and DNA was recovered by phenol/chloroform extraction and Ethanol precipitation. IRS-1 promoter regions containing ERE/Sp1 sequences were detected in the recovered DNA by PCR amplification with specific primers (Materials and Methods). To determine input DNA, the IRS-1 promoter fragment was amplified from 5 µl purified soluble chromatin before immunoprecipitation. PCR products obtained at 35 cycles are shown. ChIP with non-immune IgG was used as negative control (N), M=marker. This experiment was repeated three times with similar results.

1995) and contains thirteen AP-1- and ten Sp1-binding sites and four ERE half sites.

It appears that in addition to binding to a classic ERE element, the ER may also modulate transcription indirectly by interaction with other DNA-binding proteins. Actually, ER interaction with AP-1-bound fos and jun proteins confers E_2 responsiveness to the ovoalbumin (Gaub *et al.* 1990), *c-fos* (Weisz & Rosales 1990), collagenase (Webb *et al.* 1992) and IGF-I (Umayahara *et al.* 1994) genes. However, previous studies have demonstrated ligand- and cell-context specific differences in ERα/Ap1 and ERβ/Ap1 action. For example, in HeLa cells both estrogens and anti-estrogens activated ERα/Ap1, but only anti-estrogens activated ERβ/Ap1 (Paech *et al.* 1997). Thus, the latter observation led us to investigate whether the region of the IRS-1 promoter rich in AP-1-binding sites was responsive to E_2. Our results have shown that the AP-1-rich region failed to be up-regulated by E_2.

When we extended the molecular dissection downstream to implement the AP-1-rich region with the ERE half sites, the unresponsiveness to E_2 was still persistent. In contrast, the remaining downstream region of the IRS-1 promoter rich in Sp1-binding sites appears *per se* to be responsive to E_2 stimulation.

EMSA studies, performed in a cell-free system, using an oligonucleotide reproducing the Sp1 sequence present in the mouse IRS-1 promoter, revealed how ERα did not bind the Sp1 sequence but was able to enhance Sp1 binding to its own responsive element.

Sp1 was originally described as a *trans*-acting factor that bound to the GC box and activated transcription of the SV40 promoter (Dynan & Tjian 1983, Gidoni *et al.* 1984). However, it has been subsequently identified as a higher affinity consensus Sp1 site 5′-GGGGCGG GGC-3′ and it has been also discovered that the sequences that varied from this consensus sequence displayed decreased affinities for Sp1 (Briggs *et al.* 1986). It is worth noting how the GC-rich region, when present in the full length of the IRS-1 mouse promoter mutated for deletion in all four ERE half sites, loses its intrinsic E_2 responsiveness. This led us to investigate the potential role of ERE half site as involved in IRS-1 E_2 responsiveness, taking into account the ability of ERα to bind as a monomer to the consensus ERE half site (Wood *et al.* 1998). Among the different ERE half sites tested, only the ERE at the position nt −1500 to −1495, appears to be crucial in conferring E_2 responsiveness to the whole promoter. The latter ERE half site was the closest one to the Sp1 sequence nt −1482 to −1477. Indeed, in CHO cells, only the construct bearing the ERE/Sp1 sequence has reproduced the same pattern of E_2 responsiveness as that given by the full length IRS-1 promoter. Because of this we reasonably postulated a functional interaction between ERE half sites and the Sp1-rich region downstream.

Results from the EMSA showed that the binding of the untreated nuclear extract to the labeled ERE/Sp1 oligonucleotide, bearing both ERE half site and Sp1 sequence (5′-GGTCAN$_{(12)}$CCGCCC-3′), resulted in a single band which was enhanced in the presence of ectopic ERα and drastically increased upon prolonged E_2 exposure. In the latter condition, a clear immunodepletion occurred in the presence of either anti-Sp1 or anti-ERα antibodies.

The ability of Sp1 and ERα to bind separately was demonstrated by two distinct bands which were abrogated in the presence of an excess of cold oligonucleotide and immunodepleted in the presence of an anti-ERα antibody in a cell-free system.

Progressively increased amounts of purified ERα protein enhanced Sp1 binding to the half ERE/Sp1-binding site in a dose-dependent manner, while increased amounts of Sp1 were unable to do so.

All these data have demonstrated that ERα enhances Sp1 binding and that both ERα and Sp1 can bind directly to the half ERE/Sp1-binding site. On the other hand, the binding of ERα and Sp1 to the ERE/Sp1-containing sequence of the IRS-1 gene promoter was confirmed by ChIP assay which showed an increased occupancy of this region by the two proteins under E_2 treatment. In contrast, this was not observed when, in the ChIP assay, we used the sequence containing the first three ERE half sites. On the basis of these findings, it emerges that the ERE/Sp1-binding site is crucially involved in mediating E_2 responsiveness to the IRS-1 gene. In contrast, the three non-functional ERE half sequences upstream of the ERE/Sp1 site are not involved in the process. This finding acquired relevance when we became aware of how the functional synergism between Sp1 and ERα, through the formation of the ERα/Sp1 complex, was responsible of the activation of other E_2-responsive genes. For instance, in the promoter region of such genes the half palindromic ERE sequence and Sp1 were separated by a number of nucleotides ranging from 10 to 23 nt, such as cyclin D1, bcl2, retinoic acid receptor α1, IGF-binding protein 4, adenosine deaminase, DNA polymerase α, *c-fos*, cathepsin D, transcription factor-E2F1, creatine kinase B, human progesterone receptor A promoter and, recently, *cad* gene (Dubik & Shiu 1992, Wu-Peng *et al.* 1992, Krishnan *et al.* 1994, Rishi *et al.* 1995, Porter *et al.* 1996, 1997, Scholz *et al.* 1998, Wang *et al.* 1998, Petz & Nardulli 2000, Salvatori *et al.* 2000, Saville *et al.* 2000, Tanaka *et al.* 2000, Vyhlidal *et al.* 2000, Li *et al.* 2001, Khan *et al.* 2003).

While models of DNA are typically drawn in a linear array, the packaging of DNA and proteins into the nucleus of a cell requires tremendous compaction. This compaction could facilitate interaction between *trans*-acting factors bound to more distant *cis* elements. For instance, both ERα and SP1 are known to directly associate with the Transcription Factor (TFII) component. In particular, Sp1 has been reported to recruit TFII/TFII-binding protein and mediate formation of the transcription preinitiation complex on the TATA-less promoter (Pugh & Tjian 1991).

On the other hand, ERα as is known, interacts with the TATA-binding protein (TBP) transcription factor IIb (TFIIb) and TBP-associated factor $(TAF)_{II}30$ (Ing *et al.* 1992, Jacq *et al.* 1994, Sabbah *et al.* 1998)). Thus, we can reasonably assume that the interaction of ERα and SP1, by recruiting TFII/TFII-binding protein, could foster the formation of a protein–protein network that helps to establish an active transcriptional complex. Furthermore, the E_2-dependent recruitment of coactivators such as CREB binding protein (CBP)/p300, which can function as a histone acetyltransferase (Ogryzko *et al.* 1996), could help remodel chromatin in different promoters and enhance formation of an interconnected protein–protein and protein–DNA network involved in activation of the IRS-1 gene.

Thus, the active complex ERα/E_2-Sp1 could trigger the interaction between *trans*-acting factors bound to more distant *cis* elements, like the GC downstream elements, potentiating the transcriptional machinery at the level of the whole GC-rich region of the IRS-1 promoter, which is a region reported to have positive active elements on IRS-1 promoter activity (Araki *et al.* 1995).

Thus, with the present findings, we have demonstrated the molecular mechanism through which E_2/ERα up-regulates mouse IRS-1 expression, thereby amplifying IGF-I/insulin signaling.

Since IRS-1 is sufficient to increase rRNA synthesis and cell size (Sun *et al.* 2003), its enhanced expression, upon prolonged E_2 exposure, may establish another intriguing link between E_2, cell growth and its mitogenic potentiality.

Acknowledgements

We thank Dr Domenico Sturino for the English revision of the manuscript and Dr Pasquale Cicirelli for technical assistance. This work was supported by A.I.R.C. grant 2003. The authors declare that there is no conflict of interest that would prejudice the impartiality of this scientific work.

References

Ando' S, Panno ML, Salerno M, Sisci D, Mauro L, Lanzino M & Surmacz E 1998 Role of IRS-1 signaling in insulin-induced modulation of estrogen receptors in breast cancer cells. *Biochemical and Biophysical Research Communication* **253** 315–319.

Andrews NC & Faller DV 1991 A rapid micropreparation technique for extraction of DNA-binding proteins from limiting numbers of mammalian cells. *Nucleic Acids Research* **19** 2499.

Araki E, Haag BL, Matsuda K, Shichiri M & Kahn R 1995 Characterisation and regulation of the mouse insulin receptor substrate gene promoter. *Molecular Endocrinology* **9** 1367–1379.

Ausubel FM, Brent R, Kingston RE, Moore DD, SeidmanJD & Struhl K 1988 Enzymatic manipulation of DNA and RNA. In *Current Protocols in Molecular Biology*, vol.1. pp 3.0.1–3.17.3 Hoboken, NJ: John Wiley & Sons Inc.

Briggs MR, Kadonaga JT, Bell SP & Tjian R 1986 Purification and biochemical characterization of the promoter-specific transcription factor, Sp1. *Science* **234** 47–52.

Clackson T, Gussow D & Jones PT 1991 General application of PCR to gene cloning and manipulation. In *PCR. A Pratical Approach.* pp 185–192. Eds MJ McPherson, P Quirke & GR Taylor. New York: Oxford University Press.

Dickson RB & Lippman ME 1987 Estrogenic regulation of growth factor secretion in human breast carcinoma. *Endocrine Reviews* **8** 29–43.

Dickson RB & Lippman ME 1995 Growth factors in breast cancer. *Endocrine Reviews* **16** 559–589.

Dubik D & Shiu R 1992 Mechanism of estrogen activation of c-myc oncogene expression. *Oncogene* **7** 1587–1594.

Dynan WS & Tjian R 1983 The promoter-specific transcription factor Sp1 binds to upstream sequences in the SV40 early promoter. *Cell* **35** 79–87.

Gaub MP, Bellard M, Scheuer I, Chambon P & Sassone-Corsi P 1990 Activation of the ovalbumin gene by the estrogen receptor involves the Fos-Jun complex. *Cell* **63** 1267–1276.

Gidoni D, Dynan WS & Tjian R 1984 Multiple specific contacts between a mammalian transcription factor and its cognate promoters. *Nature* **312** 409–413.

Guvakova MA & Surmacz E 1997 Overexpressed IGF-I receptors reduce estrogen growth requirements, enhance survival, and promote E-cadherin-mediated cell–cell adhesion in human breast cancer cells. *Experimental Cell Research* **231** 149–162.

Ing NH, Beekman JM, Tsai SY, Tsai MJ & O'Malley BW 1992 Members of the steroid hormone receptor superfamily interact with TFIIB (S300-II). *Journal of Biological Chemistry* **267** 17617–17623.

Jacq X, Brou C, Lutz Y, Davidson I, Chambon P & Tora L 1994 Human TAFII30 is present in a distinct TFIID complex and is required for transcriptional activation by the estrogen receptor. *Cell* **79** 107–117.

Khan S, Abdelrahim M, Samudio I & Safe S 2003 Estrogen receptor/Sp1 complexes are required for induction of cad gene expression by 17 beta-estradiol in breast cancer cells. *Endocrinology* **144** 2325–2335.

Krishnan V, Wang X & Safe S 1994 Estrogen receptor-Sp1 complexes mediate estrogen-induced cathepsin D gene expression in MCF-7 human breast cancer cells. *Journal of Biological Chemistry* **269** 15912–15917.

Lee AV, Jackson JG, Gooch JL, Hilsenbeck SG, Coronado-Heinsohn E, Osborne CK & Yee D 1999 Enhancement of insulin-like growth factor signaling in human breast cancer: estrogen regulation of insulin receptor substrate-1 expression *in vitro* and *in vivo*. *Molecular Endocrinology* **13** 787–796.

Li C, Briggs MR, Ahlborn TE, Kraemer FB & Liu J 2001 Requirement of Sp1 and estrogen receptor alpha interaction in 17 beta-estradiol-mediated transcriptional activation of the low density lipoprotein receptor gene expression. *Endocrinology* **142** 1546–1553.

Mauro L, Salerno M, Panno ML, Bellizzi D, Sisci D, Miglietta A, Surmacz E & Ando' S 2001 Estradiol increases IRS-1 gene expression and insulin signaling in breast cancer cells. *Biochemical and Biophysical Research Communication* **288** 685–689.

Molloy CA, May FEB & Westley BR 2000 Insulin receptor substrate-1 expression regulated by estrogen in the MCF-7 human breast cancer cell line. *Journal of Biological Chemistry* **275** 12565–12571.

Morelli C, Garofalo C, Sisci D, del Roncon S, Cascio S, Tu X, Vecchione A, Sauter ER, Miller WH Jr & Surmacz E 2004 Nuclear insulin receptor substrate 1 interacts with estrogen receptor alpha at ERE promoters. *Oncogene* **23** 7517–7526.

Ogryzko VV, Schiltz RL, Russanova V, Howard BH & Nakatani Y 1996 The transcriptional coactivators p300 and CBP are histone acetyltransferases. *Cell* **87** 953–959.

Paech K, Webb P, Kuiper GG, Nilsson S, Gustafsson JA, Kushner PJ & Scanlan TS 1997 Differential ligand activation of estrogen receptors ERalpha and ERbeta at AP1 sites. *Science* **277** 1508–1510.

Petz LN & Nardulli AM 2000 Sp1 binding sites and an estrogen response element half-site are involved in regulation of the human progesterone receptor A promoter. *Molecular Endocrinology* **14** 972–985.

Porter W, Wang F,Wang W, Duan R & Safe S 1996 Role of estrogen receptor/Sp1 complexes in estrogen-induced heat shock protein 27 gene expression. *Molecular Endocrinology* **10** 1371–1378.

Porter W, Saville B, Hoivik D & Safe S 1997 Functional synergy between the transcription factor Sp1 and the estrogen receptor. *Molecular Endocrinology* **11** 1569–1580.

Pugh BF & Tjian R 1991 Transcription from a TATA-less promoter requires a multisubunit TFIID complex. *Genes and Development* **5** 1935–1945.

Quandt K, Frech K, Karas H, Wingender E & Werner T 1995 MatInd and MatInspector: new fast and versatile tools for detection of consensus matches in nucleotide sequence data. *Nucleic Acids Research* **23** 4878–4884.

Rishi A, Hhao ZM, Baumann R, Li XS, Sheikh S, Kimura S, Bashirelahi N & Fontana J 1995 Estradiol regulation of the human retinoic acid receptor gene in human breast carcinoma cells is mediated via an imperfect half-palindromin estrogen response element and Sp1 motifs. *Cancer Research* **55** 4999–5006.

Sabbah M, Kang KI, Tora L & Redeuilh G 1998 Oestrogen receptor facilitates the formation of preinitiation complex assembly: involvement of the general transcription factor TFIIB. *Biochemical Journal* **336** 639–646.

Salvatori L, Ravenna L, Felli MP, Cardillo MR, Russo MA, Frati L, Gulino A & Petrangeli E 2000 Identification of an estrogen-mediated deoxyribonucleic acid-binding independent transactivation pathway on the epidermal growth factor receptor gene promoter. *Endocrinology* **141** 2266–2274.

Saville B, Wormke M, Wang F, Nguyen T, Enmark E, Kuiper G, Gustafsson JA & Safe S 2000 Ligand-, cell-, and estrogen receptor subtype (alpha/beta)-dependent activation at GC-rich (Sp1) promoter elements. *Journal of Biological Chemistry* **275** 5379–5387.

Scholz A, Truss M & Beato M 1998 Hormone-induced recruitment of Sp-1 mediates estrogen activation of the rabbit uteroglobin gene in endometrial epithelium. *Journal of Biological Chemistry* **273** 4360–4366.

Sun H, Tu X, Prisco M, Wu A, Casaburi I & Baserga R 2003 Insulin-like growth factor receptor signaling and nuclear translocation of insulin receptor substrates 1 and 2. *Molecular Endocrinology* **17** 472–486.

Surmacz E 2000 Function of the IGF-IR in breast cancer. *Journal of Mammary Gland Biology and Neoplasia* **5** 95–105.

Tanaka N, Yonekura H, Yamagishi S, Fujimori H, Yamamoto Y & Yamamoto H 2000 The receptor for advanced glycation end products is induced by the glycation products themselves and tumor necrosis factor-alpha through nuclear factor-kappa B, and by 17 beta-estradiol through Sp-1 in human vascular endothelial cells. *Journal of Biological Chemistry* **275** 25781–25790.

Umayahara Y, Kawamori H, Watada H, Imano E, Iwama N, Morishima T, Yamasaki Y, Kajimoto Y & Kamada T 1994 Estrogen regulation of the insulin-like growth factor I gene transcription involves an AP-1 enhancer. *Journal of Biological Chemistry* **269** 16433–16442.

Vyhlidal C, Samudio I, Kladde MP & Safe S 2000 Transcriptional activation of transforming growth factor alpha by estradiol: requirement for both a GC-rich site and an estrogen response element half-site. *Journal of Molecular Endocrinology* **24** 329–338.

Wang F, Hoivik D, Pollenz R & Safe S 1998 Functional and physical interactions between the estrogen receptor Sp1 and nuclear arcyl hydrocarbon receptor complexes. *Nucleic Acid Research* **26** 3044–3052.

Webb P, Lopez GN, Greene GL, Baxter JD & Kushner PJ 1992 The limits of the cellular capacity to mediate an estrogen response. *Molecular Endocrinology* **6** 157–167.

Webb P, Nguyen P, Valentine C, Lopez GN, Kwok GR, McInerney E, Katzenellenbogen BS, Enmark E, Gustafsson JA, Nilsson S & Kushner PJ 1999 The estrogen receptor enhances AP-1 activity by two distinct mechanisms with different requirements for receptor transactivation functions. *Molecular Endocrinology* **13** 1672–1685.

Weisz A & Rosales R 1990 Identification of an estrogen response element upstream of the human *c-fos* gene that binds the estrogen receptor and the AP-1 transcription factor. *Nucleic Acids Research* **18** 5097–5106.

Wood JR, Greene GL & Nardulli AM 1998 Estrogen response elements function as allosteric modulators of estrogen receptor conformation. *Molecular and Cellular Endocrinology* **18** 1927–1934.

Wu-Peng X, Pugliese T, Dickerman H & Pentecost B 1992 Delineation of sites mediating estrogen regulation of the rat creatine kinase B gene. *Molecular Endocrinology* **6** 231–240.

Yee D & Lee AV 2000 Crosstalk between the insulin-like growth factor and estrogens in breast cancer. *Journal of Mammary Gland Biology and Neoplasia* **5** 1–5.

Received in final form 21 October 2005
Accepted 26 October 2005
Made available online as an Accepted Preprint 18 November 2005

0021-972X/05/$15.00/0
Printed in U.S.A.

The Journal of Clinical Endocrinology & Metabolism 90(8):4753–4761

doi: 10.1210/jc.2004-2233

Leptin Secretion by Human Ejaculated Spermatozoa

Saveria Aquila, Mariaelena Gentile, Emilia Middea, Stefania Catalano, Catia Morelli, Vincenzo Pezzi, and Sebastiano Andò

Department of Pharmaco-Biology (S.Aq., E.M., S.C., C.M., V.P., S.An.), Faculty of Pharmacy; Department of Cell Biology (M.G.); and Centro Sanitario (S.Aq., M.G., E.M., S.C., C.M., V.P., S.An.), University of Calabria, 87030 Arcavacata di Rende (Cosenza), Italy

Introduction: Leptin action is a dynamic area of investigation that continues to broaden beyond the basic lipostatic model originally envisaged. Here, we show that leptin is expressed in and secreted from human ejaculated spermatozoa.

Methods: By RT-PCR, Western blot, and immunofluorescence techniques, we have demonstrated that human sperm express leptin. RIA method evidenced leptin secretion. Phosphatidyl-inositol-kinase-3 (PI3K)/Akt pathway was examined by PI3K activity assay and Western blot. Leptin and insulin regulation of glycogen synthesis was evaluated by glycogen synthase activity (GSA).

Results: The large differences of leptin secretion between uncapacitated and capacitated sperm suggest a functional role for leptin in capacitation. Indeed, in uncapacitated sperm, leptin enhances both cholesterol efflux and protein tyrosine phosphorylation. In uncapacitated sperm, both insulin and leptin increased PI3K activity, Akt S473, and glycogen synthase kinase-3 S9 phosphorylation. Interestingly, during capacitation, concomitantly to the massive release of both hormones, we observed a strong reduction in the phosphorylation of glycogen synthase kinase-3 S9, kinase downstream of Akt that regulates the glycogen synthase. Our results from GSA showed that the enzymatic activity was significantly higher in uncapacitated than in capacitated sperm. Particularly, in uncapacitated sperm, GSA appeared to depend on the hormones concentration, because the enzymatic activity was stimulated at low doses, whereas it was inhibited at high doses. Moreover, both leptin and insulin regulate in autocrine fashion sperm glycogen synthesis.

Conclusion: Leptin secretion by sperm suggests that the male gamete may be able to modulate its metabolism independently by systemic leptin. These data open new considerations about leptin significance in male fertility. **(*J Clin Endocrinol Metab* 90: 4753–4761, 2005)**

RECENT OBSERVATIONS SUGGEST that leptin plays an important role in relaying energetic status to reproduction; to date, the molecular mechanisms underlying the effects of leptin in this context remain elusive (1). Various evidence has pointed to a direct role of leptin in the control of testicular function (2). However, in contrast to its well-proven effects in female fertility, the actual role of the hormone in the regulatory network controlling male reproductive function has been a matter of debate.

The ob/ob mice (lacking of functional leptin) or OB-R/OB-R mice (lacking of functional leptin receptor) are infertile and fail to undergo normal sexual maturation. Importantly, fertility of ob/ob mice is restored by leptin and not by simply reducing body weight, indicating an effect of the hormone *per se* on reproductive function (3, 4). Particularly, male mice (*ob/ob*) had small testes, azoospermia, and multinucleated spermatids. As in the female, hypogonadotropic hypogonadism and infertility are common features in male *ob/ob* mice (5). In line with results from experimental studies, in humans the absence of endogenous leptin is associated with hypogonadism and absence of pubertal development (6–8).

Leptin is expressed in the seminiferous tubules and in seminal plasma (9), but its cellular origin in these contexts is not exactly defined. Several studies support the role of serum leptin in the regulation of gonadal functions in men (10) indirectly via the central neuroendocrine system and directly via peripheral tissue membrane receptors (11, 12). Besides, compelling evidence indicates that leptin functional regulation of the male gonadal axis appears to be a tightly regulated action, carried out at different levels of the hypothalamic-pituitary-testicular system, involving not only stimulatory, but also inhibitory, effects. Recently (13), it was hypothesized that the net effect of leptin upon male reproductive function may depend on the circulating level of the molecule. Thus, predominant stimulatory effects, primarily at the hypothalamus, are observed at physiological leptin levels above a minimal threshold. In contrast, direct inhibitory actions at the testicular level may take place in the presence of a significantly elevated leptin concentration, as detected in obesity (2).

Leptin in various cell types has a range of roles, but the principal role is as a lipostat, signaling to other systems the energy reserves available to the body, mediating fuel use, and consequently energy expenditure. Recently, a new target for leptin in the male genital tract was evidenced because leptin receptor was found to be present in human spermatozoa (9). It has long been recognized that capacitated sperm display an increased metabolic rate and overall energy expenditure, presumably to affect the changes in sperm signaling and function during capacitation (14). However, the relationship between the signaling events associated with capacitation and the changes in sperm energy metabolism is

First Published Online June 8, 2005

Abbreviations: CHOD, Cholesterol-oxidase; GSA, glycogen synthase activity; GSK, glycogen synthase kinase; M-MLV, Moloney murine leukemia virus; PI3K, phosphatidyl-inositol-kinase-3; POD, peroxidase; UDP, uridine diphosphate.

poorly understood. Overall, there is a lack of information regarding how mammalian spermatozoa manage their energy status. In somatic cells, both leptin and insulin play a central role in regulation of energy homeostasis (15). Particularly, *in vitro* and *in vivo* evidence supports the hypothesis that leptin may mimic insulin action on glycogen synthesis (16). Sperm glycogen metabolism seems to be regulated by modulation of glycogen synthase in a manner similar to that observed in other tissues (17).

In the present study, we showed that leptin is expressed in, and secreted from, human ejaculated spermatozoa, providing evidence for a role of the hormone in sperm physiology.

Subjects and Methods

Chemicals

PMN cell isolation medium was from BIOSPA (Milan, Italy). Total RNA Isolation System kit, enzymes, buffers, and nucleotides 100-bp ladder used for RT-PCR were purchased from Promega Corp. (Milan, Italy). Moloney murine leukemia virus (M-MLV) was from Life Technologies Italia (Milan, Italy). Oligonucleotide primers were made by Invitrogen (Milan, Italy). DMEM-F12 medium, BSA protein standard, Laemmli sample buffer, prestained molecular weight markers, Percoll (colloidal polyvinylpyrrolidone-coated silica for cell separation), sodium bicarbonate, sodium lactate, sodium pyruvate, dimethylsulfoxide, Earle's balanced salt solution, and all other chemicals were purchased from Sigma Chemical (Milan, Italy). Acryl amide bisacrylamide was from Labtek Eurobio (Milan, Italy). Triton X-100, Eosin Y was from Farmitalia Carlo Erba (Milan, Italy). ECL Plus Western blotting detection system, Hybond ECL, [γ-^{32}P]ATP, and HEPES sodium salt were purchased from Amersham Pharmacia Biotech (Buckinghamshire, UK). Human leptin RIA kit was from Linco Research, Inc. (St. Charles, MO-Biogemini Sas, Catania, Italy). Cholesterol-oxidase (CHOD)-peroxidase (POD) enzymatic colorimetric kit was from Inter-Medical (Biogemini Sas, Catania, Italy). Monoclonal mouse p85-regulatory subunit of phosphatidyl-inositol-kinase-3 (PI3K) antibody, goat polyclonal actin antibody, polyclonal rabbit antileptin (A-20) antibody, rabbit antiinsulin antibody, rabbit antiphosphotyrosine antibody (PY99), rabbit anti-p-Akt1/Akt2/Akt3 S473 antibody, POD-coupled antirabbit and antigoat, antirabbit IgG fluorescein isothiocyanate-conjugated were from Santa Cruz Biotechnology (Heidelberg, Germany). Rabbit anti-p-glycogen synthase kinase 3 (-GSK-3) S9 antibody was from Cell Signaling (Milan, Italy). Nylon membranes were provided by Roche Diagnostics Corp. (Indianapolis, IN). Uridine diphosphate (UDP) [U-^{14}C]glucose (25 μCi/ml) was from Amersham.

Semen samples and spermatozoa preparations

Ejaculates were collected from healthy volunteers undergoing semen analysis, by masturbation (18), after 3 d of sexual abstinence. The study was approved by the local medical-ethical committees, and all participants gave their informed consent. Sperm samples with normal parameters of semen as volume, sperm count, motility, vitality, and morphology, according to the World Health Organization Laboratory Manual (18), were included in this study. In each experiment, three normal samples were pooled. Spermatozoa preparations were performed as previously described (19).

Evaluation of sperm viability

Viability was assessed using Eosin Y to evaluate potential toxic effects of different treatments. A blinded observer scored 100 cells for stain uptake (dead cells) or exclusion (live cells). Viability was evaluated before and after pooling the samples. There were no adverse effects among the different treatments on human sperm viability (data not shown).

RNA isolation, RT-PCR, and Southern blotting

Total RNA was isolated from human ejaculated spermatozoa purified as previously described (19). PCR amplification of cDNA was performed with 2 U *Taq* DNA polymerase, 50 pmol primer pair (forward, 5′-CAT TGG GGA ACC CTG TGC GGA TTC-3′; reverse, 5′-TGG CAG CTC TTA GAG AAG GCC AGC-3′) in 10 mM Tris-HCl (pH 9.0) containing 0.1% Triton X-100, 50 mM KCl, 1.5 mM $MgCl_2$, and 0.25 mM of each deoxynucleotide triphosphate. The conditions for PCR were: denaturation at 95 C for 1 min, annealing at 55 C for 1 min, and extension at 72 C for 2 min (40 cycles). A DNA marker (100-bp DNA ladder) was used to determine the size of amplified product, that is 348 bp. To check out the presence of DNA contamination, a RT-PCR was performed without M-MLV reverse transcriptase (negative control). The identity of the PCR-amplified cDNA fragment of leptin transcript from human spermatozoa was verified using Southern hybridization. A total of 1–2 ng cDNA probe (5′-CACGCAGTCAGTGTCCTCCA-3′, which corresponds to nucleotide cDNA sequence for human leptin) was labeled with [γ-^{32}P]ATP using polynucleotide kinase. Hybridization was performed overnight at room temperature. Then, membranes were washed with decreasing salt concentrations containing 0.1% sodium dodecyl sulfate, and then exposed to autoradiography with intensifying screens.

Western blot analysis of sperm proteins

Sperm samples, washed twice with Earle's balanced salt solution (uncapacitating medium), were incubated without or with the indicated treatments and then centrifuged for 5 min at 5000 $\times$ *g*. The pellet was resuspended in lysis buffer as previously described (19). Equal amounts of proteins (60 μg) were boiled for 5 min, separated by 10% PAGE, transferred to nitrocellulose sheets, and probed with an appropriate dilution of the indicated antibody. The bound of the secondary antibody was revealed with the ECL Plus Western blotting detection system according to the manufacturer's instructions. The negative control was performed using a sperm lysate that was immunodepleted of leptin (*i.e.* preincubate lysate with antileptin antibody for 1 h at room temperature and immunoprecipitate with protein A/G-agarose).

As internal control, all membranes were subsequently stripped (glycine, 0.2 M, pH 2.6, for 30 min at room temperature) of the first antibody and reprobed with antiactin antibody.

Immunofluorescence assay

Sperm cells, recovered from Percoll gradient, were rinsed three times with 0.5 mM Tris-HCl buffer (pH 7.5) and fixed with absolute methanol for 7 min at −20 C. Leptin staining was carried out, after blocking with normal horse serum (10%), using a rabbit polyclonal antihuman leptin as primary antibody and an antirabbit IgG fluorescein isothiocyanate conjugated (1:100) as secondary antibody. Sperm cells incubated without the primary antibodies were used as the negative controls. The slides were examined under a fluorescence microscope (Olympus BX41; Olympus Corp., Milan Italy), and a minimum of 200 spermatozoa per slide were scored.

Measurement of leptin secreted by human ejaculated spermatozoa

A competitive RIA was applied to measure leptin in sperm culture media. Increasing numbers of spermatozoa were washed twice with unsupplemented Earle's medium (uncapacitating medium) and were incubated in the same medium for 1 h at 37 C and 5% CO_2. Besides, some samples were incubated in Earle's balanced salt solution medium supplemented with 600 mg BSA/100 ml and 200 mg sodium bicarbonate/100 ml (capacitating medium). At the end of the sperm incubation, the culture media were recovered by centrifugation, lyophilized, and subsequently dissolved in 120 μl kit buffer. Human leptin concentrations were determined in duplicate by a human leptin RIA Kit according to manufacturer's instructions. Leptin standards ranged between 0.2–100 ng/ml. The limit of sensitivity for the assay was 0.05 ng/ml. Inter- and intraassay variations were 5.4% and 5.1%, respectively. Leptin results are presented as the original concentrations of the supernatants and are given as nanograms per milliliter.

Measurement of cholesterol in the sperm culture media

Cholesterol was measured in duplicate by a CHOD-POD enzymatic colorimetric method according to manufacturer's instructions in the incubation medium of human spermatozoa. Sperm samples, washed twice with uncapacitating medium, were incubated in the same medium or in capacitating medium for 1 h at 37 C and 5% CO_2. Other samples were incubated without (control) or in the presence of increasing leptin concentrations (10, 50, and 100 ng/ml). At the end of the sperm incubation, the culture media were recovered by centrifugation, lyophilized, and subsequently dissolved in 1 ml buffer reaction. The samples were incubated for 10 min at room temperature; then the cholesterol content was measured with the spectrophotometer at 505 nm. The cholesterol standard used was 200 mg/dl. The limit of sensitivity for the assay was 0.05 mg/dl. Inter- and intraassay variations were 0.71% and 0.57%, respectively. Cholesterol results are presented as the original concentrations and are given per 10×10^6 number of spermatozoa.

PI3K assay

Spermatozoa were washed twice in uncapacitating medium and centrifuged at $800 \times g$ for 20 min. Sperm samples were then incubated for 1 h at 37 C and 5% CO_2 without or with the indicated treatments, and the PI3K assay was performed as previously described (20). A p85 regulatory subunit of PI3K was precipitated from 500 μg sperm lysates. The negative control was performed using a sperm lysate, where p110 catalyzing subunit of PI3K was previously removed by preincubation with the respective antibody (1 h at room temperature) and subsequently immunoprecipitated with protein A/G-agarose.

Glycogen synthase activity (GSA)

The GSA was determined by the principle: glycogen + UDP[U-^{14}C]glucose→glycogen(^{14}C) + UDP.

Washed spermatozoa were incubated for 1 h at 37 C under uncapacitating or capacitating conditions as described above. Both uncapacitated and capacitating sperm were treated with leptin (10 and 50 ng/ml), insulin (3.3 or 10 nM), antileptin (or normal) rabbit serum (1:100) alone or combined with 10 ng/ml leptin, antiinsulin (or normal) rabbit serum (1:100) alone or combined with 3.3 nM insulin, wortmannin (10 μM) alone or combined with 10 ng/ml leptin or 3.3 nM insulin, monensin (25 μM), antileptin (1:100) plus antiinsulin (1:100) antibodies, LiCl (2 mM). After treatment, sperm extracts were performed in KCl (100 mM); EDTA (2 mM); HEPES (20 mM), pH 7.1; phenylmethylsulfonyl fluoride (1 mM). Aliquots of 100 μl were then assayed immediately in a reaction mixture containing glycogen (20 mg/ml), EDTA (5 mM), NaF (50 mM),

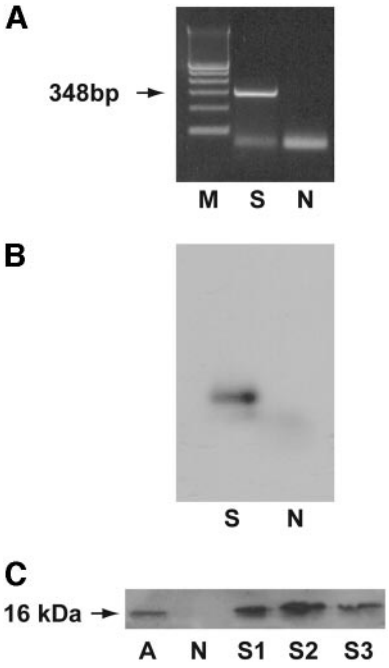

FIG. 1. Leptin expression in human ejaculated spermatozoa. A, RT-PCR analysis of human leptin gene in percolled human ejaculated spermatozoa (S), negative control (no M-MLV reverse transcriptase added) (N), and marker (lane M). *Arrow*, Expected size of the PCR product. B, Southern blot analysis of human leptin gene in percolled human ejaculated spermatozoa (S) and negative control (N). C, Western blot of leptin protein: extracts of pooled purified ejaculated spermatozoa were subjected to electrophoresis on 10% SDS-PAGEs, blotted onto nitrocellulose membranes, and probed with rabbit polyclonal antibody to human leptin. Expression in three samples of ejaculated spermatozoa from normal men (S1, S2, S3). Adipocytes extract was used as control (A). The negative control performed using sperm lysates, where leptin was previously removed by preincubation with the antibody to human leptin (1 h at room temperature) and immunoprecipitated with protein A/G-agarose, is represented in lane 2. The experiments were repeated at least three times for RT-PCR and at least six times for the Western blot, and the autoradiographs of the figure show the results of one representative experiment.

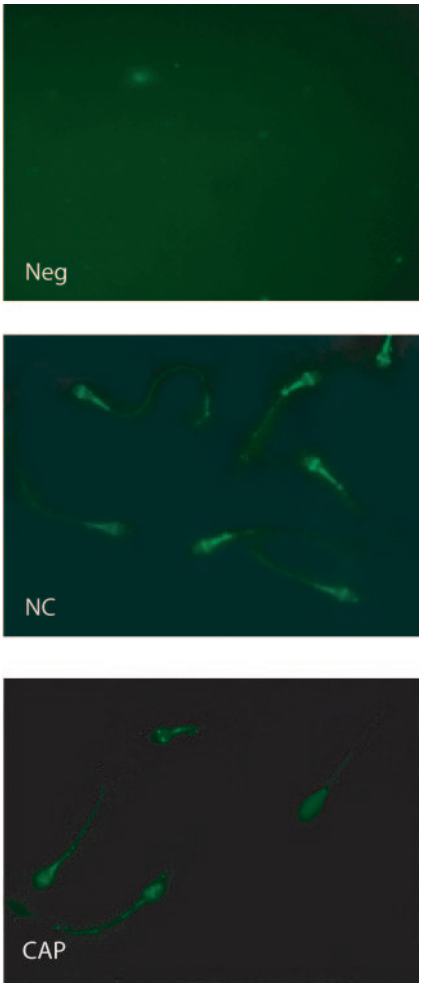

FIG. 2. Immunolocalization of leptin in human ejaculated spermatozoa. Washed spermatozoa were extensively washed and incubated in the unsupplemented Earle's medium (NC) for 1 h at 37 C and 5% CO_2, or in the presence of capacitating medium for 2 h (CAP) under the same experimental conditions. Spermatozoa were then fixed and analyzed by staining with the polyclonal antibody to human leptin. Sperm cells incubated without the primary antibody were used as negative control (Neg). The pictures shown are representative examples of experiments that were performed at least three times with repetitive results.

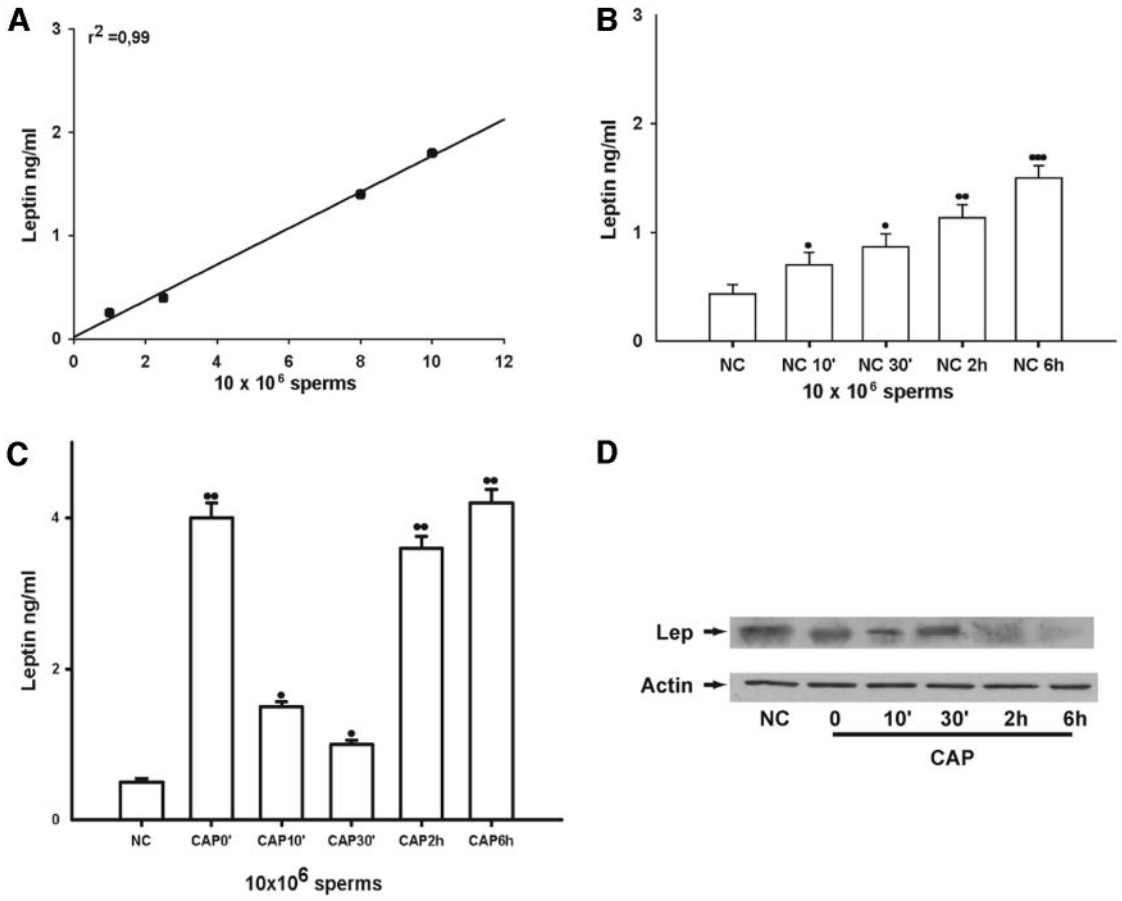

FIG. 3. Leptin secretion from human ejaculated spermatozoa. Washed human spermatozoa were incubated in unsupplemented Earle's balanced salt solution for 1 h at 37 C, 5% CO_2. Leptin secretion in culture medium from human ejaculated spermatozoa was measured by RIA. A, Increasing number of sperm were incubated in unsupplemented Earle's balanced salt solution for 1 h at 37 C, 5% CO_2. Linear regression analysis was performed, and the r was calculated ($r^2 = 0.99$). B, Time course of leptin secretion, at the indicated times, from human spermatozoa incubated in uncapacitating medium (NC). C, Time course of leptin secretion, at the indicated times, from human spermatozoa incubated in capacitating medium (CAP). D, Western blot analysis of protein lysates from sperm incubated under capacitating conditions at the indicated times. Values are means ± SEM of six determinations in a typical experiment. ●, $P < 0.05$; ●●, $P < 0.005$; ●●●, $P < 0.01$ *vs.* control.

UDP glucose (2.5 mM), Tris/HCl (25 mM), UDP [U-^{14}C]glucose (0.0005 mCi/ml), and glucose 6-phosphate (8 mM). The assay was buffered at pH 8.0. The reaction was performed at 37 C; after 15 min, 50 μl of the homogenate/assay buffer was spotted on a Whatman filter paper (1 cm × 2.5 cm). The filters were dropped into cold (4 C) 66% ethanol for 30 min to precipitate glycogen; in addition, they were washed twice at room temperature for 20 min each in 66% ethanol to remove [^{14}C]glucose 1-phosphate. After being dried, the filters were transferred to scintillation vials; 3 ml scintillation solution was added to each, and mixtures were counted for radioactivity. Data are expressed as milliunits UDP-glucose incorporated per milligram protein.

Statistical analysis

The experiments for RT-PCR were repeated on at least three independent occasions, whereas Western blot analysis was performed in at least six independent experiments. The data obtained from RIA (six replicate experiments using duplicate determinations), CHOD-POD enzymatic colorimetric method (six replicate experiments using duplicate determinations), GSA (eight replicate experiments using duplicate determinations) were presented as the mean ± SEM. The differences in mean values were calculated using a paired *t* test, with a significance level of $P < 0.05$. Regression analysis was performed using the SPSS program (SPSS, Inc., Richmond, CA).

Results

RT-PCR, Southern blot, and Western blot showed leptin expression in human sperm

To determine whether mRNA for leptin is present in human ejaculated spermatozoa, RNA, isolated from Percoll-separated samples of normal men, was subjected to reverse PCR and then to Southern blot analysis. The RT-PCR products for leptin in sperm were not a result of any DNA contamination, because the RNA samples were subjected to deoxyribonuclease treatment before RT-PCR. The primer sequences were based on the human leptin gene sequence, and the RT-PCR amplification revealed the expected PCR product size of 348 bp (Fig. 1A). To verify the identity of the amplified products, we performed Southern blot analysis (Fig. 1B). The presence of leptin protein in human ejaculated spermatozoa was investigated by Western blot using an antibody raised against the carboxyl terminus of the mature human leptin protein (Fig. 1C). One immunoreactive band was observed at the same mobility of the adipocytes extract (lane A), used as positive control.

Immunolocalization of leptin in human ejaculated sperm

Using immunofluorescence technique, we identified a positive signal for leptin in human spermatozoa (Fig. 2). Leptin immunoreactivity is specifically compartmentalized in uncapacitated sample at the equatorial segment and at the midpiece (NC), whereas capacitated sperm showed an overall decrease and a more uniform distribution in the signal intensity (CAP).

Measurement of leptin secretion by sperm

The RIA method was used to evaluate whether sperm are able to secrete leptin. After the assay was validated for sperm, we demonstrated that the increase in leptin secretion was dependent on sperm concentration (Fig. 3A). The time course of leptin secretion from spermatozoa into the uncapacitating medium is shown in Fig. 3B. Leptin secretion from 10×10^6 sperm incubated in uncapacitating medium (range, 0.2–2 ng/ml) was significantly lower than that obtained from sperm incubated in capacitating conditions (range, 0.8–4.0 ng/ml) (Fig. 3C). We have attempted to measure the amount of leptin remaining in the sperm after secretion; however, the lysis buffer somehow interferes with the kit-system, altering the binding between antigen and antibody. Then we performed the Western blot analysis of sperm lysates. The time course of capacitating sperm showed a decrease of the hormone inside the sperm (Fig. 3D), according to the increased secretion during capacitation.

Leptin affects both cholesterol efflux and protein tyrosine phosphorylation in sperm

The increased leptin secretion during capacitation suggests a possible role of the hormone in the process. Therefore, we investigated leptin effect on two different and representative aspects of capacitation: cholesterol efflux and protein tyrosine phosphorylation. The importance of the cholesterol efflux in inducing capacitation is historical known, and it has also been demonstrated that it initiates signaling events leading to tyrosine phosphorylation of sperm proteins (21, 22). Washed pooled sperm from normal samples were treated with increasing concentrations of leptin (0, 10, 50, and 100 ng/ml) and incubated under uncapacitating conditions. Then, samples were centrifuged, the upper phase was used to determinate the cholesterol levels, whereas the sperm were lysed to evaluate protein tyrosine phosphorylation. Our results showed a significant increase both in cholesterol efflux (Fig. 4A) and in protein tyrosine phosphorylation (Fig. 4B) upon leptin treatment, suggesting its involvement in the induction of capacitation. However, leptin induction of both processes was not dose-dependent; indeed, concentration as low as 10 ng/ml was able to sustain the greatest increase.

Leptin and insulin effects on PI3K/Akt pathway

The signaling events associated with capacitation and the changes in sperm energy metabolism are issues that remain to be resolved. In somatic cells, leptin and insulin play a central role in regulation of energy homeostasis. In several cell types, including muscle cells (23), adipocytes (24), and hypothalamic neurons (25), both insulin and leptin activate

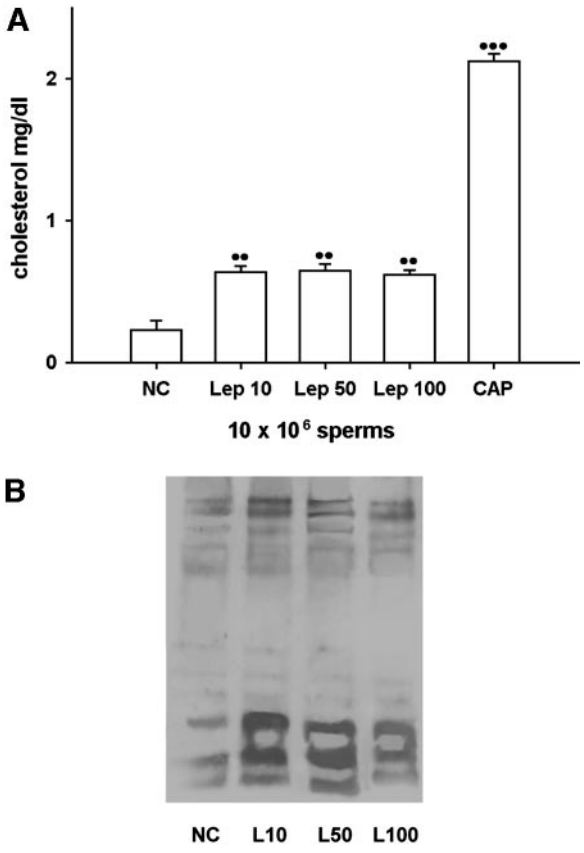

FIG. 4. Leptin affects both cholesterol efflux and protein tyrosine phosphorylation of sperm. Washed spermatozoa were incubated in the unsupplemented Earle's medium for 1 h at 37 C and 5% CO_2, in the absence (NC) or in the presence of increasing concentrations of leptin (Lep) (10, 50, and 100 ng/ml). A, Cholesterol in culture medium from human ejaculated spermatozoa was measured by enzymatic colorimetric assay. Values are means ± SEM of six determinations in a typical experiment. B, Fifty micrograms of sperm lysates were used for Western blot analysis of protein tyrosine phosphorylation. The autoradiograph presented is a representative example of experiments that were performed at least six times with repetitive results. ••, $P < 0.05$; •••, $P < 0.001$ *vs.* control.

PI3K, which may account, at least in part, for similarities in the metabolic effects of these hormones. Our results showed that, in uncapacitated sperm, both leptin and insulin stimulation increased PI3K activity (Fig. 5A) as well as the phosphorylation of Akt and GSK3, two of the major metabolic intermediates downstream of PI3K (Fig. 5B). Intriguingly, GSK3 phosphorylation was abolished in capacitating sperm, suggesting that, during capacitation, there is a block in glycogen synthesis. Concomitantly, in capacitating sperm, we observed a reduction of both hormones inside the sperm (Fig. 5C).

Leptin and insulin effects on GSA

The above reported data led us to further investigate the mechanism underlying the regulation of glycogen synthesis in sperm. Therefore, we evaluated the action of the two hormones on GSA. In somatic cells, i*n vitro* and *in vivo* evidence supports the hypothesis that leptin may mimic insulin action on glycogen synthesis (16). Our results showed that

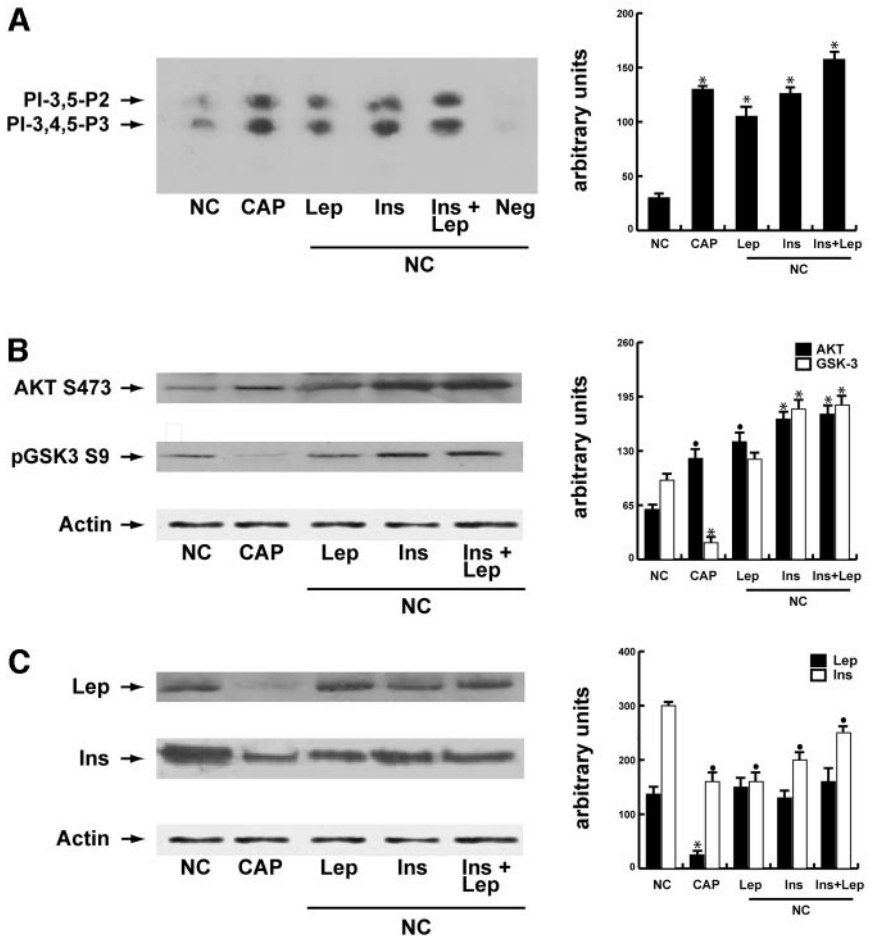

FIG. 5. Leptin and insulin action on PI3K/Akt pathway in human ejaculated spermatozoa. Washed spermatozoa were incubated in the unsupplemented Earle's medium for 1 h at 37 C and 5% CO_2, in the absence (NC) or in the presence of 10 nM leptin (Lep) or in the presence of 3.3 nM insulin (Ins) alone or combined with 10 nM leptin (Ins + Lep). Some samples were washed with the unsupplemented Earle's medium and incubated in capacitating medium for 1 h (CAP). A, A total of 500 μg sperm lysates was immunoprecipitated using anti-p85 regulatory subunit of PI3K incubated in the presence of 200 μM phosphatidylinositol and 10 μCi [γ-^{32}P]ATP for 30 min. The negative control (Neg) was performed using a sperm lysate, where p110 catalyzing subunit of PI3K was previously removed by preincubation with the respective antibody (1 h at room temperature) and subsequently immunoprecipitated with protein A/G-agarose (lane 6). PI-3,4,5-P3, phosphatidylinositol 3,4,5-triphosphate; PI-3,5-P2, phosphatidylinositol 3,5-diphosphate. B and C, A total of 50 μg sperm lysates was used for Western blot analysis of p-AKT S473 or p-GSK3 S9 (B), leptin or insulin (C). The autoradiographs presented are representative examples of experiments that were performed at least six times with repetitive results. •, $P < 0.05$; *, $P < 0.001$ *vs.* control.

GSA was significantly higher in uncapacitated than in capacitated sperm (Figs. 6 and 7). Particularly, in uncapacitated sperm, GSA appears to depend on the hormones concentration: low concentrations (leptin, 10 ng/ml; insulin, 3.3 nM) stimulated the GSA, whereas high concentrations (leptin, 50 ng/ml; insulin, 10 nM) inhibited enzymatic activity. In capacitated sperm, the GSA was unable to discriminate between low and high hormone doses.

Besides, to ascertain whether, in sperm, insulin and leptin regulation of GSA may occur through a short autocrine loop, we used a variety of experimental approaches: immune neutralization of the released hormones, blockage of the hormones release, and blockage of the intracellular messengers activity. To prove that insulin and leptin secreted by sperm are acting on GSA, we absorbed the secreted hormones with the respective antibody. In uncapacitated sperm, antileptin rabbit serum (1:100) plus leptin (Fig. 6) and antiinsulin rabbit serum (1:100) plus insulin (Fig. 7) significantly decreased GSA, compared with sperm incubated in the same conditions with normal rabbit serum (1:100) plus leptin or insulin. As further evidence of autocrine regulation of the hormones on glycogen metabolism, monensin (which blocks cell secretion) (26, 27) significantly decreased GSA. Besides, wortmannin plus leptin or wortmannin plus insulin disrupted the hormones signaling through PI3K (24–26). LiCl, an inhibitor of GSK3β (28), was used as positive control of GSA enzymatic activity. In capacitating sperm, the decrease of GSA was not observed during the same experimental conditions.

Finally, to evaluate whether, in sperm, the GSA was exclusively regulated by insulin and leptin, we used both antibodies simultaneously. Although we observed a significant decrease, the enzymatic activity still persists, suggesting that redundant actions of alternative pathways may exist in the sperm.

Discussion

Animal (4) and human (7, 8) models of leptin resistance and deficiency showed a severe impairment of the reproductive function. However, the contribution of leptin to the proper functioning of the male reproductive system is still pending (2, 29). Leptin is found in the seminiferous tubules and in seminal plasma (9, 30), but the origin of seminal plasma leptin is not exactly defined. In this study, we investigated whether leptin is expressed in and secreted from human ejaculated spermatozoa and whether the hormone may affect their fertilizing ability.

Expression of leptin in the male gamete is a novel finding. In our study, we have demonstrated the presence of leptin in human sperm at different levels: mRNA expression, protein expression and immunolocalization. New reports firmly establish the presence of messenger RNAs in mammalian

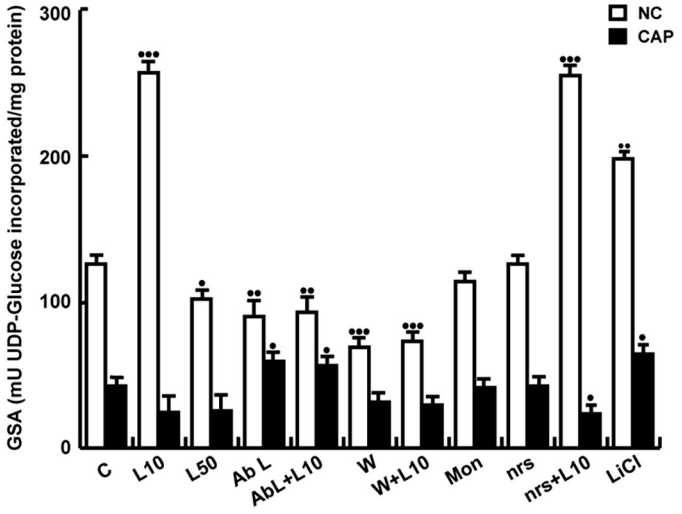

FIG. 6. Effect of leptin, antileptin antibody, wortmannin, and monensin on GSA. Washed spermatozoa were incubated for 1 h at 37 C under uncapacitating or capacitating conditions as described above. Sperm were treated with leptin (10 or 50 ng/ml) (L10 or L50), antileptin antibody (1:100) (Ab L) with or without L10, normal rabbit serum (1:100) (nrs) with or without L10, 10 μM wortmannin (W) with or without L10, 25 μM monensin (Mon), 2 mM LiCl. Data are expressed in nanomoles/min $\times$ 10^6 sperm. Values are means $\pm$ SEM of eight determinations in a typical experiment. ●, $P < 0.05$ *vs.* control (C); ●●, $P < 0.01$ *vs.* control; ●●●, $P < 0.005$ *vs.* control; □, uncapacitated sperm (NC); ■, capacitated sperm (CAP).

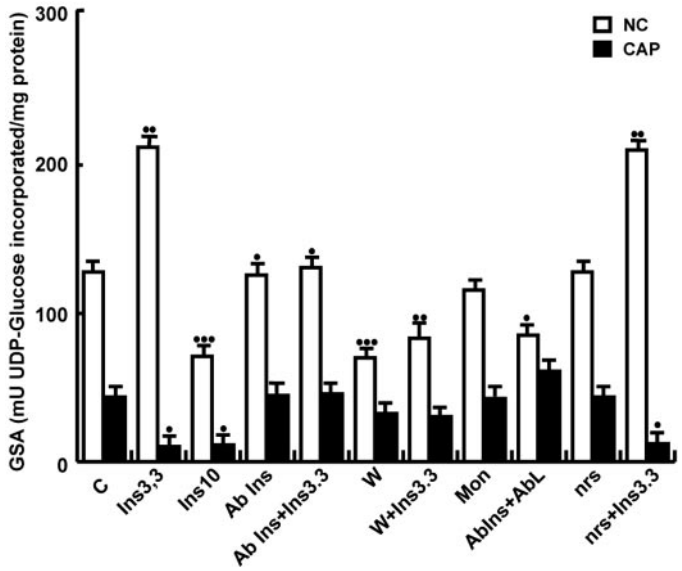

FIG. 7. Effect of insulin, antiinsulin antibody, wortmannin, and monensin on GSA. Washed spermatozoa were incubated for 1 h at 37 C under uncapacitating or capacitating conditions as described above. Sperm were treated with insulin (3.3 nM) or 10 nM (Ins3,3 or Ins10), antiinsulin (or normal, nrs) rabbit serum (1:100) (Ab Ins) alone or combined with 3.3 nM Ins (Ab Ins+Ins3.3) (nrs+Ins3.3), wortmannin 10 μM (W) alone or combined with 3.3 nM Ins, 25 μM monensin (Mon), antiinsulin plus antileptin rabbit serum (AbIns+AbL). Data are expressed in nanomoles per min per 10^6 sperm. Values are means $\pm$ SEM of eight determinations in a typical experiment. ●, $P < 0.05$ *vs.* control (C); ●, $P < 0.05$ *vs.* control; ●●, $P < 0.01$ *vs.* control; ●●●, $P < 0.005$ *vs.* control; □, uncapacitated sperm (NC); ■, capacitated sperm (CAP).

ejaculated spermatozoa. Originally, it was hypothesized that these transcripts were carried over from earlier stages of spermatogenesis, but the analysis and significance of mRNA in these cells are currently under investigation (31). Worthy new findings suggest that some of these transcripts code for proteins essential in early embryo development (32). In our study, leptin expression has also been evidenced by Western blot and by immunofluorescence. Particularly, immunocytochemical analysis showed that the hormone is specifically compartmentalized in uncapacitated sample at the equatorial segment and the midpiece, whereas capacitated sperm showed an overall decrease and a uniform distribution in the signal intensity. These data fit well with the RIA values that showed a significant increase of leptin secretion from capacitating sperm, suggesting an involvement of the hormone in capacitation.

Ejaculated spermatozoa require an extratesticular maturation termed 'capacitation' (14) that *in vivo* occurs within the female reproductive tract. It consists of several molecular events that involve different aspects of sperm physiology whose final aim is making the ejaculated sperm competent to fertilize an egg. Intriguingly, capacitation *in vitro* occurs spontaneously, after the removal of seminal plasma, without a requirement for exogenous mediator, suggesting an autocrine induction of the process (14) by endogenous sperm-derived factors. Despite the importance of capacitation, the biochemical and molecular events of the phenomenon are still poorly understood, and the identities of factors that trigger gamete activation are still unknown.

The efflux of cholesterol is historically known to be one of the first steps of capacitation, and most work has been concentrated on it (Ref. 21 and references therein). Our results showed a significant increase in cholesterol efflux upon leptin treatment in uncapacitated sperm. Moreover, leptin increases the sperm proteins tyrosine phosphorylation, which is an event tightly related to the capacitation and resulting downstream cholesterol efflux (21). However, leptin action on these two events was not dose dependent. These findings may be in context with the hypothesis of a possibly double role of leptin in the male gonads. So far, most studies indicated both positive and negative effects of leptin in gonadal functions (13, 33). Besides, seminal plasma leptin levels were significantly lower in patients with normal spermiogram parameters, compared with pathological semen samples, and showed a negative correlation with the motility of human spermatozoa (9).

It has long been recognized that capacitated sperm display an increased metabolic rate, presumably to affect the changes in sperm signaling and function during capacitation (34). The relationship between the signaling events associated with capacitation and changes in sperm energy metabolism is poorly understood. Recently, we have demonstrated that insulin is expressed in and secreted from human ejaculated spermatozoa (26). In somatic cells, both leptin and insulin play a central role in regulation of energy homeostasis, acting on PI3K/Akt pathway, which principally mediates their metabolic effects (16). Similarly, in uncapacitated sperm, both insulin and leptin increased PI3K activity, Akt S473 and GSK-3 S9 phosphorylations, leading us to hypothesize a similar action of the two hormones in modulating sperm energetic substrates availability during capacitation. Interest-

ingly, during capacitation, when the insulin and leptin secretions are maximal, we observed a strong decrease of GSK-3 S9 phosphorylation, suggesting a potential role of these hormones in modulating sperm glycogen synthesis. In somatic cells, the regulation of glycogen metabolism involves GSK-3 activity, which, in turn, is regulated by tyrosine and serine/threonine phosphorylations, the latter mediated by PI3K and Akt (35). Akt phosphorylates GSK3 on serine residue 9 and then deactivates this enzyme, which, in turn, reduces the phosphorylation and thus enhances the activity of glycogen synthase (36, 37). The conversion of UDP-glucose to glycogen by glycogen synthase is the rate-limiting step in glycogen synthesis (38); and in somatic cells, both leptin and insulin are central in the regulation of GSA.

Worthy, in our study, was the observation that GSA was significantly higher in uncapacitated than in capacitated sperm. Particularly, in uncapacitated sperm, the GSA was stimulated at low levels of both leptin and insulin, whereas it was inhibited at high concentrations. The outcome of signaling activation can depend on differences in ligand concentration (40, 41). Besides, recently it was hypothesized that the net effect of leptin upon male reproductive function may depend on the circulating level of the molecule. Thus, predominant stimulatory effects are observed at leptin levels above a minimal threshold; in contrast, direct inhibitory actions may take place in the presence of a significantly elevated leptin concentration (2, 13).

Furthermore, we have showed an autocrine regulation of GSA by both insulin and leptin in sperm. Particularly, the autocrine blockage significantly decreased GSA in uncapacitated sperm; whereas in capacitating sperm, it was not observed in the same experimental conditions. Besides, because, during capacitation, hormones efflux and multiple changes of the membrane structure rapidly occur, the autocrine blockage may be not appreciable. Our study suggests that, in uncapacitated sperm, the GSK3 is tightly blocked; whereas during capacitation, there is an activation of the enzyme, which, in turn, blocks the GSA. This effect may have physiological relevance in sperm because, during capacitation, energy demand increases, and then sperm mobilizes the glycogen reserves rather than produce it. Our results, together with the presence of leptin receptor in human ejaculated spermatozoa, create the condition for an autocrine leptin loop at this level. Upon achieving threshold concentrations, leptin may act on sperm receptors to induce signal transduction and molecular changes of capacitation.

It also has to be mentioned that mammalian spermatozoa have a fully functional glycogen metabolism, resulting in the presence of glycogen deposits and of GSK3 in the head and in the midpiece (17). Our results regarding the immunolocalization of leptin in uncapacitated sperm fit well with these findings, given that leptin works in the same sites. Glucose is needed for spermatozoa during zona pellucida penetration and sperm-oocyte fusion and to ensure that tyrosine phosphorylation occurs during capacitation (42, 43). Glucose is provided to sperm by the female reproductive tract fluid *in vivo* or by the culture medium *in vitro*; besides, several studies have indicated that stores of glycogen are endogenous sources of glucose in sperm allowing sperm to accommodate glucose-free conditions (39). It may be hypothesized that leptin in uncapacitated sperm is involved in the accumulation of energy substrates, which would be spent during capacitation.

This study shows a new possible endogenous mediator of capacitation, because we found that human ejaculated spermatozoa secrete leptin able to affect some events tightly related to this process. Leptin secretion suggests that the sperm has the ability to modulate its metabolism, according to its energy needs, independently by systemic leptin. In other words, sperm is an alternative site of leptin expression that may represent a protective mechanism in male reproduction to guarantee the accumulation of energy substrates to maintain the gamete fertilizing capability.

Acknowledgments

Our special thanks to D. Sturino (Faculty of Pharmacy, University of Calabria, Italy) for the English review of the manuscript and to Dr. V. Cunsulo (Biogemini Sas, Catania, Italy).

Received November 16, 2004. Accepted May 26, 2005.

Address all correspondence and requests for reprints to: Dr. Sebastiano Andò, Faculty of Pharmacy, University of Calabria, Arcavacata-Rende (Cosenza) 87036, Italy. E-mail: aquisav@libero.it or sebastiano.ando@unical.it.

This work was supported by PRIN 2004 Prot. N. 0067227, AIRC-2003 and MURST and Ex 60%–2004.

References

1. **Barash IA, Cheung CC, Weigle DS** 1996 Leptin is a metabolic signal to the reproductive system. Endocrinology 137:3144–3147
2. **Tena-Sempere M, Barreiro ML** 2002 Leptin in male reproduction: the testis paradigm. Mol Cell Endocrinol 188:9–13
3. **Hileman SM, Pierroz DD, Masuzaki H, Bjorbaek C, El-Haschimi K, Banks WA, Flier JS** 2002 Characterization of short isoforms of the leptin receptor in rat cerebral microvessels and of brain uptake of leptin in mouse models of obesity. Endocrinology 143:775–783
4. **Mounzih K, Lu R, Chehab FF** 1997 Leptin treatment rescues the sterility of genetically obese ob/ob males. Endocrinology 138:1190–1193
5. **Strobel A, Issad T, Camoin L, Ozata M, Strosberg AD** 1998 A leptin missense mutation associated with hypogonadism and morbid obesity. Nat Med 18: 213–215
6. **Wauters M, Considine RV, Van Gaal LF** 2000 Human leptin: from an adipocyte hormone to an endocrine mediator. Eur J Endocrinol 143:293–311
7. **Montague CT, Farooqi IS, Whitehead JP** 1997 Congenital leptin deficiency is associated with severe early-onset obesity in humans. Nature 387:903–908
8. **Farooqi IS, Jebb SA, Langmack G** 1999 Effect of recombinant leptin therapy in a child with congenital leptin deficiency. N Engl J Med 341:879–884
9. **Glander HJ, Lammert A, Paasch U, Glasow A, Kratzsch J** 2002 Leptin exists in tubuli seminiferi and in seminal plasma. Andrologia 34:227–233
10. **Steinman N, Gamzu R, Yogev L, Botchan A, Schreiber L, Yavetz H** 2001 Serum leptin concentrations are higher in azoospermic than in normozoospermic men. Fertil Steril 75:821–822
11. **Caprio M, Isidori AM, Carta AR, Moretti C, Dufau ML, Fabbri A** 1999 Expression of functional leptin receptors in rodent Leydig cells. Endocrinology 140:4939–4947
12. **Tena-Sempere M, Pinilla L, Gonzalez LC, Dieguez C, Casanueva FF, Aguilar E** 1999 Leptin inhibits testosterone secretion from adult rat testis *in vitro*. J Endocrinol 161:211–218
13. **Caprio M, Fabbrini E, Isidori AM, Aversa A, Fabbri A** 2001 Leptin in reproduction. Trends Endocrinol Metab 12:65–72
14. **Visconti PE, Galantino-Homer H, Moore GD, Baley JL, Ning X, Fornes M, Kopf GS** 1998 The molecular basis of sperm capacitation. J Androl 19:242–248
15. **Szanto I, Kahn CR** 2000 Selective interaction between leptin and insulin signaling pathways in a hepatic cell line. Proc Natl Acad Sci USA 97:2355–2360
16. **Aiston S, Agius L** 1999 Leptin enhances glycogen storage in hepatocytes by inhibition of phosphorylase and exerts an additive effect with insulin. Diabetes 48:15–11
17. **Ballester J, Fernandez-Novell JM, Rutllant J, Garcia-Rocha M, Jesus Palomo M, Mogas T, Pena A, Rigau T, Guinovart JJ, Rodriguez-Gil JE** 2000 Evidence for a functional glycogen metabolism in mature mammalian spermatozoa. Mol Reprod Dev 56:207–219
18. **World Health Organization** 1999 Laboratory manual for the examination of

human semen and sperm-cervical mucus interactions. 4th ed. Cambridge, UK: Cambridge University Press
19. **Aquila S, Sisci D, Gentile ME, Middea E, Siciliano L, Andò S** 2002 Human ejaculated spermatozoa contain active P450 aromatase. J Clin Endocrinol Metab 87:3385–3390
20. **Aquila S, Sisci D, Gentile M, Middea E, Catalano S, Carpino A, Rago V, Andò S** 2004 Estrogen receptor (ER)α and ERβ are both expressed in human ejaculated spermatozoa: evidence of their direct interaction with phosphatidylinositol-3-OH kinase/Akt pathway. J Clin Endocrinol Metab 89:1443–1451
21. **Travis AJ, Kopf GS** 2002 The role of cholesterol efflux in regulating the fertilization potential of mammalian spermatozoa. J Clin Invest 110:731–736
22. **Visconti PE, Baley JL, Moore GD, Pan D, Olds-Clarke P, Kopf GS** 1995 Capacitation in mouse spermatozoa I. Correlation between the capacitation state and protein phosphorylation. Development 121:1129–1137
23. **Berti L, Kellerer M, Capp E, Haring HU** 1997 Leptin stimulates glucose transport and glycogen synthesis in C2C12 myotubes: evidence for a PI3-kinase mediated effect. Diabetologia 40:606–609
24. **Venable CL, Frevert EU, Kim YB, Fischer BM, Kamatkon S, Neel BG, Kahn BB** 2000 Overexpression of protein-tyrosine phosphatase-1B in adipocytes inhibits insulin-stimulated phosphoinositide 3-kinase activity without altering glucose transport or Akt/Protein kinase B activation. J Biol Chem 275:18318–18326
25. **Niswender KD, Morrison CD, Clegg DT, Olson R, Baskin DG, Myers Jr MG, Seeley RJ, Schwartz MW** 2003 Insulin activation of phosphatidylinositol 3-kinase in the hypothalamic arcuate nucleus: a key mediator of insulin-induced anorexia. Diabetes 52:227–231
26. **Aquila S, Gentile M, Middea E, Catalano S, Andò S** 2005 Autocrine regulation of insulin secretion in human ejaculated spermatozoa. Endocrinology 146: 552–557
27. **Nabarra B, Andrianarison I** 1987 Pattern of secretion in thymic epithelial cells: ultrastructural studies of the effect of blockage at various levels. Cell Tissue Res 249:171–178
28. **Gould TD, Gray NA, Manji HK** 2003 Effects of a glycogen synthase kinase-3 inhibitor, lithium, in adenomatous polyposis coli mutant mice. Pharmacol Res 48:49–53
29. **Magni P, Martini L, Motta M** 2001 Leptin actions on the reproductive axis. J Clin Endocrinol Metab 86:946–947
30. **Jope T, Lammert A, Kratzsch J, Paasch U, Glander HJ** 2003 Leptin and leptin receptor in human seminal plasma and in human spermatozoa. Int J Androl 26:335–341
31. **Miller D** 2000 Analysis and significance of messenger RNA in human ejaculated spermatozoa. Mol Reprod Dev 56:259–264
32. **Ostermeier GC, Dix DJ, Miller D, Khatri P, Krawetz SA** 2002 Spermatozoal RNA profiles of normal fertile men. Lancet 360:772–777
33. **Clarke IJ, Henry BA** 1999 Leptin and reproduction. Rev Reprod 4:48–55
34. **Travis AJ, Jorgez CJ, Merdiushev T, Jones BH, Dess DM, Diaz-Cueto L, Storey BT, Kopf GS, Moss SB** 2003 Functional relationships between capacitation-dependent cell signaling and compartmentalized metabolic pathways in murine spermatozoa. J Biol Chem 276:7630–7636
35. **Van Weeren PC, De Bruyn KM, De Vries-Smits AM, Van Lint J, Burgering BM** 1998 Essential role for protein kinase B (PKB) in insulin-induced glycogen synthase kinase 3 inactivation. Characterization of dominant-negative mutant of PKB. J Biol Chem 273:13150–13156
36. **Cross DA, Alessi DR, Cohen P, Andjelkovich M, Hemmings BA** 1995 Inhibition of glycogen synthase kinase-3 by insulin mediated by protein kinase B. Nature 378:785–789
37. **Markuns JF, Wojtaszewski JF, Goodyear LJ** 1999 Insulin and exercise decrease glycogen synthase kinase-3 activity by different mechanisms in rat skeletal muscle. J Biol Chem 274:24896–24900
38. **Gomis RR, Ferrer JC, Guinovart JJ** 2000 Shared control of hepatic glycogen synthesis by glycogen synthase and glucokinase. Biochem J 3:811–816
39. **Albarracin JL, Fernandez-Novell JM, Ballester J, Rauch MC, Quintero-Moreno A, Pena A, Mogas T, Rigau T, Yanez A, Guinovart JJ, Slebe JC, Concha II, Rodriguez-Gil JE** 2004 Gluconeogenesis-linked glycogen metabolism is important in the achievement of in vitro capacitation of dog spermatozoa in a medium without glucose. Biol Reprod 71:1437–1445
40. **Marshall CJ** 1995 Specificity of receptor tyrosine kinase signaling: transient versus sustained extracellular signal-regulated kinase activation. Cell 80:179–185
41. **Castoria G, Lombardi M, Barone MV, Bilancio A, Di Domenico M, Bottero D, Vitale F, Migliaccio A, Auricchio F** 2003 Androgen-stimulated DNA synthesis and cytoskeletal changes in fibroblasts by a nontranscriptional receptor action. J Cell Biol 161:547–556
42. **Urner F, Leppens-Luisier G, Sakkas D** 2001 Protein tyrosine phosphorylation in sperm during gamete interaction in the mouse: the influence of glucose. Biol Reprod 64:1350–1357
43. **Williams AC, Ford WC** 2001 The role of glucose in supporting motility and capacitation in human spermatozoa. J Androl 22:680–695

JCEM is published monthly by The Endocrine Society (http://www.endo-society.org), the foremost professional society serving the endocrine community.

Oncogene (2004) 23, 9269–9279

www.nature.com/onc

Retinoic acid mediates degradation of IRS-1 by the ubiquitin–proteasome pathway, via a PKC-dependant mechanism

Sonia V del Rincón[1], Qi Guo[1], Catia Morelli[2], Hoi-Ying Shiu[1], Eva Surmacz[3] and Wilson H Miller Jr*,[1]

[1]*Lady Davis Institute for Medical Research, Sir Mortimer B Davis Jewish General Hospital and McGill University, Departments of Oncology and Medicine, Montreal, Quebec, Canada;* [2]*Postgraduate School in Clinical Pathology, University of Calabria, Cosenza, Italy;* [3]*Kimmel Cancer Center, Thomas Jefferson University, Philadelphia, PA 19107, USA*

Insulin receptor substrate-1 (IRS-1) mediates signaling from the insulin-like growth factor type-I receptor. We found that all-*trans* retinoic acid (RA) decreases IRS-1 protein levels in MCF-7, T47-D, and ZR75.1 breast cancer cells, which are growth arrested by RA, but not in the RA-resistant MDA-MB-231 and MDA-MB-468 cells. Based on prior reports of ubiquitin-mediated degradation of IRS-1, we investigated the ubiquitination of IRS-1 in RA-treated breast cancer cells. Two proteasome inhibitors, MG-132 and lactacystin, blocked the RA-mediated degradation of IRS-1, and RA increased ubiquitination of IRS-1 in the RA-sensitive breast cancer cells. In addition, we found that RA increases serine phosphorylation of IRS-1. To elucidate the signaling pathway responsible for this phosphorylation event, pharmacologic inhibitors were used. Two PKC inhibitors, but not a MAPK inhibitor, blocked the RA-induced degradation and serine phosphorylation of IRS-1. We demonstrate that RA activates PKC-δ in the sensitive, but not in the resistant cells, with a time course that is consistent with the RA-induced decrease of IRS-1. We also show that: (1) RA-activated PKC-δ phosphorylates IRS-1 *in vitro*, (2) PKC-δ and IRS-1 interact in RA-treated cells, and (3) mutation of three PKC-δ serine sites in IRS-1 to alanines results in no RA-induced *in vitro* phosphorylation of IRS-1. Together, these results indicate that RA regulates IRS-1 levels by the ubiquitin–proteasome pathway, involving a PKC-sensitive mechanism.
Oncogene (2004) **23,** 9269–9279. doi:10.1038/sj.onc.1208104
Published online 1 November 2004

Keywords: retinoic acid; IRS-1; ubiquitin; PKC; breast cancer

Introduction

The family of insulin receptor substrate (IRS) proteins (IRS 1–4) function as the central substrates in the insulin and insulin-like growth factor type-I (IGF-I) receptor signal transduction pathways (Sun *et al*., 1991; Lavan *et al*., 1997). Specifically, IRS-1 functions as a critical scaffolding protein between the activated IGF-IR and various downstream signaling pathways, including the PI3-kinase/AKT and MAPK pathways (Shepherd *et al*., 1998; Burks and White, 2001). Among its many functions, this protein has been shown to regulate cell proliferation and survival (White, 1997). In hematopoietic cells, IRS-1 is an essential regulator of proliferation in response to insulin (Wang *et al*., 1993), and in NIH 3T3 cells, cellular transformation can be directly induced by overexpressing IRS-1 (Ito *et al*., 1996). Several studies have highlighted the importance of IRS-1 in breast cancer pathogenesis: IRS-1 overexpression in breast cancer cells causes a loss of estrogen-dependant growth (Surmacz and Burgaud, 1995), high levels of IRS-1 in human breast tumors correlate with increased disease recurrence (Rocha *et al*., 1997; Lee *et al*., 1999), constitutive IRS-1 signaling exists in breast tumors (Chang *et al*., 2002), and expression of dominant-negative or antisense IRS-1 vectors in breast cancer cells decreases their transformation potential (Ando *et al*., 1998; Chang *et al*., 2002). This suggests that we may develop molecular strategies targeting IRS-1 by understanding the mechanisms controlling its expression and turnover.

Previous studies have suggested that the expression of IRS-1 can be regulated at the level of transcription and proteolysis. 17-β-Estradiol (E2) increases IRS-1 levels by increasing mRNA and protein levels (Lee *et al*., 1999; Molloy *et al*., 2000; Gonzalez *et al*., 2001), while antiestrogens decrease IRS-1 mRNA and/or protein levels (Salerno *et al*., 1999; Chan *et al*., 2001). Glucocorticoids also reportedly decrease the levels of IRS-1 mRNA and protein (Turnbow *et al*., 1994; Buren *et al*., 2002). Using various cellular systems, including MCF-7 breast cancer cells, it has been shown that prolonged treatment with IGF-I and high concentrations of insulin can induce degradation of IRS-1 and IRS-2 via the ubiquitin–proteasome pathway (Sun *et al*., 1999; Lee *et al*., 2000; Zhang *et al*., 2000; Haruta *et al*., 2000).

Retinoids, including all-*trans*-retinoic acid (RA), have been shown to induce G1 arrest and differentiation in

*Correspondence: WH Miller Jr, Lady Davis Institute, 3755 Cote Ste-Catherine Rd., Montreal, Quebec, Canada H3T 1E2;
E-mail: wmiller@ldi.jgh.mcgill.ca
Received 15 April 2004; revised 7 July 2004; accepted 17 August 2004; published online 1 November 2004

several cancer cell types by regulating various cellular factors. We previously showed that RA-mediated growth arrest of MCF-7 cells involves a decrease in IRS-1 protein levels (del Rincón *et al*., 2003), and others have associated G1 arrest of bronchial epithelial cells with an RA-mediated decrease of cyclin D1 protein levels (Langenfeld *et al*., 1997; Boyle *et al*., 1999) and RA-mediated differentiation of F9 embryonal carcinoma cells with a decrease in the protein levels of the transcriptional coactivator, p300 (Iwao *et al*., 1999; Brouillard and Cremisi, 2003). Although the past two decades have focused on examining transcriptional mechanisms linked to the pleiotropic effects of RA, the importance of post-translational modification of various proteins has been recently highlighted. RA has been shown to induce ubiquitination of a number of proteins, including cyclin D1 (Spinella *et al*., 1999), p300 (Brouillard and Cremisi, 2003), and Skp2 (Dow *et al*., 2001), and IRS-1 is known to be conjugated by ubiquitin (Lee *et al*., 2000). However, the ubiquitination of IRS-1 by RA has not been reported. Therefore, we tested the hypothesis that RA-mediated growth inhibition of breast cancer cells is associated with proteolytic degradation of IRS-1 by the ubiquitin–proteasome pathway.

Results

Regulation of IRS-1 protein levels in MCF-7 cells and other retinoid-responsive breast cancer cell lines

Consistent with our previous findings, exposure of MCF-7 cells to 1 μM RA for 72 h in serum-free media (SFM) results in a dose-dependant decrease in IRS-1 protein levels (Figure 1a) (del Rincón *et al*., 2003). Previous studies have shown that antiestrogens and glucocorticoids alter IRS-1 levels (Turnbow *et al*., 1994; Salerno *et al*., 1999; Chan *et al*., 2001; Buren *et al*., 2002); thus, we investigated whether other nuclear receptor-selective ligands would induce a similar decrease in IRS-1 levels. As expected, treatment of MCF-7

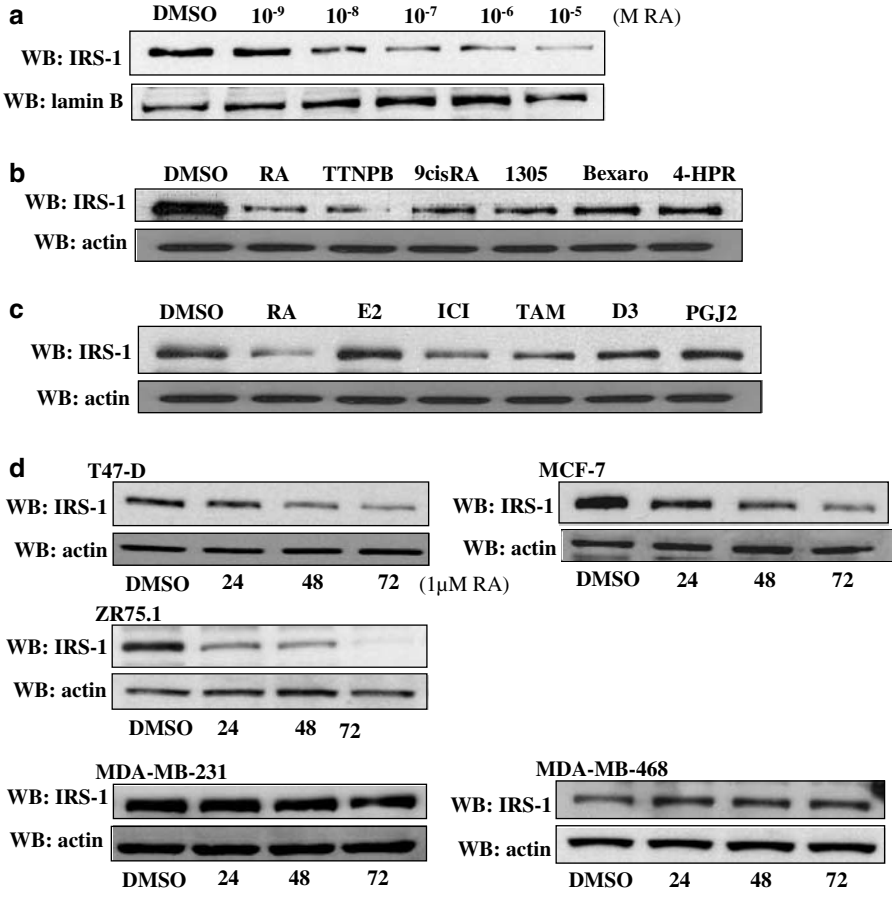

Figure 1 RA decreases IRS-1 protein levels in retinoid-sensitive breast cancer cell lines. Western blotting (WB) was used to determine the expression level of IRS-1 in (**a**)–(**d**). (**a**) MCF-7 cells were treated for 72 h in serum-free media (SFM) with increasing doses of RA (10^{-9}, 10^{-8}, 10^{-7}, 10^{-6}, 10^{-5} M). Lamin B was used as a loading control. (**b**) MCF-7 cells were treated with various retinoids: TTNPB, 9*cis*RA, LGD1305 (1305), Bexarotene (Bexaro), *N*-(4-hydroxyphenyl)retinamide (4-HPR) for 72 h in SFM. (**c**) MCF-7 cells were treated with various ligands: 17-β-estradiol (E2), tamoxifen (Tam), ICI 182780 (ICI), 1,25-dihydroxyvitamin D3 (D3), and 15-deoxy-delta 12,14-prostaglandin J2 (PGJ2) for 72 h in SFM. β-Actin (actin) was used as a loading control. (**d**) Various breast cancer cell lines (T47-D, MCF-7, ZR75.1, MDA-MB-231, MDA-MB-468) were treated with 1 μM RA for 24, 48, and 72 h in SFM

cells with Tamoxifen and ICI 182780 results in decreased IRS-1 levels (Figure 1c). We also observed a decrease with RAR-α (TTNPB), RXR-selective ligands (LGD1305 and Bexarotene), and *N*-(4-hydroxyphenyl)-retinamide (4-HPR) (Figure 1b), while no significant effect was observed after treatment with the vitamin D3 selective ligand (1,25-dihydroxyvitamin D3) or the PPAR-selective ligand (15-deoxy-delta 12,14-prostaglandin J2) for 3 days (Figure 1c).

Although the mechanism of RA-mediated growth inhibition is unclear, it has generally been found that RA inhibits the growth of breast cancer cells that are ER-positive (MCF-7, T47-D, ZR75.1), while having minimal effects on breast cancer cells that are ER-negative (MDA-MB-231, MDA-MB-468) (van der Burg *et al*., 1993; Rosenauer *et al*., 1998). We hypothesized that regulation of IRS-1 levels by RA would correlate with RA-mediated growth inhibition of breast cancer cells. We treated RA-sensitive and RA-resistant breast cancer cell lines with 1 μM RA for 24, 48 and 72 h in SFM. In support of our hypothesis, the RA-sensitive cells responded to 1 μM RA treatment with a similar decrease in IRS-1 protein levels as MCF-7 cells, while the two RA-resistant cell lines did not (Figure 1d).

RA induces a post-translational modification of IRS-1 in MCF-7 cells

Previous studies have suggested that IRS-1 can be regulated at the transcriptional level (Lee *et al*., 1999; Molloy *et al*., 2000; Huang *et al*., 2002). MCF-7 cells were treated with 10 μM RA for 24, 48 and 72 h, total RNA was extracted and IRS-1 mRNA expression was examined by Northern blot, wherein the 8.5 kb transcript is shown (Figure 2a, top panel). Using RT–PCR, we observed no change in IRS-1 mRNA expression at any of the time points examined in the presence of 1 or 10 μM RA, however, ICI 182780 was shown to decrease IRS-1 mRNA levels, consistent with previously published reports (Salerno *et al*., 1999) (Figure 2a, bottom panel).

Recently, IRS-1 has been shown to translocate to the nuclei in various cellular backgrounds stimulated with insulin or IGF-I (Boylan and Gruppuso, 2002; Tu *et al*., 2002; Sun *et al*., 2003). Since the regulation of IRS-1 nuclear/cytoplasmic trafficking is not a well-understood process, we examined whether the RA-mediated decrease in IRS-1 protein levels might involve the regulation of IRS-1 localization. We prepared cytosolic and nuclear extracts from MCF-7 cells grown in serum-free medium with or without 1 μM RA for 72 h. Under these conditions, there did not appear to be any redistribution of IRS-1 into the nucleus (Figure 2b).

Based on these results, we hypothesized post-transcriptional effect of RA on the synthesis or degradation rate of IRS-1. We first examined whether the decline in IRS-1 protein in MCF-7 cells treated with RA results from a decrease in the rate of IRS-1 synthesis. Using pulse-labeling with [^{35}S]methionine, we measured the synthesis rate of IRS-1 in MCF-7 cells pretreated with RA. The rate of IRS-1 synthesis was similar in cells treated with DMSO vehicle or RA, suggesting that this is not the mechanism by which RA alters IRS-1 protein levels (Figure 2c). We then measured the rate of degradation of IRS-1 in the presence of DMSO or RA by pulse–chase analysis and found that RA-treated MCF-7 cells showed an accelerated rate of IRS-1 degradation compared to those cells treated with DMSO alone (Figure 2d). This suggests that RA activates a proteolytic pathway in MCF-7 cells that may be responsible for the degradation of IRS-1.

Effects of proteasome and protease inhibitors on degradation of IRS-1 by RA in breast cancer cells

Previous studies have reported that the levels of IRS-1 can be regulated by IGF-I and insulin at the protein level via the ubiquitin–proteasome pathway (Sun *et al*., 1999; Lee *et al*., 2000; Zhang *et al*., 2000; Zhande *et al*., 2002). We therefore tested whether the effects of RA on IRS-1 were mediated via a similar mechanism. The proteasome inhibitors lactacystin and MG-132 are reagents that inhibit the activity of the 26S proteasome, causing the accumulation of ubiquitinated proteins otherwise degraded by the ubiquitin–proteasome pathway. As shown in Figure 3a the decrease in IRS-1 levels in MCF-7 cells treated with 10 μM RA for 48 h was rescued by the addition of lactacystin to the culture medium for the last 12 h of RA treatment. Similarly, MG-132 reversed the RA-mediated decline in IRS-1 levels (Figure 3b). Cyclin D1 is a protein known to be regulated by RA-mediated ubiquitination and subsequent proteolysis (Langenfeld *et al*., 1997; Spinella *et al*., 1999; Dow *et al*., 2001). In Figure 3b, we show a similar rescue of cyclin D1 levels by MG-132 in RA-treated MCF-7 cells.

We next assessed whether IRS-1 levels could be restored by the addition of proteasome inhibitors in other RA-sensitive breast cancer cells. In the retinoid-responsive breast cancer cell lines T47-D and ZR75.1, we added MG-132 for the last 12 h of a 48-h 10 μM RA treatment and observed a restoration of IRS-1 levels (Figure 3c). We further demonstrate the effect of RA on IRS-1 by immunofluorescence in T47-D cells (Figure 3d). Consistent with our Western blot data, treatment with RA for 48 h decreased IRS-1 protein staining, and treatment with MG-132 for the last 12 h of RA treatment blocked this effect. It has been reported that IRS-2 is regulated at the post-translational level via increased protein ubiquitination (Hirashima *et al*., 2003; Morelli *et al*., 2003); however, we failed to observe any regulation in the protein expression of IRS-2 in any of the breast cancer cell lines treated with RA (data not shown). Although MG-132 is an inhibitor of the proteasome, it also inhibits calpains, calcium-activated cysteine proteases. Furthermore, some studies have shown that IRS-1 degradation can be mediated via calpains (Smith *et al*., 1993), so we assessed whether RA induces a decline in IRS-1 levels via a mechanism involving calpains.

In our system, the addition of the cell-permeable calpain inhibitor, calpeptin, could not restore IRS-1

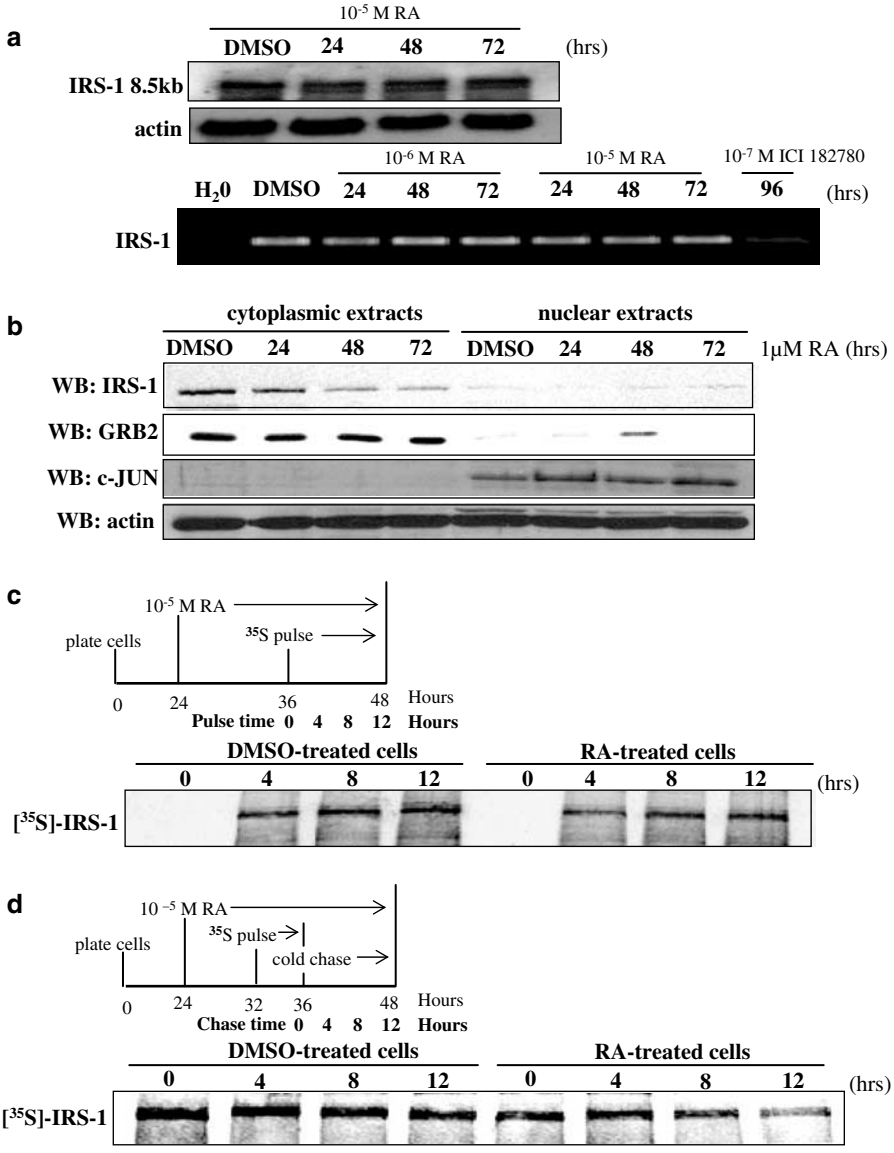

Figure 2 RA induces a post-translational modification of IRS-1 in MCF-7 cells. (**a**) MCF-7 cells were treated with 10^{-5} M RA in SFM for 24, 48, or 72 h and the expression of IRS-1 mRNA was evaluated by Northern blot (top panel). Actin was used to ensure equal loading. RT–PCR was used to detect IRS-1 levels in MCF-7 cells treated with 10^{-6} M or 10^{-5} M RA, or 10^{-7} M ICI 182780 (bottom panel). All data are representative of four independent experiments. (**b**) Subcellular fractionation was used to examine the expression of IRS-1 in cytoplasmic and nuclear protein lysates obtained from MCF-7 cells treated with RA for 24, 48, and 72 h. To control for the purity of the fractions, the levels of a nuclear protein (c-Jun), and a cytoplasmic protein (Grb2) were assessed by stripping and reprobing membranes. (**c**) The synthesis rate of IRS-1 in MCF-7 cells treated for 24 h in the presence of DMSO or 10^{-5} M RA was determined by pulse labeling with [^{35}S]methionine. IRS-1 abundance was analysed at 0, 4, 8, and 12 h time intervals after the pulse. (**d**) The degradation rate of IRS-1 in MCF-7 cells treated for 24 h in the presence of DMSO or 10^{-5} M RA was determined by pulse–chase analysis with [^{35}S]methionine. IRS-1 abundance was analysed at 0, 4, 8, and 12 h time intervals after the chase

levels (data not shown). This suggests that RA does not decrease IRS-1 levels via activation of a calpain-dependent pathway, but rather it may be increasing proteasomal activity.

RA enhances ubiquitination of IRS-1 in breast cancer cells

Proteasomal degradation of proteins involves the prior conjugation of ubiquitin to the targeted protein. We examined whether ubiquitin-IRS-1 complexes could be formed in breast cancer cells treated with RA. IRS-1 immunoprecipitation and ubiquitin Western blotting revealed that the level of ubiquitin-IRS-1 conjugates is augmented in MCF-7 cells treated with RA and MG-132 compared to either agent alone (Figure 4a). This result was supported by cotransfection experiments using expression vectors for flag-IRS-1 and HA-Ub in MCF-7 cells. The cells were transfected with both

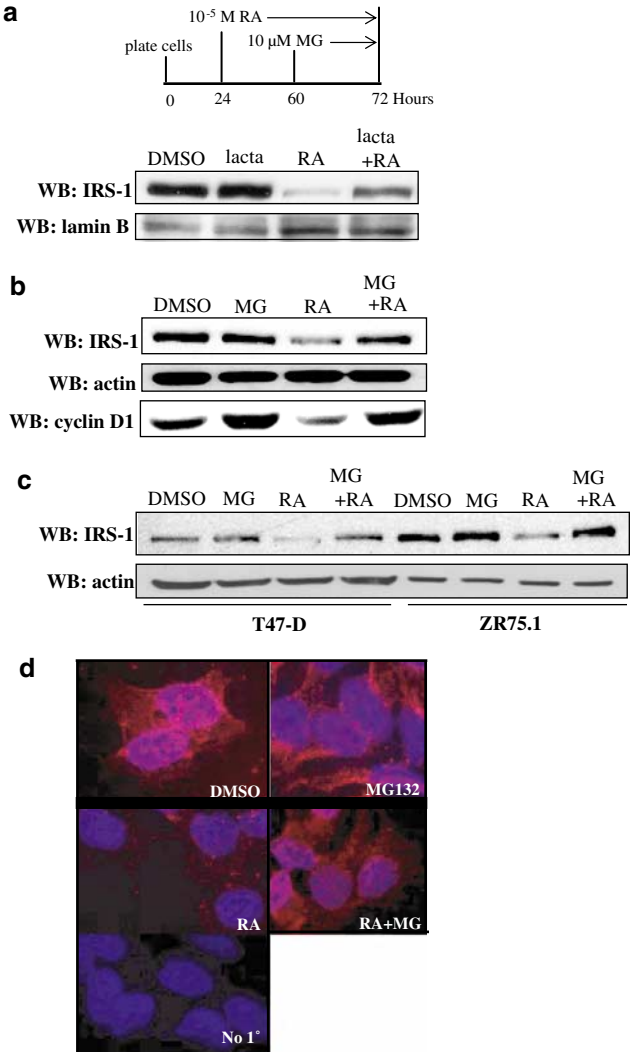

Figure 3 Proteasome inhibitors block the RA-mediated decrease in IRS-1 protein levels in retinoid-sensitive breast cancer cells. WB was used to determine the expression level of IRS-1 in (**a**)–(**c**). (**a**) MCF-7 cells were treated with DMSO or 10^{-5} M RA for 48 h in SFM. 10^{-5} M Lactacystin (lacta) was added for the last 12 h of RA treatment. (**b**) MCF-7 cells were treated with DMSO or 10^{-5} M RA for 48 h in SFM. 10^{-5} M MG-132 (MG) was added for the last 12 h of RA. Cyclin D1 levels were detected by WB. The data depicted are representative of at least three independent experiments. (**c**) T47-D and ZR75.1 cells were treated with DMSO or 10^{-5} M RA for 48 h in SFM. 10^{-5} M MG was added for the last 12 h of RA treatment. (**d**) T47-D cells were treated with DMSO or 10^{-5} M RA for 48 h in SFM. 10^{-5} M MG was added for the last 12 h of RA treatment. Immunofluorescence was used to detect IRS-1 proteins (red fluorescence) in cytoplasm of T47-D cells. DAPI staining revealed the nucleus (blue fluorescence). Similar results were repeated in MCF-7 cells (data not shown)

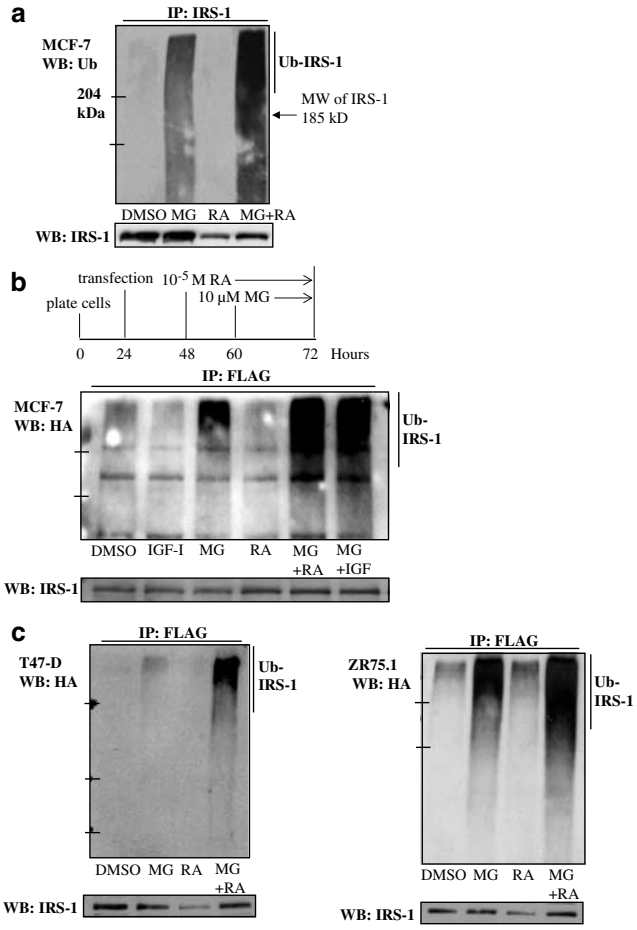

Figure 4 RA enhances ubiquitination of IRS-1 in breast cancer cells. (**a**) MCF-7 cells were treated with DMSO or 10^{-5} M RA for 48 h in SFM. 10^{-5} M MG-132 was added for the last 12 h of RA treatment. IRS-1 was immunoprecipitated (IP) from protein lysates, and the level of ubiquitination was evaluated by WB with an anti-ubiquitin (Ub) antibody. The same membrane was stripped and reprobed for IRS-1. (**b**) MCF-7 cells were transiently transfected with HA-Ub and flag-IRS-1 constructs. Cells were then treated in SFM for 24 h with 10 nM IGF-I or 10^{-5} M RA. 10^{-5} M MG-132 was added for the last 12 h of RA or IGF-I treatment. FLAG was immunoprecipitated (IP) from protein lysates, and the level of flag-IRS-1/HA-Ub interaction was evaluated by WB with an anti-HA (HA) antibody. The same membrane was stripped and reprobed for IRS-1. (**c**) T47-D and ZR75.1 cells were transfected and treated as described in (**b**)

vectors and treated with either 10 μM RA or 10 nM IGF-I for 24 h, with or without the addition of MG-132 for the last 12 h of RA treatment. To show that IRS-1-ubiquitin conjugates bound more effectively in the presence of RA, these cells were lysed and the lysate immunoprecipitated with anti-flag antibodies and immunoblotted with anti-HA antibodies (Figure 4b). RA and MG-132 induced a marked increase in the association of flag-IRS-1 and Ha-Ub compared to MG-132 alone (Figure 4b, compare lanes 3 and 5). Furthermore, consistent with prior reports, IGF-I and MG-132 also augmented the level of detectable IRS-1-Ub conjugates in MCF-7 cells compared to MG-132 alone (Figure 4b, compare lanes 3 and 6) (Lee *et al*., 2000). In two other RA-sensitive breast cancer cell lines, we found a similar dramatic increase in IRS-1-ubiquitin conjugates upon treatment with RA and MG-132 (Figure 4c). Taken together, these results show that RA enhances the ubiquitination of IRS-1.

Inhibiting the PKC pathway blocks the RA-mediated phosphorylation and degradation of IRS-1

Recent studies have shown that serine/threonine phosphorylation of IRS-1 signals its degradation, suggesting a requirement for the activation of specific kinases to regulate the levels of IRS-1. In support of this hypothesis, we find that RA-treated MCF-7 cells grown in 10% FBS have a greater and more rapid decrease in IRS-1 protein levels than when grown in serum-free media (Figure 5a). Consistent with the activation of a serine/threonine kinase in breast cancer cells treated with RA, we observe an increase in the total serine phosphorylation of IRS-1 (Figure 5b). Based on these data, we investigated the role of specific signaling pathways in mediating the RA-induced decline in IRS-1 protein levels. Using a chemical inhibitor approach, the breast cancer cell lines, MCF-7, T47-D, and ZR75.1, were pretreated for 60 min with inhibitors of the MAPK (PD98059) and PKC (Rottlerin and GF109203X) signaling cascades and then treated for an additional 48 h with RA in the presence of the inhibitors. The decrease in IRS-1 protein levels could be inhibited in all of the breast cancer cells by treatment with Rottlerin and GF109203X, but not with PD98059 (Figure 5c). Consistent with this result, we also observed a block in the RA-mediated increase in serine phosphorylation of IRS-1 when the breast cancer cells were cotreated with Rottlerin (Figure 5d). These results suggest that a PKC-sensitive pathway is involved in the RA-mediated decline in IRS-1 levels.

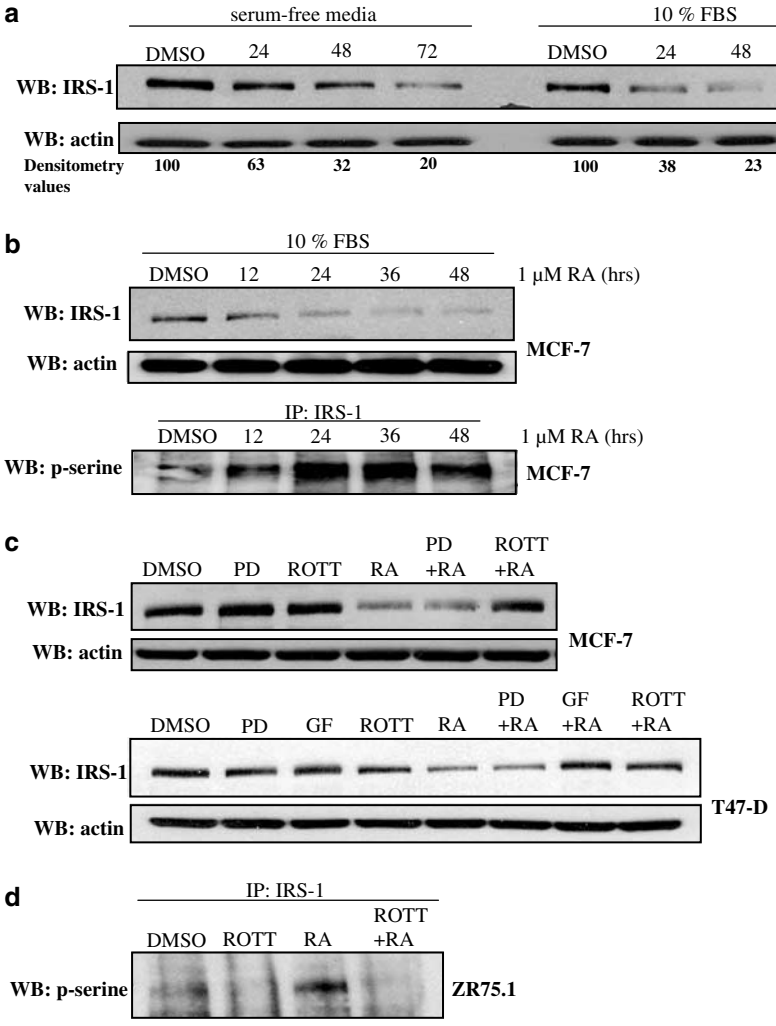

Figure 5 PKC inhibitors block the RA-mediated phosphorylation and degradation of IRS-1. WB was used to determine the expression level of IRS-1 in (**a**)–(**c**). (**a**) MCF-7 cells were treated with 1 μM RA for 24, 48, and 72 h in SFM or 10% fetal bovine serum (FBS). (**b**) Top panel: MCF-7 cells were treated with 1 μM RA for the times indicated in 10% FBS. Lower panel: the total serine phosphorylation status of IRS-1 was determined by immunoprecipitating (IP) IRS-1 from MCF-7 protein lysates and immunoblotting with an anti-phosphoserine (p-serine) antibody. (**c**) MCF-7 and T47-D cells were pretreated for 60 min with inhibitors of the MAPK (25 μM PD98059) and PKC (0.5 μM Rottlerin and 1 μM GF109203X) signaling cascades and then treated for an additional 48 h with 1 μM RA in the presence of the inhibitors. (**d**) ZR75.1 cells were treated as in (**c**), and the serine phosphorylation status of IRS-1 was determined as in (**b**)

In vitro *phosphorylation of IRS-1 by RA-activated PKC-δ in retinoid-sensitive breast cancer cells*

The PKC family of serine/threonine kinases are involved in signaling pathways controlling cell growth, transformation, and differentiation (Blobe *et al*., 1994). There are at least 10 PKC isoforms, however, Kambhampati *et al*. (2003) recently identified PKC-δ as a selective target of RA. We thus asked whether RA would activate PKC-δ in the breast cancer cell lines used in this study. We found that RA potently induces the phosphorylation of the threonine 505 residue in PKC-δ (Figure 6a). To directly measure if this increase in phosphorylation corresponded to increased activation of PKC-δ, we performed an *in vitro* kinase assays using histone H1 as a substrate. Figure 6b shows a clear increase in kinase activity with a time course of activation that is consistent with that observed for the RA-mediated decline in IRS-1 protein levels (compare, Figure 6b with Figure 5b). There was no change in PKC-δ activity in the RA-resistant breast cancer cell line MDA-MB-231, suggesting a tight correlation between activation of PKC-δ by RA and regulation of IRS-1 levels (Figure 6c). We confirm that treatment of the cells with 0.5 μM Rottlerin abrogates the RA-induced activity of PKC-δ (Figure 6d, lower panel), consistent with the ability of this inhibitor to rescue the decrease in IRS-1 levels in the RA-sensitive breast cancer cell lines. In addition, we show in Figure 6e that 0.5 μM Rottlerin also blocks basal PKC-δ activity.

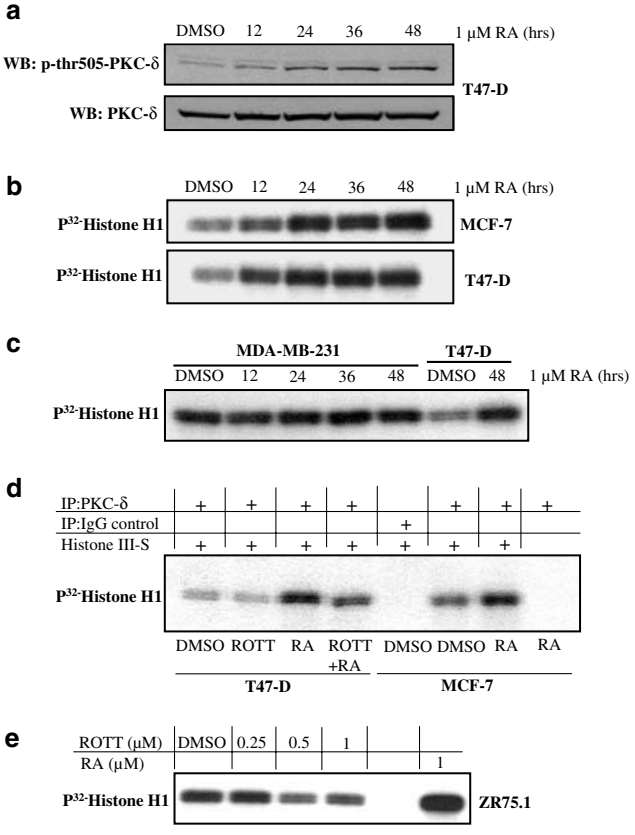

Figure 6 RA activates PKC-δ in retinoid-sensitive breast cancer cells. (**a**) T47-D cells were treated with 1 μM RA for 12, 24, 36, and 48 h in 10% FBS. Western blot was used to determine the phosphorylation status of anti-PKC-δ at threonine 505 (p-thr505-PKC-δ). This membrane was then stripped and reprobed with an antibody against total PKC-δ. (**b**) MCF-7 and T47-D cells were treated with 1 μM RA for the time indicated. Lysates were immunoprecipitated (IP) with an anti-PKCδ antibody, and immunoprecipitates were subjected to an *in vitro* kinase assay using histone H1 as an exogenous substrate. Phosphorylated histone H1 was detected by autoradiography. (**c**) The *in vitro* kinase assay using MDA-MB-231 cell extracts was performed as in (**b**). (**d**) T47-D cells were pretreated for 60 min with 0.5 μM Rottlerin and then treated for an additional 36 h with 1 μM RA in the presence of the inhibitor. The *in vitro* kinase assay was performed as in (**b**). (**e**) ZR75.1 cells were treated with 0.25, 0.5, or 1 μM Rottlerin for 36 h, and the *in vitro* kinase assay was performed as in (**b**)

Recently Greene *et al*. (2004) identified 18 PKC-δ serine/threonine phosphorylation sites on IRS-1. When three of these sites, serine 307, serine 323, and serine 574, were mutated to alanines, the phosphorylation of IRS-1 in response to activated PKC-δ was significantly decreased. To examine whether activation of PKC-δ by RA increases phosphorylation of IRS-1 on these sites, we performed an *in vitro* kinase assay using the wild-type human IRS-1-GST-fusion protein (GST-IRS-$1^{288–678WT}$) or the GST-IRS-$1^{288–678}$ with serine 307, serine 323, and serine 574 mutated to alanines (GST-IRS-$1^{288–678MUT}$) as a substrate. Our results show that PKC-δ immunoprecipitated from RA-treated breast cancer cells can phosphorylate the GST-IRS-$1^{288–678WT}$ construct, and that this phosphorylation event is abrogated by coincubation with the PKC-δ inhibitor Rottlerin (Figure 7b, left panel). In addition, when the three putative PKC-δ serine sites are mutated to alanines no RA-induced phosphorylation of the GST-IRS-$1^{288–678MUT}$ construct is observed (Figure 7b, right panel). The possibility that this phosphorylation may result from an interaction between IRS-1 and PKC-δ in the presence of RA is supported by our finding that IRS-1 coimmunoprecipitates with PKC-δ in ZR75.1 cells (and T47-D, data not shown) treated with 1 μM RA (Figure 7c).

Discussion

Although immediate/early retinoid signaling events are initiated via transcriptional activation of retinoid receptors, later retinoid signaling events can occur through the post-translational regulation of proteins. Considerable attention has been given in recent years to identifying retinoid-regulated proteins to gain insight into the mechanisms involved in their growth inhibitory and differentiating effects (Kim and Lotan, 2004). There is indeed a growing list of proteins known to be regulated by RA via mechanisms involving the ubiquitin–proteasome pathway: cyclin D1 (Spinella *et al*., 1999), PML/RAR alpha (Yoshida *et al*., 1996), RAR alpha and RAR gamma (Tanaka *et al*., 2001), CDK-4 (Sueoka *et al*., 1999), p300 (Brouillard and Cremisi, 2003), and Skp2 (Dow *et al*., 2001). Our findings support the addition of IRS-1 to this list. Using breast

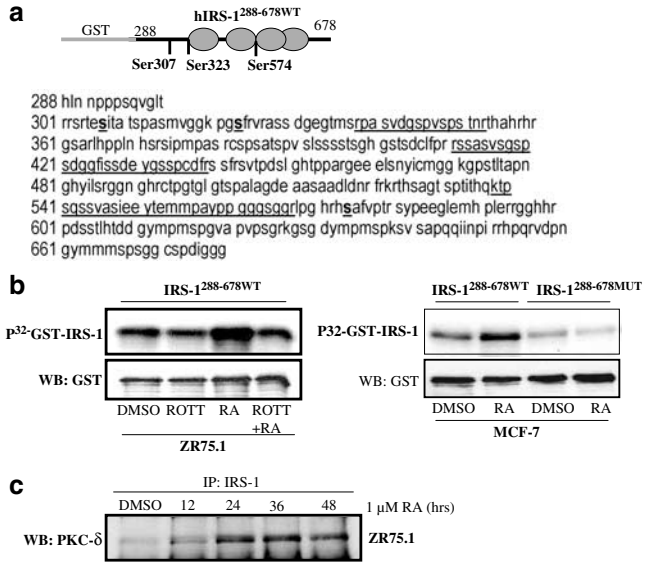

Figure 7 *In vitro* phosphorylation of IRS-1 by RA-activated PKC-δ. (**a**) Schematic showing the portion of the human IRS-1 protein used in the GST-IRS-$1^{288-678WT}$ construct. Also shown in larger font are the three serine sites phosphorylated in response to activated PKC-δ (serines 307, 323, and 574). The regions underlined in the amino-acid sequence of IRS-1 represent putative PEST domains in the region of the protein from amino acid 288 to 678. The residues in bold font and underlined represent serines 307, 323, and 574. (**b**) ZR75.1 cells were pretreated for 60 min with 0.5 μM Rottlerin and then treated for an additional 36 h with 1 μM RA in the presence of the inhibitor. Lysates were immunoprecipitated (IP) with an anti-PKC-δ antibody, and immunoprecipitates were subjected to an *in vitro* kinase assay using a GST-IRS-$1^{288-678WT}$ or GST-IRS-$1^{288-678MUT}$ (with serines 307, 323, and 574 mutated to alanines) as a substrate. Phosphorylated GST-IRS-$1^{288-678}$ was detected by autoradiography. (**c**) ZR75.1 cells were treated with 1 μM RA for 12, 24, 36, and 48 h. To detect IRS-1/PKC-δ association, cell lysate was immunoprecipitated with an anti-IRS-1 antibody and immunoblotted with an anti-PKC-δ antibody

cancer cell lines as a model, we are the first to show that RA regulates IRS-1 protein levels through a post-translational mechanism involving the ubiquitin–proteasome pathway. Moreover, we find that PKC inhibitors rescue the RA-mediated loss in IRS-1 protein, and that RA-mediated activation of PKC-δ phosphorylates IRS-1 *in vitro*.

The proteasomal degradation of proteins requires prior binding of ubiquitin to the target protein via three successive reactions. First, the ubiquitin-activating enzyme, E1, activates ubiquitin in an ATP-dependant reaction. Secondly, the ubiquitin molecule is transferred from E1 to the ubiquitin conjugating enzyme, E2. Thirdly, ubiquitin is transferred from E2 to the substrate-specific ubiquitin ligase, E3. In this paper, we show an increased level of IRS-1-ubiquitin conjugates in the presence of RA in MCF-7 cells when proteasomal activity is blocked using MG-132, and confirm this result with cotransfection experiments using flag-IRS-1 and HA-Ub constructs in the three RA-sensitive breast cancer cell lines. We observed that the RA-mediated increase in the level of IRS-1-Ub conjugates in MCF-7 cells (Figure 4b) is comparable to that previously reported in IGF-I-induced proteasomal degradation of IRS-1 (Lee *et al*., 2000). Interestingly, we did not observe a decrease in the levels of IRS-2 protein when any breast cancer cell line was treated with RA, suggesting that a specific motif in IRS-1 is responsible for the selective degradation of this protein by RA. It is believed that substrate-specificity of the ubiquitin–proteasome system is due to the specific E3, however, the E3 responsible for the degradation of IRS-1 remains unknown. One can speculate that this E3 may be an SCF ligase complex, since all identified SCF complexes target phosphorylated substrates, and prior studies have shown that IRS-1 needs to be phosphorylated on serine residues prior to its recognition by the ubiquitin machinery (Egawa *et al*., 2000; Haruta *et al*., 2000; Greene *et al*., 2003).

Our observation that RA decreases the levels of IRS-1 more rapidly in the presence of serum than in serum-free media (Figure 6a) suggested that an activated signaling pathway was involved in the degradation of IRS-1. Consistent with the idea that phosphorylated-IRS-1 is targeted for ubiquitination, we show that RA induces total serine phosphorylation of IRS-1. We used a chemical inhibitor approach to begin to clarify the signals generated that target IRS-1 for ubiquitination. We found that PKC inhibitors can rescue the RA-mediated loss in IRS-1 protein in the three RA-sensitive breast cancer cell lines examined. The activation of a number of PKC isoforms, including PKC-δ (Greene *et al*., 2004), has been linked to serine phosphorylation of IRS-1, and interestingly, Greene *et al*. mentioned an observed decrease in IRS-1 levels when CHO cells were transfected with a constitutively active PKC-δ construct, suggesting the involvement of this kinase in the regulation of IRS-1 protein levels. Our data support such a role of PKC-δ: (1) RA stimulates PKC-δ activity (Figure 6b), (2) RA-activated PKC-δ can phosphorylate IRS-1 *in vitro*, and this is blocked by the PKC-δ inhibitor Rottlerin (Figure 7b, left panel) or by mutation of three critical PKC-δ serine sites in IRS-1 (Figure 7b, right panel), and (3) PKC-δ and IRS-1 interact in the presence of RA (Figure 7c). Consistent with the inability of RA to regulate IRS-1 levels in the RA-resistant MDA-MB-231 breast cancer cell line, we also failed to observe any regulation of PKC-δ in these cells. Although activating PKC has not been previously reported to be required for the ubiquitination of IRS-1, the phosphorylation of p53 by PKC was shown to regulate p53 degradation by stimulating its ubiquitination (Chernov *et al*., 2001). Interestingly, three of the serine sites (serines 307, 323, and 574) phosphorylated by PKC-δ lie within the C-terminal domain of IRS-1 that contains potential PEST sequences, as identified by a PEST-FIND program (http://emb1.bcc.univie.ac.at/embnet/tools/bio/PESTfind/) (Figure 7a). PEST sequences are rich in proline (P), glutamate (E), serine (S) and threonine (T) residues and frequently serve as signals for proteolytic degradation (Rechsteiner and Rogers, 1996). It is tempting to speculate that

PKC-δ-mediated phosphorylation of these three serine sites may induce a conformational change in the C-terminal domain of IRS-1 that enables unmasking of these PEST domains and subsequent recognition by some component of the ubiquitin machinery. We thus propose a model of RA-mediated IRS-1 degradation whereby RA first activates PKC-δ, which in turn phosphorylates IRS-1 on serine residues, allowing for its subsequent recognition by the ubiquitin machinery.

Breast cancer cells exhibit elevated levels of known ubiquitinated proteins, such as cyclin D1 (Wang *et al*., 1994), cyclin E (Lindahl *et al*., 2004), and IRS-1 (Rocha *et al*., 1997). Although the ubiquitin ligase, or E3, for cyclin D1 and IRS-1 remain unknown, future identification of these ligases, may lead to the development of compounds that specifically activate E3, thus inhibiting the accumulation of cyclin D1 and IRS-1 in breast tumors where these proteins are stabilized. A possible novel chemotherapeutic approach for the treatment of breast tumors may be to combine RA with activation of specific E3 s to target oncogenic proteins.

Materials and methods

Reagents

All-*trans*-retinoic acid (RA), 9-*cis*-retinoic acid (9*cis*RA), TTNPB, *N*-(4-hydroxyphenyl)retinamide (4-HPR), and 17-β-estradiol (E2) were purchased from Sigma. Bexarotene was a generous gift of Ligand Pharmaceuticals, Inc. (San Diego, CA, USA). Recombinant human IGF-I was purchased from PeproTech (Princeton, NJ, USA). MG-132 (MG), 1,25-dihydroxyvitamin D3, 15-deoxy-delta 12,14-prostaglandin J2, Rottlerin and GF109203X were purchased from Calbiochem. Protein G-agarose, and Nonidet-P40 (NP-40) were purchased from Sigma (Oakville, Canada). Enhanced chemiluminescence (ECL) detection system and Protein A-sepharose were purchased from Amersham Biosciences. The following antibodies (Abs) were used for immunoprecipitations: anti-C-terminal IRS-1 pAb (Upstate Biotechnology), anti-FLAG pAb (Sigma), anti-PKC-delta (δ) pAb (Santa Cruz Biotechnology). Serine phosphorylation was detected with an anti-phosphoserine pAb (Zymed). The following antibodies were used for Western blotting: anti-IRS-1 pAb, anti-ubiquitin mAb (Santa Cruz Biotechnology), anti-HA-peroxidase mAb (clone 12CA5, Roche), anti-phospho-IRS-1 (Ser^{307}) pAb (Upstate Biotechnology), anti-GRB2 mAb (Transduction laboratories), anti-c-Jun pAB (Santa Cruz), anti-phospho-PKC-δ (Thr^{505}) pAb (Cell Signaling), anti-PKC-δ pAb (Santa Cruz), and anti-GST mAb (Santa Cruz). Equal loading in Western blotting experiments was assessed using either an anti-lamin B pAb (Santa Cruz) or anti-β-actin mAb (Sigma).

Cell maintenance and total cell lysate preparation

MCF-7 cells, ZR75.1 cells, and MDA-MB-468 cells were maintained in phenol red containing α-MEM (Life Technologies, Inc.) supplemented with 10% fetal bovine serum (FBS). T47-D cells and MDA-MB-231 cells were maintained in phenol red containing DMEM/F-12 (Life Technologies, Inc) supplemented with 10% FBS. When experiments were performed under serum-free conditions, cells at 70% confluence were washed twice with phosphate-buffered saline and changed to phenol red-free α-MEM supplemented with BSA and holo-transferrin (serum-free media – SFM). When experiments were performed in the presence of serum, cells were treated in the same media in which they were routinely maintained. For total cell lysate preparation, all cell lines were washed twice with cold phosphate-buffered saline (PBS) and lysed with RIPA buffer (50 mM Tris-HCl pH 8, 150 mM NaCl, 1% NP-40, 0.05% sodium deoxycholate, 0.1% SDS) containing protease and phosphatase inhibitors. Subsequent to incubation of lysate on ice for 30 min, the extracts were centrifuged at 13 000 *g* at 4°C for 30 min to remove insoluble material. After centrifugation, the protein content was measured by the Bradford assay using Bio-Rad reagents and BSA as standard.

Subcellular fractionation

Following the treatment periods in DMSO or RA, MCF-7 cells were washed in PBS and incubated on ice for 10 min in buffer 1 (10 mM Tris-Cl pH 7.8, 10 mM KCl, 5 mM $MgCl_2$, 0.1 mM EDTA, 300 mM sucrose, 0.5 mM DTT, plus protease and phosphatase inhibitors). A volume of 5 μl of 10% NP-40 was added to each sample and vortexed to lyse cells. The samples were centrifuged for 1 min at $\sim$1000 r.p.m., and the supernatant collected (cytosolic fraction). The pellet was washed 3 times with washing buffer (50 mM NaCl, 10 mM HEPES, pH 8, 25% glycerol, 0.1 mM EDTA, 100 mM DTT, plus protease and phosphatase inhibitors), and resuspended in buffer 2 (20 mM Tris-Cl pH 7.8, 5 mM $MgCl_2$, 320 mM KCl, 0.2 mM EDTA, 25% glycerol, 0.5 mM DTT, plus protease and phosphatase inhibitors). Tubes were incubated on ice for 30 min followed by centrifugation for 15 min at 13 000 *g*; the supernatant represented the nuclear fraction. A measure of 20 μg of cytosolic and nuclear proteins were then subjected to SDS–PAGE and transferred to nitrocellulose membrane filters. The membranes were processed for Western blotting of IRS-1, GRB-2 (for cytoplasmic purity), c-Jun (for nuclear purity), and actin (loading control).

Immunoprecipitation and Western blotting

For Western blotting, cell lysates were boiled for 3 min in 2 $\times$ SDS sample buffer (250 mM Tris-HCl pH 6.8, 8% SDS, 8 mM EDTA, 35% glycerol, 2.5% β-mercapto-ethanol, bromophenol blue) and resolved in 8–10% SDS–polyacrylamide gels (SDS–PAGE). For immunoprecipitation, 500 μg–1 mg of precleared cell lysates were incubated with the indicated antibody overnight at 4°C, followed by the addition of protein G-agarose overnight to collect immune complexes. The immunoprecipitates were washed in RIPA buffer, resuspended in SDS sample buffer, and boiled for 5 min. The solubilized proteins were resolved by SDS–PAGE. Proteins on the gel were transferred to nitrocellulose membrane (Bio-Rad) and detected by Western blotting with the indicated antibody using ECL. Some membranes were stripped to prepare them for a second round of probing.

Ubiquitination of IRS-1

The ubiquitination of IRS-1 was examined by transfecting (using FuGENE, Roche) breast cancer cells with a FLAG-tagged human IRS-1 cDNA in an expression construct provided by Dr Chris Sell, and a hemagglutinin (HA)-tagged ubiquitin cDNA in an expression construct provided by Dr Dirk Bohmann (Treier *et al*., 1994). At 24 h following transfection, cultures were washed twice with PBS and incubated in media containing 10 μM RA for 24 h in the presence or absence of 10 μM MG132 for the last 12 h of RA

treatment. FLAG-tagged IRS-1 protein was immunoprecipitated using an anti-FLAG antibody (Sigma) and after separation of the immunoprecipitated proteins by SDS–PAGE, the ubiquitinated IRS-1 was detected using an anti-HA-Peroxidase mAb (clone 12CA5, Roche).

Northern blotting

Total cellular RNA was isolated using guanidinium thiocyanate extraction as previously described (Chomczynski and Sacchi, 1987). For Northern blotting, 20 μg of RNA was electrophoresed on a 1% formaldehyde agarose gel and blotted onto Zeta probe (BioRad, Mississauga, Ontario, Canada) transfer membranes. cDNA probes were labeled by random priming (Amersham Biosciences). Hybridization and autoradiography was performed as previously described (Rosenauer *et al*., 1996). The full-length cDNA encoding IRS-1 was the generous gift of Dr Khan (Joslin Diabetes Center).

RT–PCR

Total cellular RNA was isolated using guanidinium thiocyanate extraction as previously described (Chomczynski and Sacchi, 1987). The methods described by Morelli *et al*. (2003) were used for IRS-1 RT–PCR. In brief, RNA (1 μg) was reverse transcribed (Superscript First Strand synthesis system – Gibco) and then amplified by PCR to obtain products corresponding to cDNA fragments of IRS-1. The following primers were used: IRS-1 upstream primer 5′-TCCACTGT-GACACCAGAATAAT-3′ and IRS-1 downstream primer 5′-CGCCAACATTGTTCATTCCAA-3′. The following PCR conditions were used for IRS-1: 1 min at 94°C, 1 min at 50°C, 2 min at 72°C. The amplification products obtained in 30 cycles were analysed in a 1% agarose gel.

Pulse analysis

To determine the synthesis rate of IRS-1, we followed the methods described by Zhang *et al*. with some modifications (Zhang *et al*., 2000). At 24 h after plating, MCF-7 cells were treated with DMSO vehicle or 10 μM RA for 24 h. Prior to labeling, the medium was replaced with methionine-free RPMI media (Wisent Inc.) for 1 h. During the last 12 h of RA treatment, the cells were labeled with 100 μCi of [^{35}S]methionine (Pro-mix, Amersham Biosciences) and cells were collected after 0, 4, 8, and 12-h time intervals. Total cellular proteins were isolated and IRS-1 immunoprecipitated (as described above). The IRS-1 immunoprecipitates were subjected to SDS–PAGE, and following transfer to nitrocellulose filters, labeled IRS-1 was visualized by autoradiography.

Pulse–chase analysis

To determine the degradation rate of IRS-1, we followed the methods described by Zhang *et al*. with some modifications (Zhang *et al*., 2000). At 24 h after plating, MCF-7 cells were treated with either DMSO vehicle or 10 μM RA for 24 h. Prior to labeling, the media was replaced with methionine-free RPMI media (Wisent Inc.) for 1 h. The cells were then pulsed for 4 h with 100 μCi of [^{35}S]methionine (Pro-mix, Amersham Biosciences). Following the pulse, the cells were chased for 0, 4, 8, and 12 h in 10% FBS containing media. After these chase times, total cellular proteins were isolated and processed as described above for the pulse analysis experiments.

Immunofluorescence

One day after plating on coverslips, MCF-7 cells were treated with DMSO vehicle or 10 μM RA for 48 h. For the last 12 h of RA treatment, 10 μM MG-132 was added. Following the treatment period, the cells were fixed in 3% formaldehyde in PBS for 30 min. Next, the cells were permeablized in PBS containing 0.2% Triton X-100 for 5 min. The cells were then incubated for 3 h with a rabbit anti-IRS-1 antibody (2 μg/ml), washed in PBS, and incubated for 1 h with a rhodamine-conjugated donkey anti-rabbit IgG secondary antibody. Following additional washes in PBS, the coverslips were incubated with 4,6-diamidino-2-phenylindole (DAPI) for 5 min and mounted on glass slides in antifade medium. The images were then collected using a fluorescence microscope.

In vitro *kinase assay using histone H1*

Cells were treated with RA or Rottlerin for the indicated times and then lysed in phosphorylation lysis buffer A (20 mM Tris-Cl pH 7.5, 150 mM NaCl, 1 mM EDTA, 10 mM 2-mercaptoethanol, 1% NP-40, 1 mM sodium orthovanadate, 10 mM NaF, 2 mM sodium pyrophosphate, 1 mM PMSF). Cell lysates were immunoprecipitated with anti-PKC-δ antibody, followed by the addition of protein A-sepharose overnight to collect immune complexes. Immunoprecipitates were washed twice with lysis buffer A and twice with wash buffer B (25 mM Tris-Cl pH 7.5, 5 mM $MgCl_2$). Protein A-sepharose beads were resuspended in 30 μl of kinase buffer (25 mM Tris-Cl pH 7.5, 5 mM $MgCl_2$, 0.5 mM EDTA, 1 mM dithiothreitol, 20 μg of phosphatidylserine, and 20 μM ATP) containing 5 μg of histone H1 (Sigma Type III) as an exogenous substrate, and [γ-^{32}P]ATP. The reaction was incubated for 30 min at room temperature and terminated by the addition of SDS sample buffer. Proteins were separated by SDS–PAGE, and phosphorylated histone H1 was detected by autoradiography.

In vitro *kinase assay using GST constructs*

Cells and cell extracts were treated as described above (*In vitro* kinase assay using histone H1), however, in the kinase reaction, GST-IRS-$1^{288-678WT}$, GST-IRS-$1^{288-678MUT}$, or GST alone was used as an exogenous substrate. The GST constructs were a generous gift from Dr R Roth, and have been previously described in Greene *et al*. (2004). GST-IRS-$1^{288-678WT}$ or GST were then purified from the reaction mix with GSH-Sepharose beads, resolved by SDS–PAGE, and phosphorylated GST-IRS-$1^{288-678WT}$ was detected by autoradiography. Decayed membranes were then incubated with an anti-GST antibody to ensure equal pull down of GST.

Acknowledgements
We are grateful to Dr Chris Sell for providing all FLAG-tagged IRS-1 constructs used in this manuscript. We thank Dr Dirk Bohmann for providing the HA-tagged ubiquitin construct. We extend our kindest thanks to Dr Richard A Roth for providing the GST-IRS-$1^{288-678WT}$ and GST-IRS-$1^{288-678MUT}$ constructs. We also thank Dr C Ronald Khan for his generous gift of human IRS-1 cDNA. This work was supported by a predoctoral fellowship award from the US Army Medical Research and Materiel Command Breast Cancer Research Program (Award number DAMD1701-1-0320 to SV del Rincón) and a grant from the Canadian Breast Cancer Research Initiative. Wilson H Miller Jr is an Investigator of the Canadian Institutes of Health Research.

References

Ando S, Panno ML, Salerno M, Sisci D, Mauro L, Lanzino M and Surmacz E. (1998). *Bioch. Biophys. Res. Commun.*, **253,** 315–319.

Blobe GC, Obeid LM and Hannun YA. (1994). *Cancer Metast. Rev.*, **13,** 411–431.

Boylan JM and Gruppuso PA. (2002). *Endocrinology*, **143,** 4178–4183.

Boyle JO, Langenfeld J, Lonardo F, Sekula D, Reczek P, Rusch V, Dawson MI and Dmitrovsky E. (1999). *J. Natl. Cancer Inst.*, **91,** 373–379.

Brouillard F and Cremisi CE. (2003). *J. Biol. Chem.*, **278,** 39509–39516.

Buren J, Liu HX, Jensen J and Eriksson JW. (2002). *Eur. J. Endocrinol.*, **146,** 419–429.

Burks DJ and White MF. (2001). *Diabetes*, **50,** S140–S145.

Chan TW, Pollak M and Huynh H. (2001). *Clin. Cancer Res.*, **7,** 2545–2554.

Chang Q, Li Y, White MF, Fletcher JA and Xiao S. (2002). *Cancer Res.*, **62,** 6035–6038.

Chernov MV, Bean LJ, Lerner N and Stark GR. (2001). *J. Biol. Chem.*, **276,** 31819–31824.

Chomczynski P and Sacchi N. (1987). *Anal. Biochem.*, **162,** 156–159.

del Rincón SV, Rousseau C, Samanta R and Miller Jr WH. (2003). *Oncogene*, **22,** 3353–3360.

Dow R, Hendley J, Pirkmaier A, Musgrove EA and Germain D. (2001). *J. Biol. Chem.*, **276,** 45945–45951.

Egawa K, Nakashima N, Sharma PM, Maegawa H, Nagai Y, Kashiwagi A, Kikkawa R and Olefsky JM. (2000). *Endocrinology*, **141,** 1930–1935.

Gonzalez C, Alonso A, Grueso NA, Diaz F, Esteban MM, Fernandez S and Patterson AM. (2001). *J. Pancreas*, **2,** 140–149.

Greene MW, Morrice N, Garofalo RS and Roth RA. (2004). *Biochem. J.*, **378,** 105–116.

Greene MW, Sakaue H, Wang L, Alessi DR and Roth RA. (2003). *J. Biol. Chem.*, **278,** 8199–8211.

Haruta T, Uno T, Kawahara J, Takano A, Egawa K, Sharma PM, Olefsky JM and Kobayashi M. (2000). *Mol. Endocrinol.*, **14,** 783–794.

Hirashima Y, Tsuruzoe K, Kodama S, Igata M, Toyonaga T, Ueki K, Kahn CR and Araki E. (2003). *J. Endocrinol.*, **179,** 253–266.

Huang X, Vaag A, Hansson M and Groop L. (2002). *J. Clin. Endocrinol. Metab.*, **87,** 255–259.

Ito T, Sasaki Y and Wands J. (1996). *Mol. Cell. Biol.*, **16,** 943–951.

Iwao K, Kawasaki H, Taira K and Yokoyama KK. (1999). *Nucleic Acids Symp. Ser.*, **42,** 207–208.

Kambhampati S, Li Y, Verma A, Sassano A, Majchrzak B, Deb DK, Parmar S, Giafis N, Kalvakolanu DV, Rahman A, Uddin S, Minucci S, Tallman MS, Fish EN and Platanias LC. (2003). *J. Biol. Chem.*, **278,** 32544–32551.

Kim HJ and Lotan R. (2004). *Cancer Res.*, **64,** 2439–2448.

Langenfeld J, Kiyokawa H, Sekula D, Boyle J and Dmitrovsky E. (1997). *Proc. Natl. Acad. Sci. USA*, **94,** 12070–12074.

Lavan BE, Lane WS and Lienhard GE. (1997). *J. Biol. Chem.*, **272,** 11439–11443.

Lee AV, Gooch JL, Oesterreich S, Guler RL and Yee D. (2000). *Mol. Cell. Biol.*, **20,** 1489–1496.

Lee AV, Jackson JG, Gooch JL, Hilsenbeck SG, Coronado-Heinsohn E, Osborne CK and Yee D. (1999). *Mol. Endocrinol.*, **13,** 787–796.

Lindahl T, Landberg G, Ahlgren J, Nordgren H, Norberg T, Klaar S, Holmberg L and Bergh J. (2004). *Carcinogenesis*, **25,** 375–380.

Molloy CA, May FE and Westley BR. (2000). *J. Biol. Chem.*, **275,** 12565–12571.

Morelli C, Garofalo C, Bartucci M and Surmacz E. (2003). *Oncogene*, **22,** 4007–4016.

Rechsteiner M and Rogers SW. (1996). *Trends Biochem. Sci.*, **21,** 267–271.

Rocha RL, Hilsenbeck SG, Jackson JG, VanDenBerg CL, Weng Cn, Lee AV and Yee D. (1997). *Clin. Cancer Res.*, **3,** 103–109.

Rosenauer A, Nervi C, Davison K, Lamph WW, Mader S and Miller Jr WH. (1998). *Cancer Res.*, **58,** 5110–5116.

Rosenauer A, Raelson JV, Nervi C, Eydoux P, DeBlasio A and Miller Jr W. (1996). *Blood*, **88,** 2671–2682.

Salerno M, Sisci D, Mauro L, Guvakova MA, Ando S and Surmacz E. (1999). *Int. J. Cancer*, **81,** 299–304.

Shepherd PR, Withers D and Siddle K. (1998). *Biochem. J.*, **333,** 471–490.

Smith LK, Bradshaw M, Croall DE and Garner CW. (1993). *Biochem. Biophys. Res. Commun.*, **196,** 767–772.

Spinella MJ, Freemantle SJ, Sekula D, Chang JH, Christie AJ and Dmitrovsky E. (1999). *J. Biol. Chem.*, **274,** 22013–22018.

Sueoka N, Lee HY, Walsh GL, Hong WK and Kurie JM. (1999). *Cancer Res.*, **59,** 3838–3844.

Sun H, Tu X, Prisco M, Wu A, Casiburi I and Baserga R. (2003). *Mol. Endocrinol.*, **17,** 472–486.

Sun XJ, Goldberg JL, Qiao LY and Mitchell JJ. (1999). *Diabetes*, **48,** 1359–1364.

Sun XJ, Rothenberg P, Kahn CR, Backer JM, Araki E, Wilden PA, Cahill DA, Goldstein BJ and White MF. (1991). *Nature*, **352,** 73–77.

Surmacz E and Burgaud JL. (1995). *Clin. Cancer Res.*, **1,** 1429–1436.

Tanaka T, Rodriguez de la Concepcion ML and De Luca LM. (2001). *Biochem. Pharmacol.*, **61,** 1347–1355.

Treier M, Staszewski LM and Bohmann D. (1994). *Cell*, **78,** 787–798.

Tu X, Batta P, Innocent N, Prisco M, Casaburi I, Belletti B and Baserga R. (2002). *J. Biol. Chem.*, **277,** 44357–44365.

Turnbow MA, Keller SR, Rice KM and Garner CW. (1994). *J. Biol. Chem.*, **269,** 2516–2520.

van der Burg B, van der Leede BM, Kwakkenbos-Isbrucker L, Salverda S, de Laat SW and van der Saag PT. (1993). *Mol. Cell. Endocrinol.*, **91,** 149–157.

Wang LM, Myers Jr MG, Sun XJ, Aaronson SA, White M and Pierce JH. (1993). *Science*, **261,** 1591–1594.

Wang TC, Cardiff RD, Zukerberg L, Lees E, Arnold A and Schmidt EV. (1994). *Nature*, **369,** 669–671.

White MF. (1997). *Diabetologia*, **40,** S2–S17.

Yoshida H, Kitamura K, Tanaka K, Omura S, Miyazaki T, Hachiya T, Ohno R and Naoe T. (1996). *Cancer Res.*, **56,** 2945–2948.

Zhande R, Mitchell JJ, Wu J and Sun XJ. (2002). *Mol. Cell. Biol.*, **22,** 1016–1026.

Zhang H, Hoff H and Sell C. (2000). *J. Biol. Chem.*, **275,** 22558–22562.

Oncogene (2004) 23, 7517–7526

www.nature.com/onc

Nuclear insulin receptor substrate 1 interacts with estrogen receptor α at ERE promoters

Catia Morelli[1,2,6], Cecilia Garofalo[1,2,6], Diego Sisci[1,2], Sonia del Rincon[3], Sandra Cascio[1,4], Xiao Tu[1], Andrea Vecchione[1], Edward R Sauter[5], Wilson H Miller Jr[3] and Eva Surmacz*[,1]

[1]Kimmel Cancer Center, Thomas Jefferson University, Philadelphia, PA 19107, USA; [2]Postgraduate School in Clinical Pathology, University of Calabria, Cosenza, Italy; [3]McGill University, Lady Davis Institute for Medical Research, Montreal, Canada; [4]Section of Molecular Oncology, Department of Oncology, University of Palermo, Palermo, Italy; [5]Ellis Fischel Cancer Center, University of Missouri-Columbia, Columbia, MO 65212, USA

Insulin receptor substrate 1 (IRS-1) is a major signaling molecule activated by the insulin and insulin-like growth factor I receptors. Recent data obtained in different cell models suggested that in addition to its conventional role as a cytoplasmic signal transducer, IRS-1 has a function in the nuclear compartment. However, the role of nuclear IRS-1 in breast cancer has never been addressed. Here we report that in estrogen receptor α (ERα)-positive MCF-7 cells, (1) a fraction of IRS-1 was translocated to the nucleus upon 17-β-estradiol (E2) treatment; (2) E2-dependent nuclear translocation of IRS-1 was blocked with the antiestrogen ICI 182,780; (3) nuclear IRS-1 colocalized and co-precipitated with ERα; (4) the IRS-1:ERα complex was recruited to the E2-sensitive pS2 gene promoter. Notably, IRS-1 interaction with the pS2 promoter did not occur in ERα-negative MDA-MB-231 cells, but was observed in MDA-MB-231 cells retransfected with ERα. Transcription reporter assays with E2-sensitive promoters suggested that the presence of IRS-1 inhibits ERα activity at estrogen-responsive element-containing DNA. In summary, our data suggested that nuclear IRS-1 interacts with ERα and that this interaction might influence ERα transcriptional activity.
Oncogene (2004) **23,** 7517–7526. doi:10.1038/sj.onc.1208014
Published online 16 August 2004

Keywords: breast cancer; estrogen receptor α; nuclear insulin receptor substrate 1; insulin-like growth factor; estrogen-responsive elements

Introduction

The insulin receptor substrate 1 (IRS-1) is a major signaling substrate of the insulin receptor (IR) and the insulin-like growth factor I (IGF-I) receptor (IGF-IR) (Yenush and White, 1997; White, 1998; Burks and White, 2001). Aberrant expression of IRS-1 has been associated with pathogenesis of many diseases, including diabetes and cancer (Yenush and White, 1997; White, 1998; Surmacz, 2000; Burks and White, 2001). Activated IRS-1 transmits signals from IGF-IR and IR by sequestering multiple effector molecules and stimulating different signaling pathways, including the PI-3K/Akt and ERK1/2 pathways (Yenush and White, 1997; White, 1998; Burks and White, 2001). In addition to its conventional role as a cytoplasmic signaling molecule, IRS-1 appears to function in the nuclear compartment. Several rigorously controlled studies demonstrated that nuclear IRS-1 can be found in cells transformed by oncogenic proteins, for example, T antigens of the JCV (Lassak *et al*., 2002) and SV40 (Prisco *et al*., 2002) viruses, and v-src (Tu *et al*., 2002). Nuclear translocation of IRS-1 has also been described in mouse embryo fibroblasts stimulated with IGF-I (Tu *et al*., 2002; Sun *et al*., 2003), 32D murine cells (Sciacca *et al*., 2003), osteoblasts (Seol and Kim, 2003), and hepatocytes (Boylan and Gruppuso, 2002). The mechanism by which IRS-1 is targeted to the nucleus is unknown. The observations from different cell models suggested that although IRS-1 contains putative nuclear localization signals (NLSs), it is most likely chaperoned to the nucleus by other proteins, such as viral antigens (Prisco *et al*, 2002; Tu *et al*., 2002). The nuclear localization of IRS-1 requires specific IRS-1 domains, but these requirements appear to be different depending on the experimental system. For instance, in JCV T-antigen-expressing cells, nuclear localization of IRS-1 depends on its pleckstrin homology domain (Lassak *et al*., 2002), while in IGF-I-stimulated cells, the phosphotyrosine binding domain is required (Prisco *et al*., 2002).

The biological relevance of nuclear IRS-1 in various cell backgrounds has yet to be determined. One recent study demonstrated that in mouse embryo fibroblasts stimulated with IGF-I, IRS-1 accumulated in the nucleoli and interacted with the upstream binding factor 1 (UBF1), a regulator of RNA polymerase I (Tu *et al*., 2002). In this cell model, the presence of nucleolar IRS-1 coincided with increased rRNA synthesis (Tu *et al*., 2002).

*Correspondence: E Surmacz, Kimmel Cancer Center, Thomas Jefferson University, 233 S 10th St, BLSB 631, Philadelphia, PA 19107, USA; E-mail: eva.surmacz@jefferson.edu
[6]These two authors contributed equally to this work
Received 20 January 2004; revised 24 June 2004; accepted 24 June 2004; published online 16 August 2004

In breast cancer, IRS-1 overexpression has been associated with tumor development, hormone independence, and antiestrogen resistance (Surmacz, 2000). These effects have been attributed to increased tyrosine phosphorylation of IRS-1 and potentiation of its downstream signaling to Akt (Surmacz, 2000; Sachdev and Yee, 2001). In hormone-dependent breast cancer cell lines and breast tumors, the expression of IRS-1 is strongly correlated with estrogen receptor α (ERα), and numerous studies demonstrated that IRS-1 is one of the central elements of ERα/IGF-I crosstalk (Surmacz, 2000; Chan *et al*., 2001; Sachdev and Yee, 2001). It has been well established that ERα can activate IRS-1 transcription acting on IRS-1 promoter (Lee *et al*., 1999; Molloy *et al*., 2000; Mauro *et al*., 2001). In addition, our recent data suggested that unliganded ERα can upregulate IGF-I signaling by decreasing IRS-1 degradation through proteasomal pathways (Morelli *et al*., 2003). The existence of nuclear IRS-1 in breast cancer cells and its possible role in the regulation of gene expression have never been addressed. Here we studied whether 17-β-estradiol (E2) can induce nuclear translocation of IRS-1 and if nuclear IRS-1 can associate with and modulate the action of ERα.

Results

E2 stimulates nuclear translocation of IRS-1 in MCF-7 cells, and nuclear IRS-1 interacts with ERα

The subcellular localization of IRS-1 and ERα was studied in MCF-7 cells stimulated with E2 for different times, from 15 min to 72 h. The images obtained by immunostaining and confocal microscopy are shown in Figure 1. Under serum-free medium (SFM) conditions, IRS-1 was present mainly in the cytoplasm, especially in the perinuclear area, while ERα localized in the nucleus and was weakly detectable in the cytoplasm (Figure 1). In 95% of untreated cells (SFM), colocalization of IRS-1 and ERα was not observed. At 15 min of E2 treatment, the staining of both proteins resembled that at time 0. At 1 and 4 h, 80% of cells displayed weak nuclear IRS-1 staining and strong nuclear expression of ERα. At these time points, nuclear colocalization of ERα and IRS-1 was detectable in ~25% of cells (data not shown). At 8, 24, and 48 h of E2 treatment, ERα was expressed almost exclusively in the nucleus, while IRS-1 was abundant in both cellular compartments (Figure 1). Furthermore, at these time points, evident nuclear colocalization of ERα and IRS-1 was observed in 60–70% of the cells (Figure 1). At 72 h, nuclear presence of IRS-1 became greatly reduced compared with that of earlier time points, while ERα remained nuclear. At this time, colocalization of ERα and IRS-1 was nearly undetectable (data not shown).

The above experiments were repeated several times with reproducible results. The specificity of IRS-1 staining was confirmed with other anti-IRS-1 polyclonal antibodies (pAbs), specifically anti-IRS-1 CT and anti-IRS-1 pre-CT (both from UBI), and pAb C20 (Santa Cruz). The staining was negative when the primary Abs were omitted or blocking peptide was used, as shown by us before in other cell models (Tu *et al*., 2002). In addition, we evaluated the specificity of staining procedures using BT-20 breast cancer cells, which are ERα and IRS-1 negative but express IRS-2 (Figure 1, inset). BT-20 cells were treated for 24 and 48 h with E2 and subjected to the same staining protocol as described for MCF-7 cells. Both IRS-1 and ERα were undetectable in BT-20 cells (Figure 1).

The localization of ERα and IRS-1 was further pursued in subcellular protein fractions. Cytoplasmic and nuclear proteins were obtained from MCF-7 cells

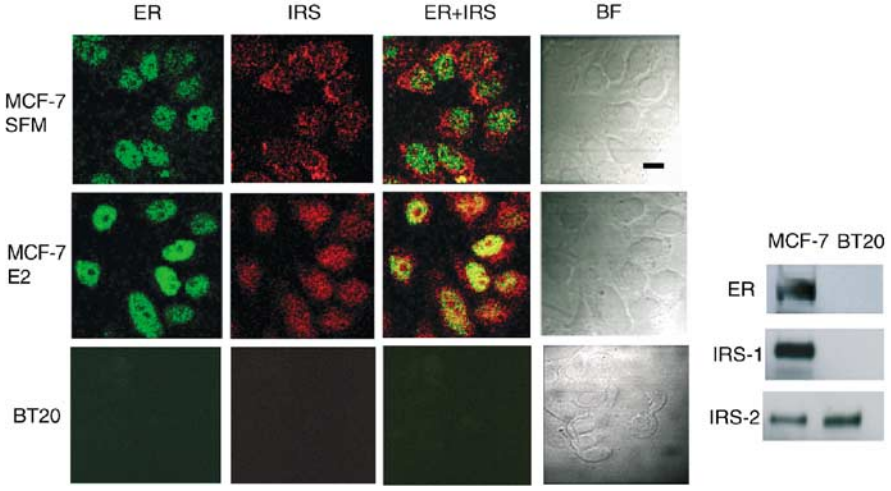

Figure 1 Subcellular localization of IRS-1 and ERα by confocal microscopy. MCF-7 cells synchronized in SFM for 24 h were treated with 10 nM E2 for 24 h (E2) or were left untreated (SFM). BT-20 cells were stimulated with E2 for 24 h. The localization of IRS-1 and ERα was studied by immunostaining and confocal microscopy as detailed in Materials and methods. The captured images of IRS-1 (IRS, red fluorescence), ERα (ER, green fluorescence), merged IRS-1 and ERα (IRS + ER, yellow fluorescence), and bright field (BF) are shown. Scale bar equals 20 μm. Inset: The expression of ERα (ER), IRS-1, and IRS-2 was detected by WB in 50 μg of total protein lysates obtained from growing MCF-7 and BT-20 cells

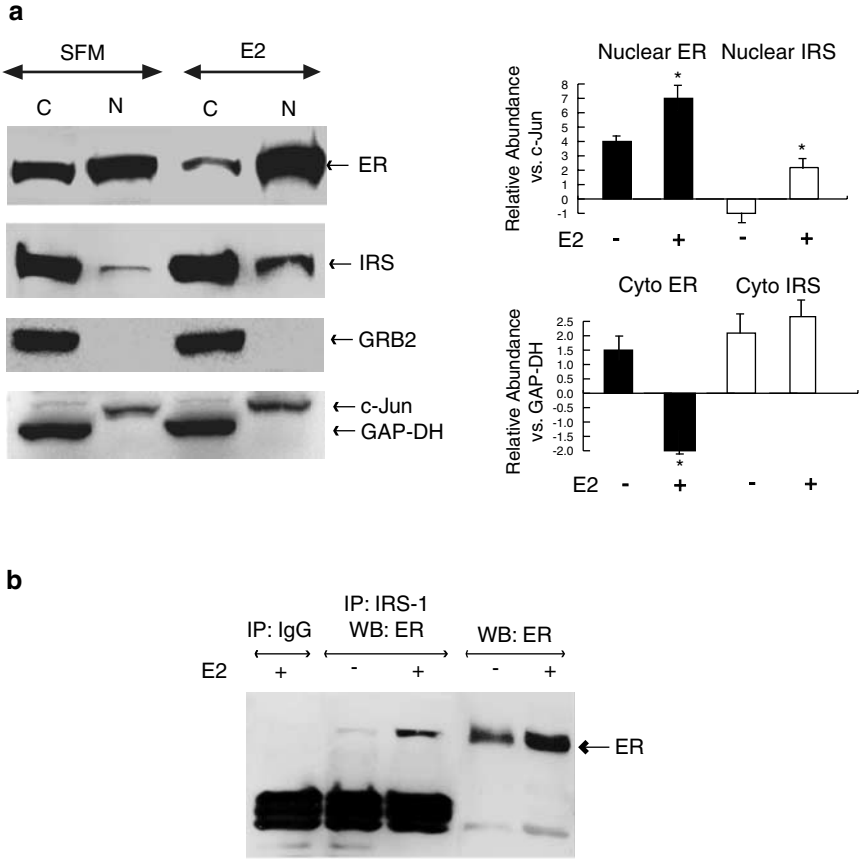

Figure 2 Subcellular localization of ERα and IRS-1 in E2-treated MCF-7 cells. (**a**) MCF-7 cells synchronized in SFM were treated with 10 nM E2 for 24 h (E2) or were left untreated (SFM). The expression of ERα (ER, ~67 kDa), IRS-1 (IRS, ~180 kDa), GRB-2 (~25 kDa), c-Jun (~39 kDa), and GAP-DH (~36 kDa) was assessed by WB in 100 μg of cytoplasmic (C) and nuclear (N) proteins using specific Abs, as described in Materials and methods. The graphs represent relative abundance of nuclear and cytoplasmic (Cyto) ERα and IRS-1 in unstimulated and E2-stimulated cells. Nuclear and cytoplasmic levels of ERα and IRS-1 were normalized to c-Jun and GAP-DH, respectively (relative values = 1). The asterisks indicate statistically significant ($P<0.05$) differences between the amounts in stimulated *vs* unstimulated cells. The results were obtained after repetitive stripping and reprobing of the same filter. (**b**) Nuclear lysates from MCF-7 cells (300 μg) were immunoprecipitated with anti-IRS-1 Ab (CT-IRS-1, UBI) or nonimmune rabbit IgG, and the amounts of ERα in the IPs were probed by WB. A 50 μg portion of nuclear proteins was run in parallel

treated with E2 for 24 h or left untreated. Under SFM conditions, ERα was present in the cytoplasmic and nuclear compartments. As expected, upon E2 treatment the nuclear abundance of ERα significantly increased, while the abundance of the cytoplasmic ERα significantly decreased (Figure 2a). In parallel, E2 stimulation significantly (~ 3.0-fold) upregulated nuclear amounts of IRS-1 (Figure 2). Despite nuclear translocation of IRS-1, its abundance in the cytoplasm remained similar in treated and untreated cells (Figure 2a), which is consistent with the fact that E2 can induce IRS-1 expression (Lee *et al*., 1999; Molloy *et al*., 2000). The expression of two cytoplasmic proteins GRB-2 and GAP-DH, and a nuclear protein c-Jun, was assessed as control of lysate purity (Figure 2a).

Confocal microscopy results suggested nuclear colocalization of IRS-1 and ERα. To confirm this observation, we studied IRS-1 and ERα interactions by immunoprecipitation (IP) and Western blotting (WB) using nuclear protein fractions obtained form MCF-7 cells grown in SFM or treated with E2 for 24 h (Figure 2b). ERα was found in IRS-1 immunoprecipitates in treated and untreated cells, with greater abundance of ERα/IRS-1 complexes in E2-stimulated cells (Figure 2b). Similarly, IRS-1 co-precipitated with nuclear ERα under E2 treatment (data not shown). Comparison of ERα content in total nuclear proteins *vs* IRS-1-associated proteins suggested that only a fraction (~10%) of ERα co-precipitates with IRS-1.

IRS-1 is recruited to the ERE-containing pS2 promoter in MCF-7 cells

Nuclear colocalization and co-precipitation of ERα and IRS-1 suggested that both molecules could be recruited to the same regulatory sequences in DNA. The binding of ERα and IRS-1 to the estrogen-responsive element (ERE)-containing domain of the pS2 gene promoter was assessed with chromatin immunoprecipitation (ChIP) and reverse ChIP (Re-ChIP) assays (Figure 3). First, we tested the dynamics of ERα association with the pS2 promoter sequences. Soluble chromatin obtained from

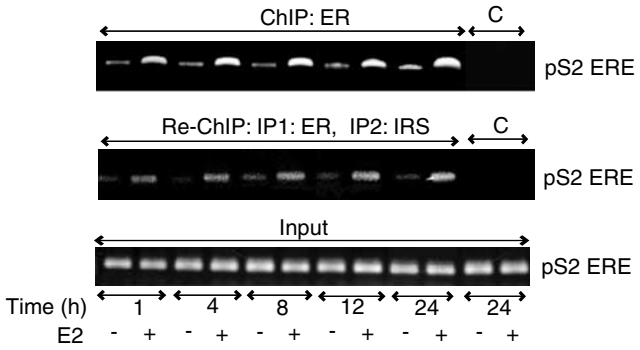

Figure 3 Time course of ERα and IRS-1 association with the pS2 promoter. Soluble chromatin was isolated from MCF-7 cells stimulated with E2 for 1, 4, 8, 12, and 24 h, and from untreated cells at the same time points. ERα ChIP (ChIP: ER) experiments were performed as described in Materials and methods. IRS-1 Re-ChIPs were obtained from ERα ChIP samples after reprecipitation with IRS-1 Abs (Re-ChIP: IP1: ER, IP2: IRS). DNA recovered from the immune complexes was tested for the presence of the ERE-containing pS2 promoter sequences (pS2 ERE) by PCR with specific primers listed in Materials and methods. PCR products obtained after 35 cycles are shown. ChIP pellets obtained using nonimmune IgG were analysed as controls of Ab specificity (C). The abundance of the pS2 promoter sequences in all samples before IP is shown as control of input DNA (Input)

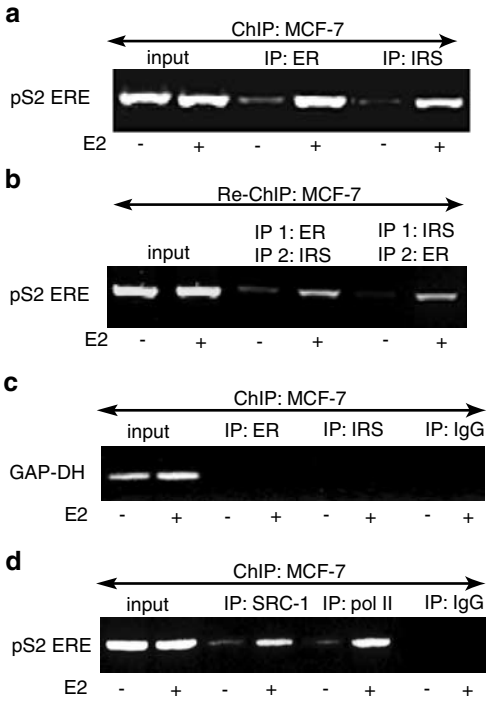

Figure 4 Association of the ERα:IRS-1 complex, SRC-1, and pol II with the pS2 promoter. MCF-7 cells were stimulated with E2 for 24 h, and the presence of the pS2 promoter sequences (pS2 ERE) in (**a**) ERα and IRS-1 ChIPs, (**b**) ERα:IRS-1 direct and reverse Re-ChIPs, and (**d**) SRC-1 and pol II ChIPs was detected by PCR as described in Materials and methods. The occupancy of ERα and IRS-1 on the GAP-DH promoter (not regulated by E2) was tested with specific GAP-DH primers in ERα and IRS-1 ChIP preparations (**c**). ChIP with nonimmune IgG was used as a control (IP: IgG)

MCF-7 cells untreated or treated with E2 for 1, 4, 8, 12, and 24 h was immunoprecipitated with anti-ERα Abs and the presence of pS2 promoter DNA in ERα precipitates was detected by PCR. As illustrated in Figure 3, E2 treatment increased ERα occupancy on the pS2 promoter at all time points. The association of ERα with pS2 DNA was maximal at 24 h after E2 addition (~3.5-fold increase *vs* untreated) (Figure 3).

To test whether IRS-1 belongs to the ERα multi-complex recruited to the pS2 promoter, we performed Re-ChIP experiments, following the protocol described for ERα interacting proteins (Reid *et al*., 2003). In our Re-ChIP experiments, the original ERα ChIP pellets were eluted and precipitated with IRS-1 Abs and the pS2 promoter sequences were detected in IRS-1 Re-ChIPs by PCR. We found pS2 DNA in IRS-1 Re-ChIPs at all time points, which indicated that IRS-1 and ERα belong to the same protein complex, and that the complex is associated with the ERE-pS2 promoter in E2-stimulated MCF-7 cells. Notably, the greatest amounts of pS2 DNA in IRS-1 Re-ChIPs were present in cells stimulated with E2 for 24 h (Figure 3).

To extend the above observations, we examined the presence of other regulatory proteins in ERα transcriptional complexes in MCF-7 cells stimulated with E2 for 24 h. Figure 4 illustrates pS2 promoter occupancy by two proteins known to regulate ERα-dependent transcription, ERα coactivator SRC-1 and polymerase II (pol II). In parallel, the association of ERα and IRS-1 under the same conditions was assessed by ChIP and two-way Re-ChIP assays. The results confirmed that E2 stimulates the recruitment of the ERα:IRS-1 complex to the pS2 promoter in MCF-7 cells (Figure 4a and b). In the same experiment, neither ERα nor IRS-1 was recruited to the GAP-DH promoter that is not regulated by ERα (Metiver *et al*., 2002) (Figure 4c). Notably, the association of ERα and IRS-1 with pS2 DNA coincided with the recruitment of SRC-1 and pol II to the same promoter (Figure 4d).

Absence of ERα blocks nuclear IRS-1 translocation

The role of ERα in the nuclear translocation of IRS-1 was probed in MCF-7 cells pretreated with the antiestrogen ICI 182,780 (ICI) for 6 h (Figure 5). This treatment has been chosen based on preliminary tests establishing the dynamics of ICI-dependent downregulation of ERα and IRS-1. IRS-1 is a stable protein with a half-life of ~10 h (Morelli *et al*., 2003) and only a long-term ICI treatment (48–74 h) can substantially decrease its levels (Salerno *et al*., 1999), while short-term ICI exposure is sufficient to degrade ERα (Reid *et al*., 2003). Indeed, a 6 h ICI treatment dramatically reduced cytoplasmatic and nuclear ERα expression without affecting IRS-1 levels (Figure 5a and b). In ICI-pretreated cells, E2 did not stimulate nuclear translocation of IRS-1, as demonstrated by WB (Figure 5a) and confocal microscopy (Figure 5b). However, E2 induced nuclear translocation of IRS-1 in untreated cells expressing normal ERα levels (Figures 1, 2 and 5a). Low amounts of nuclear IRS-1 were found under SFM

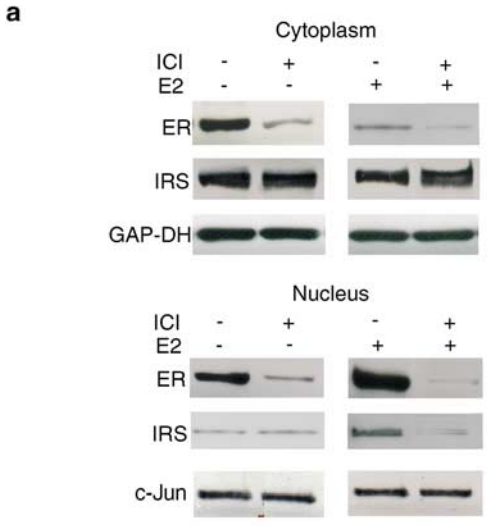

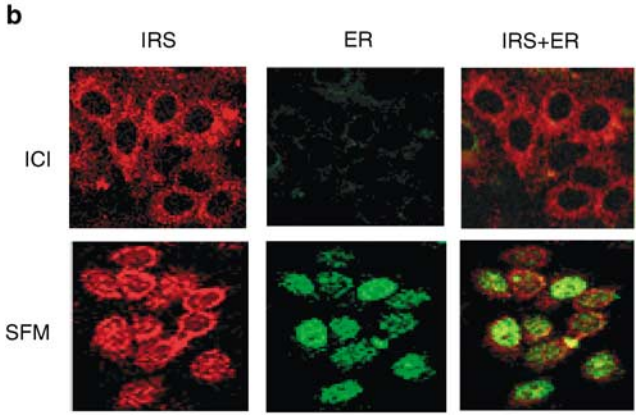

Figure 5 Effects of ERα downregulation on nuclear translocation of IRS-1. MCF-7 cells synchronized in SFM were pretreated with 10 nM ICI 182,780 for 6 h, and then stimulated with 10 nM E2 for 24 h or left untreated in SFM (**a**). The levels of IRS-1 (IRS) and ERα (ER) were detected in 50 μg of cytoplasmatic and nuclear proteins with specific Abs, as described in Materials and methods. The results were obtained after repetitive stripping and reprobing of the same filter. (**b**) MCF-7 cells were pretreated with ICI and then stimulated with E2 or left in SFM as described in (**a**). The localization of IRS-1 (IRS) and ERα (ER) was studied by confocal microscopy, as described in Figure 1. Scale bar equals 50 μm

conditions, possibly reflecting IRS-1 translocation induced by basal ERα activity (Figures 1, 2, 5a and b).

IRS-1 does not associate with the pS2 promoter in ERα-negative MDA-MB-231 cells

The requirement of ERα for E2-dependent nuclear translocation of IRS-1 was further investigated with MDA-MB-231 and MDA-MB-231/ER breast cancer cells (Figure 6). MDA-MB-231 cells are ERα negative but express IRS-1 on a level similar to that found in MCF-7 cells (Bartucci *et al*., 2001; Morelli *et al*., 2003). MDA-MB-231/ER cells have been developed in our laboratory by stable transfection of MDA-MB-231 cells with an ERα expression vector (Morelli *et al*., 2003). The association of ERα and IRS-1 with the pS2 promoter

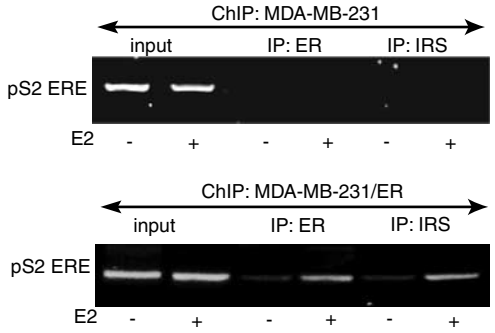

Figure 6 Recruitment of ERα and IRS-1 to the pS2 gene promoter in MDA-MB-231 and MDA-MB-231/ER cells. MDA-MB-231 and MDA-MB-231/ER cells were stimulated with E2 for 24 h or were left untreated in SFM. The presence of ERα and IRS-1 on the pS2 promoter (pS2 ERE) was detected by ChIP assays, as described in Materials and methods

was studied in both cell lines by ChIP assays. In MDA-MB-231 cells, neither ERα nor IRS-1 was found on the pS2 promoter. However, reintroduction of ERα allowed the association of both molecules with pS2 ERE sequences in response to E2 treatment (Figure 6).

IRS-1 modulates ERα transcriptional activity

Because IRS-1 and ERα are recruited to E2-sensitive promoters, we tested whether the presence of IRS-1 may affect ERα transcriptional activity at ERE sites. This possibility was examined with transactivation assays employing an ERE reporter plasmid. The plasmid, ERE-Luc, was transiently transfected into cells either together with ERα expression vector only or with a mixture of ERα and IRS-1 expression plasmids. The transfected cells were left untreated or were treated with E2 for 24 h (Figure 7).

To assess E2-dependent transcription in a controlled environment, we used ERα- and IRS-1-negative COS-7 and BT-20 cells (Figures 1 and 7b), which allowed measurements of transcriptional activity in the presence or absence of studied molecules. In addition, transactivation experiments were performed in MCF-7 cells expressing endogenous IRS-1 and ERα.

The transactivation assays indicated that the presence of IRS-1 significantly decreased ERα activation of ERE promoters in all cell lines stimulated with E2 (Figure 7a). Specifically, in COS-7, BT-20, and MCF-7 cells, cotransfection of IRS-1 reduced ERα activation of ERE by ~50, ~39, and ~44%, respectively. The transfection of IRS-1 alone did not stimulate ERE transcription (Figure 7a).

In addition to ERE reporter assays with reporter plasmids, we assessed transcriptional activation of the pS2 gene in COS-7 cells transfected with either ERα, IRS-1, or a combination of ERα plus IRS-1. COS-7 cells were selected for this assay as they proved to be the most E2-responsive and the best transfectable cell model (Figure 7a). The levels of pS2 mRNA in COS-7 cells transfected with different plasmids were studied using

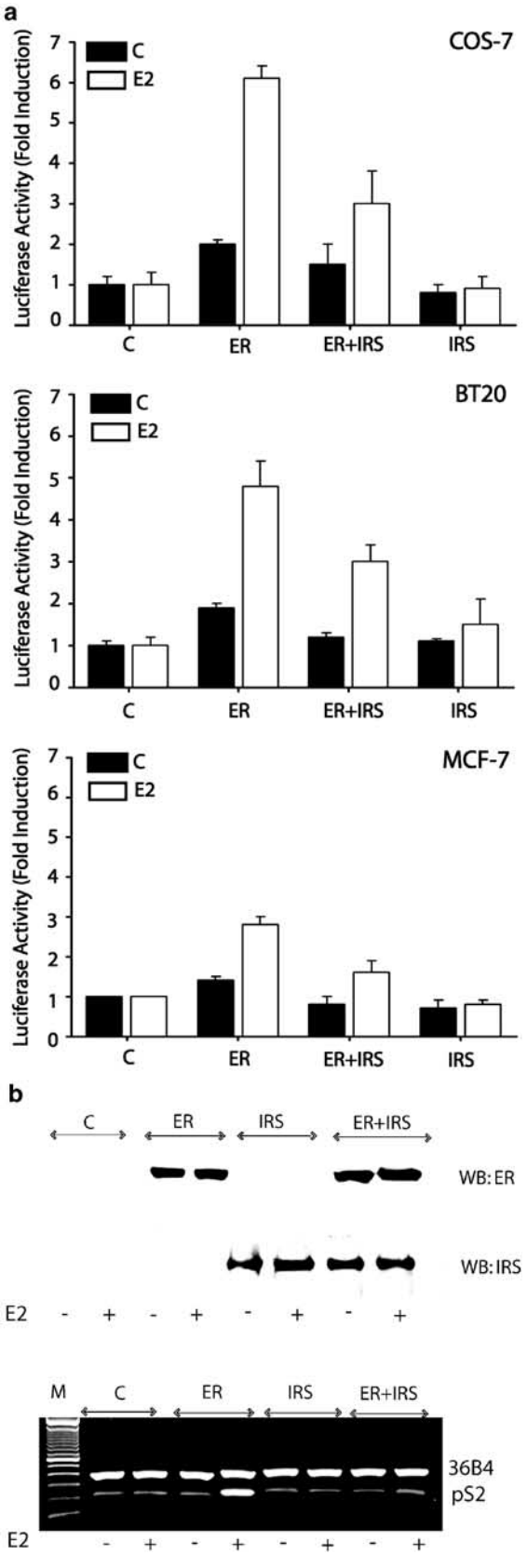

RT–PCR (Figure 7b). The amounts of a constitutively expressed 36B4 mRNA were assessed in the same samples. The results suggested that E2 stimulated pS2 mRNA expression (~3-fold) in ERα-transfected cells, compared with vector-only-transfected cells. This effect of E2 was significantly reduced in cells cotransfected with ERα and IRS-1, confirming the trend observed in ERE luciferase reporter assays. Notably, ERα expression was similar in the 'ER' and 'ER + IRS' populations, ruling out the possibility that differences in pS2 transcription were related to unequal ERα expression (Figure 7b).

Discussion

The interactions between IGF-IR and ER signaling systems have been implicated in the development of the neoplastic phenotype in mammary epithelial cells (Surmacz, 2000; Yee and Lee, 2000; Sachdev and Yee, 2001). In this context, IRS-1, a molecule that activates multiple growth and survival pathways, has been found to be one of the central elements of IGF-IR/ER crosstalk. Several reports documented that E2 can increase IRS-1 transcription, while ICI inhibits IRS-1 mRNA levels (Surmacz, 2000; Yee and Lee, 2000; Sachdev and Yee, 2001). Furthermore, the expression of ERα seems to stabilize IRS-1 protein and potentiate IRS-1 signaling through the PI-3K/Akt pathway (Morelli *et al*., 2003). In turn, the activation of IRS-1/PI-3K/Akt by growth factors can stimulate ERα by increasing its phosphorylation (Lannigan, 2003). In MCF-7 cells, overexpression of IRS-1 has been shown to induce estrogen independence (Surmacz and Burgaud, 1995), while downregulation of IRS-1 resulted in increased sensitivity to E2 (Ando *et al*., 1998).

Here we report on a novel aspect of ERα/IGF-I crosstalk involving nuclear ERα/IRS-1 interactions. Specifically, we demonstrated that (1) in MCF-7 cells, IRS-1 can be translocated from the cytoplasm to the nucleus following E2 treatment; (2) nuclear transloca-

Figure 7 Effects of IRS-1 on ERα transcriptional activity at ERE promoters. (**a**) Transactivation assays. The transcriptional activity of ERα on ERE promoters in the presence or absence of IRS-1 was evaluated using luciferase reporter system, as described in Materials and methods. COS-7, BT-20, and MCF-7 cells were transfected with DNA mixtures containing ERE reporter plasmid alone (C), ERE + plasmid pHEGO encoding ERα (ER), ERE + ER + plasmid encoding IRS-1 (ER + IRS), or ERE + IRS-1 (IRS). The activity of the ERE promoter in each experimental setting is represented by relative Luc units. The results are means ± s.e. from several experiments. In all experimental systems, the difference between E2-stimulated Luc activities in ER *vs* ER + IRS transfectants was statistically significant ($P < 0.05$). (**b**) Effect of IRS-1 expression on pS2 mRNA levels. Upper panel: COS-7 cells were transfected with different plasmids and stimulated with E2 or left untreated, as described above. ERα and IRS-1 expression in transfected cells was detected by WB in 50 μg of total protein lysates. Lower panel: The abundance of pS2 and 36B4 mRNAs in COS-7 cells transfected with different plasmids was detected by RT–PCR, as described in Materials and methods

tion of IRS-1 is blocked with ICI and does not occur in ERα-negative cells; (3) nuclear IRS-1 interacts with ERα; (4) nuclear IRS-1 is corecruited with ERα to the ERE-containing pS2 promoter; and (5) the presence of IRS-1 decreases ERα transcription at ERE promoters.

Nuclear localization of IRS-1 has recently been described in different cellular systems (Lassak *et al*., 2002; Prisco *et al*., 2002; Sun *et al*., 2003; Tu *et al*., 2002; Sciacca *et al*., 2003). The mechanism by which IRS-1 enters cell nucleus is still not clear. Although IRS-1 contains putative NLS, it is thought that IRS-1 is chaperoned to the nucleus by other proteins, for instance, by T antigens of the SV40 and JC viruses (Lassak *et al*., 2002). The transporting molecules involved in IGF-IR-dependent IRS-1 nuclear translocation are yet unknown.

In our experimental system, E2-dependent nuclear translocation of IRS-1 and its interaction with the pS2 promoter were totally blocked when ERα was down-regulated by ICI (Figure 5) and did not occur in MDA-MB-231 cells that are ERα negative but express ERα (Vladusic *et al*., 2000) (Figure 6). However, re-expression of ERα allowed association of IRS-1 with the pS2 sequences. These observations suggest that nuclear function of IRS-1 in response to E2 requires ERα. Notably, a small amount of nuclear IRS-1 was found in unstimulated MCF-7 cells, which could result from basal ERα activity.

The prerequisite for nuclear translocation of IRS-1 in response to E2 is most likely the formation of the ERα:IRS-1 complex in the cytoplasm. ERα association with cytoplasmic signaling molecules is not unusual. Recently, ERα has been shown to bind the PI-3K/Akt complex (Simoncini *et al*., 2000; Sun *et al*., 2001), and to interact with growth factor receptor docking protein Shc (Song *et al*., 2002) as well as with IGF-IR (Kahlert *et al*., 2000). Similarly, we reported that unliganded ERα can associate with cytoplasmic IRS-1 in MDA-MB-231/ER cells (Morelli *et al*., 2003). Our preliminary data suggest that ERα/IRS-1 binding involves at least two different IRS-1 domains, and does not depend on IRS-1 tyrosine phosphorylation (Surmacz *et al*., unpublished data).

Our previous findings (Morelli *et al*., 2003) and this report suggest that only a fraction of ERα binds to IRS-1 (~10% of nuclear ERα) (Figure 2b), according to rough estimations based on coprecipitation procedures. However, if the linkage between ERα and IRS-1 is labile, coprecipitation assays might underestimate the actual extent of their association. In fact, the results obtained with confocal microscopy in intact cells suggested that in some cells, ~30% of ERα colocalized with IRS-1. Because only a fraction of ERα associates with IRS-1, it is understandable that nuclear accumulation of IRS-1 upon E2 stimulation might occur slower than that of ERα. The nuclear presence of IRS-1 in E2-treated MCF-7 cells was limited to ~72 h, while ERα remained nuclear for longer times. It needs to be discovered whether IRS-1 disappearance from the nucleus is caused by proteolysis or by translocation to the cytoplasmic compartment.

In this work, we report for the first time that nuclear IRS-1 can interact with ERα on ERE-containing chromatin regions. In our experimental system, IRS-1 was recruited together with ERα and other proteins involved in ERα transcription (SRC-1 and pol II) to the pS2 promoter (Figures 3, 4, and 6). The possibility that IRS-1 modulates ERα-dependent transcription was addressed with transient transfection reporter assays. With this methodology, we noted inhibition of ERα activity by IRS-1 in several cell lines (Figure 7a). We also found that overexpression of IRS-1 inhibits E2/ERα-dependent transcription of the endogenous pS2 gene in COS-7 cells (Figure 7b). A hypothetical model explaining the inhibitory effect of IRS-1 could be proposed on the basis of the recent discovery that ERα-dependent transcription from ERE sites requires cyclic proteasomal degradation of ERα (Reid *et al*., 2003). Because IRS-1 and ERα compete for the same degradation machinery (Morelli *et al*., 2003), it is possible that the presence of nuclear IRS-1 interferes with ERα proteolysis, and thus with ERα transcription.

IRS-1 modification of ERα activity is probably restricted to certain transcriptional complexes, as we did not observe significant effects of IRS-1 on ERα-dependent transcription at AP-1 sites. In addition, our new data suggest that the association of IRS-1 with ERE promoters can be transiently inhibited by its recruitment to activated IGF-I receptors (Surmacz *et al*., unpublished data).

The presence of nuclear IRS-1 in cellular systems needs to be further evaluated in human clinical material. The expression of nuclear IRS-1 in primary breast tumors has been reported by Schnarr *et al*. (2000), but the authors did not speculate on the biological relevance of this phenomenon. Our preliminary data confirmed that nuclear IRS-1 can be detected in mammary tissue sections and that its expression correlates with ERα (data not shown). Larger studies evaluating the correlations of cytoplasmatic and nuclear IRS-1 with other tumor markers are underway in our laboratory.

In summary, our data suggest that IRS-1 can interact with ERα in the nucleus of breast cancer cells and modulate ERα transcriptional activity. We postulate that nuclear ERα/IRS-1 interactions represent a new paradigm in IGF-IR/ER crosstalk.

Materials and methods

Cell lines

MCF-7, MDA-MB-231, BT-20, and COS-7 cells were obtained from ATCC. MDA-MB-231 cells stably expressing ERα have been developed in our laboratory (Morelli *et al*., 2003).

Cell culture

MCF-7 and MDA-MB-231 cells were grown in DMEM:F12 containing 5% calf serum (CS). MDA-MB-231/ER cells were grown in DMEM:F12 plus 5% CS plus 0.05 mg/ml

G418. BT-20 cells were grown in DMEM:F12 with 10% fetal bovine serum (FBS). COS-7 and HeLa cells were grown in DMEM supplemented with 10% FBS. In the experiments requiring E2- and serum-free conditions, the cells were cultured in phenol red-free SFM (Guvakova and Surmacz, 1997).

Cell treatments

E2 (Sigma) and the antiestrogen ICI 182,780 (Tocris Cookson) were used at a concentration of 10 nM.

Detection of IRS-1 and ERα by confocal microscopy

Confluent cultures (50%) grown on coverslips were fixed in 3% paraformaldehyde, permeabilized with 0.2% Triton X-100, washed three times with PBS, and incubated for 1 h with a mixture of primary Abs (pAbs) recognizing IRS-1 and ERα. The anti-IRS-1 CT pAb (UBI) or anti-IRS-1 pre-CT pAb (UBI) at 2 μg/ml was used for IRS-1 staining; F-10 monoclonal Ab (mAb) (Santa Cruz) at 2 μg/ml was used to detect ERα. Following the incubation with primary Abs, the slides were washed three times with PBS, and incubated with a mixture of secondary Abs. A fluorescein-conjugated donkey anti-mouse IgG (Calbiochem) was used as a secondary Ab for ERα and a rhodamine-conjugated donkey anti-rabbit IgG (Calbiochem) was used for IRS-1. The cellular localization of IRS-1 and ERα was studied with Bio-Rad MRC 1024 confocal microscope connected to a Zeiss Axiovert 135M inverted microscope with ×600 magnification. The optical sections were taken at the central plane. The fluorophores were imaged separately to ensure no excitation/emission wavelength overlap. In control samples, the staining was performed with the omission of the primary Abs.

Immunoprecipitation and Western blotting

The cytoplasmic and nuclear proteins were obtained from 70% cultures. The cytoplasmic lysis buffer contained the following: 50 mM HEPES pH 7.5, 150 mM NaCl, 1% Triton X-100, 1.5 mM $MgCl_2$, EGTA 10 mM pH 7.5, glycerol 10%, inhibitors (0.1 mM Na_3VO_4, 1% PMSF, 20 μg/ml aprotinin). Following the collection of cytoplasmic proteins, the nuclei were lysed with the buffer containing 20 mM HEPES pH 8, 0.1 mM EDTA, 5 mM $MgCl_2$, 0.5 M NaCl, 20% glycerol, 1% NP-40, inhibitors (as above). A 25–50 μg portion of protein lysates was used for WB, while 500 μg was used for IP. The following mAbs and pAbs were employed: anti-IRS-1 CT pAb (UBI) for WB and IP; anti-ERα F-10 mAb (Santa Cruz) for WB and IP; anti-GAP-DH mAb (Research Diagnostics Inc.) for WB, anti-c-Jun mAb (Santa Cruz) for WB, anti-GRB2 mAb (Transduction Laboratories) for WB.

In all IPs, protein lysates were first incubated with primary Abs at 4°C for 4 h in HNTG buffer (20 mM HEPES pH 7.5, 150 mM NaCl, 0.1% Triton X-100, 10% glycerol, 0.1 mM Na_3VO_4), and then immune complexes were precipitated for 1 h with appropriate beads, specifically with protein A agarose (Calbiochem) for IPs with polyclonal Abs and anti-mouse IgG agarose (Sigma) for IPs with mouse mAbs. In control samples, the primary Abs were substituted with nonimmune IgGs (rabbit or mouse, depending on the source of the primary Abs). The immunoprecipitated proteins were washed three times with HNTG buffer, separated on a 4–15% polyacrylamide denaturing gel, analysed by WB, and visualized by ECL chemiluminescence (Amersham). The intensity of bands representing relevant proteins was measured by Scion Image laser densitometry scanning program.

Luciferase reporter assays

The experiments were performed using COS-7, BT-20, and MCF-7 cell lines. The cells were grown in 24-well plates. At 70% confluence, the cultures were transfected for 6 h with 0.5 μg DNA/well using Fugene 6 (Roche) (DNA : Fugene 3 : 1). All transfection mixtures contained 0.3 μg of the reporter plasmid, ERE-Luc, encoding the firefly luciferase (Luc) cDNA under the control of the TK promoter and three ERE sequences. ERE-Luc was cotransfected with the ERα expression vector pSG5-HEGO, alone or in combination with the IRS-1 expression vector pCMV-IRS-1. To maintain the same DNA input in all transfection mixtures, the samples were adjusted with an empty vector (pcDNA3 or pSG5). In addition, to assess transfection efficiency, each of the DNA mixtures contained 50 ng of pRL-TK-Luc, a plasmid encoding *Renilla* luciferase (RI Luc) (Promega). Upon transfection, the cells were shifted to SFM for 12 h and then treated with 10 nM E2 for 24 h, or left untreated in SFM. Luciferase activity (Luc and RI Luc) in cell lysates was measured using Dual Luciferase Assay System (Promega) following the manufacturer's instructions. The values obtained for Luc were normalized to that of RI Luc to generate relative Luc units representing ERE-dependent transcription.

Chromatin immunoprecipitation

We followed ChIP methodology described by Shang *et al*. (2000) with minor modifications. MCF-7, MDA-MB-231, and MDA-MB-231/ER cells were grown in 100 mm plates. Confluent cultures (90%) were shifted to SFM for 24 h and then treated with 10 nM E2 for 1–24 h, or left untreated in SFM. Following treatment, the cells were washed twice with PBS and crosslinked with 1% formaldehyde at 37°C for 10 min. Next, the cells were washed twice with PBS at 4°C, collected and resuspended in 200 μl of lysis buffer (1% SDS, 10 mM EDTA, 50 mM Tris-HCl pH 8.1) and left on ice for 10 min. Then, the cells were sonicated four times for 10 s at 30% of maximal power (Fisher Sonic Dismembrator) and collected by centrifugation at 4°C for 10 min at 14 000 rpm. The supernatants were collected and diluted in 1.3 ml of IP buffer (0.01% SDS, 1.1% Triton X-100, 1.2 mM EDTA, 16.7 mM Tris-HCl pH 8.1, 16.7 mM NaCl) followed by immunoclearing with 80 μl of sonicated salmon sperm DNA/protein A agarose (UBI) for 1 h at 4°C. The precleared chromatin was immunoprecipitated for 12 h with specific Abs, specifically anti-ERα C-terminus mAb F-10 (Santa Cruz) for ERα, and anti-IRS-1 C-terminus pAb (UBI) for IRS-1, anti-pol II CTD4H8 mAb for pol II (UBI), and anti-SRC1 1135 mAb for SRC1 (UBI). After this, 60 μl of salmon sperm DNA/protein A agarose was added and precipitation was continued for 2 h at 4°C. After pelleting, precipitates were washed sequentially for 5 min with the following buffers: Wash A (0.1% SDS, 1% Triton X-100, 2 mM EDTA, 20 mM Tris-HCl pH 8.1, 150 mM NaCl), Wash B (0.1% SDS, 1% Triton X-100, 2 mM EDTA, 20 mM Tris-HCl pH 8.1, 500 mM NaCl), and Wash C (0.25 M LiCl, 1% NP-40, 1% sodium deoxycholate, 1 mM EDTA, 10 mM Tris-HCl pH 8.1), and then twice with TE buffer (10 mM Tris, 1 mM EDTA). The immune complexes were eluted with elution buffer (1% SDS, 0.1 M $NaHCO_3$). The eluates were reverse crosslinked by heating at 65°C for 12 h and digested with proteinase K (0.5 mg/ml) at 45°C for 1 h. DNA was obtained by phenol and phenol/chloroform extractions. A 2 μl portion of 10 mg/ml of yeast tRNA was added to each sample and DNA was precipitated with EtOH for 12 h at 4°C and then resuspended in 20 μl of TE buffer. A 5 μl volume of each sample was used for PCR with pS2 promoter primers

flanking ERE-containing pS2 promoter fragment: upstream 5′-GATTACAGCGTGAGCCACTG-3′, and downstream 5′-TGGTCAAGCTACATGGAAGG-3′. The primers for GAPDH promoter were 5′-GCTACTAGCGGTTTTACGGG-3′ (forward) and 5′-AAGATGCGGCTGACTGTCGAA-3′ (reverse). The PCR conditions were 45 s at 94°C, 40 s at 58°C, and 90 s at 72°C. The amplification products obtained in 25 and 35 cycles were analysed in a 2% agarose gel and visualized by ethidium bromide staining. The intensity of bands representing relevant proteins was measured by Scion Image laser densitometry scanning program. In control samples, non-immune IgG (rabbit for IRS-1 Abs and mouse for all other Abs, Santa Cruz) was used instead of the primary Abs.

Reverse ChIP

We followed the methodology described by Reid *et al*. (2003). The pellets obtained by IP of soluble chromatin with IRS-1 and ERα Abs were eluted with 500 μl of Re-ChIP buffer (0.5 mM DTT, 1% Triton X-100, 2 mM EDTA, 150 mM NaCl, 20 mM Tris-HCl pH 8.1). Next, the eluate from ERα IP was precipitated with IRS-1 pAb (UBI) and the eluate from IRS-1 IP was precipitated with ERα mAb (Santa Cruz). The presence of the pS2 promoter sequences in the resulting Re-ChIP pellets was examined as described above for one-step ChIP.

RT–PCR

COS-7 cells were transfected with different plasmids for 24 h, as described in the transactivation assays methodology. Total RNA was isolated using TRIzol reagent (Invitrogen) according to the manufacturer's instructions. A 5 μg portion of total RNA was reverse transcribed (RT) at 37°C for 30 min in 20 μl of buffer containing 200 U of M-MLV reverse transcriptase (Promega), 0.4 μg oligo-dT, 0.5 μM deoxynucleotide triphosphate (dNTP), and 24 U RNAsin. The reaction was terminated by heat denaturation for 5 min at 95°C.

A 2 μl portion of RT products was used to simultaneously amplify pS2 and 36B4 (control) DNA sequences. The pS2 cDNA fragment (210 bp) was amplified using the following primers: 5′-TTCTATCCTAATACCATCGACG-3′ (forward) and 5′-TTTGAGTAGTCAAAGTCAGAGC-3′ (reverse). The 408 bp fragment of the 36B4 ribosomal phosphoprotein DNA was amplified with the following primers: 5′-CTCAACATCTCCCCCTTCTC-3′ (forward) and 5′-CAAATCCCATATCCTCGTCC-3′ (reverse) (Maggiolini *et al*., 2001). The PCR amplification was performed using 1.25 U GoTaq DNA polymerase (Promega), 1 × PCR buffer (10 mM Tris-HCl, 50 mM KCl), 2.5 mM $MgCl_2$, 0.2 mM of each dNTP, and 1.5 pM of primers for pS2 or 0.5 pM primers for 36B4. PCR conditions were 30 s at 94°C, 40 s at 59°C, and 60 s at 72°C for 30 cycles. PCR products (10 μl) were separated on a 1.2% agarose gel.

Statistical analysis

Student's *t*-test was used to analyze WB and transactivation data. Statistical significance was assumed at $P<0.05$.

Acknowledgements
This research was supported in part by the following grants and awards: DOD Breast Cancer Research Program DAMD17-99-1-9407 (ES), DAMD17-01-1-0651 (ES), DAMD17-01-1-0320 (SdR), NIH CA87391 (ERS); Cancer Research Foundation of America F55401 (CG and ES).

References

Ando S, Panno ML, Salerno M, Sisci D, Mauro L, Lanzino M and Surmacz E. (1998). *Biochem. Biophys. Res. Commun.*, **253,** 315–319.
Bartucci M, Morelli C, Mauro L, Ando' S and Surmacz E. (2001). *Cancer Res.*, **61,** 6747–6754.
Boylan JM and Gruppuso PA. (2002). *Endocrinology*, **143,** 4178–4183.
Burks DJ and White MF. (2001). *Diabetes*, **50,** S140–S145.
Chan TW, Pollak M and Huynh H. (2001). *Clin. Cancer Res.*, **7,** 2545–2554.
Guvakova MA and Surmacz E. (1997). *Cancer Res.*, **57,** 2606–2610.
Kahlert S, Nuedling S, van Eickels M, Vetter H, Meyer R and Grohe' C. (2000). *J. Biol. Chem.*, **275,** 18447–18453.
Lannigan DA. (2003). *Steroids*, **68,** 1–9.
Lassak A, Del Valle L, Peruzzi F, Wang JY, Enam S, Croul S, Khalili K and Reiss K. (2002). *J. Biol. Chem.*, **277,** 17231–17238.
Lee AV, Jackson JG, Gooch JL, Hilsenbeck SG, Coronado-Heinsohn E, Osborne CK and Yee D. (1999). *Mol. Endocrinol.*, **10,** 787–796.
Maggiolini M, Bonofiglio D, Marsico S, Panno ML, Cenni B, Picard D and Andò S. (2001). *Mol. Pharmacol.*, **60,** 595–602.
Mauro L, Salerno M, Panno ML, Bellizzi D, Sisci D, Miglietta A, Surmacz E and Ando S. (2001). *Biochem. Biophys. Res. Commun.*, **288,** 685–689.
Metiver R, Stark A, Flouriot G, Hubner MR, Brand H, Penot G, Manu D, Denger S, Reid G, Kos M, Russel RB, Kah O, Pakdel F and Gannon F. (2002). *Mol. Cell*, **10,** 1019–1032.
Molloy CA, May FEB and Westley BR. (2000). *J. Biol. Chem.*, **275,** 12565–12571.
Morelli C, Garofalo C, Bartucci M and Surmacz E. (2003). *Oncogene*, **22,** 4007–4016.
Prisco M, Santini F, Baffa R, Liu M, Drakas R, Wu A and Baserga R. (2002). *J. Biol. Chem.*, **277,** 32078–32085.
Reid G, Hubner M R, Metivier R, Brand H, Denger S, Manu D, Beaudouin J, Ellenberg J and Gannon F. (2003). *Mol. Cell*, **11,** 695–707.
Sachdev D and Yee D. (2001). *Endocr. Relat. Cancer*, **8,** 197–209.
Salerno M, Sisci D, Mauro L, Guvakova M, Ando S and Surmacz E. (1999). *Int. J. Cancer*, **81,** 299–304.
Schnarr B, Strunz K, Ohsam J, Benner A, Wacker J and Mayer D. (2000). *Int. J. Cancer*, **89,** 506–513.
Sciacca L, Prisco M, Wu A, Belfiore A, Vigneri R and Baserga R. (2003). *Endocrinology*, **144,** 2650–2658.
Seol KC and Kim SJ. (2003). *Biochem. Biophys. Res. Commun.*, **306,** 898–904.
Shang Y, Hu X, DiRenzo J, Lazar MA and Brown M. (2000). *Cell*, **103,** 843–852.
Simoncini T, Hafezi-Moghadam A, Brazil DP, Ley K, Chin WW and Liao JK. (2000). *Nature*, **407,** 538–541.
Song R, Mcpherson RA, Adam L, Bao Y, Shupnik M, Kumar R and Santen RJ. (2002). *Mol. Endocrinol.*, **16,** 116–127.
Sun H, Tu X, Prisco M, Wu A, Casaburi I and Baserga R. (2003). *Mol. Endocrinol.*, **17,** 472–486.
Sun M, Paciga JE, Feldman RI, Yuan Z, Coppola D, Lu YY, Shelley SA, Nicosia SV and Cheng JQ. (2001). *Cancer Res.*, **61,** 5985–5991.
Surmacz E. (2000). *J. Mammary Gland Biol. Neopl.*, **5,** 95–105.
Surmacz E and Burgaud JL. (1995). *Clin. Cancer Res.*, **1,** 1429–1436.

Tu X, Batta P, Innocent N, Prisco M, Casaburi I, Belletti B and Baserga R. (2002). *J. Biol. Chem.*, **277,** 44357–44365.
Vladusic EA, Hornby AE, Guerra-Vladusic FK, Lakins J and Lupu R. (2000). *Oncol. Rep.*, **7,** 157–167.
White MF. (1998). *Mol. Cell. Biochem.*, **182,** 3–11.
Yee D and Lee AVJ. (2000). *J Mammary Gland Biol. Neopl.*, **5,** 107–115.
Yenush L and White MF. (1997). *BioEssays*, **19,** 491–500.

E. R. Sauter
C. Garofalo
J. Hewett
J. E. Hewett
C. Morelli
E. Surmacz

Leptin Expression In Breast Nipple Aspirate Fluid (NAF) and Serum Is Influenced By Body Mass Index (BMI) But Not by the Presence of Breast Cancer

Abstract

While obesity is a known risk factor for postmenopausal breast cancer, the molecular mechanisms involved are unclear. Systemic levels of leptin, the product of the *ob* (obesity) gene, are increased in obese individuals (body mass index, BMI, over 25) and are higher in women than men. Leptin has been found to stimulate the growth of breast cancer cells *in vitro*. Our goal was to determine whether leptin was 1) present in nipple aspirate fluid (NAF), and 2) whether NAF leptin levels were associated with a) levels in serum, b) obesity, and c) breast cancer. We collected and evaluated NAF specimens from 83 subjects and serum specimens from 49 subjects. NAF leptin was detectable in 16/41 (39%) of premenopausal and 21/42 (50%) postmenopausal subjects. NAF leptin was significantly lower ($p = 0.042$) in premenopausal than postmenopausal women with a BMI < 25, but not in those with a higher BMI. NAF leptin was significantly associated with BMI in premenopausal ($p = 0.011$) but not in postmenopausal women. Serum leptin was associated with BMI in both premenopausal and postmenopausal women ($p = 0.0001$ for both). NAF and serum leptin were associated in premenopausal ($p = 0.02$) but not postmenopausal women. Neither NAF nor serum leptin was associated with premenopausal or postmenopausal breast cancer. Our findings include that 1) leptin is present in the breast and detectable in a subset of NAF samples, 2) NAF leptin in premenopausal but not postmenopausal women parallels serum leptin levels, and 3) neither NAF nor serum levels of leptin were associated with premenopausal or postmenopausal breast cancer.

Key words
Obesity · Premenopause · Postmenopause · Protein concentration · Leptin release

Abbreviations: BCA, bicinchoninic acid; BMI, body mass index; DCIS, ductal carcinoma *in situ*; ELISA, enzyme linked immunosorbent assay; IBC, invasive breast cancer; IRB, institutional review board; NAF, nipple aspirate fluid; ob, obesity; OB-R, obesity receptor; OB-Rs, short form of the obesity receptor

Introduction

Leptin, the product of the *ob* gene, is a 16 kDa cytokine acting as a circulating satiety factor [1] concentrated in adipose tissue. The expression of leptin is 2 – 3 times as high in women as in men [2]. This is likely both because women have a higher percentage of subcutaneous fat [3] and because leptin expression may be affected by female sex hormones [2]. Leptin mRNA is detectable in human mammary epithelial cells, and immunoreactive leptin has

Affiliation
Ellis Fischel Cancer Center, University of Missouri-Columbia, Columbia, MO [E.R.S., J.H., J.E.H.] and Kimmel Cancer Center, Thomas Jefferson University, Philadelphia, PA [C.G., C.M., E.S.]

Correspondence
E. R. Sauter · University of Missouri – Columbia · One Hospital Drive · Rm 588 · Columbia · MO 65212 · Phone: +1(573)8824471 · Fax: +1(573)8844585 · E-Mail: sautere@health.missouri.edu

Received 8 October 2003 · **Accepted after revision** 24 January 2004

Bibliography
Horm Metab Res 2004; 36: 1–5 © Georg Thieme Verlag Stuttgart · New York · DOI 10.1055/s-2004-814490 · ISSN 0018-5043

been found in breast milk [4,5]. Leptin is considered a mammary hormone that may induce differentiation of breast cells [6].

The association between leptin and breast cancer has been addressed by recent studies. *In vitro* experiments demonstrate that estrogen receptor-positive MCF-7 [7] and T47-D [8] cells express leptin receptors and are stimulated to proliferate by leptin. In clinical studies, leptin has been directly associated with breast cancer in one report [9], and inversely associated with premenopausal breast cancer in another [10]; no association was found in the third report [11].

Obesity seems to protect premenopausal women and increase a postmenopausal woman's breast cancer risk [12]. The ideal method of evaluating the role of leptin in the breast should be non-invasive and organ-specific. Nipple aspiration, which provides NAF, is organ-specific (unlike plasma or serum), causes minimal or no discomfort, is non-invasive and provides both cells and extracellular fluid from the breast ductal epithelium, the cells which give rise to cancer. NAF can be reliably collected from both premenopausal and postmenopausal subjects [13] and biological markers measured in the fluid using as little as 1 µl of sample [14].

Material And Methods

Subjects

Informed consent was obtained from 91 subjects using a protocol approved by the Institutional Review Board. Eighty-two enrolled subjects had NAF samples collected in the breast evaluation clinics at our institutions. Forty-nine of the subjects provided blood for serum leptin analysis, including nine who did not have nipple aspiration attempted. The median age was 47 (range 23–81) years. Forty (49%) subjects who provided NAF were premenopausal. Women who had nursed or been pregnant within two years before enrollment were excluded. Subjects provided their height and weight as part of a comprehensive breast health history questionnaire. Women belonging to any breast cancer risk category were enrolled, including women with breast cancer, those with an abnormal mammogram or a palpable mass, or women undergoing nipple aspiration without breast cancer concerns. Women who required diagnostic breast surgery had NAF and serum samples obtained just prior to (within three weeks) or on the same day as definitive surgery to treat their cancer. Women that had received prior radiation to the breast from which NAF was collected were also excluded from the study.

Specimen collection and preparation

Nipple fluid was aspirated from the breast by a trained physician or nurse clinician using a modified breast pump [15]. Samples were collected into capillary tubes and stored at – 80 °C until use; 8 ml of blood was also collected if the subject agreed, and stored after serum separation at – 80 °C until use.

Leptin analysis

NAF and serum leptin were measured using a human leptin ELISA kit (Linco Research, St. Charles, MO) following the manufacturer's instructions. Total protein concentration in NAF was assessed by the BCA method (Pierce Chemicals, Rockford, IL). Pure NAF samples were adjusted to 100 µl with PBS. Leptin was measured in 50 µl of adjusted samples in duplicate. Leptin in serum was analyzed in pure form. Several NAF and serum samples were measured repeatedly to determine the interassay variation. The interassay variation was < 9% for NAF and < 12% for serum.

Statistical analysis

Since the data were not normally distributed, ranking procedures were used for all analyses with continuous variables. Data were analyzed using all NAF leptin results, including those below the level of detection, which were considered as zero. To compare leptin expression between the premenopausal and postmenopausal groups, the Wilcoxon Rank Sum Test or Fisher's Exact Test was used. Spearman Rank Correlations were calculated to measure the association between leptin expression and BMI and between NAF leptin and serum leptin.
Where multiple samples contained detectable leptin, the median value of these samples was used for our analyses. In all BMI analyses, controlling for total NAF protein identified a stronger association than when total protein was not controlled for. For this reason, all Spearman's calculations are reported as NAF leptin/mg total protein.

Results

Leptin is measurable in NAF and serum

Leptin was measurable in the NAF of 44.6% (37/82) of subjects (Table **1**), 39% of premenopausal and 50% of postmenopausal women. When comparing premenopausal and postmenopausal women based on BMI (0 – 24.99, 25 – 29.99, and > = 30), NAF leptin levels were lower (p = 0.042) in premenopausal than postmenopausal women for the lowest but not for the intermediate (p = 0.33) or highest (p = 0.60) BMI groups. The ability to detect leptin increased with increasing BMI among premenopausal (p = 0.011) but not postmenopausal women (Table **1**, Fig. **1**). When considering only women without breast cancer (Table **2**), the ability to detect leptin in NAF remained associated with increased BMI in premenopausal women.

Leptin was detectable in the serum of 49/49 subjects (Table **3**). Median serum leptin was 11.0 ng/ml in premenopausal subjects

Table **1** Detection of NAF Leptin Expression (ng/g total protein) Based on Body Mass Index (BMI)

	BMI (kg/m²)			
	0 – 24.99	*25 – 29.99*	*≥ 30*	*P value*
Overall				
Yes[1]	12	9	16	
No	23	8	15	0.15
Premenopausal				
Yes	4	5	7	
No	18	2	5	**0.011**
Postmenopausal				
Yes	8	4	9	
No	5	6	10	0.56

Yes[1]: NAF leptin level was measurable; No: NAF leptin was not measurable.

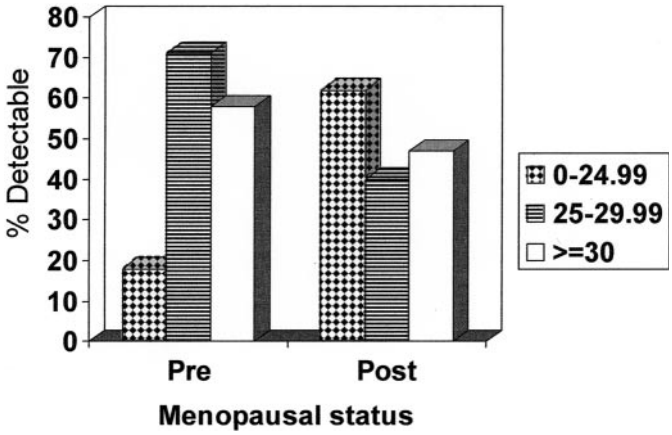

Fig. **1** Percentage of NAF samples in which leptin was detectable based on body mass index and menopausal status.

and 21.4 ng/ml in postmenopausal subjects. The difference was not statistically significant. Serum leptin was associated with BMI in both premenopausal ($r = 0.79$, $p = 0.0001$, $n = 23$) and postmenopausal ($r = 0.73$, $p = 0.0001$, $n = 26$) women.

NAF leptin levels are associated with BMI and serum leptin levels in premenopausal women

We next evaluated NAF leptin expression based on the actual measurement (Table **4**), rather than whether classified as detectable or not. Using this approach, NAF leptin expression was associated with BMI in premenopausal ($r = 0.38$, $p = 0.01$) but not in postmenopausal women ($r = -0.003$, $p = 0.98$). There were 40 subjects in whom we had matched NAF and serum samples. NAF and serum leptin levels were associated in premenopausal ($r = 0.51$, $p = 0.02$, $n = 20$) but not in postmenopausal women ($r = -0.12$, $p = 0.60$, $n = 20$).

Table **2** Detection of NAF Leptin Expression in Women with/without Breast Cancer

	BMI 0–24.99		*25–29.99*		*≥30*		*P value*	
Overall subjects (%)	CA	No CA	CA	No CA	CA	No CA	CA	No CA
NAF								
Yes	4	7	5	4	6	10		
No	4	19	1	7	8	7	0.24	0.11
Premenopausal								
Yes	0	4	2	3	2	5		
No	2	16	0	2	2	3	0.14	**0.053**
Postmenopausal								
NAF								
Yes	4	3	3	1	4	5		
No	2	3	1	5	6	4	0.39	0.32

CA: cancer; Yes, No: Indicates whether NAF leptin was detectable

Table **3** Serum Leptin Expression (ng/ml) Based on Body Mass Index (BMI)

	BMI (kg/m²) 0–24.99	*25–29.99*	*≥30*
Overall			
n	21	8	20
Median	7.80	16.39	27.10
Range	0.71–29.41	10.06–22.56	20.47–88.41
Premenopausal			
n	14	1	8
Median	5.96	10.06	30.63
Range	0.71–29.41	10.06–10.06	22.71–71.06
Postmenopausal			
n	7	7	12
Median	9.67	17.32	25.11
Range	3.32–26.14	10.28–22.56	20.47–88.41

Table **4** NAF Leptin Expression (ng/g total protein) Based on Body Mass Index (BMI)

	BMI (kg/m²) 0–24.99	*25–29.99*	*≥30*
Overall			
n	35	17	31
Median	0	0.047	0.037
Range	0–0.47	0–1.52	0–0.73
Premenopausal			
n	22	7	12
Median	0	0.068	0.067
Range	0–0.47	0–1.52	0–0.42
Postmenopausal			
n	13	10	19
Median	0.013	0	0
Range	0–0.41	0–0.74	0–0.73

Overall[1]: Eight women who had blood serum analyzed for leptin did not provide NAF samples. n: Number of subjects.

Table **5** Detection of NAF Leptin in Ductal Carcinoma In Situ (DCIS) and Invasive Breast Cancer (IBC)

Diagnosis		*BMI*					
		19.3 – 24.9		*25 – 29.9*		*≥ 30*	
	n	*Yes*	*No*	*Yes*	*No*	*Yes*	*No*
NAF							
DCIS	*6*	1	2	1	0	2	0
IBC	*22*	3	2	4	1	4	8

Association of NAF and serum leptin with breast cancer

We used two approaches for evaluating the association of NAF leptin with breast cancer. In the first approach, we considered whether there was an association between our ability to detect leptin and breast cancer. The two were not associated in pre ($p = 0.14$) nor in postmenopausal ($p = 0.39$) subjects (Table **2**). In the second approach, we considered the actual leptin measurement. Using this approach and Spearman's rank correlation, NAF leptin was not associated with breast cancer in either premenopausal ($p = 0.59$) or postmenopausal women ($p = 0.60$). Similarly, there was no association between serum leptin levels and the presence of breast cancer in either premenopausal ($p = 0.28$) or postmenopausal women ($p = 0.68$).

Finally, we evaluated whether there was an association between our ability to detect NAF leptin and breast cancer progression (Table **5**). Specifically, we compared non-invasive (ductal carcinoma *in situ*, DCIS) and invasive breast cancer (IBC). The limited number of samples from subjects with DCIS did not allow statistical analysis comparing NAF leptin detection in DCIS *vs.* IBC, nor leptin detection in DCIS based on BMI. There was no association between leptin detection and IBC.

Discussion and Conclusions

The link between obesity and breast cancer has been established fairly well [16]. Since circulating leptin levels rise with increasing BMI, we hypothesized that leptin expression might be associated with breast cancer risk. As a first step, we assessed the expression of this hormone in NAF, an organ specific specimen, and compared it to systemic levels in serum. Because leptin has been found in breast milk [4], we anticipated that it would be measurable in NAF. Indeed, leptin was detectable in 34% of samples. Leptin was probably also expressed in some samples below the threshold level of sensitivity of our ELISA detection kit (0.5 ng/ml).

Leptin was detectable in all serum samples (mean 21.2, median 20.3 ng/ml). Consistent with published findings, the expression of leptin in serum was significantly correlated with BMI [17]. According to previous reports, there is no consensus on the correlation between serum leptin and menopausal status [18]. In our study, serum leptin levels did not differ by menopausal status. Interestingly, the expression of leptin in NAF only correlated with BMI in premenopausal women. We speculate that leptin in NAF is transported from neighboring adipose tissue by the means of transcellular and intracellular passage. Although the mechanism of transcellular leptin transport is still unclear, some data suggest that this process could be controlled by premenopausal female sex hormones. Experiments demonstrated that transcellular transport of leptin is mediated by short-form leptin receptors (Ob-Rs) [19] whose expression appears to be regulated by estrogens [20, 21].

We observed that leptin levels in NAF and serum are significantly associated ($p = 0.02$). Generally, leptin concentration in NAF was lower than in serum. NAF leptin was detectable in 44.6% of samples overall, and was significantly lower ($p = 0.042$) in premenopausal than in postmenopausal women with a BMI less than 25, but not in those with a higher BMI. There are at least two explanations for the lower leptin levels in NAF than in serum. First, NAF leptin may originate in and be secreted from mammary epithelial cells, which produce only small amounts of the hormone. Indeed, normal mammary cells and breast cancer cells have been reported to express leptin mRNA in vitro, even though leptin protein is not consistently detected [22]. Second, it is possible that in addition to (or instead of) local leptin secretion, the hormone is transported from neighboring breast adipose tissue or serum, which results in its dilution. The mechanism of such passage could involve transepithelial transport similar to that suggested in the transport of leptin through the blood-brain barrier [23]. The association between NAF leptin levels and BMI suggests that the second possibility should be considered.

Prior reports link obesity with both premenopausal and postmenopausal breast cancer [12] and two clinical reports analyzing leptin levels in serum have linked the protein with breast cancer risk, although the conclusions were conflicting, one report indicating a direct [9] and the other [10] an inverse associated with premenopausal breast cancer. Our findings are consistent with and extend a third report [11], which evaluated serum leptin levels in premenopausal women with DCIS, while our study evaluated women with both DCIS and invasive breast cancer (combined into one group as cancer) and both premenopausal and postmenopausal women, concluding that there was no significant association between serum leptin and breast cancer.

In conclusion, our study indicates that leptin can be detected in a subset of NAF samples, that NAF leptin is associated with BMI and serum leptin in premenopausal women, and that serum leptin is associated with BMI in both premenopausal and postmenopausal women. Contrary to some other reports suggesting that serum leptin was associated with breast cancer, we did not observe an association between leptin and cancer in either NAF or serum. It would be important to test our hypothesis on transcellular transport of leptin by measuring the level of the Ob-R in mammary epithelium in premenopausal and postmenopausal women and correlating the levels with NAF leptin.

Acknowledgements

This work was supported in part by the following grant awards: National Cancer Institute CA87391, Department of Defense 17-01-1-0651, and Cancer Research Foundation of America F55401

References

[1] Friedman JM, Halaas JL. Leptin and the regulation of body weight in mammals. Nature 1998; 395: 763 – 770
[2] Wauters M, Considine RV, Van Gaal LF. Human leptin: from an adipocyte hormone to an endocrine mediator. Eur J Endocrinol 2000; 143: 293 – 311
[3] Hube F, Lietz U, Igel M, Jensen PB, Tornqvist H, Joost HG et al. Difference in leptin mRNA levels between omental and subcutaneous abdominal adipose tissue from obese humans. Horm Metab Res 1996; 28: 690 – 693
[4] Smith-Kirwin SM, O'Connor DM, de Johnston J, Lancey ED, Hassink SG, Funanage VL. Leptin expression in human mammary epithelial cells and breast milk. J Clin Endocrinol Metab 1998; 83: 1810 – 1813
[5] Uysal FK, Onal EE, Aral YZ, Adam B, Dilmen U, Ardicolu Y. Breast milk leptin: its relationship to maternal and infant adiposity. Clin Nutr 2002; 21: 157 – 160
[6] Neville MC, McFadden TB, Forsyth I. Hormonal regulation of mammary differentiation and milk secretion. J Mammary Gland Biol Neoplasia 2002; 7: 49 – 66
[7] Dieudonne MN, Machinal-Quelin F, Serazin-Leroy V, Leneveu MC, Pecquery R, Giudicelli Y. Leptin mediates a proliferative response in human MCF7 breast cancer cells. Biochem Biophys Res Commun 2002; 293: 622 – 628
[8] Laud K, Gourdou I, Pessemesse L, Peyrat JP, Djiane J. Identification of leptin receptors in human breast cancer: functional activity in the T47-D breast cancer cell line. Mol Cell Endocrinol 2002; 188: 219 – 226
[9] Tessitore L, Vizio B, Jenkins O, de Stefano I, Ritossa C, Argiles JM et al. Leptin expression in colorectal and breast cancer patients. Int J Mol Med 2000; 5: 421 – 426
[10] Petridou E, Papadiamantis Y, Markopoulos C, Spanos E, Dessypris N, Trichopoulos D. Leptin and insulin growth factor I in relation to breast cancer (Greece). Cancer Causes Control 2000; 11: 383 – 388
[11] Mantzoros CS, Bolhke K, Moschos S, Cramer DW. Leptin in relation to carcinoma in situ of the breast: a study of pre-menopausal cases and controls. Int J Cancer 1999; 80: 523 – 526
[12] Harvard Health Letter 2001
[13] Sauter ER, Ross E, Daly M, Klein-Szanto A, Engstrom PF, Sorling A et al. Nipple aspirate fluid: a promising non-invasive method to identify cellular markers of breast cancer risk. Br J Cancer 1997; 76: 494 – 501
[14] Sauter ER, Ehya H, Babb J, Diamandis E, Daly M, Klein-Szanto A et al. Biological markers of risk in nipple aspirate fluid are associated with residual cancer and tumour size. Br J Cancer 1999; 81: 1222 – 1227
[15] Sauter ER, Daly M, Linahan K, Ehya H, Engstrom PF, Bonney G et al. Prostate-specific antigen levels in nipple aspirate fluid correlate with breast cancer risk. Cancer Epidemiol Biomarkers Prev 1996; 5: 967 – 970
[16] Friedenreich CM. Review of anthropometric factors and breast cancer risk. Eur J Cancer Prev 2001; 10: 15 – 32
[17] Considine RV, Sinha MK, Heiman ML, Kriauciunas A, Stephens TW, Nyce MR et al. Serum immunoreactive-leptin concentrations in normal-weight and obese humans. N Engl J Med 1996; 334: 292 – 295
[18] Di Carlo C, Tommaselli GA, Nappi C. Effects of sex steroid hormones and menopause on serum leptin concentrations. Gynecol Endocrinol 2002; 16: 479 – 491
[19] Hileman SM, Tornoe J, Flier JS, Bjorbaek C. Transcellular transport of leptin by the short leptin receptor isoform ObRa in Madin-Darby Canine Kidney cells. Endocrinology 2000; 141: 1955 – 1961
[20] Chan JL, Bluher S, Yiannakouris N, Suchard MA, Kratzsch J, Mantzoros CS. Regulation of circulating soluble leptin receptor levels by gender, adiposity, sex steroids, and leptin: observational and interventional studies in humans. Diabetes 2002; 51: 2105 – 2112
[21] Duggal PS, Weitsman SR, Magoffin DA, Norman RJ. Expression of the long (OB-RB) and short (OB-RA) forms of the leptin receptor throughout the oestrous cycle in the mature rat ovary. Reproduction 2002; 123: 899 – 905
[22] O'Brien SN, Welter BH, Price TM. Presence of leptin in breast cell lines and breast tumors. Biochem Biophys Res Commun 1999; 259: 695 – 698
[23] Hileman SM, Pierroz DD, Masuzaki H, Bjorbaek C, El-Haschimi K, Banks WA et al. Characterizaton of short isoforms of the leptin receptor in rat cerebral microvessels and of brain uptake of leptin in mouse models of obesity. Endocrinology 2002; 143: 775 – 783

■ Remark for the author: please check carefully Fig. **1**. In the data you sent us the picuture was not the same as in the paper version of the manuscript. ■

SYNTHESIS OF MESOPOROUS SILICA MICROSPHERE FOR DRUG TARGETING

L. Pasqua[a], C. Morelli[b], F. Testa[a], D. Sisci[b], R. Aiello[a] and S. Andò[c]

a) Dipartimento di Ingegneria Chimica e dei Materiali, Università degli Studi della Calabria, Via Pietro Bucci, 87030 Rende, Italy;
b) Dipartimento Farmaco-Biologico, Facoltà di Farmacia, Università degli Studi della Calabria Via Pietro Bucci, 87030 Rende, Italy.
c) Dipartimento di Biologia Cellulare Università degli Studi della Calabria, Via Pietro Bucci, 87030 Rende, Italy;

INTRODUCTION

In the last years, in the field of highly ordered mesoporous silicates, much effort has been devoted to the development of organic-inorganic supramolecular self-assemblies and their subsequent polycondensation. These syntheses involved organic structuring agents such as long chain quaternary ammonium cationic [1, 2] and anionic surfactants [3]. Also non-ionic surfactants, such as long chain alkylamine [4] and polyethylene oxides-type copolymers [5-7], were shown to produce synergistic assembly of silica. The hybridization of the inorganic precursor allows the development of innovative multifunctional materials with complex architectures and combining properties of organic, bio and inorganic components.

Hybrid inorganic-organic materials are produced when chemically active groups are covalently linked to the inorganic framework of mesoporous materials either by post-synthetic grafting or by simultaneous condensation of siloxane and organic siloxane precursors, the last containing a non-hydrolysable Si-C bond [8-14].

This method was also applied for bulky chromophores [15]. The synthesis of mesoporous hydrophobic materials by simultaneous removal of surfactant template and modification of the external surface, has been achieved by treating uncalcined MCM-41 with trialkylchlorosilanes [16].

The preparation of mesoporous silicate and alumino-silicate by different synthesis methods are reported together with their surface modification by reaction with benzoyl chloride [17]. Mesoporous materials synthesized using sodium silicate and an industrial neutral surfactant, are activated by calcination or solvent extraction and modified by reaction with benzoyl chloride to compare surface properties of both samples [18].

Mesoporous macroscale structures were obtained by oil-water interface templating systems at acid pH. TEOS is used as silica source and is hydrolyzed just at the oil-water interface where mesostructures are formed reflecting, on a larger scale, size and shape of the oil spheres because the inorganic materials condense around them. Stirring is one of the parameters for controlling emulsion properties through modification of long-range hydrodynamic forces. Under slow stirring fiber-type morphologies are predominantly observed while with increasing stirring rate more and more sphere-like particles are formed. The two-level byphase control was also used on a larger scale to produce self-supporting membranes at a static interface between an aqueous and an inorganic phase [19].

Successively, a method has been described where mesoporous silica particles of macroscopic dimensions, functionalized with organic ligands, can be produced from alkaline medium in a one-step emulsion process [20]. Furthermore, hard mesoporous silica spheres have been described according to a procedure closely related to that initially reported for the synthesis of MCM-41 [1-2]; the primary difference is that phase separation and emulsion chemistry which result from the hydrophobic nature of tetrabutylorthosilicate and butanol, are used in order to create the

desired morphology [21]. More recently, the conditions favouring the formation of mesoporous film over bulk material through the separation of the ingredients into two stratified phases, both in acid and in basic media, have been defined [22].

Recently, mesoporous materials and functionalized mesoporous materials have been obtained from two-level byphase emulsions. The upper one is an organic phase and contains the silica source; the lower phase is a water or water-ethylene glycol solution of the neutral surfactant. Micelles are feed by the silicon alcoxide, precursor of the inorganic coverage, in the interfacial region and, after condensation, the particles move to the bottom part of the synthesis vessel [23].

The possibility of synthesizing mesoporous materials with regularly sized pores by means of the supramolecular templating of a sol-gel process represents a starting point for the design of functional nanostructured materials. Mesoporous silicas with ordered porosity have been investigated for hosting non-steroidal anti-inflammatory drugs bearing a carboxylic acid through a confinement procedure consisting in either physisorption on the pure silica surface or *via* chemical anchoring on modified silica surface [24-27]. Furthermore, they have been also used as cell markers [28], in MALDI-TOF mass spectrometry because they selectively bind low molecular weight proteome [29] and to engineer systems able to activate the drug release through a photocatalyzed reaction [30].

In the present work mesoporous silica materials are synthesized from two-level by-phase emulsions according to the synthesis methodology reported in ref. 23 but employing new organic phases such as cyclohexane, hexane and decane. The synthesis procedures are aimed to produce mesoporous silica particles with controlled size and morphology and test then the suitability for the design of drug targeting devices through the evaluation of their behaviour in tumor cels culture media.

EXPERIMENTAL

Synthesis

The neutral polioxyethylene(10)octylphenylether, named Triton X-100 (Alfa Aesar), tetraethylortosilicate (Aldrich) as silica source and the hybrid silica source was (3-aminopropyl)-triethoxysilan (APTES, Aldrich) were used. The molar composition of the synthesis mixtures investigated are shown in Table 1. In a typical preparation of a mesoporous silica (Synthesis system 2) 13.80g of the surfactant are completely dissolved in 150g of distilled H_20 at room temperature.

A solution of TEOS (13,8 g) in n-decane (10 g) is slowly runned along the vessel wall of the aqueos solution so that the upper organic phase is easily established. The mixture is aged at room temperature for 8 days under slow magnetic stirring. The organic phase is finally removed and the resulting suspension filtered, washed and dried for 8 hours at 80° C.

Syntheses	Upper Phase				Lower Phase	
	TEOS	Decane	Hexane	Cyclohexane	Nonfix 10	H_2O
1	1	2.1			0.324	126.2
2	1	1.05			0.324	126.2
3	1	0.52			0.324	126.2
4	1		4.2		0.324	126.2
5	1			4.2	0.324	126.2

Table 1. Molar ratios in two-level byphase emulsions used for the synthesis of mesoporous materials.

Fluorescence labeling

APTES (1.42 g; 0.0064 moles) and Fluoresceine isothiocyanate (FITC) (0.004 g; 0.0103 mmoles) have been stirred in ethanol (3 ml) at room temperature for 24 hours; then a suspension of 700 mg of material 3 in ethanol (700 mg in 2.5 ml) has been added to the first solution and the whole mixture has been stirred for 2 days.

Characterization

X-Ray powder diffraction patterns were measured on a Philips PW1710 diffractometer using Cu-Kα radiation (40 Kv, 20 mA) over the range $1°<2\theta<15°$.

The N_2 adsorption-desorption volumetric isotherms at 77 K were measured on a Micromeritics Asap 2010 apparatus. Samples were pre-treated under vacuum at 300°C to a residual pressure of 2 μmHg. Surface area of the samples was calculated by BET linearization in the pressure range 0.05 to 0.2 P/P_0.

Lattice pore volume was obtained from the amount of nitrogen gas adsorbed at the top of the rising section of the isotherms of type I or IV. The amount of surfactant was measured by TG analysis. The measurements were carried out with a Netzsch STA 409 instrument between 20°C and 850°C at a ramp of 10°C/min in air with a flow rate of 10 ml/min. Micrographs were collected by a SEM Jeol JSTM 330A.

Cell lines and culture

MCF-7 and HeLa cells were obtained from ATCC. MCF-7 cells were grown in DMEM:F12 containing 5% calf serum (CS). HeLa cells were grown in DMEM plus 10% FCS. During the experiments cells were left in the same culture media.

Cell treatment

MCF-7 and HeLa cells were incubated with FITC labeled Mesoporous Silica Microspheres (FITC-MSM) at a final concentration of 50μg/ml.

Fluorescence microscopy

Cells were grown on coverslips up to 80% confluency. Then they were fixed in 3% paraformaldehyde, permeabilized with 0.2% Triton X-100, washed three times with PBS, and mounted with Vectashield mounting medium containing DAPI for nuclear counterstain (VECTOR Laboratories).

The cellular localization of FITC-MSM was examined under a fluorescence microscope (Olympus BX41; Olympus Corp.). Images were taken at x1000 magnification. The fluorophores were imaged separately to ensure no excitation/emission wavelength overlap. Untreated cells were used as control samples.

RESULTS AND DISCUSSION

All the samples (Table 2) show S_{BET} specific surface ranging from 800 to 1100 m^2/g and high pore volume up to 1,1 cm^3/g. Figure 2 shows nitrogen adsorption-desorption isotherms for materials obtained from systems 4 and 5 (Table 1). In both cases a type IV not reversible isotherm is obtained.

Pore volume for materials 1, 2 and 3 decreases with decane amount in byphasic emulsions probably because permeation of decane inside surfactant micelles decreases with decreasing decane concentration. This trend regards particularly high relative pressures pore volume.

Figures 1a and 1b show the XRD powder diffraction pattern of as-made and calcined sample obtained from system 3 (decane-water byphase system), respectively. As-made material shows the expected bymodal mesoporous structure [23], mantained after calcination.

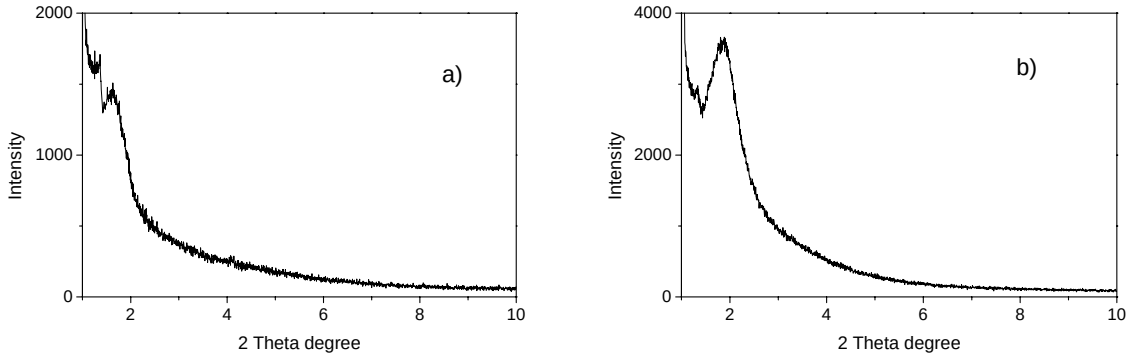

a) b)

Figure 1. XRD powder diffraction pattern of as-made (a) and calcined (b) sample obtained from decane-water byphase syntheses system 3 in Table 1.

Table 2

d-spacing values, for as-made (d_0), calcined (d_c) samples, specific surface areas (S_{BET}), pore volume and total mass loss of mesoporous silica samples obtained from systems in Table1.

Material	d_0 (Å)	d_c (Å)	S_{BET} (m^2/g)	Pore Volume (P/P_0=0.9;cm3/g)	Total mass loss (%)
1	62.38	53.34	908	0.81	55.18
2	53.33 66.12	48.63 63.12	886	0.57	51.63
3	53.33 66.12	46.58 66.12	924	0.53	48.62
4	59.04	66.12	1129	0.84	54.54
5	50.87 66.12	75.12	814	0.97	61.36

Material 3 shows typical bimodal nitrogen adsorption-desorption isotherm where two main mesopore filling steps are detectable. Material 4 shows a not reversible Type IV isotherm typical of capillary condensation in regularly-sized mesopores with a high relative pressure nitrogen adsorption step, while a bymodal isotherm is shown by material 5, probably because of cyclohexane permeation inside micelles surfactant.

Data obtained from XRD of as-synthesized materials evidence that the properties of the interfacial region affect surfactant chemistry. Micelles with different size are formed during the assembly of the materials. This is clearly shown by the observation of the XRD patterns of as-synthesized and calcined materials. The double peak XRD patterns, representative of two main reflecting elements,

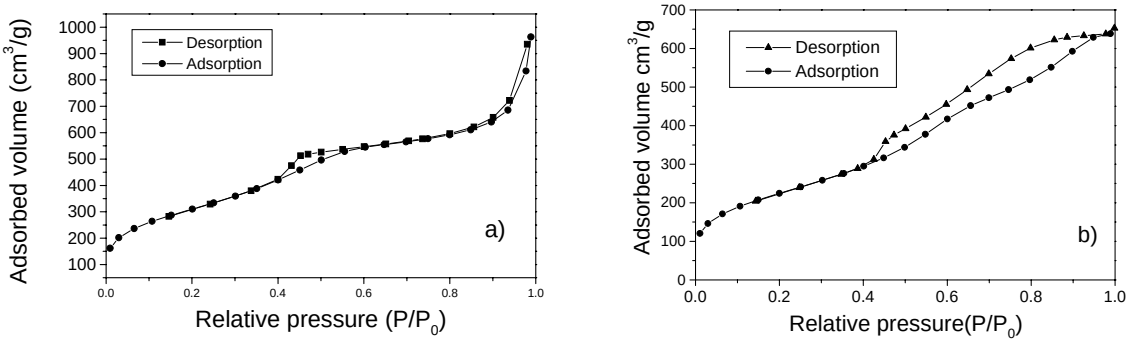

Figure 2. Nitrogen adsorption-desorption isotherms of materials 4 (a) and 5 (b) obtained from hexane- and cyclohexane-water byphase synthesis systems (Table 1).

confirms the co-existence of two templating systems with different diameters in accordance with the nitrogen adsorption on calcined materials showing two distinct capillary condensation steps.

The occurrence of heterogeneous formation of surfactant templating-micelles can be explained on the basis of solvent inclusion in the hydrophobic core of the micelles.

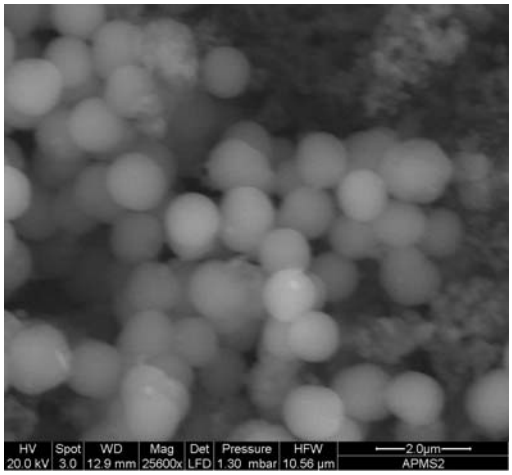

Figure 3. SEM micrograph of material 3.

SEM micrograph (Figure 3) shows that regular spheres, around 1 micron in size, are obtained from material 3. Regular spheres below 1 micron are obtained for all the preparation except for material 5 obtained from cyclohexane-water synthesis system that exhibits not regular formations several microns in size.

Mesoporous silica microspheres (material 3) have been modified on the external surface, before surfactant extraction, to provide the particles with imaging capabilities to evaluate the suitability of this regularly-sized mesoporous material for localized release by tracking interaction with tumor cells.

Fluoresceine isothiocyanate isomer I (FITC) was used as fluorescence label and covalently linked in ethanol to amino-propyltriethoxysilane (APTES).

The fluorescent silicon alkoxide was successively grafted at room temperature to the external surface of mesoporous silica microsphere using the as-synthesized material before surfactant extraction. Figure 4 (a and b) shows DRFT-IR spectra of material 3 as-synthesized and after FITC conjugation. The first one presents a very important surfactant contribute in the region around 2900 cm^{-1}, while the latter presents vibrations in the region 1020-1560 cm^{-1}, as expected for thiourea

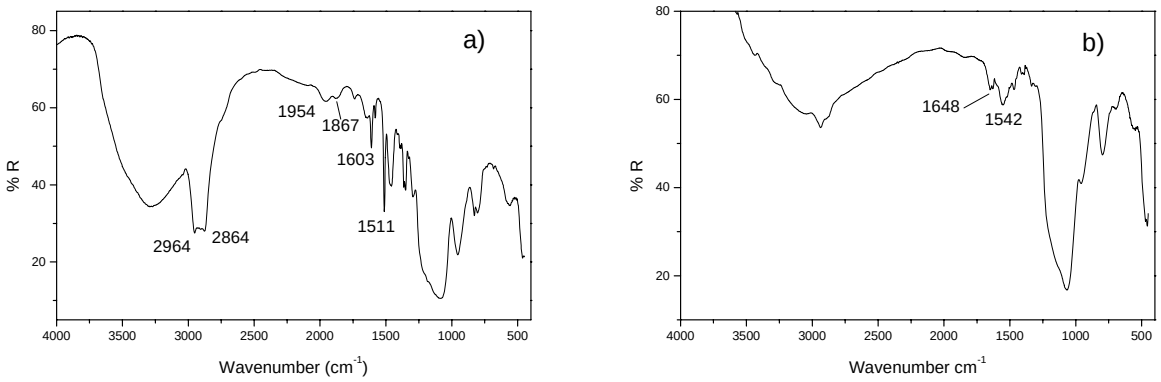

Figure 4. DRFT-IR spectra of sample 3 as-synthesized (a) and after conjugation with fluoresceine isothiocyanate (b).

derivatives, but shows decreased intensity for surfactant vibrations probably because soaking in ethanol for long time during FITC coupling partially removes surfactant; this is confirmed from thermogravimetric analysis that shows a decrease in total mass loss from 48.62 % for material 3 (Table 2) to 25.8 % for the corrispondent FITC-MSM material. Powder XRD of FITC-MSM shows a low-order single reflection pattern evidencing a silica reorganization during FITC coupling and ethanol soaking.

Microspheres have been suspended in water (1mg/ml) and successively incubated with two different tumor cell lines (MCF-7 and HeLa cells). Suspensions remained stable during months.

Cells were monitored up to 24 h at different times (1 h, 6 h, 24 h) under a fluorescence microscope. Figure 5 shows representative images of HeLa cells at 24h. The localization of labelled microparticles was studied by fluorescence microscopy as detailed in Experimental. The captured images of FITC-MSM (green fluorescence, Figure 5 a), merged FITC-MSM with DAPI (Figure 5 b), and bright field (BF, Figure 5c) are shown. In both cell lines the microparticles interact with cells and, more importantly, are retained on cell surface (Fig. 5 b).

Cell viability experiments showed that silica microparticles are well tolerated from biological systems (data not shown), so that they can be utilized for localized drug release purposes or, through their conjugation to a cell receptor specific ligand, for the design of an active drug targeting device.

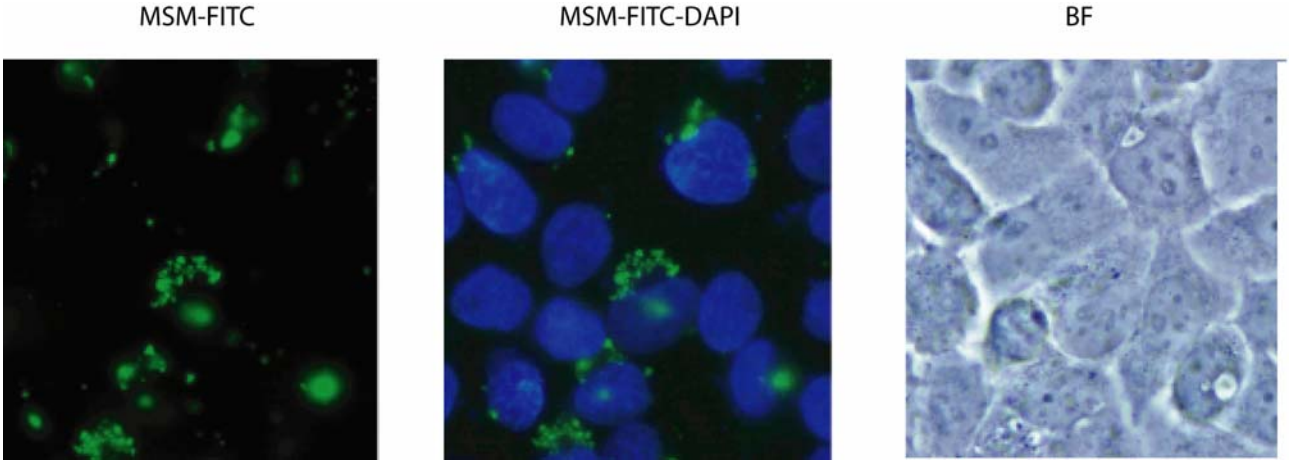

Figure 5. HeLa cells were incubated for 24h with 50μg/ml of FITC-MSM. Captured images of FITC-MSM green fluorescence (a), merged FITC-MSM with DAPI (b), and bright field (BF; c)

CONCLUSIONS

The above reported results show that the above reported results show that byphase emulsion synthesis systems are able to produce mesoporous silica particles with controlled morphology and submicronic size, as required for drug targeting purposes.
Due to their size these mesoporous silica particles, present a great potentiality for localized drug release as they are able to interact with cell surface where they are retained without showing any toxicity effect.

Aknowledgements

The authors acknowledge the financial Support from the Ministry of Instruction, University and Research (P.R.I.N. Project "Nanostructured Materials with Controlled Porosity for Innovative Technological Applications")

References

[1] C. T. Kresge, M.E, Leonowicz, W.J. Roth, J. C Vartuli, J. S. Beck, Nature ,**359** (1992) 710.
[2] J.S. Beck, J.C. Vartuli, W.J. Roth, M.E. Leonowicz, C.T. Kresge, K.D. Schmitt, C.T-W. Chu, D.H. Olson, E.W. Sheppard, S.B. McCullen; et al. J. Am. Chem. Soc., **114** (1992) 10834.
[3] Q. Huo, D.I. Margolese, U. Cielsa, P. Feng, T.E. Gier, P. Sieger, R. Leon, P.M. Petroff, F. Schüth, G.D. Stucky, Nature, **368** (1994) 317.
[4] P.T. Tanev, T.J. Pinnavaia, Science, **267** (1995) 865.
[5] G. Attard, J.C. Glyde, C.G. Göltner, Nature, **378** (1995) 366.
[6] S.A. Bagshaw, E. Prouzet and T.J. Pinnavaia, Science, **269** (1995) 1242.
[7] D. Zhao, J. feng, Q. Huo, N. Melosh, G.H. Fredrickson, B.F. Chmelka, G.D. Stucky, Science, **279** (1998) 548; D. Zhao, Q. Hou, J. Feng, B.F. Chmelka, G.D. Stucky, J. Am. Chem. Soc., **120** (1998) 6024
[8] S.L. Burkett, S.D. Sims and S. Mann, Chem. Commun., (1996) 1367.
[9] M.H. Lim and A. Stein, Chem. Mater., **11** (1999) 3285.
[10] Brunel D. , Microporous Mesoporous Mater. **10** (1999) 329.
[11] M. Park, S. Komarneni, Microporous Mesoporous Mater., **25** (1998) 75.
[12] D. J. Macquarrie, M. Rocchia, B. Onida, E. Garrone, P. Lentz, D. Brunel, A. C. Blanc, F. Fajula, Stud. Surf. Sci. Catal. **135** (2001) 29-P-31.
[13] D. J. Macquarrie, D. Brunel, G. Renard, A.C. Blanc, Stud. Surf. Sci. Catal., **135** (2001) 29-P-10.
[14] D.Brunel, F.Fajula, J.B. Nagy, B. Deroide, M.J. Verhoef, L. Veum, J.A. Peters and a. Van Bekkum, Appl. Catal. A, **213** (2001) 73.
[15] C.E. Fowler, B. Lebeau and S. Mann, Chem. Commun., (1999) 201.
[16] V. Antochshuk and M. Jaroniec, Chem. Commun., (1999) 2373
[17] L. Pasqua, F.Testa, R. Aiello, J. B.Nagy, G. Madeo, Phys. Chem. Chem. Phys, **5** (2003) 640.
[18] L. Pasqua, f. Testa, R. Aiello, Stud. Surf. Sci. Catal., **146** (2003) 497.
[19] S. Schacht, Q. Huo, I.G. Voigt-Martin, G.D. Stucky, F. Schuth, Science, **273** (1996) 768.
[20] R.I. Nooney, M. Kalyanaraman, G. Kennedy, E.J. Magin, Langmuir, **17** (2001) 528.
[21] Q. Huo, J. Feng, F. Schuth, G.D. Stucky, Chem. Mater., **9** (1997) 14.
[22] L. Faget, A Bergman, O. Regev, Thin Solid Films, **386** (2001) 6.
[23] Pasqua, L.; Testa, F.; Aiello, R. *Stud. Surf. Sci. Catal.* **2005**, *158*, 557.
[24] Vallet-Regi, M.; Ramila, A.; Del Real, R.P.; Perez-Pariente, J. *Chem. Mater.* 2001, **13**, 308.
[25] Cavallaro, G.; Pierro P.; Palumbo, F.S.; Testa, F.; Pasqua, L.; Aiello R. *Drug Deliv.* **2004** *11*, 41.

[26] Munoz, B.; Ramila, A.; Perez-Pariente, J.; Diaz, I.; Vallet-Regi, M. *Chem. Mater.* 2003, *15***,** 500.
[27] Tourné-Péteilh, C.; Brunel, D.; Bégu, S.; Chiche, B.; Fajula, F.; Lerner, D. A.; Devoisselle, J.M. *New. J. Chem.* 2003, **27**, 1415.
[28] Kishor Mal, N.; Fujiwara, M.; Tanaka, Y. *Nature* 2003, **421**, 350.
[29] Lin, Y.-H.; Tsai, C.-P.; Huang, H.Y.; Kuo, C.-T.; Hung, Y.; Huang, D.-M.; Chen, Y.-C.; Mou, C.-Y. *Chem. Mater.* 2005, **17,** 4570.
[30] R. Terracciano, M. Gaspari, F. Testa, L. Pasqua, P. Tagliaferri,M. Ming-Cheng Cheng, A. J. Nijdam,E. F. Petricoin, L. A. Liotta, G. Cuda, M. Ferrari, Salvatore Venuta, *Proteomics*, in press.
[31] L.Pasqua, F. Testa, R. Aiello, F. Di Renzo and F. Fajula, Stud. Surf. Sci. Catal. **135** (2001) 06-P-28.
[32] M. Grun, K.K. Unger, A. Matsumoto, K. Tsutsumi, Microporous Mesoporous Mater., **27** (1999) 207.
[33] Y. Zhong-Yong, S. Bao-Lian, Colloid Surface A, **241** (2004) 95.